Escola Tècnica Superior d'Enginyeria de Telecomunicació de Barcelona

UNIVERSITAT POLITÈCNICA DE CATALUNYA

PROJECTE FINAL DE CARRERA (PFC)

GEOSAR Mission:

Orbit Determination Methods and Techniques

Marc Fernàndez Uson

PFC Advisor: Prof. Antoni Broquetas Ibars

May 2016

PROJECTE FINAL DE CARRERA (PFC)

GEOSAR Mission:

Orbit Determination Methods and Techniques

Marc Fernàndez Uson

ABSTRACT

Multiple applications such as land stability control, natural risks prevention or accurate numerical weather prediction models from water vapour atmospheric mapping would substantially benefit from permanent radar monitoring given their fast evolution is not observable with present Low Earth Orbit based systems. In order to overcome this drawback, GEOstationary Synthetic Aperture Radar missions (GEOSAR) are presently being studied.

GEOSAR missions are based on operating a radar payload hosted by a communication satellite in a geostationary orbit. Due to orbital perturbations, the satellite does not follow a perfectly circular orbit, but has a slight eccentricity and inclination that can be used to form the synthetic aperture required to obtain images.

Several sources affect the along-track phase history in GEOSAR missions causing unwanted fluctuations which may result in image defocusing. The main expected contributors to azimuth phase noise are orbit determination errors, radar carrier frequency drifts, the Atmospheric Phase Screen (APS), and satellite attitude instabilities and structural vibration. In order to obtain an accurate image of the scene after SAR processing, the range history of every point of the scene must be known. This fact requires a high precision orbit modeling and the use of suitable techniques for atmospheric phase screen compensation, which are well beyond the usual orbit determination requirement of satellites in GEO orbits. The other influencing factors like oscillator drift and attitude instability, vibration, etc., must be controlled or compensated.

In order to determine the satellite orbit, GEOSAR mission propose a group of Active Radar Calibrators (ARCs). These ARCs will be placed in well-known positions of the observed scene providing range and range-rate measurements. From such measurements, the satellite position and velocity may be initially calculated. Then, the initial state may be refined by means of differential correction techniques such as Least Squares or Kalman filter techniques. In this way, the satellite orbit may be calculated more precisely, which is crucial in order to achieve well focused images.

This document will present the methods for computing the initial state of the satellite orbit, and will study the use of Least Squares technique as a method to determine the satellite orbit precisely. Since there is no real data available, ideal data will be created in order to perform different simulations of all methods and techniques presented within this document. Thus, the results will be used as a first approximation to the future satellite orbit determination.

ACNOWLEDGEMENTS

I would like to specially thank my PFC advisor, Prof. Antoni Broquetas, for introducing me to the orbit determination topic, and for his guidance during all project. I would also appreciate the support and exchange of ideas among all colleagues of the working group, especially Roger Martín. I hope this document may help you when dealing with orbit determination in your future PhD.

On the other hand, I would like to thank all people that have shared time with me during all university studies. I will begin with Marc Arànega and Manak Bhambi. I started the Telecommunications Engineering with them, but they became engineers first some years ago, and they are now supporting me. I will continue with Luís Aldana who is the first person I met after returning to university life. And, I will conclude with Eduardo Delgado, Juan Arimany, David Tomuletiu, Susana Amorós, Miquel Àngel Corbella, Milena Ten, Jordi Nonell, Meritxell Liria, Àlex Peiró, Laura Samos…, people that have helped me to finalize my university studies, so that my warm thanks to all of them.

Finally, I would like to thank my family for being always there during good and bad times.

This work has been financed by the Spanish Science, Research and Innovation Plan (Ministerio de Economía y Competitividad) with Project Code TIN2014-55413-C2-1-P.

TABLE OF CONTENTS

ACRONYMS AND ABBREVIATIONS

APS	Atmospheric Phase Screen
ARC	Active Radar Calibrator
BPA	Back Propagation Algorithm
COE	Classical Orbital Elements
ECEF	Earth-Centred, Earth-Fixed
ECI	Earth Centred Inertial
ENVISAT	ENVIronmental SATellite
ERS	European Remote Sensing
FFT	Fast Fourier Transform
FM	Frequency Modulated
GEO	Geostationary Earth Orbit
GEOSAR	GEOstationary Synthetic Aperture Radar
GMST	Greenwich Mean Sidereal Time
$\boldsymbol{IJK}$	Geocentric Equatorial Coordinate System
InSAR	Interferometric Synthetic Aperture Radar
ITRF	International Terrestrial Reference Frame
ITRS	International Terrestrial Reference System
JD	Julian Date
LEO	Low Earth Orbit
LEOSAR	Low Earth Orbit Synthetic Aperture Radar
LS	Least Squares
LST	Local Sidereal Time
Matlab	MATrix LABoratory
NWP	Numerical Weather Prediction
PFC	Projecte Final de Carrera
$\boldsymbol{PQW}$	Perifocal Coordinate System
PRF	Pulse Repetition Frequency
RADAR	RAdio Detection And Ranging
RCS	Radar Cross Section
RMS	Root Mean Square
SAR	Synthetic Aperture Radar
SES	Société Européenne des Satellites
SLL	Side Lobe Level
SNR	Signal-to-Noise Ratio
STD	Standard Deviation
SV	State Vector
TLE	Two-Line Element
UT1	Universal Time 1
UTC	Coordinated Universal Time
VLBI	Very Large Baseline Interferometer
WGS-84	World Geodetic System 1984

LIST OF FIGURES

LIST OF TABLES

LIST OF SYMBOLS

a	Semi-major axis
$\mathbf{b}$	Observation matrix
$\tilde{\mathbf{b}}$	Residual matrix
c	Speed of light
d	Interval of time between two consecutive time samples when linear interpolation is performed
e	Eccentricity
$e_{\oplus}$	Eccentricity of the Earth
f^{-1}	Flattening of the Earth
f_D	Frequency Doppler
f_{i}	Instantaneous frequency
f_{s}	Sampling frequency
f_0	Carrier frequency
h	Altitude
$\mathbf{h}$	Angular momentum
i	Inclination
k_0	Wave number
m_{sat}	Mass of the satellite
$m_{\oplus}$	Mass of the earth
n	Mean motion
p	Semi-latus rectum
$\mathbf{r}$	Satellite position state vector
$\mathbf{r}_{\mathbf{site}}$	Site position state vector
$\bar{r}$	Residuals
t_{f}	Final epoch
t_{max}	Maximum time to reach the farthest image pixel
t_{min}	Minimum time to reach the closest image pixel
t_{p}	Time of periapsis passage
t_{r}	Delay between the transmitted and received pulse
t_0	Initial epoch
u	Argument of latitude
u_0	Argument of latitude at epoch t_0
$\mathbf{v}$	Satellite velocity state vector
v_{r}	Radial velocity
$\mathbf{v}_{\mathbf{rel}}$	Relative velocity of the satellite to the site
$\mathbf{v}_{\mathbf{site}}$	Site velocity state vector
x_{0_i}	Observed values of the dependent variable
y_{c}	Computed values of the dependent variable
y_0	Observed values of the dependent variable
$\mathbf{A}$	Partial-derivative matrix
B	Band-limited width of the signal
E	Eccentric anomaly
E/N_0	Signal-to-Noise Ratio

G	Antenna gain
G	Gravitational constant
$\mathbf{H}$	Observation partial derivatives
J	Cost function
JD_{UT1}	Julian Date in UT1
L	Losses
L_{a}	Antenna length
L_{min}	Minimum length of the radar along track direction
L_{s}	Synthetic aperture
M	Mean anomaly
P_{t}	Transmitted peak power
P_{r}	Echo power delivered by the antenna
R	Distance between the radar antenna and target
R_{eq}	Equatorial radius of the Earth
R_0	Radar-target closest approach
SLL_{az}	Azimuth cut SLL
SLL_{rg}	Range cut SSL
T	Orbital period
T	Pulse duration
T_{s}	Sample time
T_{UT1}	Number of Julian centuries from a particular epoch in UT1
$\mathbf{W}$	Weighting matrix
$\mathbf{X}$	State vector
$\hat{\mathbf{X}}$	Solution, state vector or state space
$\hat{\mathbf{X}}_{\mathrm{mod}}$	Modified state vector
$\hat{\mathbf{X}}_{\mathrm{nom}}$	Nominal state vector
α	Oversampling factor
α	RMS time duration
α_{i}	Interpolation factor
β	RMS bandwidth
γ	Linear FM rate
δ_i	Difference between modified and nominal state vector (component i)
$\delta\tilde{\mathbf{x}}$	Estimated correction to the state
θ_{bw}	Azimuth beam width
θ_{GMST}	Greenwich Mean Sidereal Time
$\theta_{\mathrm{GMST\ 0h}}$	Greenwich Mean Sidereal Time at 0 h
θ_{LST}	Local Sidereal Time
λ	Longitude
λ	Radar wavelength
λ_{sat}	Initial satellite longitude
λ_{true}	True longitude
$\lambda_{\mathrm{true}_0}$	True longitude at epoch t_0
μ	Gravitational parameter
ν	True anomaly
ν_0	True anomaly at epoch t_0
ξ	Error

ρ	Compression factor
ρ	Range measurement/observation
$\boldsymbol{\rho}$	Vector range
$\dot{\rho}$	Range-rate measurement/observation
$\hat{\boldsymbol{\rho}}$	Unit range vector
σ	RCS of the target
$\sigma_{v_{\mathrm{r}}}$	Standard deviation of range-rate measurements/observations
σ_{ρ}	Standard deviation of range measurements/observations
$\sigma_{f_D}^2$	Cramer-Rao lower bound on frequency estimation
σ_{τ}^2	Cramer-Rao lower bound for delay estimation
τ_0	Pulse duration
ϕ	Geodetic latitude
$\phi_{\mathrm{com.pulse}}$	Phase peak of the compressed pulse
ϕ_{gc}	Geocentric latitude
ϕ_{peak}	Pulse phase peak
ϕ_{pulse}	Pulse phase
ϕ_{sat}	Satellite geodetic latitude
ω	Argument of periapsis
ω_0	Carrier angular frequency
$\omega_{\oplus}$	Mean angular rotation of the Earth
$\widetilde{\omega}_{\mathrm{true}}$	True longitude of periapsis
Δf	Bandwidth
Δt	Interval of time between two consecutive time samples
Δx	Theoretical azimuth resolution
$\Delta x'$	Nominal azimuth resolution
$\Delta x'$	Approximate azimuth resolution
ΔR	Theoretical range resolution
$\Delta R'$	Approximate range resolution
$\Delta UT1$	Time difference between UT1 and UTC at one particular epoch
$\Delta\rho$	Range resolution
$\boldsymbol{\Phi}$	Matrix of variational equations
Ω	Right ascension of the ascending node
Υ	Vernal equinox

1

GEOSAR Mission

GEOstationary Synthetic Aperture Radar (GEOSAR) missions are presently being studied in order to provide continuous monitoring of the Earth on a continental scale (Tomiyasu, 1983). Nowadays, LEOSAR (Low Earth Orbit Synthetic Aperture Radar) missions offer Earth imaging, but they cannot provide continuous information about events that suffers rapid changes in short periods of time (LEO satellites have a revisit time of 11-14 days). This permanent monitoring will allow GEOSAR missions to cover a new set of applications that will be discussed in this chapter (Wadge et al., 2014).

GEOSAR missions are based on operating a radar payload hosted by a communication satellite in a geostationary orbit. One can think that a satellite located in a geostationary orbit remains fixed from an Earth observer. In practice, residual inclination and eccentricity of the satellite orbit results in a small elliptical motion relative to Earth. This fact will allow the radar to form the synthetic aperture required to obtain images. The shape of this synthetic aperture and other important parameters of GEOSAR missions will be explained in this chapter.

As the radar payload will be placed on a platform over 42 000 km from the Earth's centre, some limitations will affect the design of the system in order to get well focused images. One of these limitations arises from the fact that the satellite orbit is not known with the required precision. That lack of knowledge will affect the range history of the signal received by the radar, and therefore will produce image defocusing. In this chapter, the main limitations of GEOSAR missions will be described paying more attention on the limitation about the satellite orbit determination. In this way, the starting point of this document will be introduced.

Once the mission has been introduced and in order to conclude the chapter, the objective of this project will be explained as well as the main aspects of the following chapters will be discussed.

1.1. GEOSAR MISSION: APPLICATIONS

The major scientific advantage in geostationary radar is the ability to provide an early warning and monitor short-lived (less than a day) phenomena that would otherwise be missed, aliased or confused with noise. Many of such short-lived phenomena represent hazards at the Earth's surface (e.g., earthquakes, volcanic eruptions, flooding), and others may be hazardous only at certain times (e.g., landslides, urban subsidence). On the other hand, there are some phenomena that do not entail a risk at the Earth's surface but require short-interval radar measurements in order to reveal valuable information (e.g., snow mass, agricultural events).

Hereafter, the main applications of GEOSAR missions will be listed and briefly explained.

Atmospheric Phase Screen (APS)

In SAR acquisition, particularly in interferometry, the APS is an undesired artefact that affects the target phase estimation. The APS variations are related to the changes in the atmospheric properties such as water vapour content, temperature and pressure. These parameters cause a change in the refractivity index, mostly in the tropospheric layer, and produce an undesired atmospheric phase delay.

In typical LEOSAR missions, with integration times around 1 s, the atmospheric phase map is considered invariant during the acquisition. However, in GEOSAR missions, the atmospheric phase decorrelation during the integration time (up to hours) must be characterized and compensated from the acquired raw data in order to avoid image defocusing.

In Figure 1.1, an example of an input phase map and the retrieved one is shown (Ruiz Rodon et al., 2014).

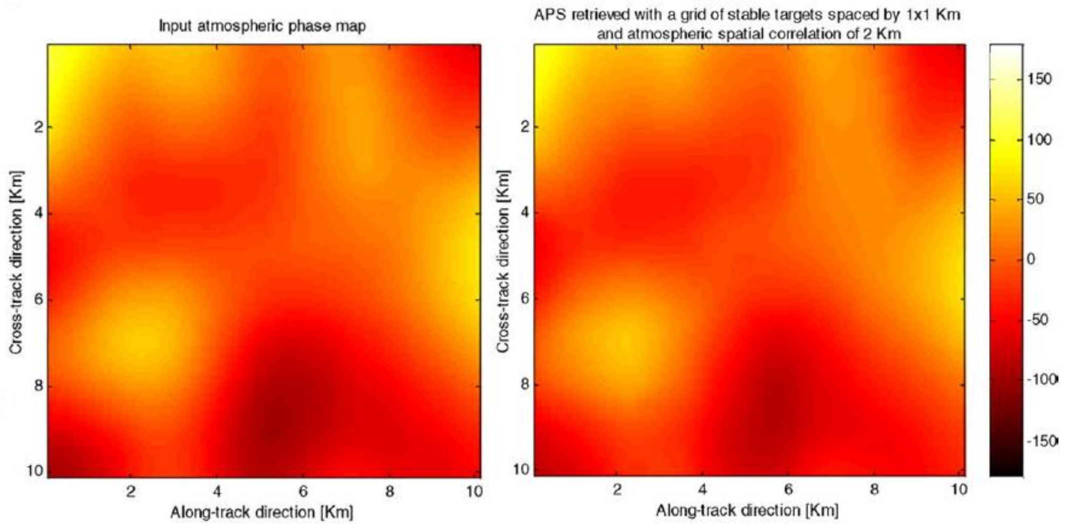

Figure 1.1: *Phase map estimation considering a grid of stable targets with APS correlation of 2 km.*

The APS data can be also used in Numerical Weather Prediction (NWP) by means of the information about water vapour content in the atmosphere (Monti Guarnieri et al., 2011).

Flooding

Hydrological flood models can be run to predict inundation if the topography, the water flux, the nature of the surface, and the flow paths taken are known. Images showing the flood boundary every 2 hours would be a major advance on current and planned capabilities, though they would not be available at all times. Thus, this boundary information could then be assimilated into hydrological models.

Hydrology

Soil moisture is an essential climate variable with major satellites dedicated to its measurement. However, these measurements are too coarse and infrequent to record good quality data from precipitation events. A backscatter-based retrieval of soil moisture at a scale of 1 km/1 h is required to do this. Therefore, continuous monitoring is needed.

Agriculture

Field-to-field comparisons when farming activities will be provided by using geostationary radar. Such data would feed into farming-centric concerns and management on the one hand, and land surface vegetation models and hydrological, small catchment-scale models on the other.

Cryosphere

The motion of glaciers can be measured by the advance or retreat of the glacier front and by the vectors of motion on the flow surface. The speed of many glaciers (metres/day) cannot be daily monitored by LEO satellites. In addition, the much more frequent observations from geostationary radar will enable studies of even fast moving glaciers to be made.

With two radars using different frequencies, the snow mass can also be estimated. They could be together used to retrieve the mass of dry snow and the location of the region over which snow was melting.

Earthquakes

The damage done to buildings when an earthquake occurs (the main determinant of deaths and injuries) may take a long time to discover due to a lack of communications, remoteness and darkness. On the other hand, the elastic part of the Earth's crust slowly deforms over distances of hundreds of kilometres between earthquakes. Mapping these phenomena will be important in order to support the emergency services response and help forecast future major earthquakes.

Volcanoes

LEO satellites cannot capture the complex pattern of deformation that magma makes prior to and during an eruption. To understand the location, motion and threat posed of lava flows, pyroclastic flows and ash falls is vital to advice the civil authorities on evacuations and other mitigation measures.

In Figure 1.2, an example of displacement due to volcanic activity in Tenerife (Canary Islands) is shown. This image was taken by ENVISAT (Environmental Satellite) satellite during 2005-2008.

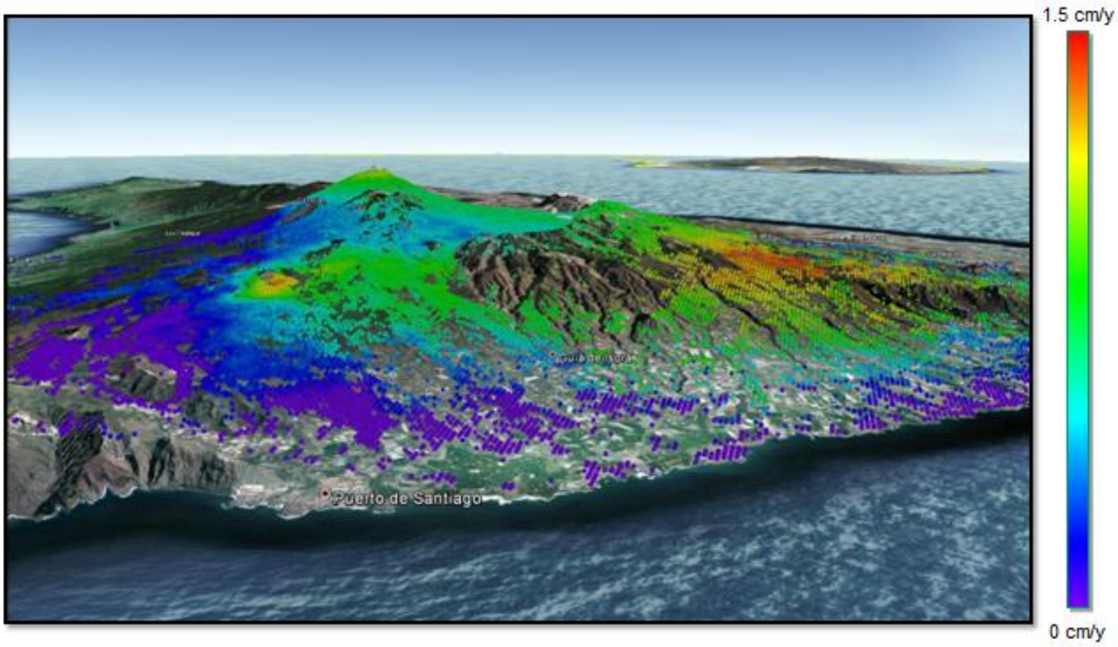

Figure 1.2: *Displacement due to volcanic activity in Tenerife (2005-2008).*

Landslides
Continuous monitoring and detection of soil displacements would help to asses and prevent landslides. After debris avalanches and landslides have produced, a timely map covering an area from hundreds to thousands of square kilometres in extent is required. Some individual landslides can be monitored by ground-based InSAR (Interferometric Synthetic Aperture Radar) but regional surveillance requires satellite-based methods.

Subsidence
The removal of liquids from the pore spaces of rocks or the rocks themselves cause the surrounding rock mass to subside. LEO radars are good at monitoring the long-term secular deformation signal from regional subsidence; however, the more rapidly accelerating deformation due to sinkhole formation (e.g., in building structures) is missed. This local deformation will be measured by means of geostationary radar.

1.2. SYNTHETIC APERTURE

The Geostationary Earth Orbit (GEO) is a circular orbit located in the Earth's equatorial plane with a radius over 42 000 km from the Earth's centre. The peculiarity of this orbit is that a satellite placed into this orbit has a period of one sidereal day (i.e. the satellite follows the Earth's rotation about its axis). Hence, the geostationary orbit clearly offers unique advantages for global communications. Its primary attribute is that the sub-satellite point is fixed at a selected longitude with 0° latitude. GEO satellites may therefore provide fixed-point to fixed-point communications to any site within the beam of their antennas. In this way, an almost complete global coverage (except for the intermediate polar regions) may be achieved from merely three satellites, and with no need for the ground antenna to switch between satellites.

However, perturbations such as the force exerted by the Earth's equatorial bulge, the solar radiation pressure and the gravitational attraction of the Sun and the Moon affect the satellite trajectory in the GEO orbit. Due to these perturbations, the satellite orbit is no longer circular and equatorial. A slight eccentricity and inclination appear in the orbit that both have to be corrected from time to time in order to keep the satellite into the GEO orbit.

GEOSAR missions can take benefit of this slightly elliptical orbit in order to form the synthetic aperture needed to obtain images (Ruiz Rodon et al., 2014). In Figure 1.3, an example of this elliptical movement for an observer on the Earth's surface is shown. The satellite used in the figure is located in 19.2° E longitude to cover, for example, Europe. Thus, the green line of the satellite orbit could be used as a synthetic aperture in order to obtain images from the European region.

Up to now, it has only been described the advantages of placing a radar payload in a GEO orbit; however, as the radar will be far away from the Earth's surface, some limitations must be overcome (see Section 1.4). Before seeing them, another important aspect of GEOSAR missions will be explained in the next section.

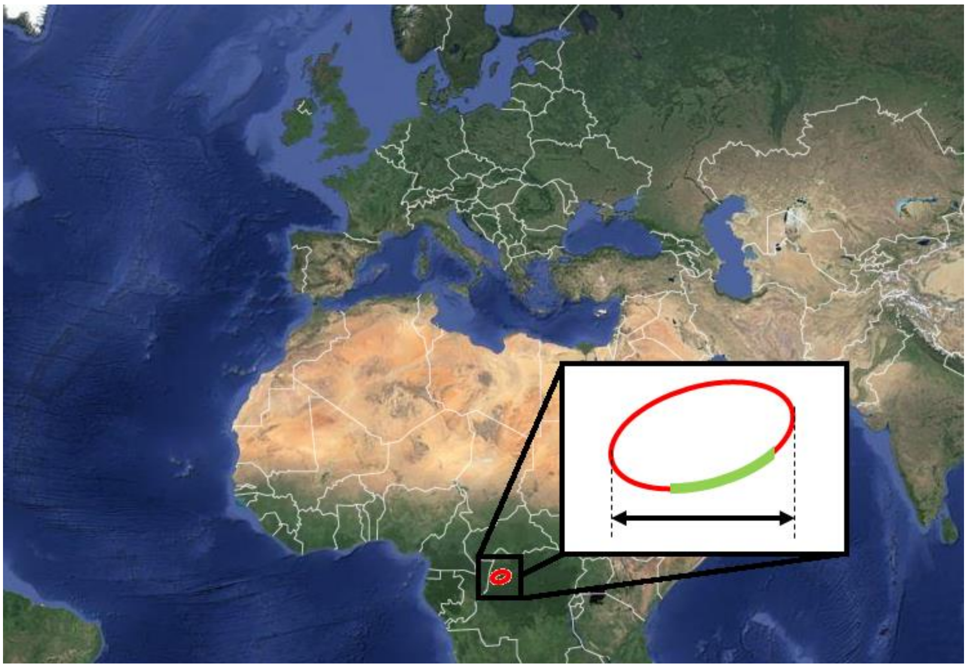

Figure 1.3: *Typical GEO satellite-Earth relative motion. A portion of the track (in green) can be used to form a radar synthetic aperture.*

1.3. L-BAND AND X-BAND RADARS

A dual band GEOSAR mission has been recently proposed: one working at L-band and the other at X-band (Wadge et al., 2014).

The L-band wide coverage beam will offer continental coverage (~3 000 km) with coarse 1 km resolution considering an integration time of 20-30 minutes. Thus, low resolution water vapour maps will be obtained in order to provide interesting meteorological information for weather forecast. At the same time, these atmospheric maps will be important in order to compensate the tropospheric delay in the higher resolution X-band images acquisition. As it will be explained in Section 1.4 in more detail, GEOSAR missions will need long integration time (up to hours) in order to obtain higher resolution images. Under these conditions, the atmosphere cannot be considered invariant. The L-band radar will consequently have to monitor continuously the atmosphere in order to retrieve its temporal evolution (Ruiz Rodon et al., 2012).

On the other hand, the X-band radar will be used to cover smaller areas (~ 500 km). With observation times of few hours, medium resolution images (10-20 metres) will be obtained.

In Figure 1.4, the geometry of the system acquisition in GEOSAR missions, for example over Europe, is shown. The red circle represents the L-band beam coverage covering most of Europe, whereas the yellow circles show the X-band beam coverage covering smaller areas.

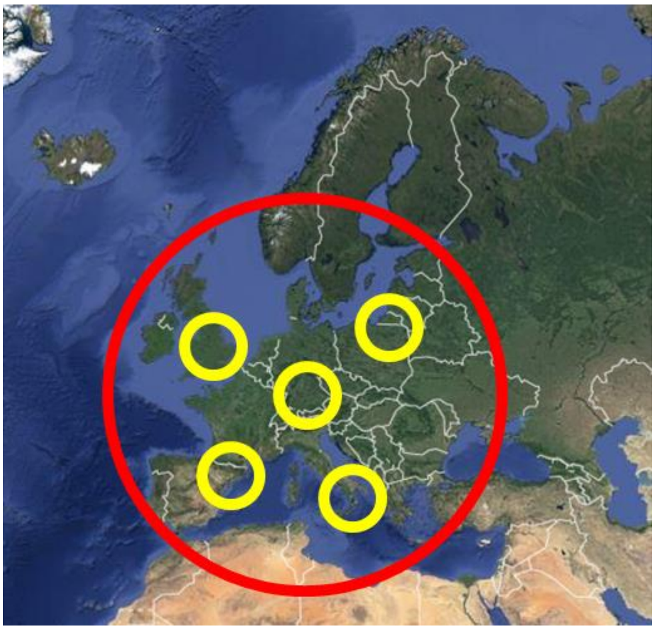

Figure 1.4: *GEOSAR L-band beam coverage (red circle) and X-band beam coverage (yellow circles).*

1.4. GEOSAR MISSION LIMITATIONS

Once the advantages and suitability of GEOSAR missions have been explained, let us consider the difficulties and limitations of the mission.

As it has been said, GEOSAR missions will place a radar payload in a satellite platform of a GEO orbit. The radar payload will consequently be far away from the Earth's surface receiving a low power echo from the targets and resulting in a low Signal-to-Noise Ratio (SNR). In order to increase the SNR, a first option could be to increase the transmitted power and use larger antennas; however, this fact would suppose higher development and exploitation costs. Therefore, the possibility to launch GEOSAR missions working with typical LEOSAR power and antenna parameters is being studied. In this case, SNR can be increased using along-track oversampling with a PRF (Pulse Repetition Frequency) well above the Doppler bandwidth, and operating the radar with a long integration time.

In order to obtain medium resolution images (10-20 metres) by means of the X-band radar, the integration time should be increased up to hours; thus, the illumination energy can substantially increase. However, what is the problem of using this long integration time? During this time, the atmosphere changes and radar signals can be decorrelated significantly. The effect of the atmosphere on radar signals cannot be considered invariant as it is in LEOSAR missions where the integration time is around 1 s. The temporal evolution of the atmosphere must consequently be compensated before doing the azimuth SAR compression in order to avoid image defocusing. This atmosphere retrieval will be performed by means of the atmospheric phase screen maps obtained by using the L-band radar (Ruiz Rodon et al., 2013).

Besides the APS, several sources affect the along-track phase history in GEOSAR missions causing unwanted fluctuations which may result in image defocusing. Thus, the main expected contributors to azimuth phase noise are:

- Atmospheric Phase Screen.
- Radar carrier frequency drifts.
- Satellite attitude instabilities and structural vibration.
- Orbit determination errors.

In order to obtain an accurate image of the scene after SAR processing, the range history of every point of the scene must be known. This fact requires a high precision orbit modelling and the use of suitable techniques for atmospheric phase screen compensation. The other influencing factors such as carrier frequency drifts or satellite attitude or structural fluctuations must be controlled or compensated.

It has to be considered that the processes responsible of the synthetic aperture phase changes are slow in comparison to the pulse duration. For this reason, no degradation is expected in the processor pulse compression task in GEOSAR missions.

The usual orbit modelling requirements to manage repositioning of satellites in GEO orbits are well beyond of the exposed orbital determination requirements for this mission. Such expected precision is in the order of magnitude of the radar wavelength. As GEOSAR missions will work in the X-band, the expected errors in the range history of every location under the satellite L-band beam coverage must be less than or equal to centimetres during the radar synthetic aperture.

The methods and techniques used to find such precision are discussed later in the following chapters. First, it has to be explained the radar measurements that are going to be used in order to determine the satellite orbit in GEOSAR missions. Such measurements will be the starting point to develop all theory of this document.

1.5. RADAR OBSERVABLES AND PROPOSED SYSTEMS TO OBTAIN THEM

Assuming a group of suitable radar reflectors are deployed at well-known Earth surface positions, radar observables can be of three types:

- Pointing Angles: Direction of arrival of reflected signals (with respect to the radar antenna using an appropriate reference system). This direction is defined in the 3 dimension space by a couple of angles.

- Range: Distance from radar antenna to reflectors deployed on the Earth's surface, computed from the echo time delay.

- Range-rate: Line-of-sight radial velocity component of the relative motion of reflectors as observed by the radar antenna. It can be easily derived from the Doppler shift measured from the received signal.

Two possible systems in order to obtain precise measurements suitable for accurate orbit determination are presently being studied in GEOSAR missions. First, a group of Active Radar Calibrators (ARCs) will provide range and range-rate measurements by means of a well-located transponders network. These transponders will act as active reflectors by using the known transmitted signal of the radar (Casado, 2016). On the other hand, an alternative or complementary technique based on ground interferometric measurements of the radar transmissions is also being studied (Martín, 2016). Such system will provide high resolution angular data using a VLBI (Very Large Baseline Interferometer) configuration.

This document will study the precise orbit determination from range and range-rate measurements. In Figure 1.5, a block diagram of a proposed ARC system for GEOSAR missions is shown. Such system consists in a linear transponder that includes a receiver antenna, a high gain amplifier and a transmitter antenna plus complementary electronics. Consult Casado (2016) for further information about the ARC system.

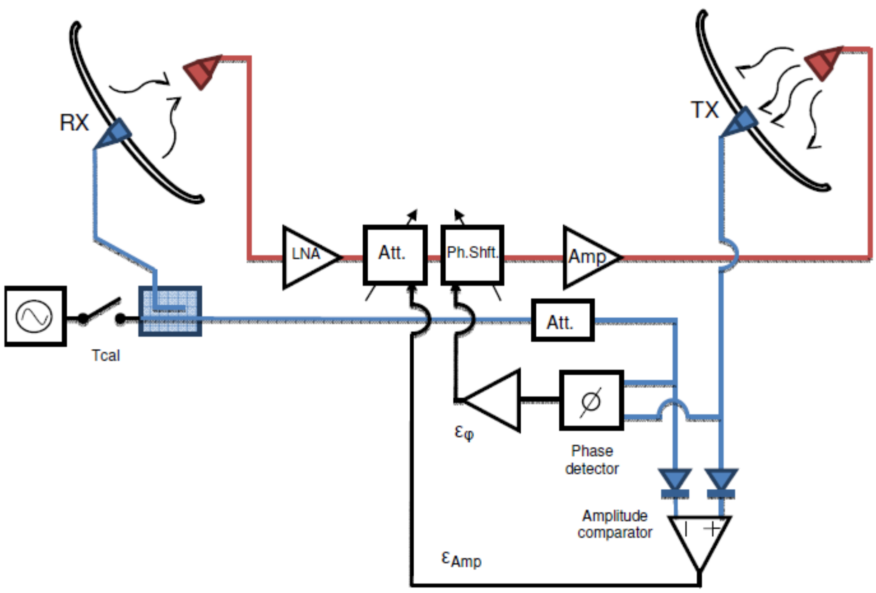

Figure 1.5: *Block diagram of a proposed ARC system for GEOSAR missions.*

1.6. PROJECT OBJECTIVE

The aim of this project is to perform a first study on the satellite determination methods and techniques available in the literature in order to calculate the satellite orbit of GEOSAR mission from range and range-rate measurements. These methods or techniques must consider the requirements of the mission, so that the expected relative errors in the range history of every location under the satellite L-band beam coverage must be less than or equal to centimetres (i.e., the radar X-band wavelength). It is worth mentioning that bias errors in range history have no impact on the synthetic aperture focusing, which means high precision is needed but not high accuracy. In addition, autofocus synthetic aperture techniques can be used to refine the range history predicted from the orbital model. Taking into account the small magnitude of orbital perturbations, in practice, the precision requirement could be relaxed in the order of magnitude of tens of centimetres.

In the following chapters, the methodology to determine the satellite orbit from range and range-rate measurements will be explained. This methodology will be accompanied by theoretical and practical results obtained from Matlab simulations. The errors found in each section will also be discussed since the magnitude of these errors will play a major role on the focused image acquisition. In this way, the structure of this document has been designed as follows.

Chapter 2 will introduce the Synthetic Aperture Radar to the reader. It will explain the reason why the synthetic aperture is needed. In addition, two basic examples will illustrate how a SAR forms a well-focused image from the received echoes and the accurate knowledge of the acquisition geometry. Then, this chapter will conclude including a third example reproducing the GEOSAR data acquisition case over the city of Barcelona (Spain).

Chapter 3 will begin the introduction and study of the initial orbit determination methods from range and range-rate measurements given by an ideal ARC system. As there is no real data available yet, an ideal simulated system will be designed in order to provide ideal data without considering any kind of perturbations involving the satellite movement around the Earth (i.e., only taking into account the interaction between the satellite and the Earth). Once the ideal data is achieved, the precision of the initial orbit determination methods evaluated will be assessed by Matlab simulations considering two different environments: a) initial range and range-rate data completely ideal, and b) adding expected noise to such initial data. All the results within this chapter will be shown by means of numerical results and the use of different plots.

Chapter 4 will conclude the explanation of orbit determination methods and techniques of this document introducing the Least Squares technique. The methods presented in Chapter 3 do not fulfil the GEOSAR mission requirements, so that there is the need to study the use of differential correction techniques in order to increase the precision of the satellite orbit determination. As in Chapter 3, the theoretical fundamentals of such technique will be accompanied by numerical results and different plots performed by Matlab simulations in order to show the Least Squares feasibility on GEOSAR mission.

Finally, the conclusions and future work of this document will be addressed. Some appendices are also added, so that the reader may have a complete description of the results obtained and the Matlab functions involved in all simulations performed throughout this document.

2

Synthetic Aperture Radar Techniques. Examples

This chapter aims to provide the fundamental basis of a Synthetic Aperture Radar (SAR) and some techniques that it uses in order to form images. In this way, the chapter is organised as follows. Section 2.1 will introduce the reader to SAR explaining the basic operation principles. Then, two basic examples related to SAR are shown in Sections 2.2 and 2.3 in order to complement the explanations done in Section 2.1. Finally, Section 2.4 will show a real range history example between a satellite located in a geostationary orbit and one site placed over the Earth's surface. Thus, the reader will be familiarized with the main aspects involved in the SAR image acquisition.

The reader may consult Cumming and Wong (2005) in order to complete all explanations given into this chapter about Synthetic Aperture Radar and related techniques.

2.1. SYNTHETIC APERTURE RADAR (SAR) INTRODUCTION

The objective of Synthetic Aperture Radar is to obtain high-resolution images. This resolution for Earth Observation applications is in the order of magnitude of metres both in distance (or range) resolution and lateral (or azimuth) resolution.

The radar can easily obtain metre resolutions in distance since it implies working with an appropriate pulse bandwidth and matched filter. In addition, distance resolution is not degraded by the operating distance (i.e., the same distance resolution is obtained whether the radar is closer or further to the scene where the radar is taking an image). However, problems appear when considering lateral resolution. Such resolution is determined by the antenna beam-width projected to the ground, and therefore lateral resolution degrades with the operating distance. The further the radar is from the scene, the coarser the lateral resolution will be. For instance, considering the radar at a distance of hundreds of kilometres, the achieved lateral resolution would be in the order of magnitude of kilometres in spite of using large antennas in the order of 10 m long. Thus, there is a need to improve the lateral resolution in order to obtain lateral or cross-range resolutions in the order of metres, required for remote sensing applications from aircraft and satellites.

Reducing the lateral beam-width of an antenna can be realised by replicating a small antenna at regular intervals. Thus, an array of antennas may be built with much larger dimensions compared to a single element antenna. However, such big antennas cannot be placed in a satellite since an array of kilometres of length will be needed in order to obtain metric resolutions.

In order to circumvent this limitation, if the radar is installed on a moving platform it is possible to record the radar echoes obtained with a single antenna along the track in order to combine them later on with appropriate focusing weights. This array is called synthetic array since it does not exist physically. Therefore, high radar resolutions can be obtained by using a small antenna and large synthetic apertures. This kind of instruments is named Synthetic Aperture Radars (SAR).

The synthetic aperture is usually limited by the antenna beam-width, which results in a synthetic aperture length proportional to scene to radar distance. This fact will compensate the distance impact over the radar lateral resolution discussed above.

In order to form high-resolution images, two orthogonal dimensions of the imaged surface must be sensed with similar spatial resolution. Using broadband transmitted pulses and matched receiving filters, radars can maximize both Signal-to-Noise Ratio (SNR) and time-delay resolution in the echo waveform. Since the time delay of each scene scattering object is proportional to the distance from the radar, the required range resolution orthogonal to the lateral synthetic aperture resolution can be obtained with appropriate transmitted pulse design and subsequent filtering in the receiver.

The Chirp signal is the most used radar pulse in SAR systems in order to obtain high range resolution images. It has the particularity that both pulse time duration and bandwidth can be very large resulting in a high-energy pulse. By processing a Chirp with a matched filter, a narrow impulse is obtained, being ideal for high range resolution applications. This technique is known as pulse compression.

In order to form the synthetic aperture, the pulse transmission is repeated regularly during the flight, and the echoes stored in a 2D matrix are called raw-data. The matrix dimensions are the echo time delay and flight distance (also called slow-time). Every point of the scene generates a two-dimensional holographic patch on the raw-data matrix, which is not directly interpretable. From this hologram, a focused image is obtained by means of a SAR processor, which performs two compressions on the received raw-data: a) pulse range compression, and b) azimuth compression (see Figure 2.20).

The first compression is implemented along the range direction. It uses a matched filter in order to achieve the best possible SNR of the signal at the output of the filter. This matched filter is the optimal one and provides the signal autocorrelation at its output. The following section will illustrate an example of pulse compression considering a static radar and a point target. Thus, the reader will be able to understand better how the pulse compression works since mathematical formulation and intermediate results are given.

The second compression of SAR processor is performed in a similar way to the previous one but now along the azimuth direction. In this case, the signal is compressed by using a SAR algorithm. Section 2.3 will show a basic and complete SAR processor example. In this case, it has been considered to use a Back Propagation Algorithm (BPA) in order to address the azimuth compression due to its flexibility (Soumekh, 1999). BPA, compared to other algorithms, is suitable for synthetic aperture curved tracks, which is the case of GEOSAR mission. As in the pulse compression example, Section 2.3 will provide all mathematical formulation used and will show many figures in order to illustrate the geometry of the example and the intermediate results obtained. In this way, the reader will have a better understanding of how a SAR processor works.

Once the bases of the SAR processor have been explained, Figure 2.1 illustrates a real SAR image of Barcelona city (Spain), which is a composite of ERS (European Remote Sensing satellite) and ENVISAT (Environmental Satellite) satellites.

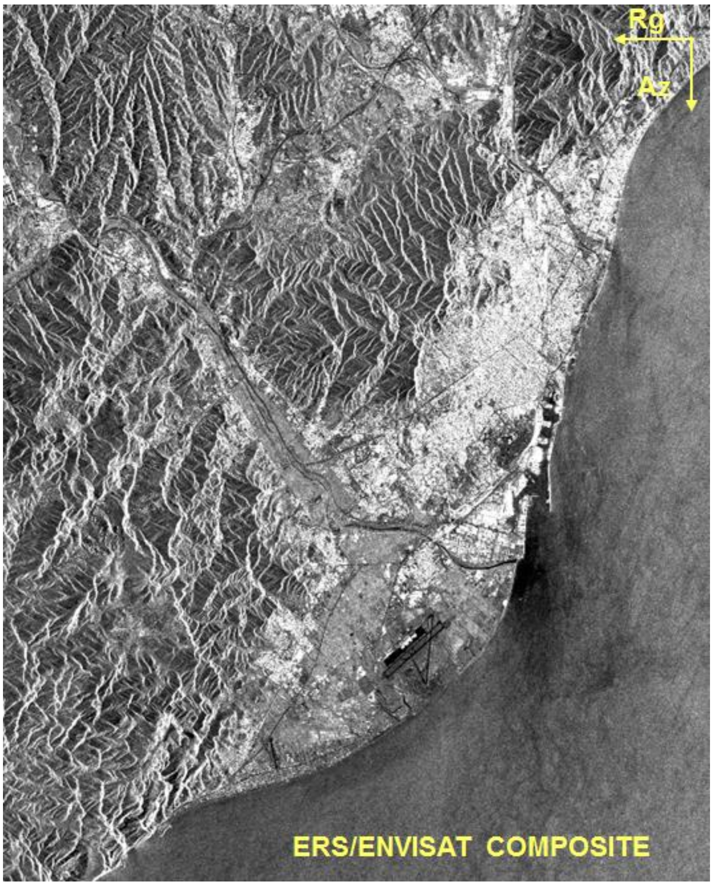

Figure 2.1: *SAR image of Barcelona city (Spain).*

2.2. PULSE COMPRESSION EXAMPLE

We have a target at distance R from a radar antenna and we want to derive and plot the matched filter output after a pulse compression is performed. In Figure 2.2, we can see the sketch of the example.

The transmitted signal $s_e(t)$ is a chirp pulse given by

$$s_{\mathrm{e}}(t) = \mathrm{Re}\left\{ \prod\left(\frac{t}{\tau_0}\right) e^{j2\pi f_0 t} \, e^{j\pi\gamma t^2} \right\} \tag{2.1}$$

where τ_0 is the pulse duration, f_0 is the carrier frequency, and γ is the linear FM rate.

If we now write the low pass equivalent of the transmitted signal (i.e., we get rid of the carrier term $e^{j2\pi f_0 t}$), Equation (2.1) *becomes*

$$\widetilde{s_{\mathrm{e}}}(t) = \prod\left(\frac{t}{\tau_0}\right) e^{j\pi\gamma t^2} \tag{2.2}$$

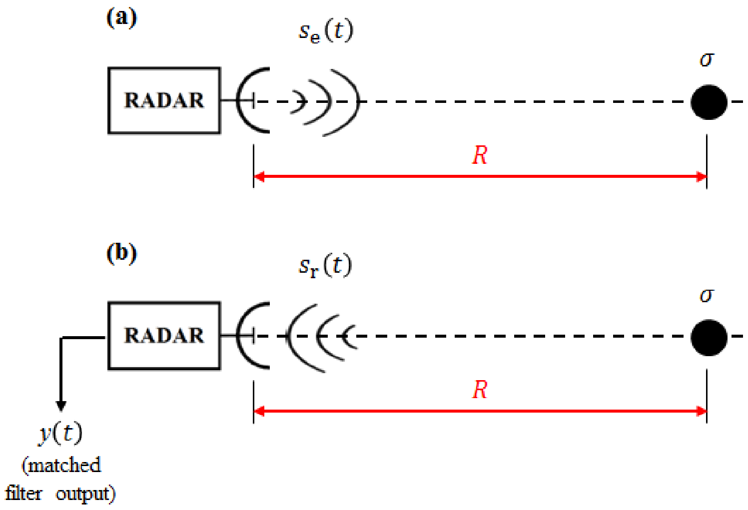

Figure 2.2: *(a) Transmitted signal $s_e(t)$, and (b) Target echo $s_r(t)$ and matched filter output $y(t)$.*

Assuming an isolated point target, the target echo received on the radar can be expressed as

$$s_r(t) = \mathrm{Re}\left\{ \prod\left(\frac{t - t_r}{\tau_0}\right) e^{j2\pi f_0 (t - t_r)} \, e^{j\pi\gamma (t - t_r)^2} \right\} \tag{2.3}$$

where t_r is the delay between the transmitted and received pulse given by

$$t_r = \frac{2R}{c} \tag{2.4}$$

where c is the speed of light.

If we now write Equation (2.3) *on its low pass equivalent expression, we obtain*

$$\tilde{s}_r(t) = \prod\left(\frac{t - t_r}{\tau_0}\right) e^{-j2\pi f_0 t_r} \, e^{j\pi\gamma (t - t_r)^2} = \prod\left(\frac{t - \frac{2R}{c}}{\tau_0}\right) e^{-j2k_0 R} \, e^{j\pi\gamma \left(t - \frac{2R}{c}\right)^2} \tag{2.5}$$

where k_0 is the wave number given by

$$k_0 = \frac{\omega_0}{c} = \frac{2\pi f_0}{\lambda_0 f_0} = \frac{2\pi}{\lambda_0} \tag{2.6}$$

where λ_0 is the carrier wavelength.

The matched filter of the receiver performs the pulse compression. Hence, the matched filter output $\tilde{y}(t)$ is simply the convolution between the target echo and matched filter.

$$\tilde{s}_r(t) \longrightarrow \boxed{\tilde{h}_m(t)} \longrightarrow \tilde{y}(t)$$

Then, the matched filter output can be expressed as

$$\tilde{y}(t) = \frac{1}{2} \, \tilde{s}_r(t) * \tilde{h}_m(t) \tag{2.7}$$

where the matched filter $\widetilde{h}_{\mathrm{m}}(t)$ is the time-reversed, complex conjugate of the transmitted signal $\tilde{s}_{\mathrm{e}}(t)$

$$\widetilde{h}_{\mathrm{m}}(t) = \tilde{s}_{\mathrm{e}}^{\,*}(-t) = \prod\left(\frac{t}{\tau_0}\right) e^{-j\pi\gamma t^2} \tag{2.8}$$

Note that the convolution is multiplied by $1/2$ because it is shown on low pass equivalent terms.

A convolution is computationally costly since an integral must be computed for every t.

$$\tilde{y}(t) = \frac{1}{2}\int \tilde{s}_{\mathrm{r}}(\tau)\ \widetilde{h}_{\mathrm{m}}(t-\tau)\, d\tau \tag{2.9}$$

Thus, it is appropriate to obtain the filter output in the spectral domain (fast convolution technique) in order to gain computational efficiency,

$$\tilde{S}_{\mathrm{r}}(f) \longrightarrow \boxed{\widetilde{H}_{\mathrm{m}}(f)} \longrightarrow \tilde{Y}(f)$$

$$\tilde{Y}(f) = \frac{1}{2}\,\tilde{S}_{\mathrm{r}}(f)\,\widetilde{H}_{\mathrm{m}}(f) \tag{2.10}$$

where the matched filter spectrum $\widetilde{H}_{\mathrm{m}}(f)$ is the complex conjugate of the transmitted signal spectrum.

$$\widetilde{H}_{\mathrm{m}}(f) = \mathcal{F}\{\tilde{s}_{\mathrm{e}}^{\,*}(-t)\} = \tilde{S}_{\mathrm{e}}^{\,*}(f) \tag{2.11}$$

Finally, to derive the expression of the matched filter output in the time domain, an inverse Fourier transform must be performed.

$$\tilde{y}(t) = \mathcal{F}^{-1}\{\tilde{Y}(f)\} = \mathcal{F}^{-1}\left\{\frac{1}{2}\,\tilde{S}_{\mathrm{r}}(f)\,\widetilde{H}_{\mathrm{m}}(f)\right\} \tag{2.12}$$

Radar and target specifications:

- *Carrier frequency:* $f_0 = 9.65$ GHz *(X-Band radar)*
- *Pulse duration*: $\tau_0 = 100$ ns
- *Bandwidth*: $\Delta f = 100$ MHz
- *Linear FM rate*: $\gamma = \frac{\Delta f}{\tau_0} = \frac{100\cdot 10^6\ \mathrm{Hz}}{100\cdot 10^{-9}\ \mathrm{s}} = 10^{15}\ \frac{\mathrm{Hz}}{\mathrm{s}}$
- *Compression factor*: $\rho = \Delta f\ \tau_0 = 100\cdot 10^6\ \mathrm{Hz}\cdot 100\cdot 10^{-9}\ \mathrm{s} = 10$
- *Target distance*: $R = 30$ m
- *Transmitted peak power*: $P_{\mathrm{t}} = 1$ W
- *Echo power delivered by the antenna*: $P_{\mathrm{r}} = \frac{P_{\mathrm{t}}\, G^2\, \sigma\, \lambda^2}{(4\pi)^3\, R^4\, L}$
- *Target RCS (Radar Cross Section)*: $\sigma = 1\ \mathrm{m}^2$
- *Antenna gain*: $G = 20$ dB
- *Losses*: $L = 6$ dB

Hereafter, the script steps are provided:

1. *Declare constants.*
2. *Define the time step which has to satisfy Nyquist, so that* $T_{\max} = \frac{1}{B} = \frac{1}{\Delta f}$. *Oversample the sampling frequency* $\times 2$ *or* $\times 4$ *(better) for better performance.*
3. *Obtain the transmitted pulse* $\tilde{s_e}(t)$ *and plot its amplitude and phase.*
4. *Obtain and plot the instantaneous frequency of the transmitted pulse to see the FM linear sweep.* $f_i(t) = \frac{1}{2\pi}\frac{d\phi_{\text{pulse}}}{dt}$.
5. *Obtain and plot the spectrum of the transmitted signal.* $\tilde{S_e}(f) = \text{FFT}\{\tilde{s_e}(t)\}$.
6. *Obtain the matched filter in the frequency domain and plot its amplitude and phase.* $\widetilde{H_m}(f) = \tilde{S_e}^*(f)$. *Check whether the phase is inverted with respect to the pulse phase.*
7. *Obtain and plot the radar matched filter output* $\tilde{y}(t)$ *and compare it to Figure 2.3 (Levanon, 1988: Figure 7.4).*
8. *Check the phase at the peak of the compressed pulse. It should be* $-2k_0R$.

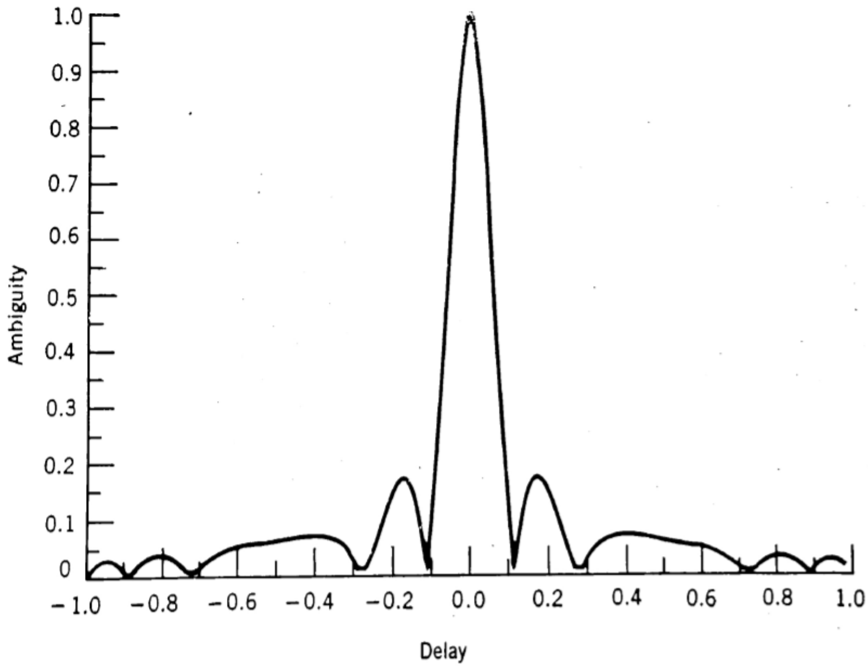

Figure 2.3: *A zero-Doppler cut of the ambiguity function of a linear FM pulse with* $\rho = 10$.

SOLUTION:

A Matlab script has been used in order to solve this example. Here, in this solution, the main results obtained will be shown as well as the main steps to achieve them will also be explained.

Once the radar and target parameters have been defined into the script, the following step is to define the sample time. We know that Nyquist must be satisfied and it must be done with an oversampling factor $\alpha = 4$. Since the sample time is just the inverse of the sampling frequency,

$$f_s = \alpha\, B = \alpha\, \Delta f = 4 \cdot 100 \cdot 10^6 \text{ Hz} = 400 \text{ MHz} \tag{2.13}$$

we can obtain the sample time as

$$T_s = \frac{1}{f_s} = \frac{1}{400 \cdot 10^6 \text{ Hz}} = 2.5 \text{ ns} \tag{2.14}$$

From this sample time, we can build a time axis large enough to cover the transmitted pulse and the target echo. We can now plot the amplitude and phase of the low pass equivalent of the transmitted signal via Equation (2.2) (see Figure 2.4).

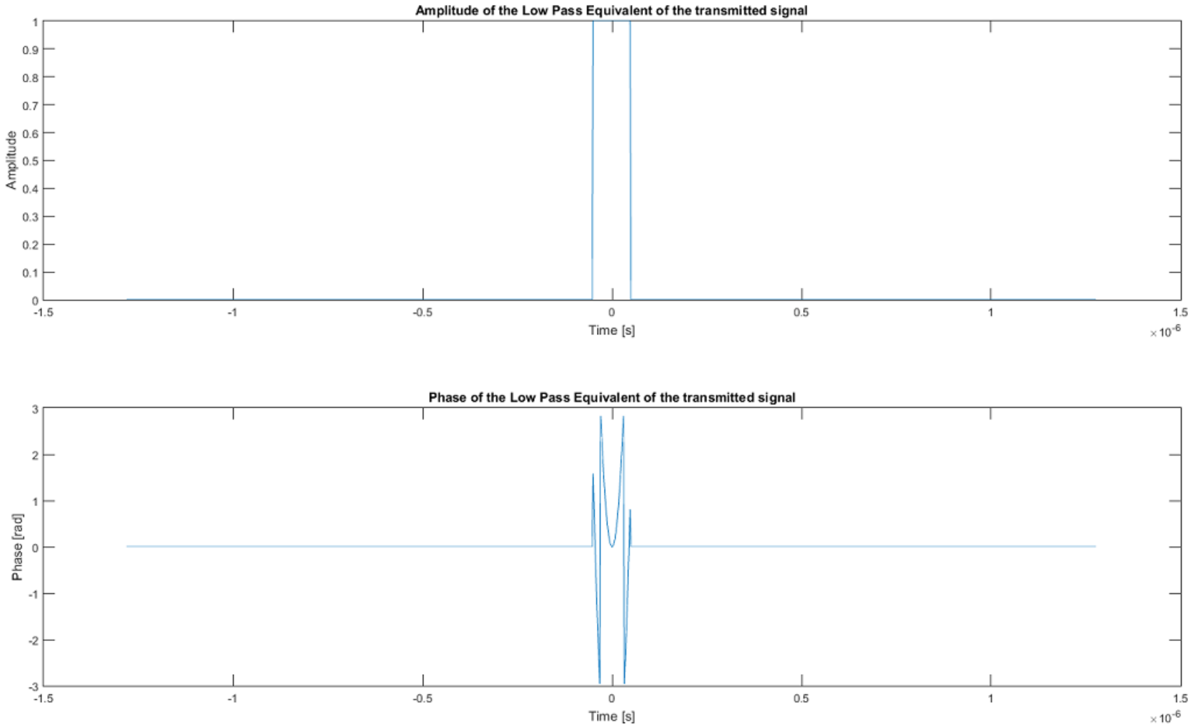

Figure 2.4: *Amplitude and phase of the low pass equivalent of the transmitted signal.*

Note that the amplitude and phase have been plotted in a centred format to provide a better view of the results. However, all the calculations done into the script have been carried out using an FFT format.

In order to obtain the instantaneous frequency, we must solve the following derivative

$$f_i(t) = \frac{1}{2\pi} \frac{d\phi_{\text{pulse}}}{dt} \tag{2.15}$$

where $\phi_{\text{pulse}} = \pi\gamma t^2$. Thus,

$$f_i(t) = \frac{1}{2\pi} \frac{d(\pi\gamma t^2)}{dt} = \frac{1}{2\pi} \cdot 2\pi\gamma t = \gamma t \tag{2.16}$$

In Figure 2.5, we can see the shape of the instantaneous frequency along the transmitted signal. If we zoom in the pulse area, we can notice the linear behaviour of the transmitted pulse. The straight line of slope γ sweeps all bandwidth Δf of the transmitted pulse during the pulse duration τ_0 (see Figure 2.6).

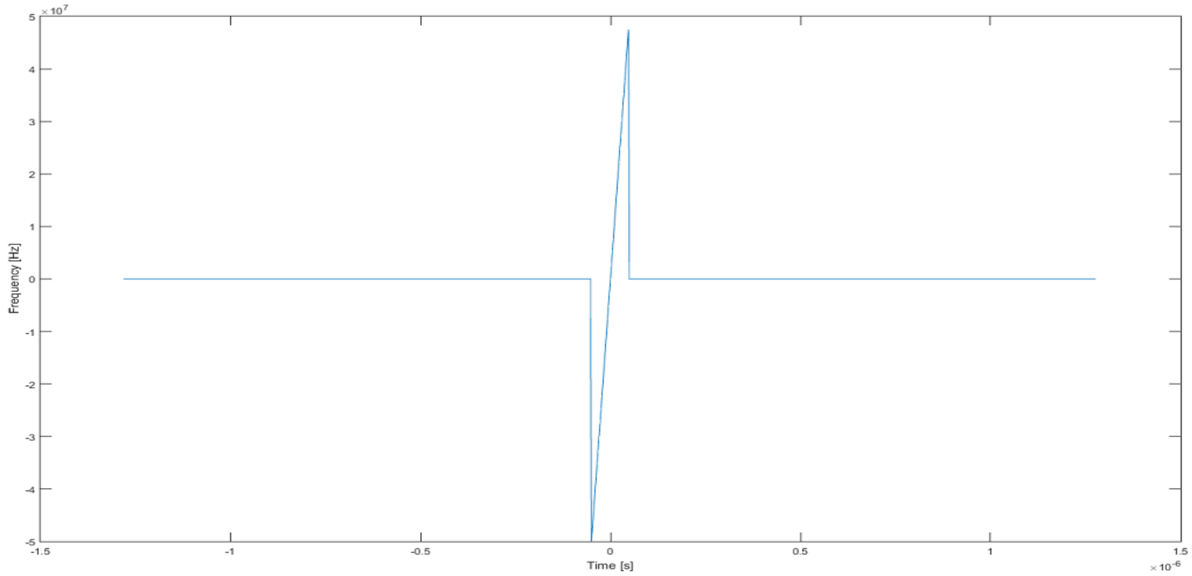

Figure 2.5: *Instantaneous frequency of the transmitted signal.*

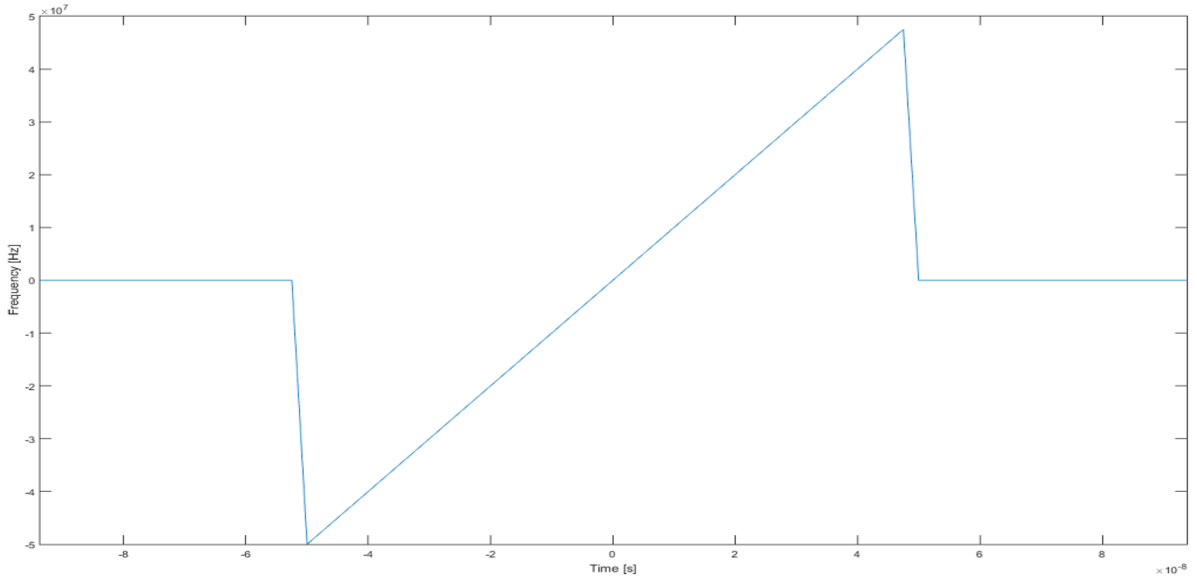

Figure 2.6: *Instantaneous frequency of the transmitted signal (zoom in).*

Now, we need to obtain the matched filter. Therefore, we have to compute the transmitted signal spectrum by using the Fast Fourier Transform (FFT) in Equation (2.2).

$$\widetilde{S}_{\mathrm{e}}(f) = \mathrm{FFT}\{\widetilde{s}_{\mathrm{e}}(t)\} \tag{2.17}$$

We can see the amplitude and phase of the transmitted signal spectrum in Figure 2.7.

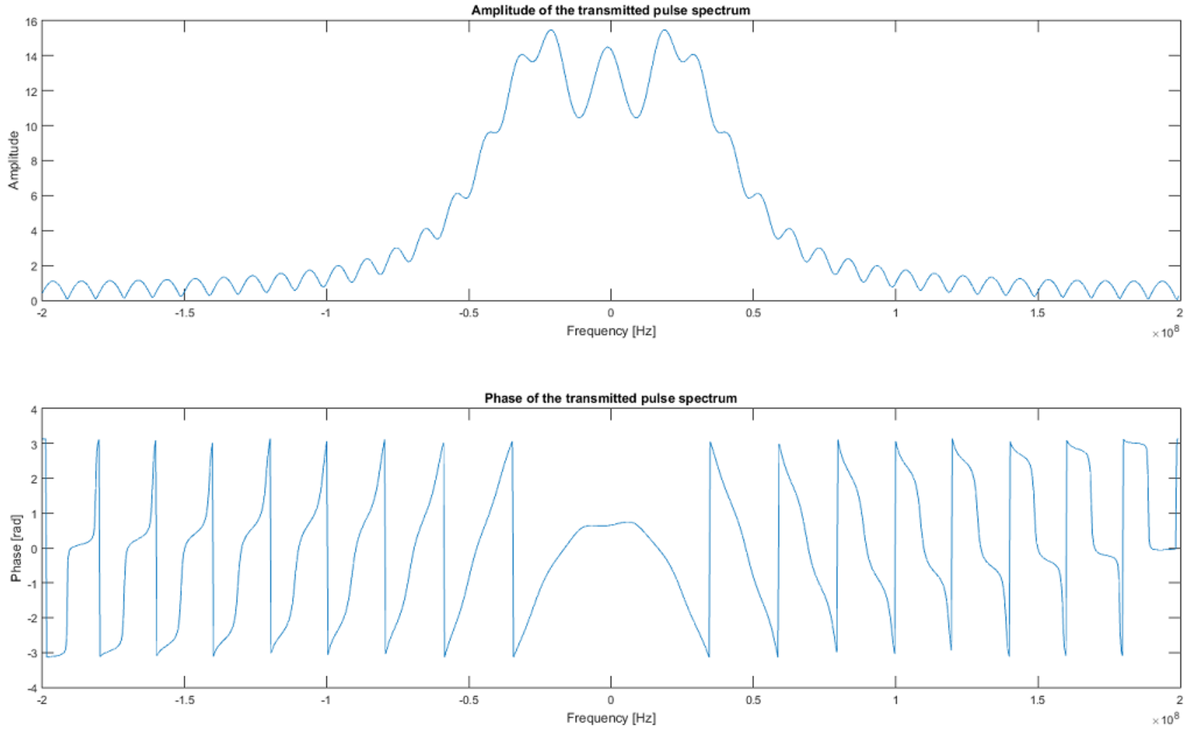

Figure 2.7: *Amplitude and phase of the transmitted signal spectrum.*

From Equation (2.11), we can compute the matched filter in the frequency domain. Thus, the amplitude and phase of the matched filter spectrum are plotted in Figure 2.8.

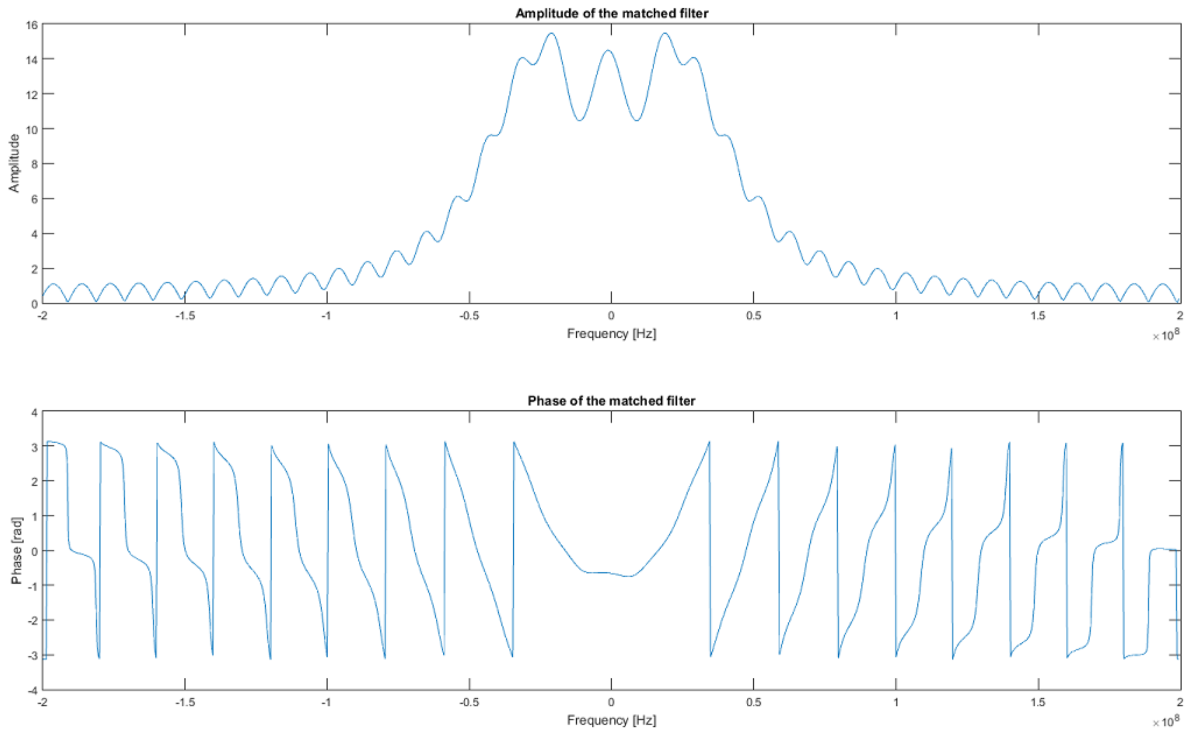

Figure 2.8: *Amplitude and phase of the matched filter spectrum.*

Note that the matched filter phase (from Figure 2.8) is inverted with respect to the phase of the transmitted signal spectrum.

At this point, we can compute the radar matched filter output from Equation (2.12) and plot its amplitude (see Figure 2.9). Before using Equation (2.12), you must take into account to compute the spectrum of the target echo.

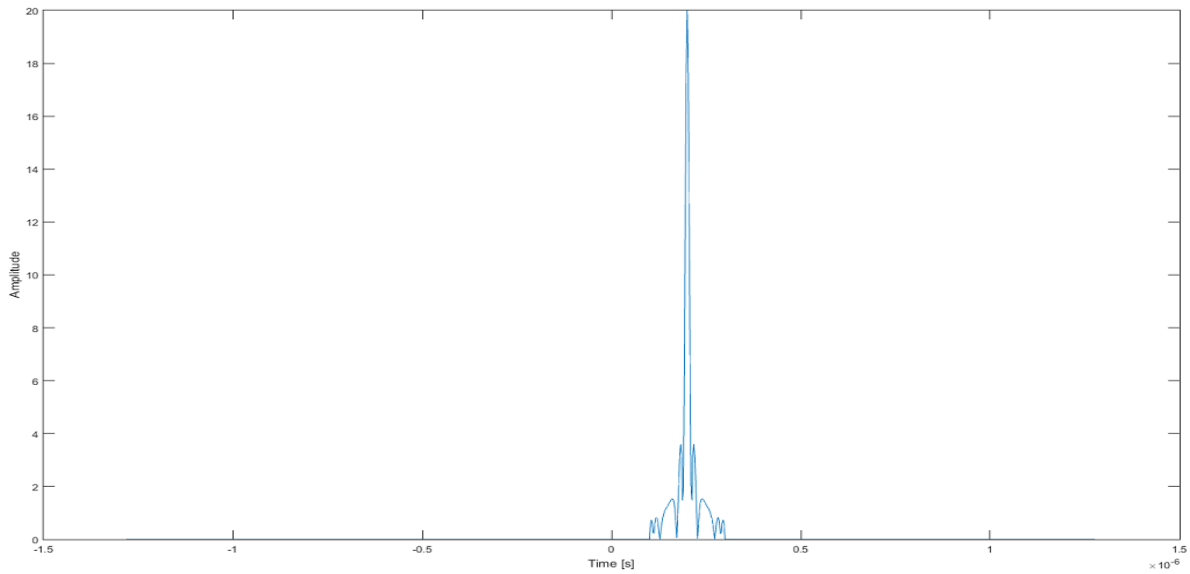

Figure 2.9: *Amplitude of the radar matched filter output.*

In order to compare the result obtained in Figure 2.9 to Figure 2.3, the radar matched filter output has been normalized with respect to its maximum value (peak value), and centred to the time origin (i.e., the delay between the transmitted and received signals has been removed). Thus, you can see the resulting signal in Figure 2.10.

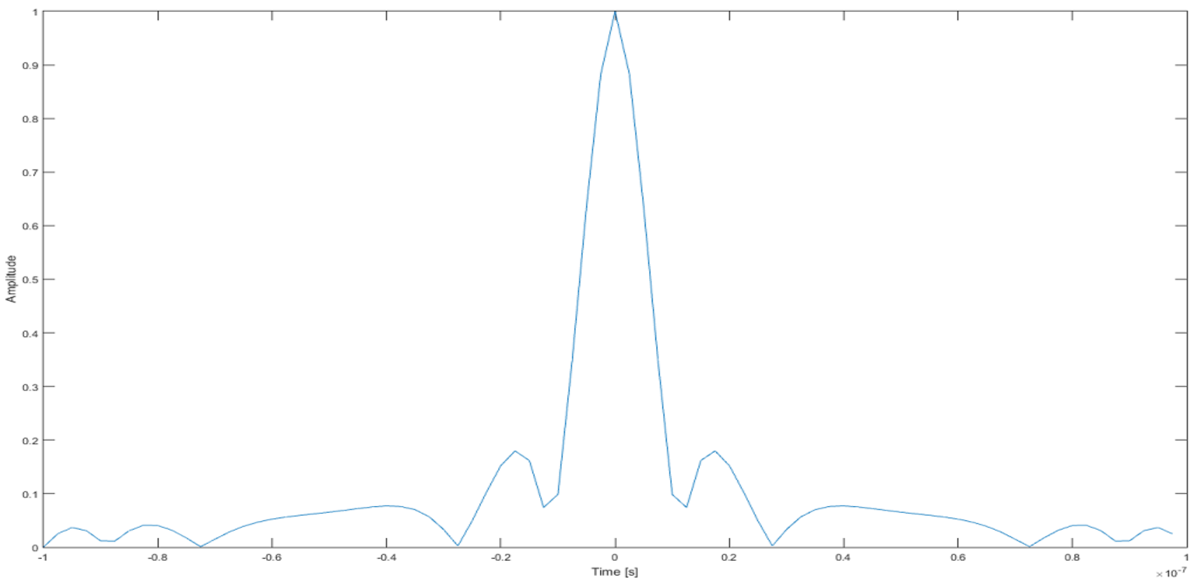

Figure 2.10: *Normalized and centred amplitude of the radar matched filter output.*

From Figures 2.10 and 2.3., we can see the similarity between both signals, which validates the calculations.

Finally, we have to check whether the phase at the peak of the compressed pulse is equal to the theoretical phase (i.e., $-2k_0R$). Hence, let us first compute this theoretical phase.

$$\phi_{\text{peak}} = -2k_0R = -2\,\frac{2\pi f_0}{c}\,R = -2\cdot\frac{2\cdot\pi\cdot 9.65\cdot 10^9\ \text{Hz}}{3\cdot 10^8\ \frac{\text{m}}{\text{s}}}\cdot 30\ \text{m} \approx 12126.55\ \text{rad}$$

In order to compare this result to the phase at the peak of the compressed pulse, we have to compute ϕ_{peak} modulo 2π. Thus, the theoretical phase becomes $\phi_{\text{peak}} = 0$ rad, and therefore, as the phase of the compressed pulse is $\phi_{\text{com.pulse}} = 2.3\cdot 10^{-13}$ rad (result given in Matlab), we can conclude that both phases are practically equal.

Since the signal obtained in Figure 2.10 has an abrupt shape compared to the signal of Figure 2.3, make use of the interpolation to smooth the radar matched filter output by means of zero padding its spectrum. Use an interpolation factor $\alpha_{\text{i}} = 8$.

SOLUTION:

In order to obtain the interpolated radar matched filter output, we have to define a new vector of the radar matched filter output spectrum (e.g., Y'). The length of this new vector must be α_{i} times the length of the same vector without interpolation (e.g., Y) used in the previous section. Then, vector Y' must be filled of zeros. And, finally, the first half of vector Y must be copied at the beginning of vector Y', and the second half of vector Y must be copied at the end of vector Y'. In this way, the zero padding interpolation has been performed.

After computing the inverse Fourier transform of Y', we can obtain and plot the interpolated radar matched filter output (see Figure 2.11).

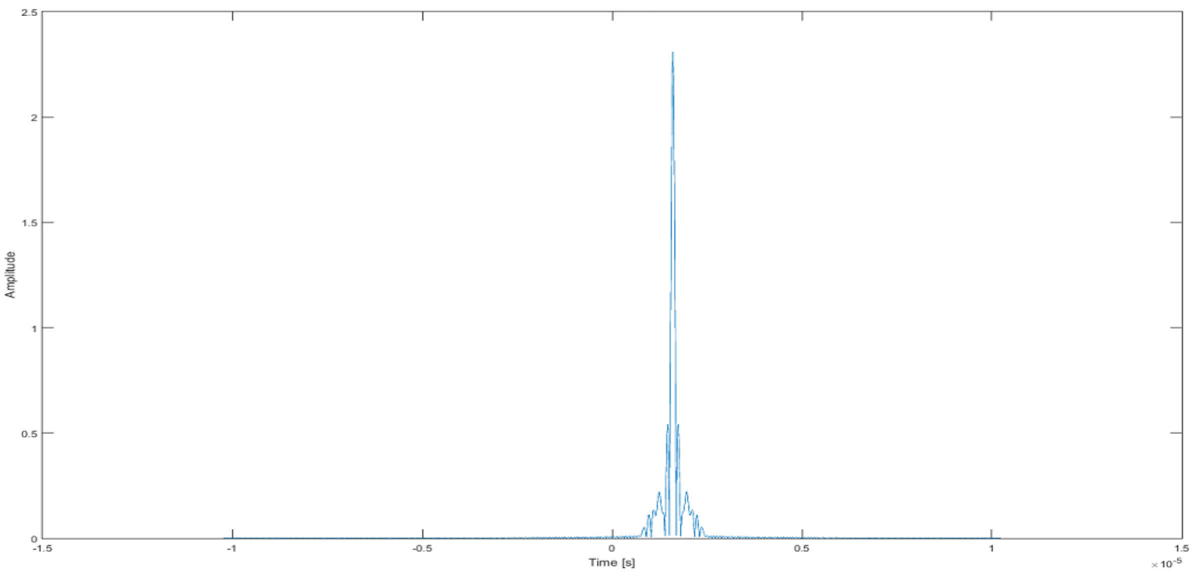

Figure 2.11: *Amplitude of the interpolated radar matched filter output.*

Now, we can proceed as the previous section in order to plot the radar matched filter output on a normalized and centred way. Hence,

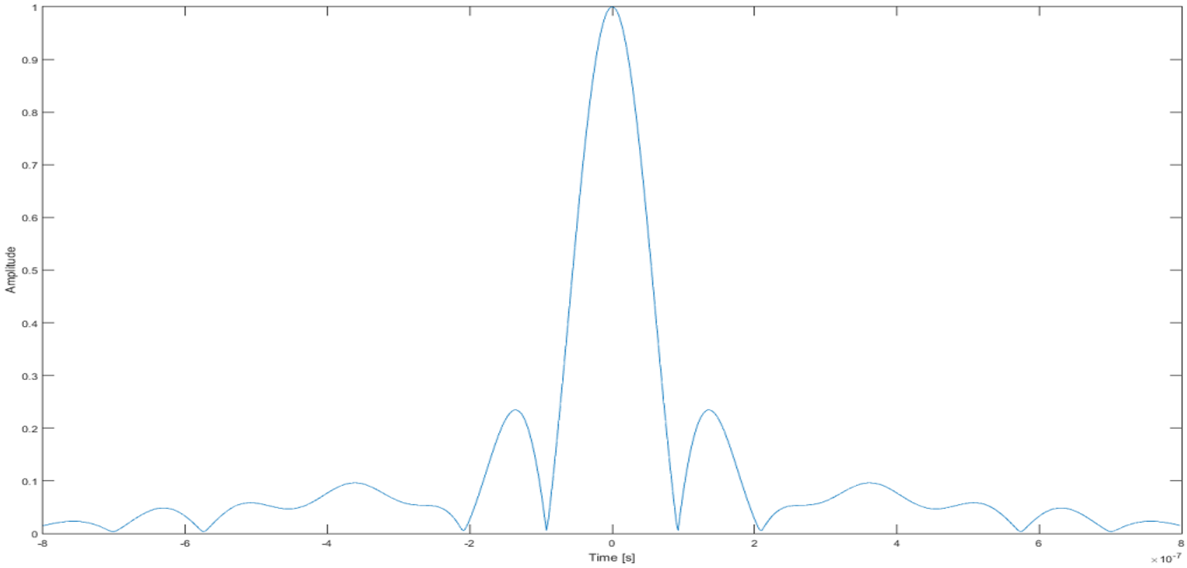

Figure 2.12: *Amplitude of the interpolated, normalized and centred radar matched filter output.*

In Figure 2.12, we can note that the signal has smoothed with respect to the signal from Figure 2.10. Now, the signals of Figures 2.12 and 2.3 are practically equal.

In order to conclude this example, we want to reduce the side lobes of the radar matched filter output. Therefore, we suggest adding a window in the radar receiver. Do it for two different windows (e.g., a triangular window and a Hanning window).

SOLUTION:
The suggested solution is to multiply the matched filter by the window in the frequency domain to achieve a new filter $\widetilde{H}'(f)$. We will use this new filter, which will not be the matched filter, in order to obtain the radar filter output $\widetilde{y}'(t)$ from the target echo $\widetilde{s}_\mathrm{r}(t)$.

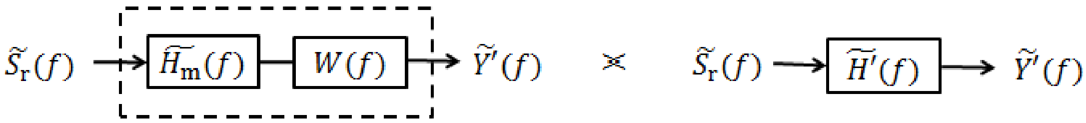

$$\widetilde{H}'(f) = \widetilde{H}_\mathrm{m}(f)\, W(f) \tag{2.18}$$

In Figures 2.13 and 2.14, we can see the amplitudes of: (a) the matched filter, (b) the window used in each case, and (c) the resulting filter.

Finally, the radar filter outputs are shown altogether in Figure 2.15 on a normalized and centred way for easier comparison. We can note how the side lobes have diminished with respect to the radar matched filter output case.

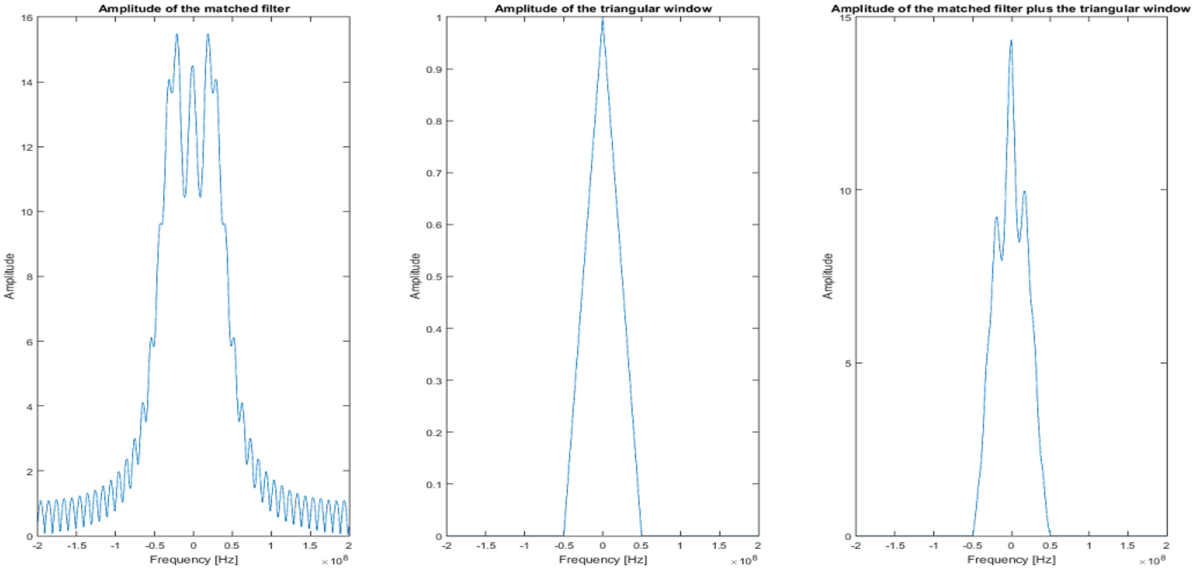

Figure 2.13: *Amplitudes of: (a) the matched filter, (b) the triangular window and (c) the resulting filter.*

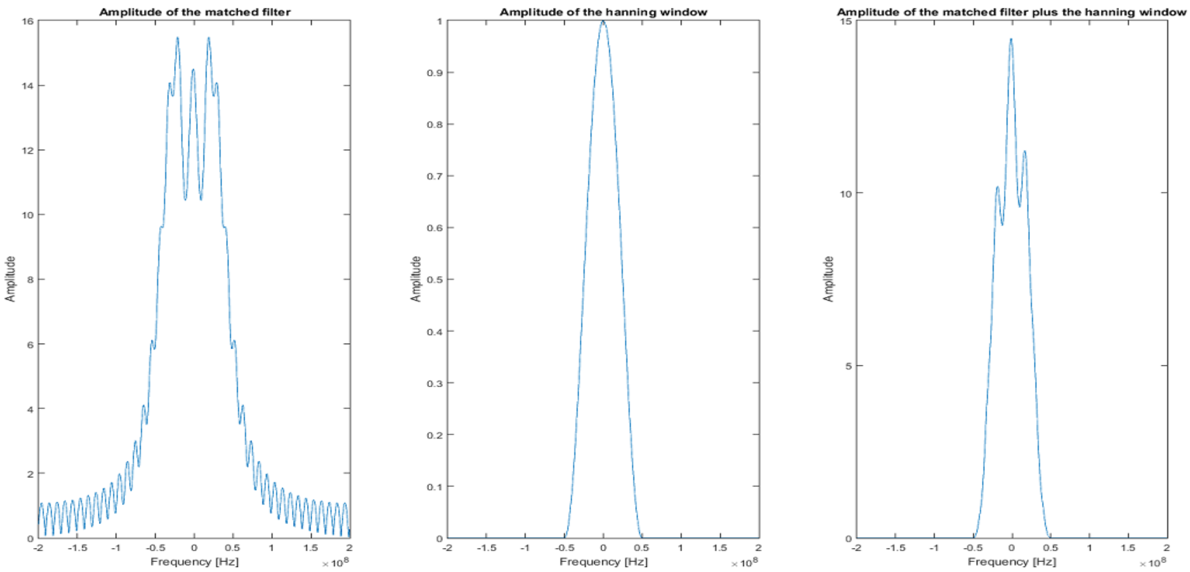

Figure 2.14: *Amplitudes of: (a) the matched filter, (b) the Hanning window and (c) the resulting filter.*

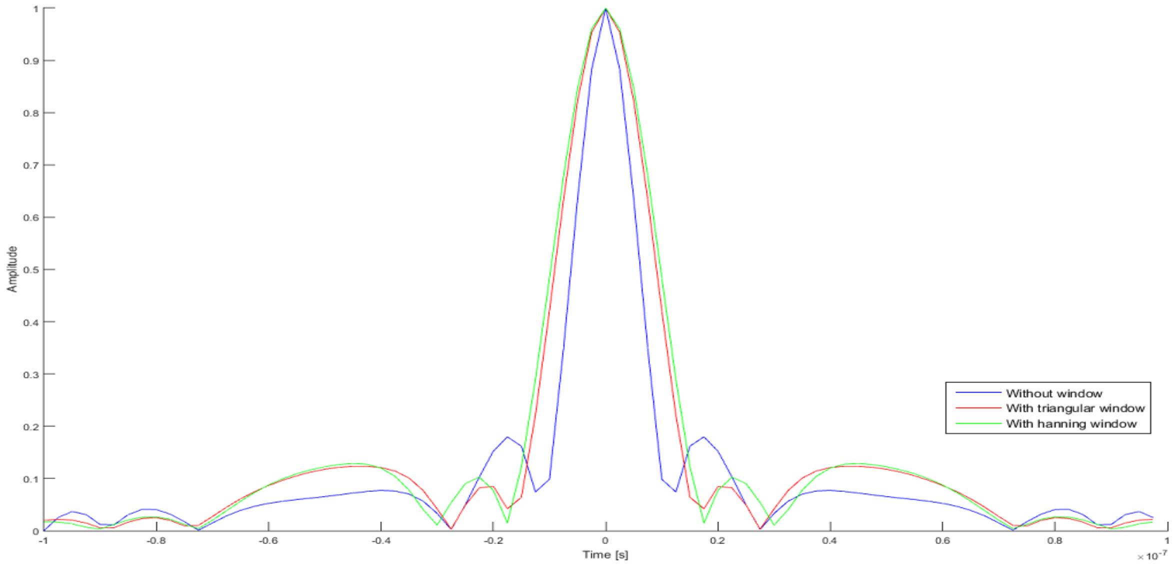

Figure 2.15: *Radar filter outputs.*

2.3. SAR PROCESSOR EXAMPLE

The aim of this example is to achieve a radar reflectivity image $\Psi_I(z,x)$ of a set of single points spread over an area $\Psi(z,x)$. You can see a sketch of the example in Figure 2.16. The radar is moving along axis x' in a straight line and constant speed, and the distance R_0 shows the closest approach between the radar and the origin of axes z, x.

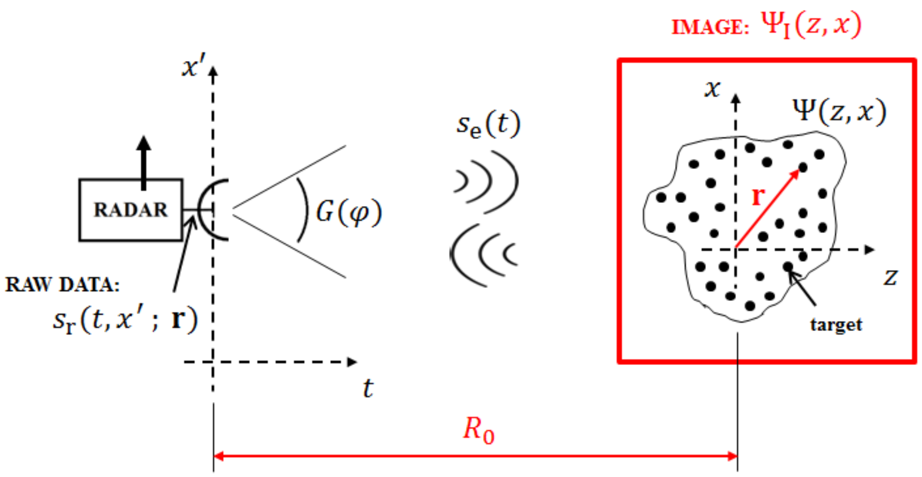

Figure 2.16: *Raw data acquisition of an area $\Psi(z,x)$.*

In order to obtain the image $\Psi_I(z,x)$, we will use a Back Propagation algorithm into the radar SAR processor. Taking into account superposition, the algorithm is designed to focus the data over every single point of the scene $\Psi(z,x)$.

Figure 2.17: *Image acquisition from raw data.*

In order to perform the SAR processor, we will first need to know the cause-and-effect relationship (i.e., the scattered fields over the measured geometry that a single target would cause). This is what we call "the direct problem of scattering" (see Figure 2.18).

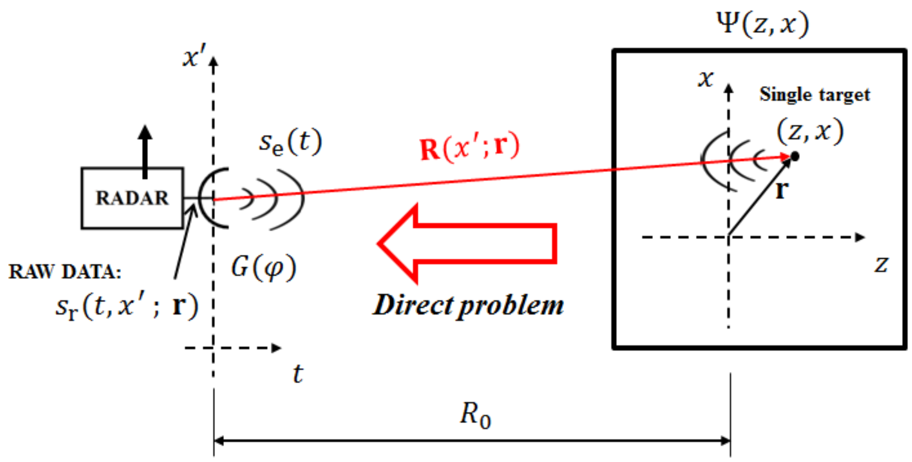

Figure 2.18: *Direct problem of scattering.*

In order to cope the direct problem of scattering, let us consider the transmitted signal $s_e(t)$ a chirp pulse given by

$$s_e(t) = \text{Re}\left\{ \prod\left(\frac{t}{\tau_0}\right) e^{j2\pi f_0 t} \, e^{j\pi\gamma t^2} \right\} \tag{2.19}$$

where τ_0 is the pulse duration, f_0 is the carrier frequency, and γ is the linear FM rate. Equation (2.19) *can be also written on its low pass equivalent expression as*

$$\tilde{s}_e(t) = \prod\left(\frac{t}{\tau_0}\right) e^{j\pi\gamma t^2} \tag{2.20}$$

The received signal on the radar antenna depends on: (a) the position of the radar along the axis x', (b) the time between the transmitted and received signals (this variable may also be expressed as a spatial variable), and (c) the position of each target along the axes z, x. Hence, we can write the expression of the received signal as

$$s_r(t, x' ; \mathbf{r}) = \text{Re}\left\{ \prod\left(\frac{t - t_r}{\tau_0}\right) \frac{\sqrt{\sigma}}{4\,\pi\, R^2(x' ; \mathbf{r})} \, G[\varphi(x' ; \mathbf{r})] \, e^{j2\pi f_0 (t - t_r)} \, e^{j\pi\gamma (t - t_r)^2} \right\} \tag{2.21}$$

where σ is the radar cross section of the target, $G[\varphi(x' ; \mathbf{r})]$ is the radiation diagram of the radar antenna, and t_r is the delay between the transmitted and received pulse given by

$$t_{\mathrm{r}} = \frac{2\,R(x'\,;\,\mathbf{r})}{c} \tag{2.22}$$

where c is the speed of light.

The collected echo signals described by Equation (2.21) *along the radar track are stored in a 2D matrix, which is usually named "raw data". If we now write the raw data on its low pass equivalent expression, we obtain*

$$\tilde{s}_{\mathrm{r}}(t, x'\,;\,\mathbf{r}) = \prod\left(\frac{t - \frac{2\,R(x'\,;\,\mathbf{r})}{c}}{\tau_0}\right) \frac{\sqrt{\sigma}\,G[\varphi(x'\,;\,\mathbf{r})]}{4\,\pi\,R^2(x'\,;\,\mathbf{r})}\; e^{-j2k_0R(x';\,\mathbf{r})}\; e^{j\pi\gamma\left(t-\frac{2\,R(x';\,\mathbf{r})}{c}\right)^2} \tag{2.23}$$

where k_0 is the wave number given by

$$k_0 = \frac{\omega_0}{c} = \frac{2\pi f_0}{\lambda_0 f_0} = \frac{2\pi}{\lambda_0} \tag{2.24}$$

where λ_0 is the carrier wavelength.

Now, our objective is to recover the point reflectivity from the measured fields. We must do an "inverse problem".

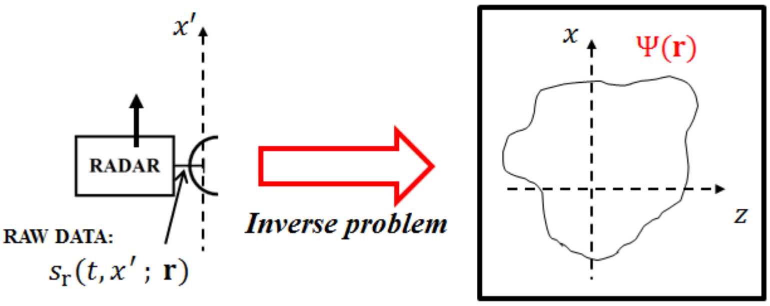

Figure 2.19: *Inverse problem.*

Therefore, we need to design a SAR processor that gets the radar reflectivity image from the acquired raw data fulfilling the following condition

$$\Psi_{\mathrm{I}}(\mathbf{r}) \approx \Psi(\mathbf{r}) \tag{2.25}$$

In this way, our SAR processor will consist of two blocks: (a) the range compressor and (b) the azimuth compressor (see Figure 2.20).

The range compressor must compress the raw data along the axis t by using a matched filter. Thus, the range compressed signal must be

$$\widetilde{s_{\mathrm{r}}}'(x'\,;\,\mathbf{r}) = \frac{1}{2}\,\tilde{s}_{\mathrm{r}}(t, x'\,;\,\mathbf{r}) * \widetilde{h_{\mathrm{m}}}(t) \tag{2.26}$$

or, if we write the expression above in a range frequency domain to avoid the convolution computation costly, we obtain

$$\widetilde{S_r}'(x' \,;\, \mathbf{r}) = \frac{1}{2}\, \widetilde{S_r}(f, x' \,;\, \mathbf{r})\, \widetilde{H_m}(f) \tag{2.27}$$

where

$$\widetilde{S_r}(f, x' \,;\, \mathbf{r}) = \mathcal{F}\{\widetilde{s_r}(t, x' \,;\, \mathbf{r})\} \tag{2.28}$$

$$\widetilde{H_m}(f) = \mathcal{F}\{\widetilde{s_e}^*(-t)\} = \widetilde{S_e}^*(f) \tag{2.29}$$

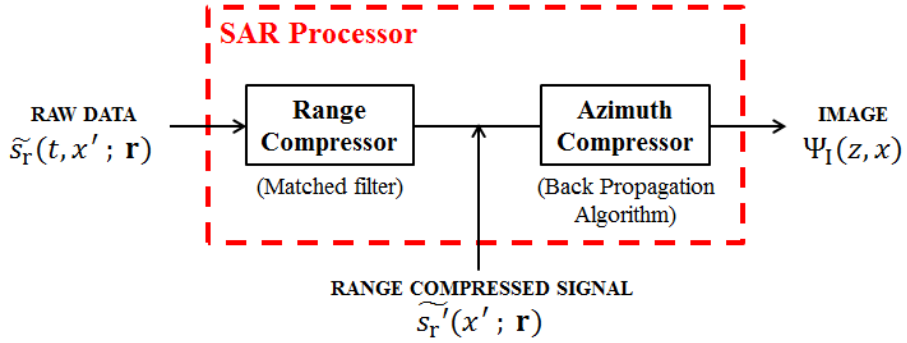

Figure 2.20: *SAR processor blocks.*

In Figure 2.21, we can see an example of the range compressed signal of a point target derived from Equation (2.26) *where the horizontal axis can be expressed either in time or spatial domain* ($z = c\,t/2$)*.*

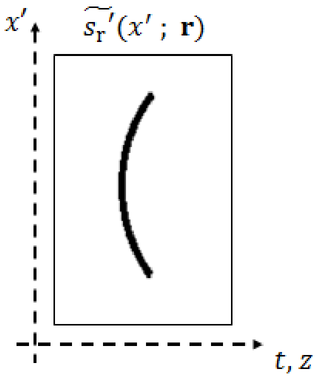

Figure 2.21: *Example of range compressed signal of a single target.*

Now, we must transform the range compressed signal of 2 dimensions in an image that fulfils Equation (2.25)*. That is what we will obtain after the back propagation algorithm implementation into the azimuth compressor will be performed. The BPA algorithm is based on a coherent addition of the measured data (pixel) by compensating the amplitude and phase lost in the direct problem.*

Although the range compressed signal has 2 dimensions, every scene point in the range compressed domain generates a hyperbolic line of data (curved line of Figure 2.21). Thus, we can integrate the compensated amplitude and phase data along this measured compressed data line and derive the final image $\Psi_I(\mathbf{r})$ *as*

$$\Psi_{\mathrm{I}}(\mathbf{r}) = \int_{x'} \widetilde{s_{\mathrm{r}}}'[l(x'\,;\,\mathbf{r})\,;\,\mathbf{r}]\, \frac{4\,\pi\, l^2(x'\,;\,\mathbf{r})}{\sqrt{\sigma}\, G[\varphi(x'\,;\,\mathbf{r})]}\, e^{j2k_0 l(x';\mathbf{r})}\, dx' \tag{2.30}$$

In Figure 2.22, we can see the geometry used to solve Equation (2.30).

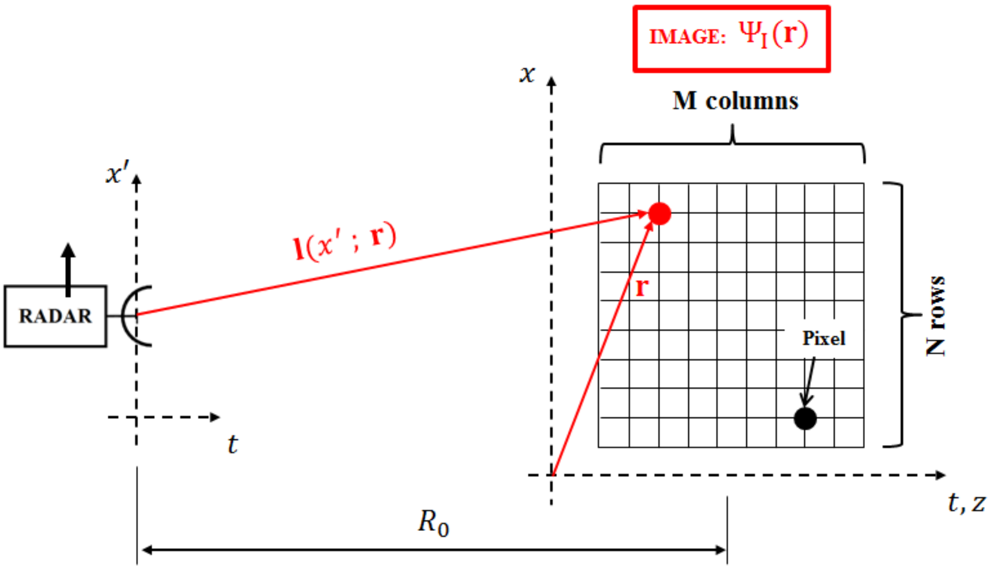

Figure 2.22: *Geometry used in Equation* (2.30).

The image will contain NxM pixels. The N and M values will depend on the size of the evaluated area $\Psi(\mathbf{r})$*, and the desired range and azimuth resolutions. The distance* l *must be computed for each radar antenna position and pixel of the image, and must be used to achieve the appropriate value of the range compressed signal on each case. Therefore, interpolation is needed on this latter step for better accuracy in the result of Equation* (2.30).

In order to avoid errors in the integral computation, the inverse of the radiation diagram of the radar antenna $F[\varphi(x'\,;\,\mathbf{r})]$ *may be computed as*

$$F[\varphi(x'\,;\,\mathbf{r})] = \frac{1}{G[\varphi(x'\,;\,\mathbf{r})]} = \begin{cases} 0 & \text{if } \; G[\varphi(x'\,;\,\mathbf{r})] = 0 \\ \dfrac{1}{G[\varphi(x'\,;\,\mathbf{r})]} & \text{other case} \end{cases} \tag{2.31}$$

Once the direct problem for a simple target has been successfully solved, the same problem with a scene of multiple targets should not be difficult to deal with. Therefore, you are asked to solve the direct and inverse problems for a simple target located at the origin of the axes z, x.

Radar and target specifications:

- *Carrier frequency*: $f_0 = 9.65\ \mathrm{GHz}$ *(X-Band radar)*
- *Oversampling factor*: $\alpha = 4$ *(To satisfy Nyquist* $\times$ *4)*
- *Pulse duration*: $\tau_0 = 100\ \mathrm{ns}$
- *Bandwidth*: $\Delta f = 1\ \mathrm{GHz}$
- *Linear FM rate*: $\gamma = \frac{\Delta f}{\tau_0} = \frac{10^9\ \mathrm{Hz}}{100 \cdot 10^{-9}\ \mathrm{s}} = 10^{16}\ \frac{\mathrm{Hz}}{\mathrm{s}}$
- *Range compression ratio*: $\rho = \Delta f\ \tau_0 = 10^9\ \mathrm{Hz} \cdot 100 \cdot 10^{-9}\ \mathrm{s} = 100$
- *Radar-target closest approach*: $R_0 = 3000\ \mathrm{m}$
- *Antenna length*: $L_\mathrm{a} = 0.3\ \mathrm{m}$
- *Azimuth beam width*: $\theta_\mathrm{bw} = \frac{\lambda_0}{L_\mathrm{a}} = \frac{c}{f_0\ L_\mathrm{a}} = \frac{3 \cdot 10^8\ \frac{\mathrm{m}}{\mathrm{s}}}{9.65 \cdot 10^9\ \mathrm{Hz} \cdot 0.3\ \mathrm{m}} = 0.1036\ \mathrm{rad}$
- *Synthetic aperture*: $L_\mathrm{s} = \theta_\mathrm{bw}\ R_0 = 0.1036\ \mathrm{rad} \cdot 3000\ \mathrm{m} = 310.88\ \mathrm{m}$
- *Nominal azimuth resolution*: $\Delta x' = \frac{L_\mathrm{a}}{2} = 0.15\ \mathrm{m}$
- *Target RCS*: $\sigma = 1\ \mathrm{m}^2$
- *Radiation diagram of the radar antenna (see Figure 2.23).*

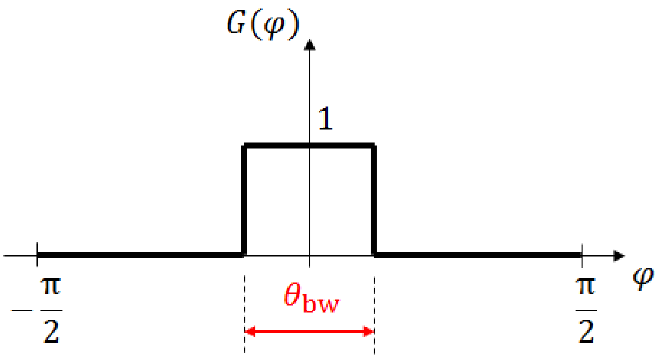

Figure 2.23: *Radiation diagram of the radar antenna.*

Hereafter, the steps of the Back Propagation Algorithm are provided:

- *For every* $\mathbf{r}$ *point (2 loops: one for coordinate* x *and another for coordinate* z*).*
  - *For every antenna position* (x')*.*
    - *Compute the range of the travel signal* $l(x'\ ;\ \mathbf{r})$*.*
    - *Obtain* $\widetilde{s_\mathrm{r}}'[l(x'\ ;\ \mathbf{r})\ ;\ \mathbf{r}]$ *by linear interpolation.*
    - *Apply amplitude and phase corrections.*
    - *Sum the integral results in the same variable pixel.*
  - *Save the value of the variable pixel into the matrix image.*
  - *Reset the value of the variable pixel.*

SOLUTION:
As in the previous section, it has been used a Matlab script in order to solve this example. The solution will show the main results obtained as well as the main steps to achieve them.

After the radar and target parameters have been defined into the script, we must build all the coordinate systems[1] we need to obtain the image of the single target. First, we must delimit the length of the range and azimuth axes of the image which we define as t_i (time axis) or z_i (space axis) and x_i respectively. There are two options for expressing the length of these axes: (a) by means of a number of meters or (b) by means of a number of pixels. Second, we must build the axes of the radar antenna. The azimuth radar antenna axis (defined as x) must be large enough for being able to depict the curved line of Figure 2.21. Thus, in Figure 2.24, we can see that the required minimum length is L_s. In order to add a little margin at the upper and lower parts of the curve, let us set the length of axis x, $1.5 \cdot L_s$. In order to obtain the range radar antenna axis (defined as t), we need to know the maximum time delay corresponding to the farthest pixel of the image (in Figure 2.25, we can see the geometry of this problem). Thus, we can derive the maximum time $t_{\max}$ as

$$t_{\max} = \frac{2\sqrt{(x_{\min} - x\_i_{\max})^2 + (R_0 + z\_i_{\max})^2}}{c} \tag{2.32}$$

Therefore, we could obtain the length of axis t doubling the value $t_{\max}$. However, if our target is far from the radar, we will need many samples to depict signals on axis t and many of these samples will not provide us useful information. So that, let us delimit the length of axis t to the subtraction between $t_{\max}$ and $t_{\min}$, where $t_{\min}$ can be expressed as

$$t_{\min} = \frac{2\,(R_0 - |x\_i_{\min}|)}{c} \tag{2.33}$$

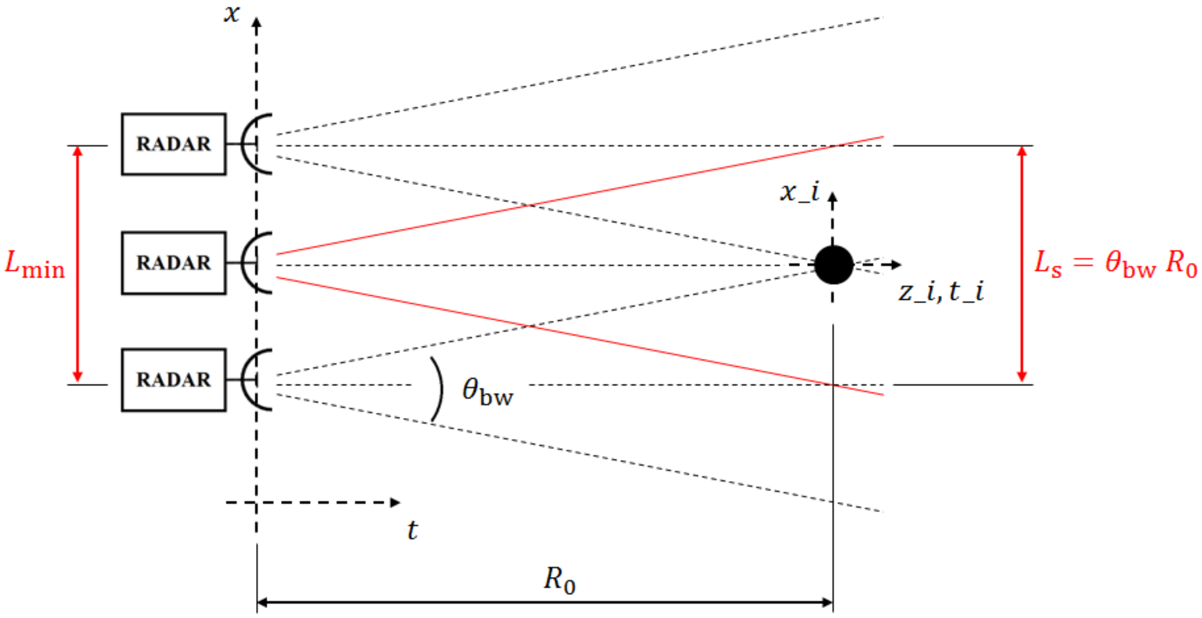

Figure 2.24: *Minimum length of axis x.*

[1] All the coordinate systems we will use in this example are built in an FFT format. Therefore, this format will be taken into account on the derived expressions from now on.

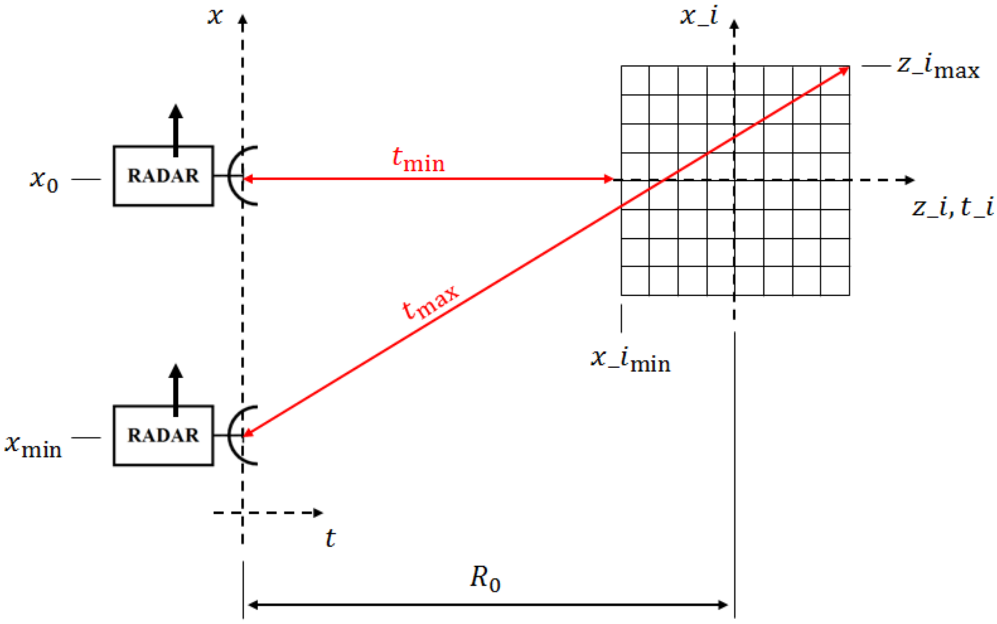

Figure 2.25: *$t_{\min}$ and $t_{\max}$.*

Now, we can derive the last coordinate system to depict the raw data. We will use the same coordinate system as for the radar antenna case, but the origin of the time axis will be changed to take into account the delay. Thus,

$$t\_raw = t + \frac{2\,R_0}{c} \tag{2.34}$$

To conclude the definition of the coordinate systems, we must build the slant range array R to compute the distance between the radar antenna and target on each radar antenna location along axis x. Hence,

$$R = \sqrt{R_0^2 + x^2} \tag{2.35}$$

Once the example geometry is defined, let us deal with the transmitted and received signals. As the problem definition says, the transmitted signal is a chirp pulse given by Equation (2.20). In order to obtain the raw data from this transmitted signal, we will compute the target echo at each radar antenna location following Equation (2.23). In this way, we will achieve a good approximation in modelling a real radar acquisition. Since the angle between the radar and target on each radar location may not match to a sample value of the radiation diagram, a *nearest neighbour* approximation has been used.

In Figure 2.26, we can see the amplitude and phase of the raw data obtained following all the steps mention above.

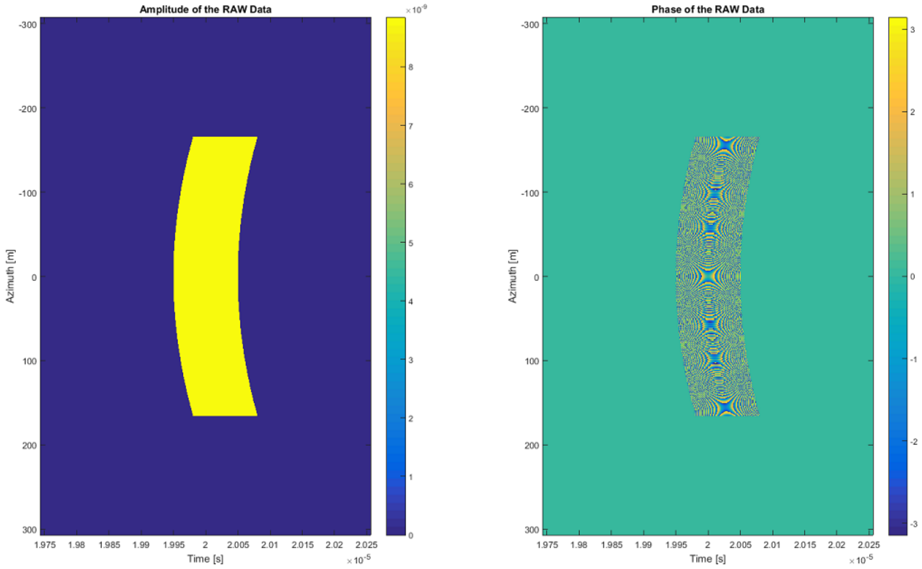

Figure 2.26: *Amplitude and phase of the raw data.*

At this point, we must process the raw data using the described SAR processor in order to achieve the range compressed signal first, and then the final image. Thus, we can proceed following the steps shown in the previous section (Range Compression Example) in order to obtain the range compressed signal. However, in this case, we have more than one signal along axis x, so that the range FFT must be performed on each radar antenna location along axis x. In Figure 2.27, we can see the amplitude and phase of the compressed signal of the data, as expressed by Equation (2.27).

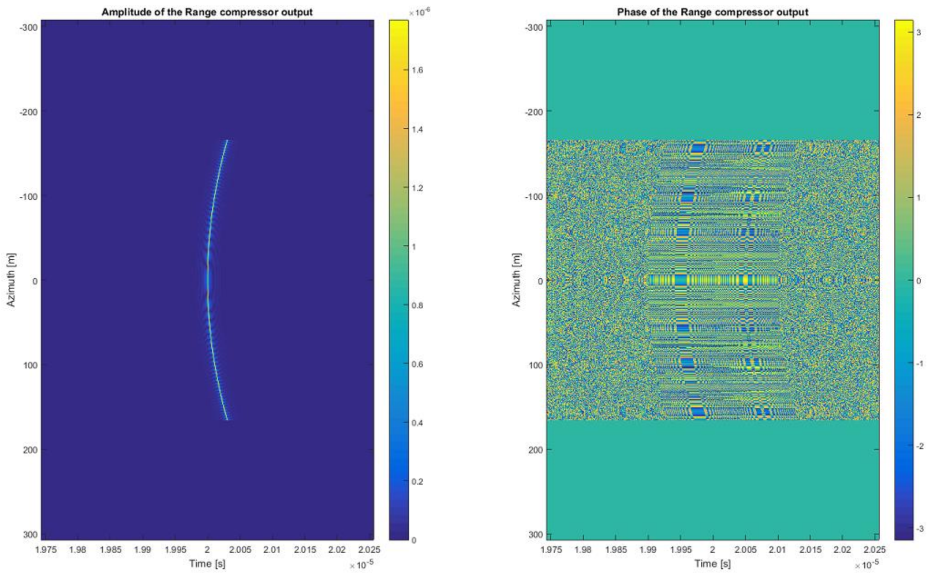

Figure 2.27: *Amplitude and phase of the range compressed signal.*

The next step is to implement the back propagation algorithm on the range compressed signal, which has been described in the problem definition. Therefore, we must first compute the distance $l(x\,;\,\mathbf{r})$ of each pixel of the image. Since the range axis of the range compressed signal is in seconds, we will also obtain the distance $l(x\,;\,\mathbf{r})$ in seconds. Thus,

$$l(x\,;\,\mathbf{r}) = \frac{2\sqrt{(x - x\_i)^2 + (R_0 + z\_i)^2}}{c} \tag{2.36}$$

Then, we must derive the value of the signal $\widetilde{s_r}'[l(x\,;\,\mathbf{r})\,;\,\mathbf{r}]$ per each pixel and time $l(x\,;\,\mathbf{r})$. In Figure 2.28, we can see a sketch of the linear interpolation to be done on, for example, the amplitude of the signal. However, this kind of interpolation may be extended to whole signal. In this way, the value for each radar antenna location of signal $\widetilde{s_r}'[l(x\,;\,\mathbf{r})\,;\,\mathbf{r}]$ can be obtained as

$$\widetilde{s_r}'[l(x_0\,;\,\mathbf{r})\,;\,\mathbf{r}] = \widetilde{s_r}'(x_0,\, t_{n+1})\,\frac{d}{T_s} + \widetilde{s_r}'(x_0,\, t_n)\,\frac{T_s - d}{T_s} \tag{2.37}$$

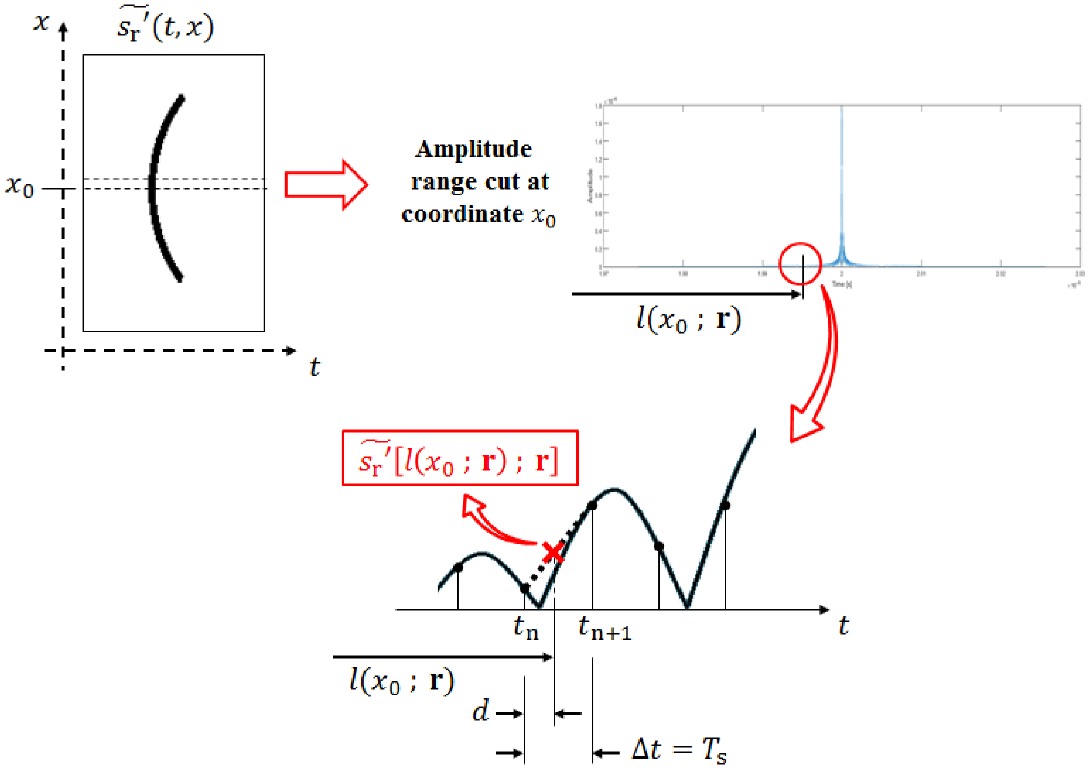

Figure 2.28: *Linear interpolation computation of the signal range compressed amplitude.*

Next, we must apply the amplitude and phase corrections to fulfil Equation (2.30) and we must compute the integral per each radar antenna location. Finally, we must sum all the integral results of one pixel and restart the algorithm for another pixel. Once all pixels have been computed, we can obtain the image of the single target as it is shown in Figure 2.29.

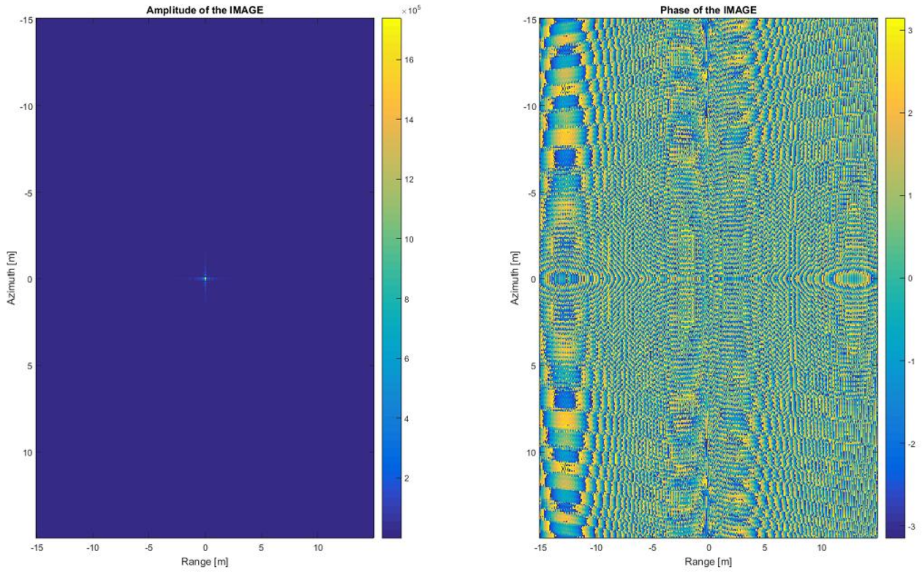

Figure 2.29: *Amplitude and phase of the image* $\Psi_{\mathrm{I}}(z,x)$.

As we can see in the amplitude plot of Figure 2.29, the point target placed at the scene centre has appeared. Therefore, the example seems to be correctly solved. However, in order to evaluate the quality of this result, we must compute the resolutions of the range cut and azimuth cut on the target location, and compare them to the theoretical ones.

Let us first obtain the theoretical resolutions on both range and azimuth directions.

$$\textit{Theoretical range resolution}: \quad \Delta R = \frac{c}{2\,B} = \frac{c}{2\,\Delta f} = \frac{3\cdot 10^8\ {}^{\mathrm{m}}/_{\mathrm{s}}}{2\cdot 10^9\ \mathrm{Hz}} = 0.15\ \mathrm{m}$$

$$\textit{Theoretical azimuth resolution}: \quad \Delta x = \frac{L_{\mathrm{a}}}{2} = \frac{0.3\ \mathrm{m}}{2} = 0.15\ \mathrm{m}$$

In Figures 2.30 and 2.31, we can see the image range and azimuth cuts on the target location respectively. In order to obtain both resolutions, we must compute the main lobe width at 3 dB below its peak ($1/\sqrt{2} \approx 0.707$ in amplitude). As very few samples depict both main lobes, both target lobe range and azimuth cuts have been interpolated in order to obtain a better approximation of the range and azimuth resolutions. Thus, a zero padding interpolation has been used with an interpolation factor of 32.

In Figures 2.32 and 2.33, we can see the final results after the interpolation and also normalization have been done. From the main lobe labels, we can now obtain the approximate range and azimuth resolutions as

$$\textit{Approximate range resolution}: \quad \Delta R' \approx 2\cdot 0.06797\ \mathrm{m} = 0.136\ \mathrm{m}$$

$$\textit{Approximate azimuth resolution}: \quad \Delta x' \approx 2\cdot 0.06328\ \mathrm{m} = 0.127\ \mathrm{m}$$

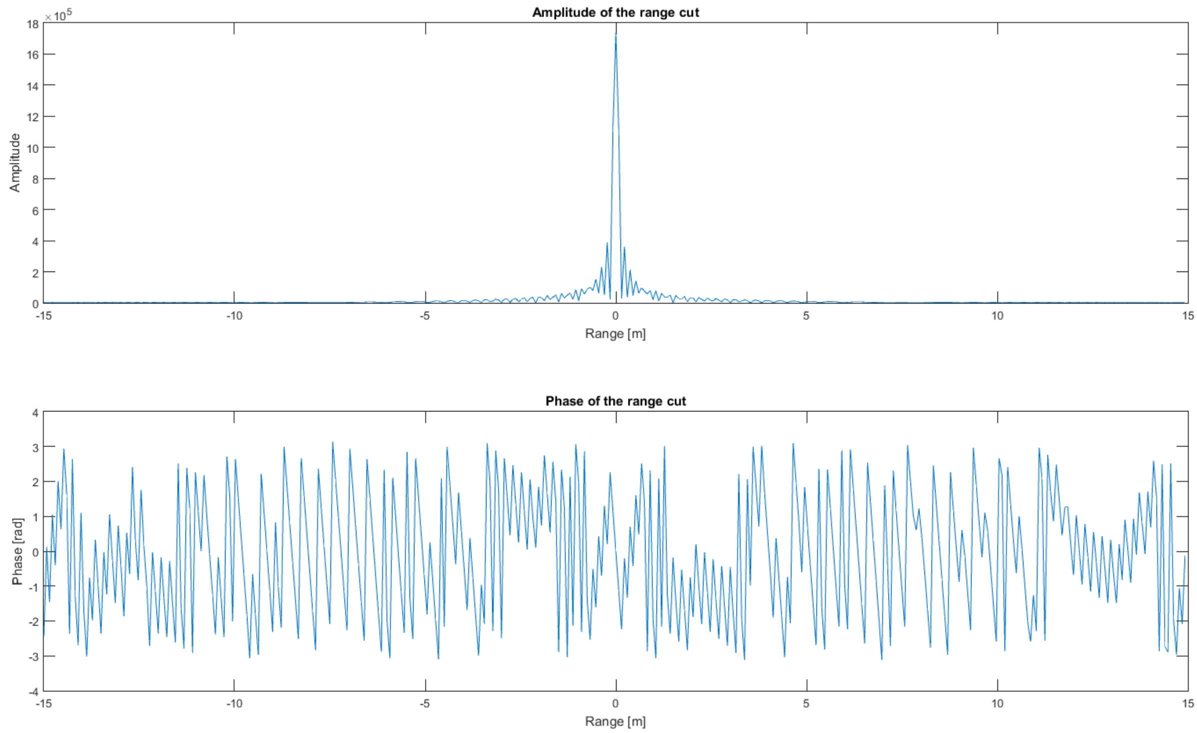

Figure 2.30: *Amplitude and phase of the image range cut on the target location.*

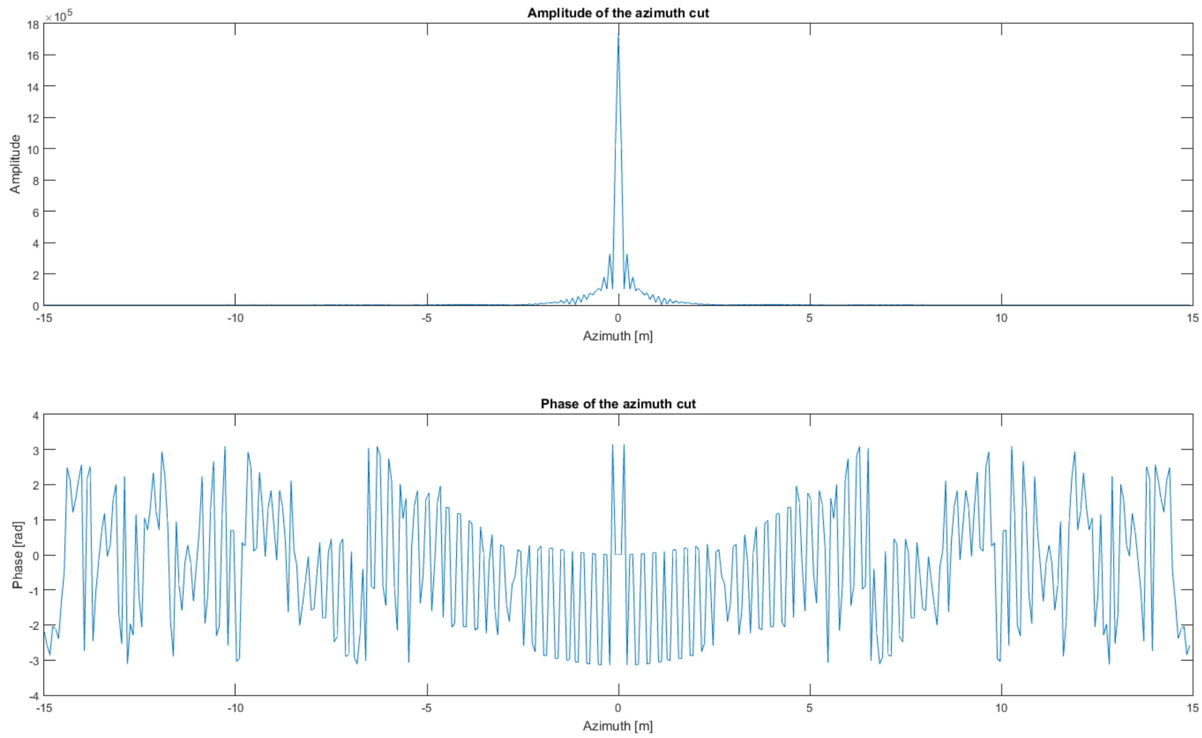

Figure 2.31: *Amplitude and phase of the image azimuth cut on the target location.*

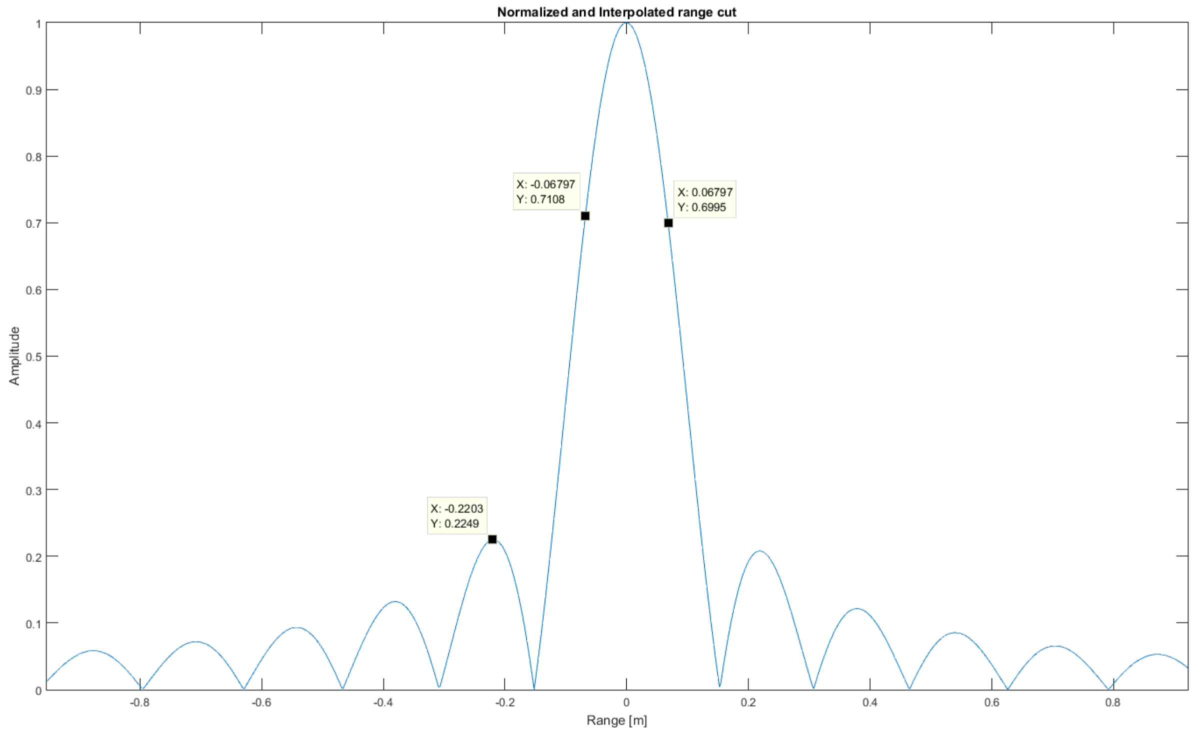

Figure 2.32: *Interpolated and normalized amplitude of the image range cut on the target location.*

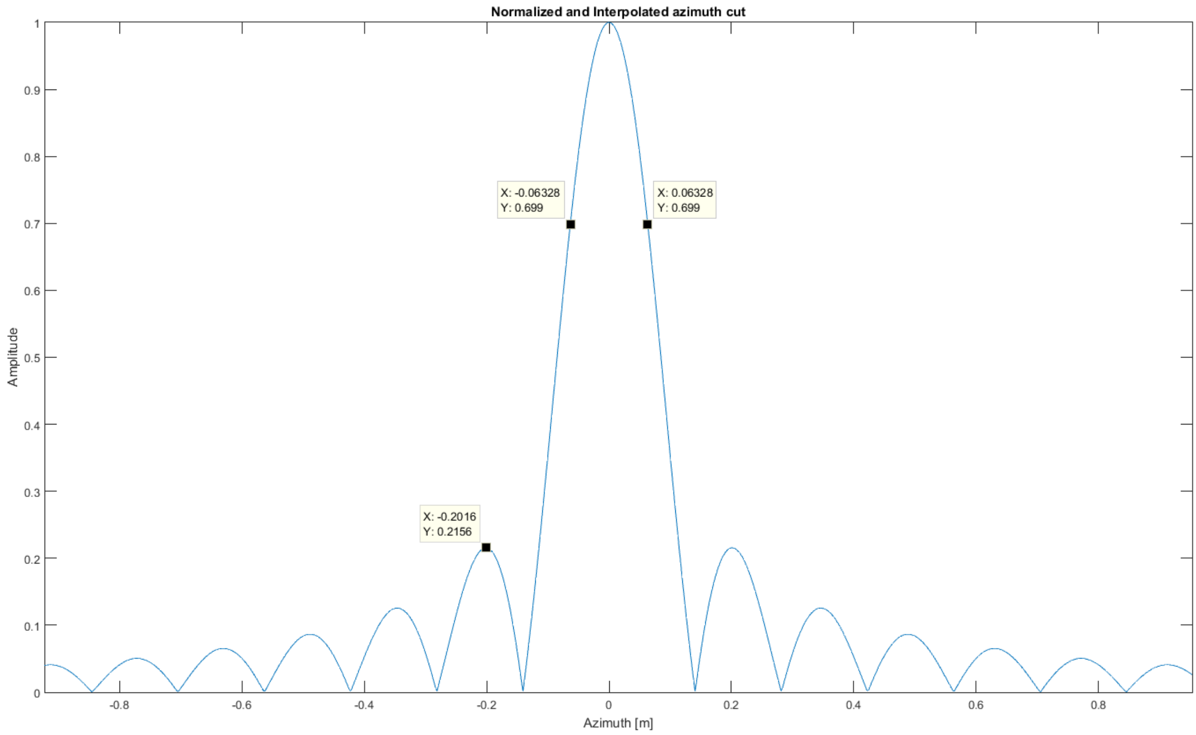

Figure 2.33: *Interpolated and normalized amplitude of the image azimuth cut on the target location.*

From Figures 2.32 and 2.33, we can also compute the Side Lobe Level (SLL) of both cuts. Thus,

$$\textit{Range cut SLL:} \quad SLL_{\mathrm{rg}} \approx 20 \cdot \log\left(\frac{1}{0.2249}\right) = 12.96\ \mathrm{dB}$$

$$\textit{Azimuth cut SLL:} \quad SLL_{\mathrm{az}} \approx 20 \cdot \log\left(\frac{1}{0.2156}\right) = 13.33\ \mathrm{dB}$$

As we can see, the approximate range and azimuth resolutions are very close to the theoretical ones. In addition, the SLL of both cuts are also very close for a rectangular aperture antenna having a uniform amplitude distribution (i.e. ~ 13.26 dB). Therefore, we can conclude that the example has been correctly solved.

2.4. REAL RANGE HISTORY EXAMPLE

In the previous section, the SAR processor has been applied to data simulated from a radar moving in a straight line. However, in the GEOSAR mission case, the radar hosted by the satellite in the GEO orbit does not follow a rectilinear movement. Thus, the signal of Equation (2.36) cannot be obtained from such a straightforward way. As seen in the previous example, this signal plays a major role when performing the image focusing by means of the BPA algorithm, so that it must be calculated precisely. Such signal will be called range history from now on since it collects the distances between the radar antenna and every point of the observed scene over time.

The following example will illustrate a real range history that could be obtained from a satellite orbiting in a GEO orbit. In this way, the reader will have an overview of the real movement between the satellite and one point of the scene. On the other hand, the example will introduce the reader to the explanation of the satellite orbital determination methods and techniques of next chapters.

The satellite that is going to be used is located on longitude 19.2° E and is operated by SES S.A. (Société Européenne des Satellites) providing Satellite TV and Telecommunication Data services with the commercial name ASTRA. In order to place the satellite in a certain point in the space at a given time, a Two-Line Element set[1] (TLE) is going to be used. TLEs are periodically published in the Space Track program website [19], which keeps track of the vast majority of the objects orbiting the Earth. From a TLE, one may obtain the satellite position and velocity vectors with regard to a proper coordinate frame, which has its origin on the Earth's centre. However, the location error of the satellite from such TLEs is well beyond the precision requirement of GEOSAR mission. Anyway, the TLE can still be used as a first approximation of iterative methods such as Least Squares technique. The methods and techniques explained in the following chapters will determine the satellite orbit more precisely.

Having located the satellite, the next step is to place a site (i.e., a base station) over the Earth's surface in order for being able to calculate the range history between the satellite and the site. At this point, one must consider that there is visibility of the satellite from the site. In this way, a base station

[1] A Two-Line Element set (TLE) is a data format encoding a list of orbital elements of an Earth-orbiting object for a given point in time. Consult reference [12] for further information about the TLE format.

placed in Barcelona city (Spain) has been chosen. Table 2.1 summarizes the location parameters needed to obtain the position and velocity vectors of Barcelona site in a particular coordinate frame. This coordinate frame may not be the same coordinate frame which locates the satellite, so that some relations between both coordinate frames are needed to be found in order not to calculate the range history in a wrong way. Such relations involve perturbations, such as nutation, precession or polar motion, which affect the Earth's motion, and whose effects will not be considered within the example. Thus, the position of the site with regard to the position of the satellite will only be calculated by means of time.

Location parameters of the base station placed in Barcelona	
Geodetic Latitude	$41°\ 23'\ 20.0''$ N
Longitude	$2°\ 9'\ 20.0''$ E
Altitude	0.020 km

Table 2.1: *Location parameters of a base station placed in the city of Barcelona (Spain).*

The time is given into the TLE, so that the satellite position and velocity vectors calculated are specific of this time. Chapter 3 shows how to calculate time for a particular site via Equation (3.8). In this example, as time is given as a date (i.e., year, month, day, hour, minutes and seconds), the Greenwich Mean Sidereal Time (GMST), θ_{GMST}, can be obtained as

$$\begin{gathered}\theta_{\mathrm{GMST}} = 67310.54841\ \mathrm{s} + (876600\ \mathrm{h} + 8640184.812866\ \mathrm{s}) \cdot T_{\mathrm{UT1}} \\ +0.093104 \cdot T_{\mathrm{UT1}}^2 - 6.2 \times 10^{-6} \cdot T_{\mathrm{UT1}}^3\end{gathered} \tag{2.38}$$

where T_{UT1} is the number of Julian centuries from a particular epoch (i.e. J2000.0[1]) in UT1[2] (Universal Time 1) time scale. The general formula referencing J2000.0 is

$$T_{\mathrm{UT1}} = \frac{JD_{\mathrm{UT1}} - 2451545.0}{36525} \tag{2.39}$$

where JD_{UT1} is the Julian Date (i.e., the interval of time measured in days from the epoch January 1, 4713 B.C., 12:00) in UT1 time scale. The reader may consult (Vallado, 2013) for further information about this topic.

In order to be more precise when computing the GMST, one must take into account that the time given in a TLE is in UTC[3] (Coordinated Universal Time) time system. Thus, a conversion between UTC and UT1 must consequently be performed since Equation (2.38) is in UT1. The relation between both time scales follows Equation (2.40)

$$\Delta UT1 = UT1 - UTC \tag{2.40}$$

where $\Delta UT1$ value can be achieved from [7]. Since the example will show the range history between the satellite and the base station during the first week of January 2012, the value of $\Delta UT1$ is -0.4 s. One can see that this value is not high; however, it is required for precise computations.

[1] J2000.0 refers to January 1, 2000 12:00:00.000.
[2] UT1 is a variation of Universal Time (UT), which is based on a fictitious mean Sun in order to define the time of an event.
[3] Coordinated Universal Time (UTC), is the most commonly used time system, which is derived from an ensemble of atomic clocks. It is designed to follow UT1 within ± 0.9 s.

Once the position of the satellite and the site has been obtained in the same coordinate frame and time, the range observation can be calculated via Equation (3.14). Thus, using different TLEs of the first week of January 2012, one may compute different values of range, and therefore the range history of the site.

Figure 2.34 illustrates a general overview of the satellite orbit around the Earth along all week. From this figure, one can perfectly see the GEO orbit described by the satellite. In order to notice the minor differences among consecutive satellite orbits around the Earth, Figure 2.35 plots these orbits alone (i.e., without the Earth). As seen in the figure, the satellite orbits do not remain fixed because the satellite is affected by many perturbations during its movement around the Earth. Examples of such perturbations are the asphericity of the Earth, the solar-radiation pressure, the third body effects… These perturbations can cause important deviations on the satellite orbit (Vallado, 2013), sometimes comparable to the primary attracting force (i.e., the two-body gravitation).

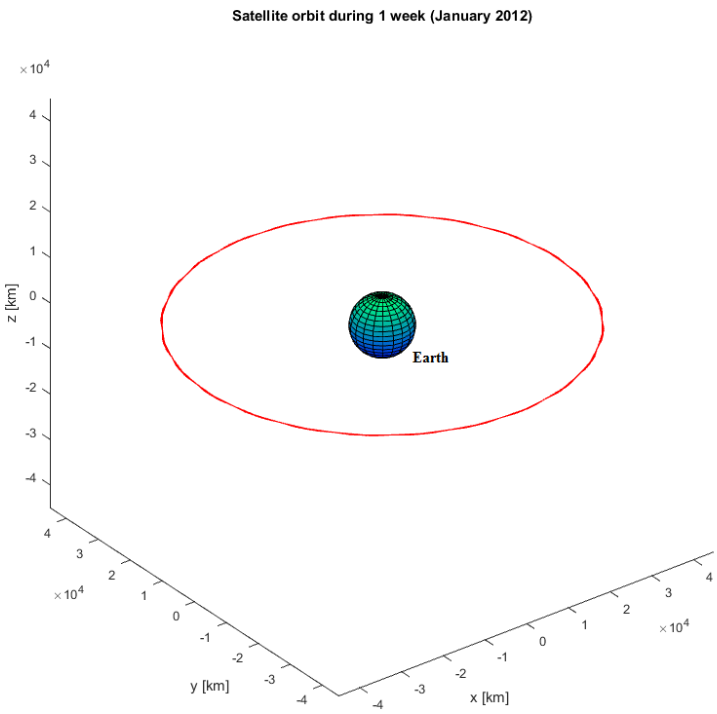

Figure 2.34: *Satellite orbit around the Earth during the first week of January 2012.*

Finally, in Figure 2.36, the range history between the satellite and the base station placed in Barcelona has been depicted. Two facts can be derived from this latter figure. The first one is that the satellite orbit is not perfectly circular as an ideal GEO orbit should be, but it has a small eccentricity. One can see this from the fact that the range history is not a constant straight line. The non-circularity of the satellite orbit was already known from the data given in the TLEs since all of them had an eccentricity different to 0. However, this fact was unknown for the reader. The second issue that can be derived from Figure 2.36 is related to consecutive satellite orbits are not equal, which it could already be seen from Figure 2.35. Thus, the degradation suffered by the satellite orbit along time and how it affects the range history determination can be observed in another way. Table 2.2 lists the maximum and minimum ranges calculated per orbit in order to notice such degradation more clearly.

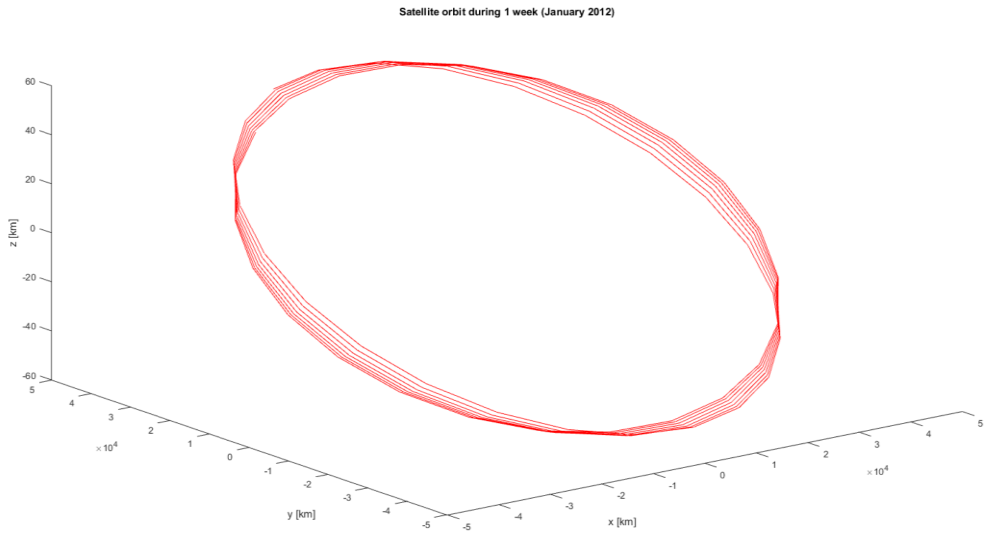

Figure 2.35: *Satellite orbit alone during the first week of January 2012.*

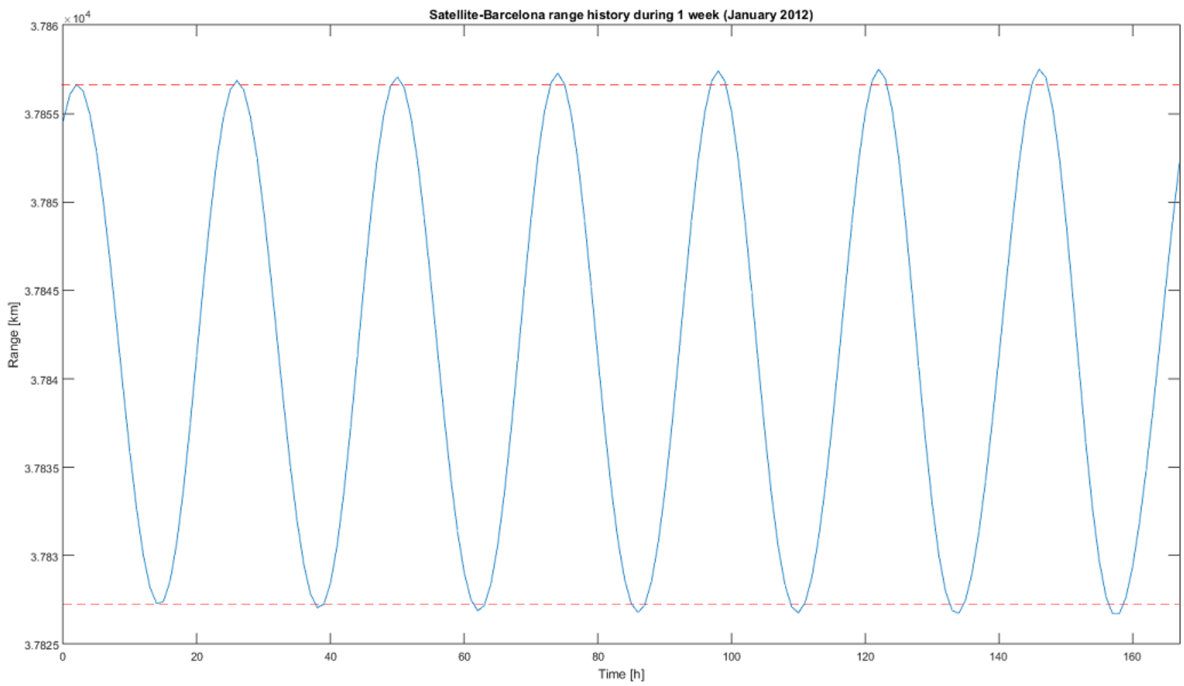

Figure 2.36: *Satellite-Barcelona range history during the first week of January 2012.*

Maximum and minimum ranges per satellite orbit		
Orbit number	**Maximum range [km]**	**Minimum range [km]**
1	37 856.644	37 827.290
2	37 856.858	37 827.061
3	37 857.072	37 826.886
4	37 857.283	37 826.794
5	37 857.420	37 826.773
6	37 857.508	37 826.745
7	37 857.510	37 826.702

Table 2.2: *Maximum and minimum ranges per orbit between the satellite and base station.*

The examples shown in this chapter give a basic overview of how a SAR works. In this way, well-focused images can be obtained by means of the BPA algorithm of the SAR processor. GEOSAR orbit determination requirements are well beyond those used in other applications such as telecommunications or TV Broadcasting. In the following chapters, different methods and techniques suitable for satellite high precision orbit estimation are assessed.

3

Initial Orbit Determination

Initial orbit determination involves various analytical methods that relate observation data produced by sensor sites to orbital elements describing the movement of a body in motion in space. These observation data may be of different types depending on the observations that the sensor performs of the body in movement. Thus, angular data, range measurements, rates of each measurement, etc., may be used for determining initial orbits. One could not process data in order to calculate the satellite orbit without the individual vectors determined through one of the techniques used for initial orbit determination.

In the context of GEOSAR mission, the radar payload hosted by a communications satellite in a geostationary orbit will provide range and range-rate measurements thanks to well-located ARCs (Active Radar Calibrators) over the Earth's surface. Such measurements will be used to track the satellite orbit around the Earth. However, the position of the satellite in space will remain unknown unless the range and range-rate measurements are processed into orbital elements.

Escobal (1965) suggests a method called Trilateration, which converts simultaneous range and range-rate information coming from different sensor sites to an initial position and velocity vectors of the satellite under study. This chapter will analyse this method and will also discuss Gibbs method in case the sensor site may only provide range measurements.

In order to perform such analysis, ideal data must be created since there is no real measured data available yet. In this way, the first part of this chapter will be dedicated to explain the fundamentals of how the ideal data is built. This ideal data involves the design of a satellite orbit that fulfils a geostationary orbit from which ideal range and range-rate observations may be calculated. In addition, some basic Astrodynamics concepts will be introduced first in order to better understand all parameters that are going to be used along the text.

Once the ideal data is obtained, the analysis of Trilateration and Gibbs will be performed. To this end, some Matlab simulations will be discussed in order to have an extensive description of the precision of both methods on determining the satellite orbit. In this way, Trilateration and Gibbs methods will be analysed ideally first (i.e., only using the ideal data) to conclude the study of both methods adding noise to the ideal data.

At the end of the chapter, a summary of all results obtained will be shown. Thus, the reader will easily compare the performance of all simulations evaluated.

This chapter aims to be as complete as possible, but the reader is encourage to consult Bate, Mueller and White (1971), Escobal (1965), and Vallado (2013) for further explanations about topics discussed along this text or other concepts related to Astrodynamics.

3.1. COORDINATE SYSTEMS

Before starting to describe all orbit elements and methods in order to find the satellite orbit, one must know the coordinate systems that are going to be considered in order to locate the satellite with regard to an Earth position. This document will take into account three coordinate systems: two of them are Earth-based systems and the third one is a satellite-based system.

a) Geocentric Equatorial Coordinate System, IJK

This system originates at the centre of the Earth and is generically designated with the letters IJK. The fundamental plane contains the Earth's equator as shown in Figure 3.1a. The I axis points towards the vernal equinox[1]; the J axis is 90° to the east in the equatorial plane; and the K axis extends through the North Pole.

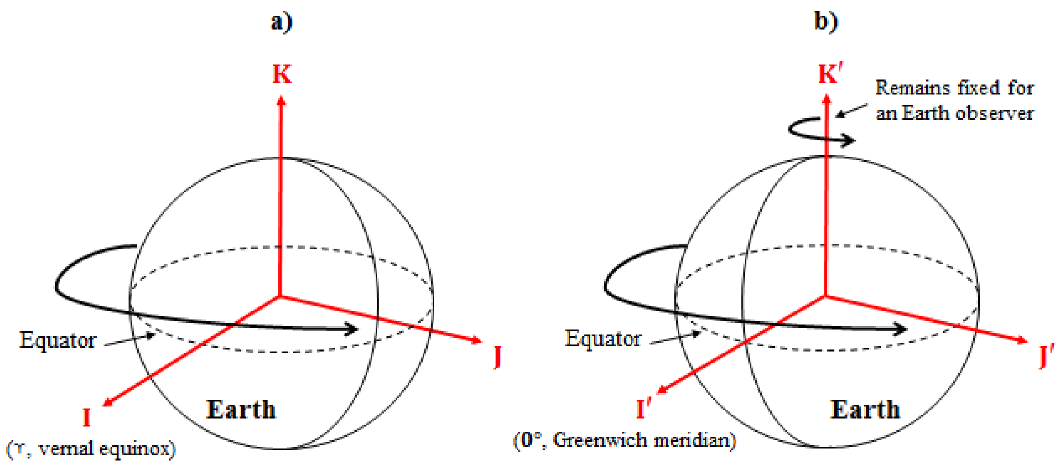

***Figure 3.1: a)** ECI Coordinate System, and **b)** ECEF Coordinate System.*

The geocentric frame, IJK, is often used interchangeably with an Earth-Centred Inertial (ECI) nomenclature. The equinox and plane of the equator move very slightly over time so that the term "inertial" can cause confusion. $J2000$ is an example of a quasi-inertial frame realized in the IAU-76/FK5 system (Vallado, 2013), which was the standard pseudo-inertial system for geocentric coordinates for many years.

b) Body-Fixed Coordinate System, ITRF

A geocentric coordinate system fixed to the rotating Earth results in the Body-Fixed (BF) or International Terrestrial Reference Frame (ITRF) coordinate system. Its origin is at the centre of the Earth and the axes are realized by the adopted coordinates of defining stations on the Earth's surface. Confusion may exist because the ITRF system is frequently called the Earth-Centred, Earth-Fixed (ECEF) coordinate frame. The term "Earth-Fixed" describes a terrestrial reference system whose net global orientation remains unchanged over time with respect to the crust of the Earth.

[1] A formal definition for the vernal equinox is that it occurs when the Sun's declination is 0° as it changes from negative to positive values. The direction of the vernal equinox is designated ♈ and often referred as the first point of Aries.

In order to simplify complexity, this document will use the ECEF coordinate system. Its fundamental plane contains the Earth's equator (see Figure 3.1b). The I axis points towards the Greenwich meridian (0°); the J axis is 90° to the east in the equatorial plane; and the K axis extends through the North Pole. ECEF system rotates with the Earth, and therefore coordinates of a point fixed on the Earth's surface do not change.

In addition, this document will not take into account precession and nutation effects of the Earth's equatorial plane as well as polar motion, which affect the movement of the Earth around the Sun. In this way, the I axis of the ECEF coordinate system and the previous ECI coordinate system will always remain fixed and the conversion between both systems will be performed as finding the angle between both I axes in a given time (see Section 3.4).

c) Perifocal Coordinate System, PQW

In this system, the fundamental plane is the satellite orbit, and the origin is at the centre of the Earth. The P axis points towards perigee[1]; the Q axis is 90° from the P axis in the direction of the satellite motion; and the W axis is normal to the orbit (see Figure 3.2).

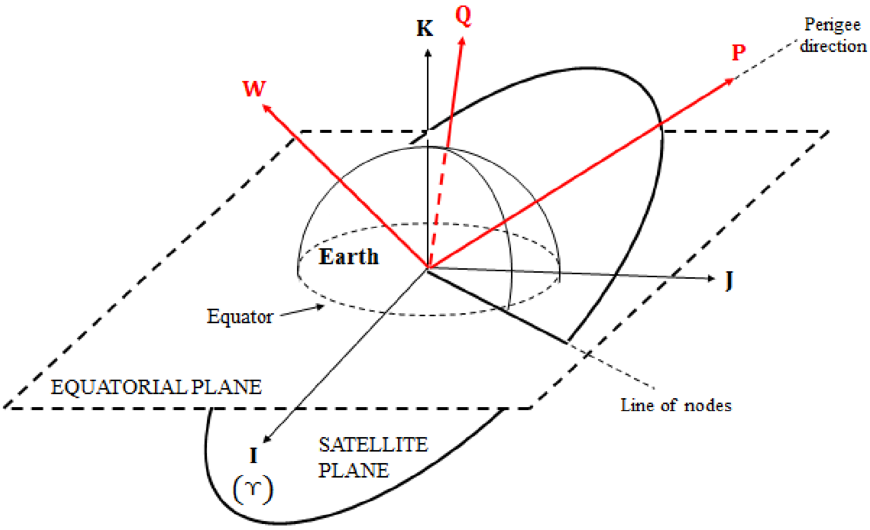

Figure 3.2: *Perifocal Coordinate System, PQW.*

The perifocal frame, PQW, will be needed when defining some orbital elements that are going to be used to describe the satellite orbit in the following section.

3.2. SATELLITE STATE REPRESENTATIONS

The state of a satellite in space is defined by six quantities, which may take many equivalent forms. Whatever the form, the collection of these six quantities can be called either a state vector, **X**, or an element set. The state vector is usually associated with position and velocity vectors. Thus, the state of

[1] The perigee is the nearest point of an elliptical satellite orbit from the centre of the Earth.

a satellite in space can be defined by the Cartesian coordinates of both vectors (r_{x0}, r_{y0}, r_{z0}, v_{x0}, v_{y0}, and v_{z0}) completing a set of six quantities (see Figure 3.3). The subscript 0 refers to the time where the state vector is given since, as the time changes, so does the state vector. On the other hand, an element set is a collection of scalar magnitudes and angular representations of the orbit, which are called orbital elements. The most common element sets are the Classical Orbital Elements (COE), also called Keplerian elements, two-body elements or osculating elements. However, several other element sets have been developed (e.g., two-line, equinoctial, Delaunay, and Poincaré) for convenience or to avoid the difficulties the classical orbital elements suffer for certain orbital geometries. As seen, there are many ways to define the state of a satellite in space; but this document will only address the state vector in Cartesian coordinates, which will also be called satellite state vector, and elements sets of classical orbital elements.

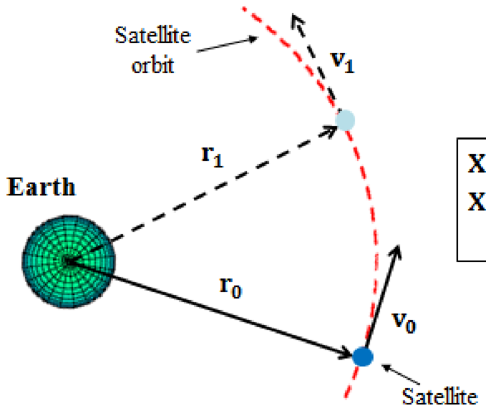

$$\mathbf{X_0} = (\mathbf{r_0}, \mathbf{v_0}) = (r_{x0}, r_{y0}, r_{z0}, v_{x0}, v_{y0}, v_{z0})$$
$$\mathbf{X_1} = (\mathbf{r_1}, \mathbf{v_1}) = (r_{x1}, r_{y1}, r_{z1}, v_{x1}, v_{y1}, v_{z1})$$
$$\vdots$$

Figure 3.3: *Satellite state vector at time t_0, $\mathbf{X}_0$, and satellite state vector at time t_1, $\mathbf{X}_1$.*

There are many classical orbital elements in order to perform the element set. The fact of choosing one or another will mainly depend on the satellite orbit that is going to be analysed. For example, the most common way to represent the classical orbital elements in an element set is the semi-major axis, a; eccentricity, e; inclination, i; right ascension of the ascending node, Ω; argument of perigee, ω; and true anomaly, ν. All of these orbital elements are going to be defined below as well as other important elements that are going to be used in the following sections. As seen in Chapter 1, the satellite orbit of GEOSAR mission will describe a geostationary orbit, which is a case of special orbit since it is equatorial and nearly circular. For this reason, it is necessary to add more orbital elements in the explanation in order to define the satellite orbit correctly.

The first classical orbital elements shown are related to the shape of the satellite orbit. As commented before, the satellite describes a near circular orbit so that the explanations will only consider circular and elliptical orbits, and will not talk about parabolic and hyperbolic orbits. In this way, the orbital elements that are going to be used are:

- The semi-major axis, a: it is the radius of an orbit at the orbit two most distant points (see Figure 3.4). If the orbit is circular, then the semi-major axis is simply the radius of the orbit. The semi-major axis always has a positive value for circular and elliptical orbits.

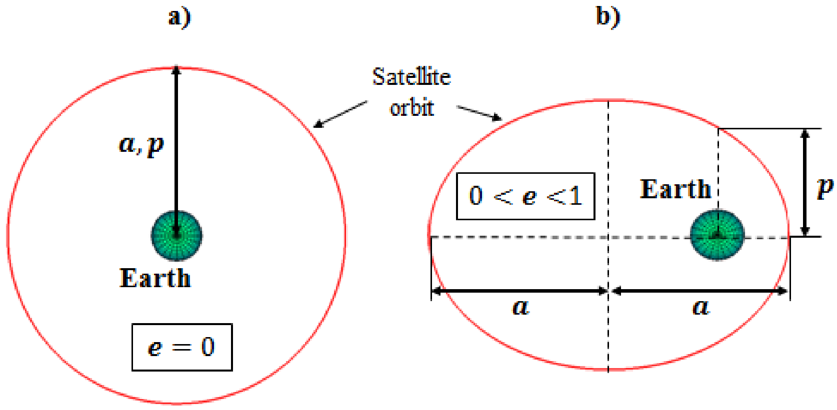

Figure 3.4: *a, e, and p orbital elements of* ***a)*** *circular orbit, and* ***b)*** *elliptical orbit.*

- The eccentricity, e: it indicates the shape of the orbit, i.e. its "roundness" or "flatness". Its value is zero for circular orbits and varies from zero to one for elliptical orbits.

- The semi-latus rectum (also called semi-parameter), p: it describes the size of the orbit by defining the width at the primary focus[1]. If the orbit is circular, then the semi-latus rectum coincides with the radius of the orbit. Instead of using the semi-major axis, one can choose the semi-latus rectum following Equation (3.1).

$$p = a(1 - e^2) \tag{3.1}$$

- The mean motion, n: it describes the satellite average angular rate of motion over one orbit. The mean motion can be used instead of the semi-major axis following Equation (3.2),

$$n = \sqrt{\frac{\mu}{a^3}} \tag{3.2}$$

where μ is the gravitational parameter, which value is

$$\mu = G\left(m_{\oplus} + m_{\text{sat}}\right) \approx Gm_{\oplus} = 3.986\,004\,418 \times 10^5\ \frac{\text{km}^3}{\text{s}^2}$$

$$G = 6.673 \times 10^{-20} \pm 0.001 \times 10^{-20}\ \frac{\text{km}^3}{\text{kg} \cdot \text{s}^2} \qquad m_{\oplus} \cong 5.973\,332\,0 \times 10^{24}\ \text{kg}$$

where G is the gravitational constant, $m_{\oplus}$ is the mass of the Earth, and m_{sat} is the mass of the satellite. As seen, the satellite mass can be neglected because it is too small relative to the Earth's mass. The values of μ and G are subtracted from WGS-84[2], whereas $m_{\oplus}$ is a derived quantity.

[1] In Astrodynamics, the gravitational centre of attraction coincides with one focus for all orbital motion, called the primary focus.

[2] The World Geodetic System 1984 (WGS-84) is an Earth-centered, Earth-fixed terrestrial reference system and geodetic datum based on a consistent set of constants and model parameters that describe the Earth's size, shape, and gravity and geomagnetic fields [13].

From the orbital elements described above, one must choose between to of them in order to form the element set. The shape of the orbit is usually expressed through the semi-major axis and eccentricity; however, one can select the semi-latus rectum or mean motion instead of a.

The second group of classical orbital elements relates the Earth-based system to the satellite-based system. In particular, the coordinate systems that are going to be related are the Geocentric Equatorial Coordinate System (IJK) and the Perifocal Coordinate System (PQW). Thus, the classical orbital elements that relate both coordinate systems are:

- The inclination, i: it is the angle measured from the unit vector $\hat{K}$ to the angular momentum vector $\mathbf{h}$[1]. The inclination refers to the tilt of the orbit plane and ranges from $0°$ to $180°$. Inclinations of $0°$ and $180°$ are equatorial orbits, whereas all others are inclined orbits.

- The right ascension of the ascension node, Ω: it is the angle in the equatorial plane measured positive eastward from the unit vector $\hat{I}$ to the location of the ascending node[2]. The right ascension of the ascending node values may range from $0°$ to $360°$ since all locations in the $I - J$ plane must be taken into account.

- The argument of periapsis (also called argument of perigee when the central body attracting the satellite is the Earth), ω: it is the angle measured from the ascending node to the periapsis point[3] in the direction of the satellite motion and in the plane of the satellite orbit. The argument of periapsis may vary from $0°$ to $360°$.

In order to form the element set, three orbital elements that relate the Earth-based system to the satellite-based system are needed. The three orbital element introduced above are the usual ones to this fact (see Figure 3.5).

The third group of classical orbital elements locates the satellite into the PQW coordinate system. These orbital elements are:

- The true anomaly, ν: it is the angle, in the plane of the satellite orbit, that determines the satellite current position relative to the location of the periapsis. The true anomaly may vary from $0°$ to $360°$.

- The time of periapsis passage, t_{p}: it is the time when the satellite was at periapsis. This orbital element can be used instead of the true anomaly.

[1] The angular momentum vector, **h**, is the vector cross product between the satellite position state vector, **r**, and the satellite velocity state vector, **v**. Therefore, it must lie perpendicular to the plane of the orbit (i.e., following the direction of W axis of the PQW coordinate system).
[2] The ascending node is the point on the equatorial plane at which the satellite crosses the equator from south to north. All inclined orbits also have a descending node, at which the satellite crosses from north to south across the equatorial plane. The line segment connecting both nodes defines a line of nodes.
[3] The extreme points of an elliptical orbit are the apoapsis and periapsis, representing the farthest and nearest points in the orbit, respectively, from the centre of attraction. The ending of these words can be changed in order to indicate a particular planet or central body attracting the satellite. They are the aphelion and perihelion in the case of the Sun, the apogee and perigee for the Earth, the aposelenium and periselenium for the Moon, and so forth.

The element set is completed with one of the two orbital elements described above, which is usually the true anomaly. However, it may also be used the time of perigee passage or the mean anomaly (introduced later) instead of ν.

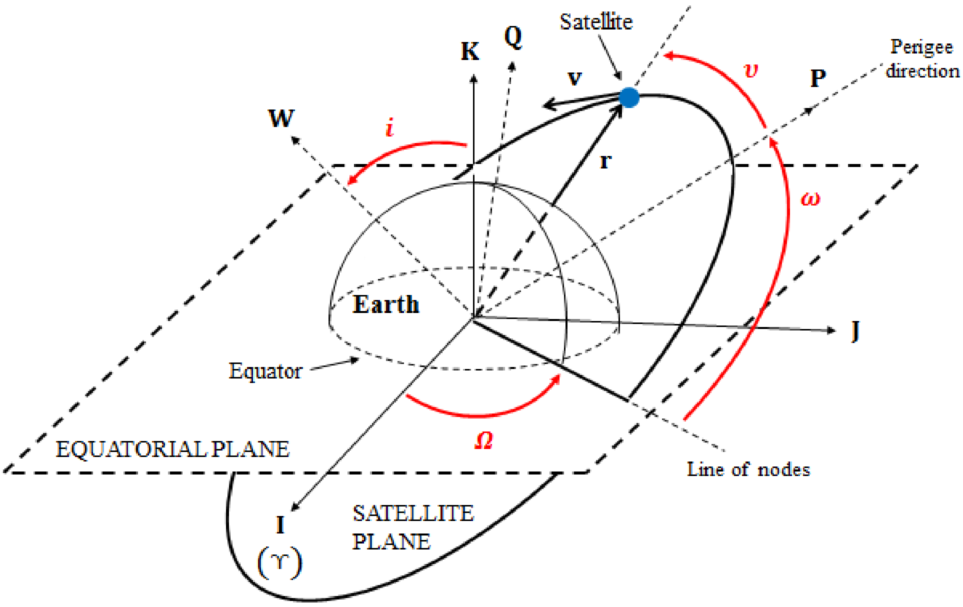

Figure 3.5: *i, Ω, ω, and ν orbital elements.*

As the satellite orbit of GEOSAR mission is equatorial, there is a need to define other orbital elements. In this particular case, the line of nodes does not exist (i.e., both the equatorial plane and the satellite plane are the same plane) and orbital elements such as the right ascension of the ascending node and the argument of periapsis remain undefined. In addition, the satellite orbit is near circular meaning that the periapsis point could not exist and the true anomaly could be undefined. Thus, some other orbital elements can replace the use of Ω, ω, and ν to better describe the satellite orbit such as:

- The true longitude of periapsis, $\tilde{\omega}_{\text{true}}$: it is the angle measured eastward from the unit vector $\hat{I}$ in the geocentric coordinate system to the periapsis point. The true longitude of periapsis is used when the line of nodes does not exist and the orbit is not circular. It may vary from 0° to 360°.

- The argument of latitude, u: it is the angle measured between the ascending node and the satellite position vector in the direction of the satellite motion. The argument of latitude is used in circular inclined orbits where there is no periapsis point to measure ω, and ν. It may vary from 0° to 360°.

- The true longitude, λ_{true}: it is the angle measured eastward from the unit vector $\hat{I}$ to the position of the satellite. It may vary from 0° to 360°. The true longitude can be calculated via Equation (3.3) of different ways depending on whether the line of nodes and the perigee are defined or not.

$$\lambda_{\text{true}} = \Omega + \omega + \upsilon = \tilde{\omega}_{\text{true}} + \nu = \Omega + u \tag{3.3}$$

Figure 3.6 illustrates the angles mentioned above in order to clarify their definitions.

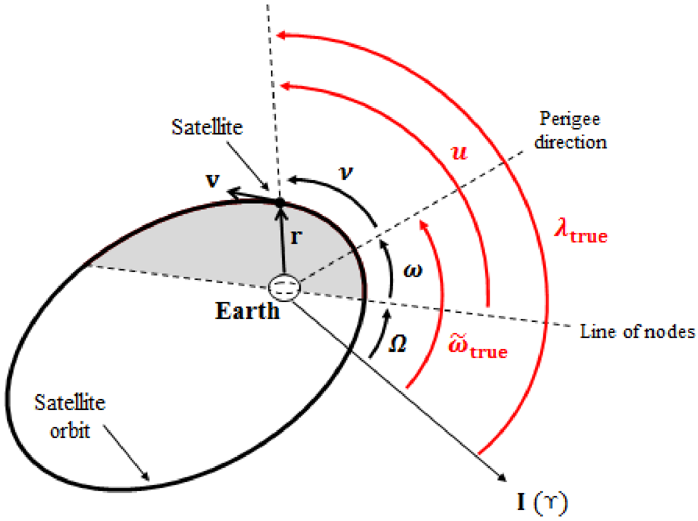

Figure 3.6: *$\tilde{\omega}_{\text{true}}$, u, and λ_{true} orbital elements.*

Finally, the two last orbital parameters must be introduced. As it will be seen later, there is a need to determine the relation of the time and angular displacement within an orbit. This is solved by the so-called Kepler's equation (see Equation [3.4]), which includes two new orbital elements that must be defined.

$$M = E - e\sin(E) = n\left(t - t_{\text{p}}\right) \tag{3.4}$$

- The eccentric anomaly, E: it is an angle related to the true anomaly and the circle drawn around the ellipse of the satellite orbit, which is called the auxiliary circle (see Figure 3.7). The eccentric anomaly may vary from 0° to 360° as the true anomaly does.

- The mean anomaly, M: it is an angle measured from the periapsis point corresponding to uniform angular motion on a circle of radius a. The mean anomaly may vary from 0° to 360°.

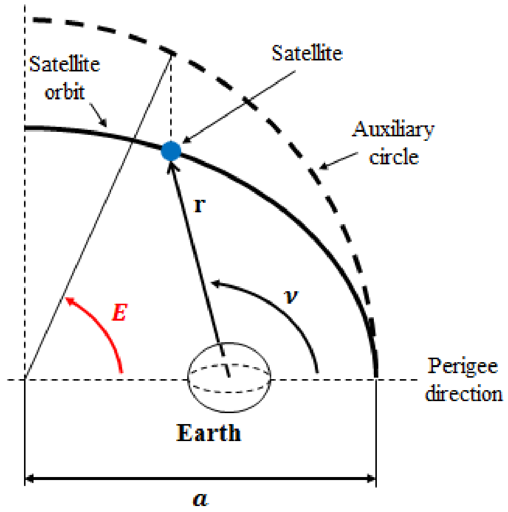

Figure 3.7: *Eccentric anomaly, E.*

Kepler's equation can be solved in two different ways. First, determining eccentric (and true) anomaly given the mean anomaly is a transcendental operation and is the form most commonly identified as Kepler's equation. The inverse problem (i.e., determining mean anomaly, and therefore time, when the eccentric anomaly or true anomaly and eccentricity are given) is a straightforward operation. In order to solve the transcendental operation, the Newton-Raphson iteration is usually used. Equation (3.5) must be solved in an iterative way until some tolerance is achieved. In addition, it must be considered that initial estimates must be close enough to the true solution in order not to violate the linear assumption of the Newton-Raphson method.

$$E_{n+1} = E_n + \frac{M - E_n + e\sin(E_n)}{1 - e\cos(E_n)} \quad \textbf{until} \ |E_{n+1} - E_n| < \text{tolerance} \tag{3.5}$$

To conclude this section, it must be said that finding the satellite state vector from an element set of classical orbital elements or vice versa is quite straightforward but implies several equations and requirements depending on the satellite orbit. When doing the transformation, it must be taken into account that the state vector must be given or will be given in the Geocentric Equatorial Coordinate System (IJK). The reader can find more information about this topic in the references listed at the introduction of the chapter. In addition, there are algorithms available online in Matlab and other programming languages, for example on the web of Vallado (2013), which perform such operations.

3.3. PROPOSED METHODS TO INITIALLY DETERMINE THE SATELLITE ORBIT

In Chapter 1, it has been explained which measurements GEOSAR mission will provide in order to determine the satellite orbit. As seen in this chapter, the proposed ARC system will offer range and range-rate measurements.

Escobal (1965) discusses a method of Trilateration. This method utilizes as data the range and range-rate (ρ_i and $\dot{\rho}_i$) of a satellite from a minimum of three observation stations (i.e., $i = 1, 2, 3$) that are in contact with each other. The main requirement is that all these measurements must be obtained at the same time. Trilateration method is exact and yields a precise orbit due to the fact that only geometric principles are involved.

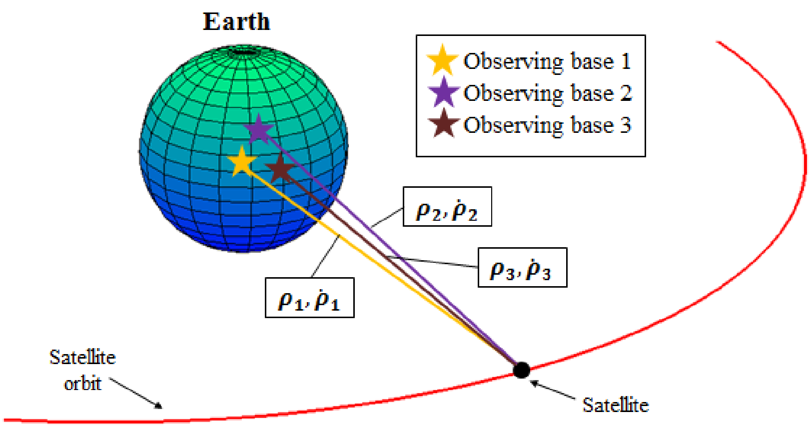

Figure 3.8: *Sketch of Trilateration method.*

The complete algorithm is given in Escobal (1965) so that this document will only show the main inputs and the final outputs that the algorithm uses. Figure 3.8 illustrates the initial conditions of Trilateration method. The algorithm needs the coordinates of each observing base (i.e., the Geodetic latitude[1], ϕ_i, the longitude, λ_i, and the altitude, h_i), and their range and range-rate measurements (ρ_i and $\dot{\rho}_i$). All of these parameters must be provided at a given time, t. Then, by using geometric relationships, the algorithm is capable to obtain a satellite state vector, which is given in the IJK coordinate system (see Figure 3.9).

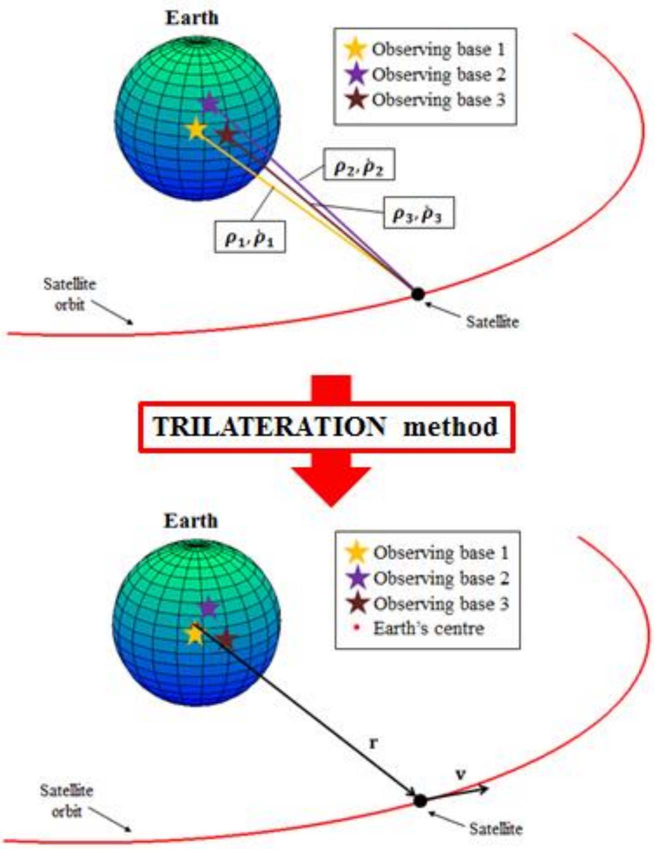

Figure 3.9: *Obtaining the satellite state vector by using Trilateration method.*

It may happen that the observing stations can only provide range measurements. In that case, Trilateration method could also be used to obtain the satellite state vector. If only range measurements of three different observing stations were given, Trilateration method would only provide a position satellite state vector at the time of range measurements. Repeating the same operation at another time, a new position state vector can be obtained, and so forth. There are some methods that calculate a velocity state vector from two or three different position state vectors; however, this document will only use Gibbs method because of its simplicity and geometrical solution. Thus, by using Trilateration and Gibbs methods when range-rate measurements are not available, the satellite state vector may also be obtained. It must be taken into account that Gibbs method fails when the position vectors are closely spaced due to its geometrical solution, so that one must take care of it before implementing Gibbs method.

[1] As it will be seen in Section 3.4a, the model of the Earth that this document will follow is WGS-84. Therefore, variables such as the Earth's equatorial radius, the Earth's flatness, etc., will be taken from this model.

The reader can find the complete explanation of Gibbs method in Bate, Mueller, and White (1971). The Gibbs method needs three nonzero, coplanar position vectors, which represent three time-sequential vectors of a satellite in its orbit. Then, from these three vectors, a velocity vector at the time of the second position vector is calculated. In this way, the satellite state vector is provided (see Figure 3.10).

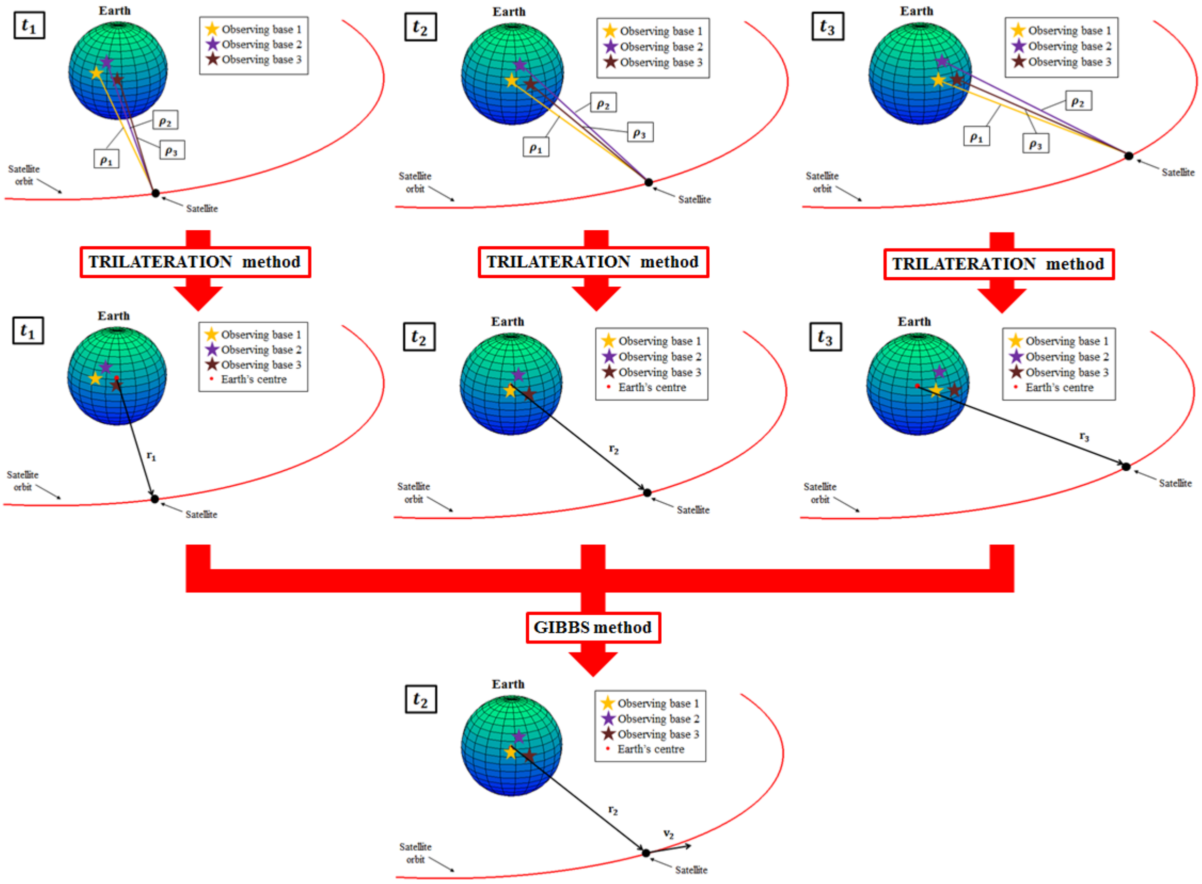

Figure 3.10: *Obtaining the satellite state vector by using Trilateration and Gibbs methods.*

Once the methods to obtain the satellite state vector have been introduced, the next step is to evaluate the precision of these methods. From Chapter 1, it has been explained that the precision expected in GEOSAR mission in order to obtain focused images is in the order of magnitude of the radar wavelength, λ (i.e., $\lambda \approx 3$ cm taking into account the most restrictive case, the X-band). As there are not real measured data available, there is a need to simulate ideal range and range-rate observations in order to assess the suitability of Trilateration and Gibbs methods. In this way, the measurement of precision may be calculated comparing the initial ideal satellite state vector and the one obtained after the implementation of both methods.

In the following sections, it will be explained the methodology used in order to build the ideal observations and the results that will be obtained after using Trilateration and Gibbs methods. Thus, the structure of the following sections can be summarized as follows:

1) Create an ideal simulated satellite orbit.

2) From this simulated orbit, obtain all ideal observations.
3) Do the inverse operation, i.e. obtain the satellite state vector and the satellite orbit from these ideal observations.
4) Obtain the precision comparing both the ideal and retrieved observations.

3.4. OBTAINING THE IDEAL DATA

This section will cover the explanation of how the ideal observations will be calculated. It will start defining the model of the Earth that is going to be used as well as how the time will be computed. Both topics are important in order to place the observing bases over the Earth's surface. Then, this section will define the parameters related to the initial position of the satellite and the position of the observing bases over the Earth's surface. These observing bases will be called sites from now on. Finally, the ideal simulated satellite orbit will be created and all ideal observations will be calculated.

Since GEOSAR orbit determination is required for a short interval of few hours, the satellite orbit will first be modelled based on the unperturbed two-body problem. The possible impact of perturbations from third bodies, atmospheric drag, solar radiation pressure, etc. is left for a future extension of this analysis.

a) The Earth Model

This document will follow WGS-84[1] in order to define the Earth's size, shape, and gravity and geomagnetic fields. WGS-84 defines four parameters, which are listed in Table 3.1.

WGS-84		
Parameter	**Notation**	**Value**
Semi-major axis (Equatorial Earth's radius)	a (R_{eq})	$6\,378.137\ \text{km}$
Flattening of the Earth	$\frac{1}{f}$	$\frac{1}{298.257\,223\,563}$
Earth's mean angular rotation	$\omega_{\oplus}$	$7.292\,115 \times 10^{-5}\ \frac{\text{rad}}{\text{s}}$
Earth's gravitational parameter	μ	$398\,600.441\,8\ \frac{\text{km}^3}{\text{s}^2}$

Table 3.1: *Defining parameters of WGS-84.*

The Earth is not a perfect geometric sphere. In order to increase the accuracy of the calculations, a model for the geometric shape of the Earth must consequently be adopted. WGS-

[1] WGS-84 is an Earth-Centred, Earth-Fixed terrestrial reference system and geodetic datum. WGS84 is the standard U.S. Department of Defence definition of a global reference system for geospatial information and is the reference system for the Global Positioning System (GPS). It is compatible with the International Terrestrial Reference System (ITRS).

84 defines the shape of the Earth as an oblate spheroid[1] whose semi-major axis and flattening[2] values are listed in Table 3.1. The Earth's mean angular rotation, $\omega_{\oplus}$, will be assumed to be constant and will be used when computing time between the ECI and ECEF coordinate systems. Finally, the Earth's gravitational parameter, μ, has previously been defined in section 3.2 and it will be needed, for example, to compute the COE when the satellite state vector is known.

After describing the shape of the Earth, the location of different sites over the Earth's surface can now be explained. Remember that three sites are needed in order to compute the satellite state vector, so that the parameters in order to locate a site over the Earth's surface must be described.

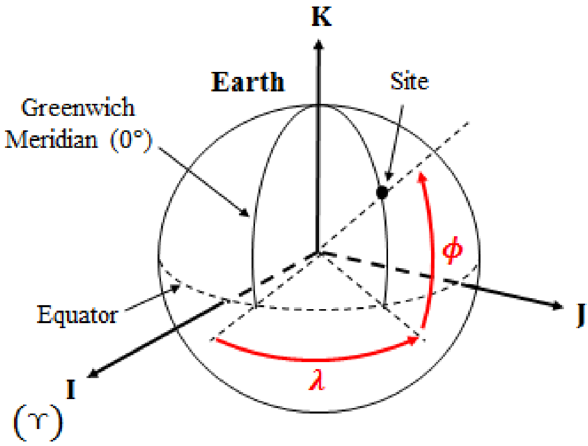

Figure 3.11: *Longitude, λ, and geodetic latitude, ϕ.*

First, one must know the longitude, λ, of the site. The longitude is defined as the east-west angular displacement measured positive to the east from a primary meridian[3] in a plane (see Figure 3.11). The second parameter needed is the geodetic latitude, ϕ, of the site. The geodetic latitude is the angle between the equatorial plane and the normal to the surface of the ellipsoid. One must be careful not to confuse this angle with the geocentric latitude, ϕ_{gc}, which is the angle measured at the Earth's centre from the plane of the equator to the point of interest. Figure 3.12 illustrates the difference between both angles. Finally, the third parameter is the height, h, above the ellipsoid. By means of these three parameters, one may calculate the Cartesian coordinates of any site located over the Earth's surface in an ECEF system following Equations (3.6).

$$r_{x_{\mathrm{ECEF}}} = \left(\frac{R_{\mathrm{eq}}}{\sqrt{1 - e_{\oplus}^2 \sin^2(\phi)}} + h\right)\cos(\phi)\cos(\lambda)$$
$$r_{y_{\mathrm{ECEF}}} = \left(\frac{R_{\mathrm{eq}}}{\sqrt{1 - e_{\oplus}^2 \sin^2(\phi)}} + h\right)\cos(\phi)\sin(\lambda) \tag{3.6}$$

[1] Oblate spheroids result from the revolution of an ellipse around its minor axis.
[2] The flattening is a parameter related to the eccentricity of the ellipsoid of revolution.
[3] The primary meridian for the Earth is the Greenwich meridian whose longitude is 0°.

$$r_{z_{\mathrm{ECEF}}} = \left(\frac{R_{\mathrm{eq}}(1 - e_{\oplus}^2)}{\sqrt{1 - e_{\oplus}^2 \sin^2(\phi)}} + h \right) \sin(\phi)$$

The parameter $e_{\oplus}$ is the eccentricity of the Earth whose value is related to the flattening of the Earth via Equation (3.7).

$$e_{\oplus} = \sqrt{2\frac{1}{f} - \left(\frac{1}{f}\right)^2} \tag{3.7}$$

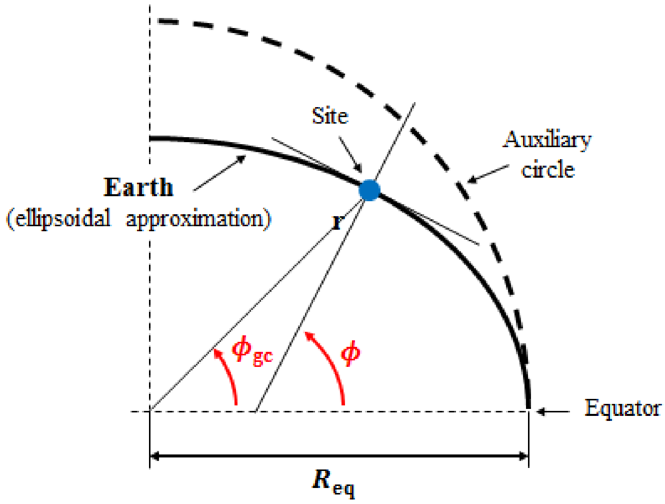

Figure 3.12: *Geodetic latitude, ϕ, vs. Geocentric latitude, ϕ_{gc}.*

b) Time

The moment of a phenomenon must be defined precisely. This moment will be called the epoch of the event and will designate a particular instant described as a date. Nowadays, there are four time scales providing timekeeping for scientific, engineering, and general purposes: sidereal time, solar (universal time), dynamical time, and atomic time. The complexity on determining the epoch of an event will be simplified within this document by using the sidereal time as follows.

Sidereal time is a direct measure of the Earth's rotation and it is measured positively in the anti-clockwise direction when viewed from the North Pole. Specifically, the sidereal time will be defined as the hour angle of the vernal equinox relative to the local meridian. Since the vernal equinox is the reference point, the sidereal time associated with the Greenwich meridian is termed Greenwich Mean Sidereal Time (GMST), θ_{GMST}. The sidereal time at a particular longitude is called Local Sidereal Time (LST), θ_{LST}. In this context, time is an angle measured from the observer's longitude to the equinox (see Figure 3.13).

The conversion between GMST and LST at a particular longitude, λ, can be performed by means of Equation (3.8).

$$\theta_{\mathrm{LST}} = \theta_{\mathrm{GMST}} + \lambda \tag{3.8}$$

This formula requires a convention for east and west longitudes. The convention for this document is positive for east longitudes, and negative for west longitudes. Remember that the vernal equinox direction will be considered fixed into this document, as precession is not taken into account. Thus, the local sidereal time will provide the exact longitudes of each site in the ECI coordinate system, IJK. Equations (3.6) may consequently be reformulated now considering the LST. In this way, the ECI Cartesian coordinates of any site over the Earth's surface can now be obtained via Equations (3.9).

$$r_I = \left(\frac{R_{\mathrm{eq}}}{\sqrt{1 - e_{\oplus}^2 \sin^2(\phi)}} + h\right)\cos(\phi)\cos(\theta_{\mathrm{LST}})$$

$$r_J = \left(\frac{R_{\mathrm{eq}}}{\sqrt{1 - e_{\oplus}^2 \sin^2(\phi)}} + h\right)\cos(\phi)\sin(\theta_{\mathrm{LST}}) \tag{3.9}$$

$$r_K = \left(\frac{R_{\mathrm{eq}}\left(1 - e_{\oplus}^2\right)}{\sqrt{1 - e_{\oplus}^2 \sin^2(\phi)}} + h\right)\sin(\phi)$$

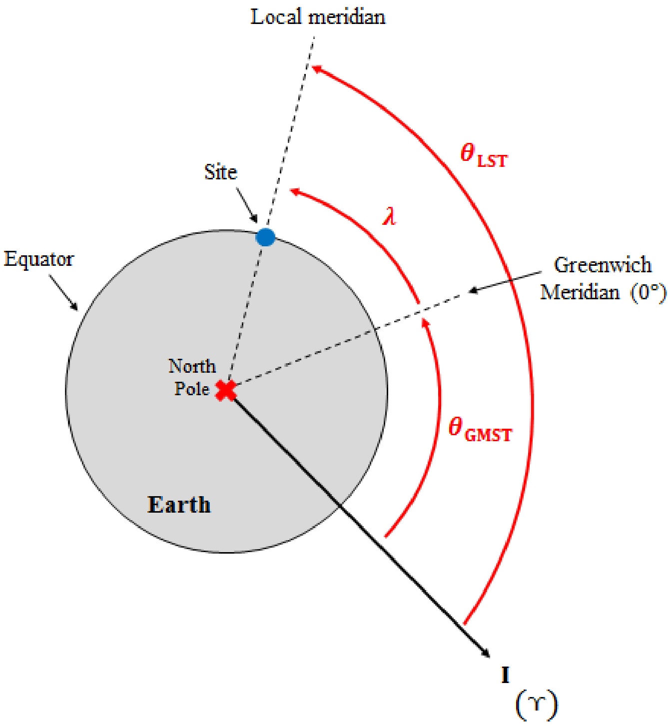

Figure 3.13: *Greenwich Mean Sidereal Time, θ_{GMST}, and Local Sidereal Time, θ_{LST}.*

Equation (3.8) relates LST to GMST but do not provide information of how to calculate GMST. The GMST will be defined as follows:

$$\theta_{\mathrm{GMST}}(t) = \theta_{\mathrm{GMST\ 0h}} + \omega_{\oplus} t \qquad (3.10)$$

where $\theta_{\mathrm{GMST\ 0h}}$ is the Greenwich Mean Sidereal Time at 0 h in radians or degrees, $\omega_{\oplus}$ is the Earth's mean angular rotation in radians per second or degrees per second, and t will be the elapsed time from the initial epoch (i.e., $\theta_{\mathrm{GMST\ 0h}}$).

In this way, setting an initial value to $\theta_{\mathrm{GMST\ 0h}}$, and knowing the location parameters of each site (i.e., λ, ϕ, and h), one will be able to calculate the ECI Cartesian coordinates of the site at different epochs by means of changing the values of the variable t.

Now, the location parameters of each site may be defined. Remember that an ideal orbit must be created, so that the initial location of the satellite must also be described. Then, from the satellite-sites locations, the ideal range and range-rate observations will be obtained.

c) Satellite Parameters

The initial satellite parameters that are going to be used in order to create the satellite orbit are listed in Table 3.2. The term "initial" refers to the fact that the satellite orbit will not describe a perfect circular orbit, so that the satellite longitude will slightly vary over time when an ECEF coordinate system is considered. Having mentioned this fact, the initial satellite longitude chosen is 19.2° E, which is related to a longitude of one of the satellites of SES ASTRA company. On the other hand, the ideal simulated satellite orbit will be completely equatorial. Thus, the geodetic latitude will be 0° all the time.

SATELLITE PARAMETERS		
Parameter	**Notation**	**Value**
Initial longitude	λ_{sat}	$19°\ 12'\ 0.0''$ E ≈ 0.335 rad
Geodetic latitude	ϕ_{sat}	$0°\ 0'\ 0.0'' = 0.0$ rad

Table 3.2: *Satellite parameters.*

d) Site Parameters

Three sites are needed in order to calculate the satellite state vector from range and range-rate observations. These three sites have been chosen accordingly to places where the ARCs of GEOSAR mission might be located. Thus, Barcelona (Spain), Betzdorf (Luxemburg), and Milan (Italy) are places that fulfil such requirement and complete the main configuration of this document. The specific location parameters of these places are listed in Table 3.3. In addition, all these sites are placed in a map in red colour (see Figure 3.14) in order to have a better overview of their locations.

As Trilateration method is geometric, it will also be studied how the separation of the sites affects to the satellite state vector calculation. For this reason, a second configuration, which includes specific locations of Las Palmas de Gran Canaria (Spain), Reykjavik (Iceland), and Ankara (Turkey) have also being added in Table 3.3 and Figure 3.14 (yellow colour) despite not being under the proposed satellite L-band beam coverage.

Finally, it has also been listed other specific locations of different places of Europe in order to evaluate the errors in the range and range-rate observations when either the main or the second configurations are chosen. This third group of places has been plotted in purple in Figure 3.14.

SITE LOCATION PARAMETERS				
Map number	**Site**	**Longitude (λ_i)**	**Geodetic latitude (ϕ_i)**	**Height (h_i)**
01	Barcelona (Spain)	$2°\ 9'\ 20.0''$ E (≈ 0.038 rad)	$41°\ 23'\ 20.0''$ N (≈ 0.722 rad)	0.020 km
02	Betzdorf (Luxemburg)	$6°\ 19'\ 47.8''$ E (≈ 0.110 rad)	$49°\ 41'\ 34.6''$ N (≈ 0.867 rad)	0.288 km
03	Milan (Italy)	$9°\ 9'\ 56.3''$ E (≈ 0.160 rad)	$45°\ 30'\ 19.9''$ N (≈ 0.794 rad)	0.120 km
04	Las Palmas de Gran Canaria (Spain)	$15°\ 25'\ 41.1''$ W (≈ -0.269 rad)	$28°\ 7'\ 59.4''$ N (≈ 0.491 rad)	0.000 km
05	Reykjavik (Iceland)	$21°\ 49'\ 3.6''$ W (≈ -0.381 rad)	$64°\ 7'\ 29.7''$ N (≈ 1.119 rad)	0.000 km
06	Ankara (Turkey)	$32°\ 41'\ 46.9''$ E (≈ 0.571 rad)	$39°\ 44'\ 33.8''$ N (≈ 0.694 rad)	0.020 km
07	Bern (Switzerland)	$7°\ 27'\ 1.7''$ E (≈ 0.130 rad)	$46°\ 56'\ 52.0''$ N (≈ 0.819 rad)	0.540 km
08	Lisbon (Portugal)	$9°\ 8'\ 36.2''$ W (≈ -0.160 rad)	$38°\ 42'\ 38.1''$ N (≈ 0.676 rad)	0.040 km
09	London (United Kingdom)	$0°\ 7'\ 41.3''$ W (≈ -0.002 rad)	$51°\ 30'\ 29.6''$ N (≈ 0.899 rad)	0.035 km
10	Berlin (Germany)	$13°\ 22'\ 43.4''$ E (≈ 0.234 rad)	$52°\ 30'\ 59.2''$ N (≈ 0.917 rad)	0.034 km
11	Warsaw (Poland)	$21°\ 0'\ 44.0''$ E (≈ 0.367 rad)	$52°\ 14'\ 58.8''$ N (≈ 0.912 rad)	0.100 km
12	Athens (Greece)	$23°\ 43'\ 36.3''$ E (≈ 0.414 rad)	$37°\ 58'\ 17.0''$ N (≈ 0.663 rad)	0.100 km

Table 3.3: *Location parameters of each site.*

Once the initial satellite parameters and the location parameters of each site have been described and the theoretical bases have been explained, let us define the ideal simulated satellite orbit and obtain the ideal range and range-rate observations.

e) Ideal Simulated Satellite Orbit

A geostationary orbit must be circular ($e = 0$), equatorial ($i = 0$) and a satellite orbiting this kind of orbit must have a period of one sidereal day. A sidereal day is defined as the time between successive transits of the stars over a particular meridian. The reader should not confuse sidereal time with solar time, which is defined as the time between successive transits of the Sun over a particular meridian. Figure 3.15 shows the difference between both times. Thus, one sidereal day has $23^{\mathrm{h}}\ 56^{\mathrm{m}}\ 4.09^{\mathrm{s}}$ whereas a solar day has 24^{h}.

However, as seen in the example of Section 2.4, the geostationary satellite does not perfectly match a geostationary orbit since the orbit described by the satellite has a slight eccentricity and inclination. For this reason, the satellite must be relocated in order not to escape from the geostationary orbit from time to time.

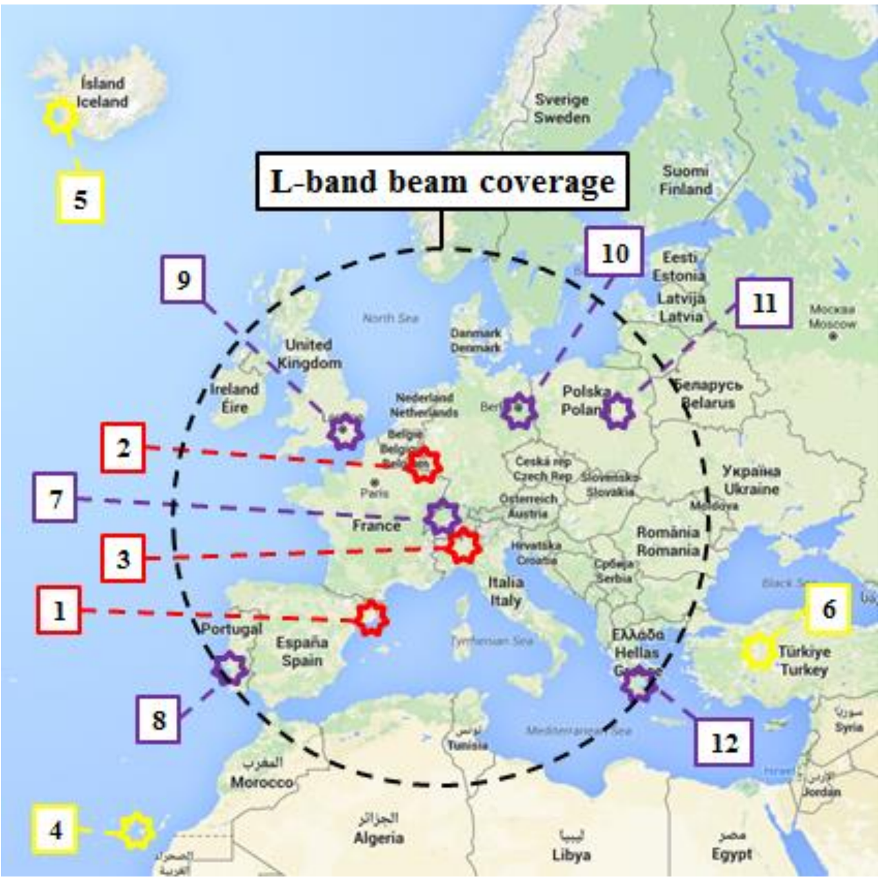

Figure 3.14: *Sites location.*

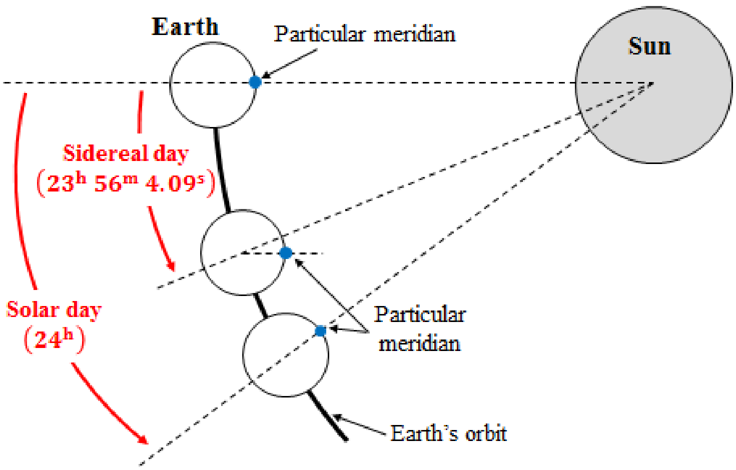

Figure 3.15: *Sidereal day vs. Solar day (exaggerated view).*

The ideal simulated satellite orbit that is going to be created will have a slight eccentricity ($e = 2.0 \times 10^{-4}$), so that the synthetic aperture may be performed. In addition, it will be perfectly equatorial ($i = 0.0$ rad) and it will have a period of one sidereal day. From this initial point, let us define the remaining orbital elements in order to complete the element set of classical orbital elements.

The period, T, of a satellite orbit is related to the semi-major axis, a, via Equation (3.11).

$$T = 2\pi \sqrt{\frac{a^3}{\mu}} \tag{3.11}$$

Isolating a from Equation (3.11), one can obtain the value of the semi-major axis as follows

$$a = \left(\left(\frac{T}{2\pi}\right)^2 \mu\right)^{1/3} = \left(\left(\frac{(23 \times 3600 + 56 \times 60 + 4.09)\ \mathrm{s}}{2\pi}\right)^2 \times 398\,600.441\,8\ \frac{\mathrm{km}^3}{\mathrm{s}^2}\right)^{1/3} =$$

$$= 42\,164.169\ \mathrm{km}$$

Then, the semi-latus rectum, p, can be calculated via Equation (3.1)

$$p = a(1 - e^2) = 42\,164.169\ \mathrm{km} \times (1 - (2 \times 10^{-4})^2) = 42\,164.168\ \mathrm{km}$$

As the orbit has been defined as perfectly equatorial, the angles right ascension of the ascending node, Ω, argument of perigee, ω, and argument of latitude, u, will remain undefined. In order to calculate the true anomaly, ν, and the true longitude of perigee, $\tilde{\omega}_{\mathrm{true}}$, the perigee point of the orbit must be defined. Let us put the perigee point on the intersection between the satellite orbit and the axis I of the ECI coordinate system. Thus, the value of the true longitude of perigee is

$$\tilde{\omega}_{\mathrm{true}} = 0.0\ \mathrm{rad}$$

Now, the initial epoch of the entire system must also be defined in order to find the value of the true anomaly. Let us consider the initial epoch called t_0 and its value be

$$t_0 = 00{:}00{:}00\ \mathrm{h} = 0\ \mathrm{s}$$

At this initial epoch, it is defined that the Greenwich meridian match the direction of the axis I, so that $\theta_{\mathrm{GMST\ 0h}} = 0.0$ rad, and therefore $\theta_{\mathrm{GMST}}(t_0) = 0.0$ rad. In this case, the true anomaly at t_0, i.e. ν_0, is defined equal to the initial satellite longitude, λ_{sat}.

$$\nu_0 = \lambda_{\mathrm{sat}} = 0.335\ \mathrm{rad} = 19.2°$$

Note the use of the subscript 0 in order to define the epoch t_0 of the true anomaly. As the value of the true anomaly changes along the period of the satellite orbit, it must be clarified the epoch where ν is given. This also happens to other orbital elements such as u, λ_{true}, E, or M.

Finally, the last orbital element needed to complete the element set is the true longitude at t_0, $\lambda_{\mathrm{true}_0}$. It can be calculated following one of the expressions of Equation (3.4).

$$\lambda_{\text{true}_0} = \tilde{\omega}_{\text{true}} + \nu_0 = \lambda_{\text{sat}} = 0.335 \text{ rad} = 19.2°$$

Table 3.4 summarizes all COE computed from the ideal satellite orbit at epoch t_0. This table also highlights those orbital elements that can be used, as an element set, to compute all points of the satellite orbit. The procedure to obtain these points is as follows: a) calculate the satellite state vector from this initial element set (see Section 3.2), b) change the value of ν and recalculate the satellite state vector using this new value of ν, and c) repeat b) until completing one revolution of the values of ν (i.e., from 0 to 2π rad). These steps are correct because the system used fulfills a two-body problem and no perturbations have been taken into account. Vallado (2013) provides further information when perturbations are considered. Figure 3.16 illustrates the ideal simulated satellite orbit obtained by using the classical orbital elements of Table 3.4.

COE OF THE IDEAL SIMULATED SATELLITE ORBIT AT t_0		
Orbital element	**Notation**	**Value**
Semi-major axis	a	42 164.169 km
Eccentricity	$\boldsymbol{e}$	$\mathbf{2.0 \times 10^{-4}}$
Semi-latus rectum	$\boldsymbol{p}$	$\mathbf{42\,164.168}$ **km**
Inclination	$\boldsymbol{i}$	$\mathbf{0.0}$ **rad** $(\mathbf{0.0°})$
Right ascension of the ascending node	Ω	undefined
Argument of perigee	ω	undefined
True anomaly	$\boldsymbol{\nu_0}$	$\mathbf{0.335}$ **rad** $(\mathbf{19.2°})$
True longitude of perigee	$\boldsymbol{\tilde{\omega}_{\text{true}}}$	$\mathbf{0.0}$ **rad** $(\mathbf{0.0°})$
Argument of latitude	u_0	undefined
True longitude	$\boldsymbol{\lambda_{\text{true}_0}}$	$\mathbf{0.335}$ **rad** $(\mathbf{19.2°})$

Table 3.4: *COE computed for the ideal simulated satellite orbit (in bold, the element set).*

In order to conclude the definition of the ideal simulated satellite orbit, the relationship between a particular epoch and the position of the satellite at this particular epoch must be established. In the previous paragraph, it has been described how one may plot the satellite orbit from an element set; however, as true anomaly changes along the satellite orbit, which is the true anomaly value that corresponds at one particular epoch? The location of a satellite in orbit after certain amount of time is so-called Kepler's problem or more generally, propagation.

The simplest way to solve Kepler's problem involves classical orbital elements. In the time between successive positions in the orbit, the only variable to change when no perturbations are included is the true anomaly, ν, or associated parameters for the special orbits (u, $\tilde{\omega}_{\text{true}}$, λ_{true}). Knowing the conversion between the anomalies and the mean motion solved with Kepler's equation (see Equation [3.4]), the individual anomalies can be updated, and then the position and velocity vectors can also be updated. Below, it is shown the procedure in order to solve Kepler's problem via classical orbital elements.

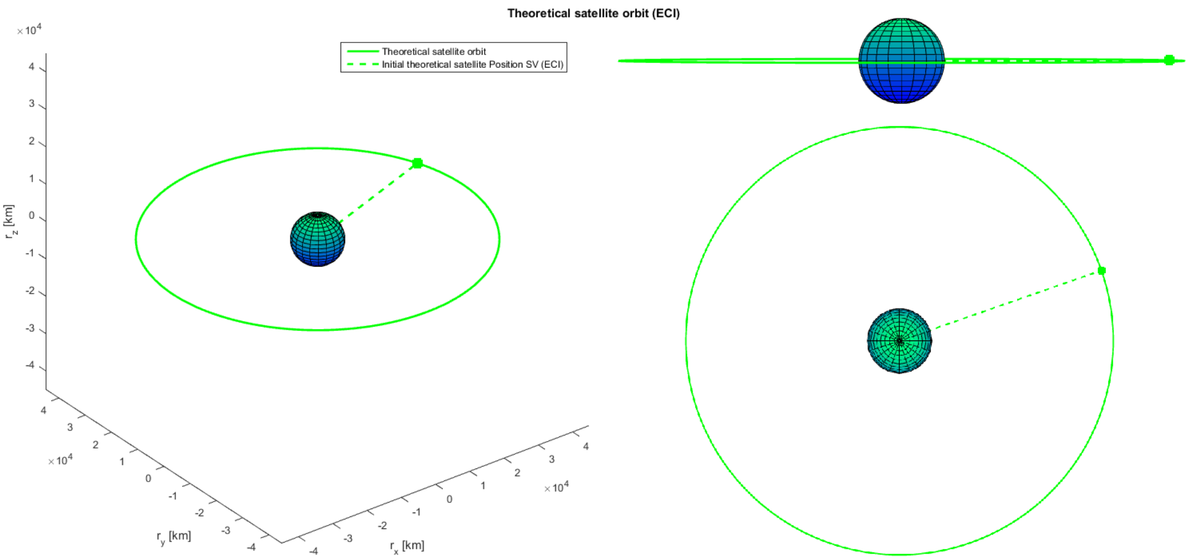

Figure 3.16: *Different views of the ideal simulated satellite orbit around the Earth from COE of Table 3.4.*

First, obtain the COE from the initial satellite state vector. Let us call this initial epoch t_0. Second, calculate the eccentric anomaly at t_0, E_0, via Equations (3.12).

$$\sin(E) = \frac{\sqrt{1-e^2}\sin(\nu)}{1+e\cos(\nu)}$$
$$\cos(E) = \frac{e+\cos(\nu)}{1+e\cos(\nu)} \tag{3.12}$$

One of the two formulas above can be used to find the value of E_0 by using ν_0, taking care of resolving the angle to the proper quadrant. Third, find the mean anomaly at t_0, M_0, via Equation (3.4) (Kepler's equation).

$$M_0 = E_0 - e\sin(E_0)$$

Forth, calculate the mean anomaly at new epoch. Let us call this new epoch t_1, so that the mean anomaly at t_1 is M_1.

$$M_1 = M_0 + n\Delta t$$

Δt corresponds to the elapsed time between the initial and new epochs ($\Delta t = t_1 - t_0$). Fifth, obtain the eccentric anomaly at t_1, E_1, by solving the transcendental operation of Kepler's equation by means of the Newton-Raphson iteration (Equation [3.5]).

$$M_1 = E_1 - e\sin(E_1) \;\Rightarrow\; E_{1_{n+1}} = E_{1_n} + \frac{M_1 - E_{1_n} + e\sin\left(E_{1_n}\right)}{1 - e\cos\left(E_{1_n}\right)}$$

Sixth, find the true anomaly at t_1, ν_1, via one of the two Equations below considering the eccentric anomaly value obtained in the previous step.

$$\sin(\nu) = \frac{\sqrt{1-e^2}\sin(E)}{1-e\cos(E)}$$
$$\cos(\nu) = \frac{\cos(E)-e}{1-e\cos(E)} \tag{3.13}$$

Finally, calculate the satellite state vector at t_1 by using the same classical orbital elements of epoch t_0, but substituting the initial true anomaly, ν_0, by the new value obtained at t_1, ν_1.

All this procedure can be repeated for all epochs where the ideal satellite state vector must be computed. As an example, Figures 3.17 and 3.18 show the evolution that the ideal satellite state vector obtained from Table 3.4 suffers along one orbit (i.e., one sidereal day). This evolution has been depicted for all six Cartesian components forming the satellite state vector in order to have a different view of Figure 3.16.

In this way, the ideal simulated satellite orbit has been completely described. Let us now explain how to obtain the ideal range and range-rate observations from the satellite state vectors in the following sub-section.

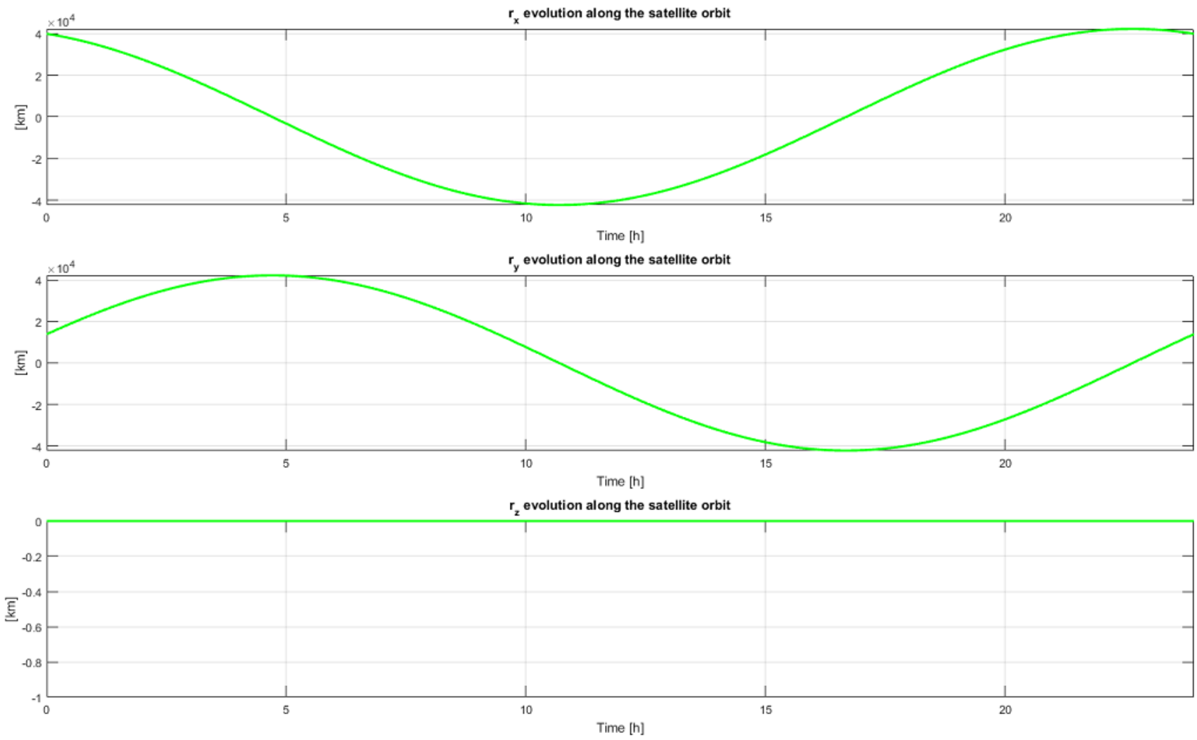

Figure 3.17: *Ideal satellite position state vector evolution along one satellite orbit.*

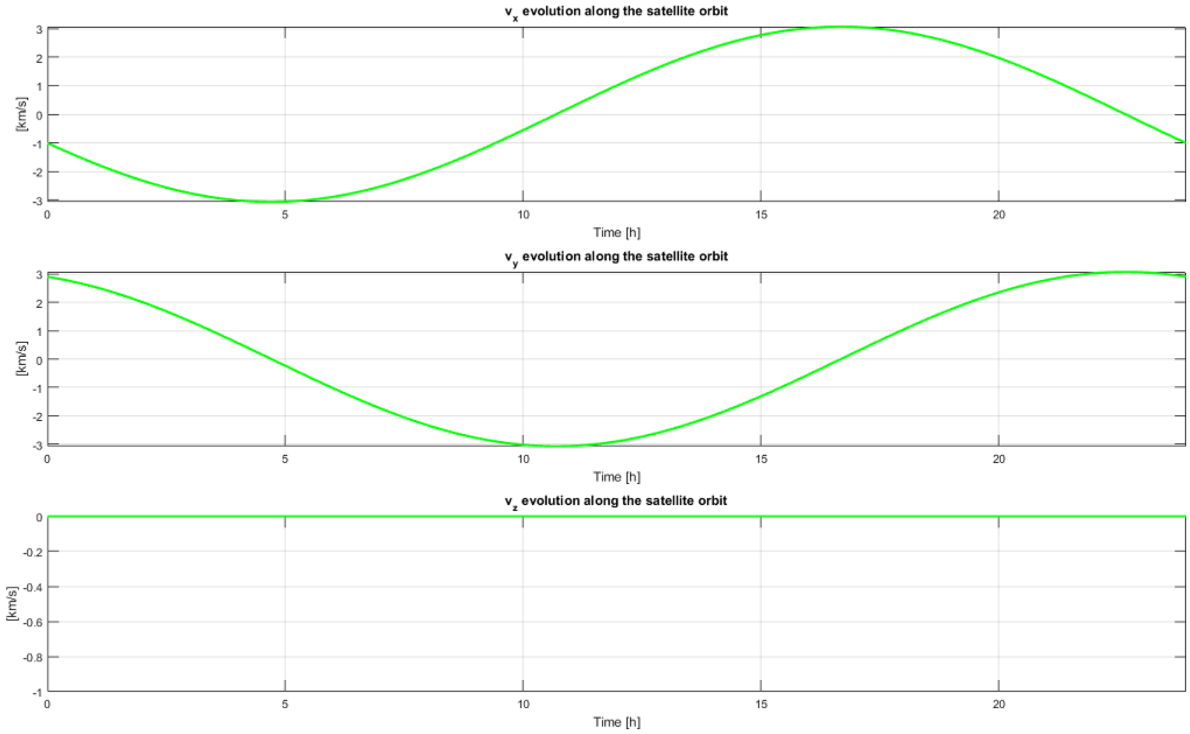

Figure 3.18: *Ideal satellite velocity state vector evolution along one satellite orbit.*

f) Ideal Range and Range-rate Observations

Figure 3.19 illustrates the geometry involved on the range observations computation.

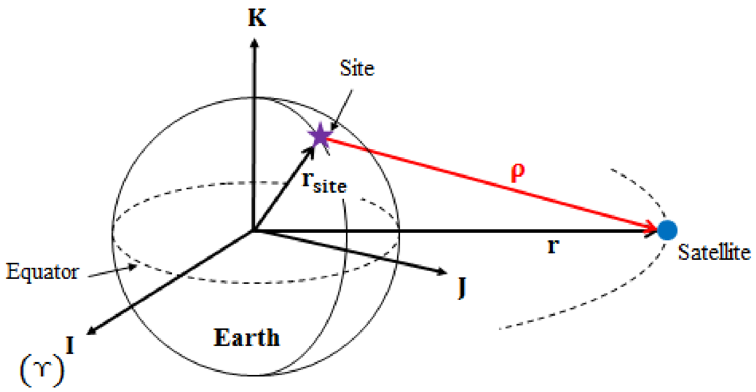

Figure 3.19: *Geometry of range observations computation.*

The ideal range observations of each site, ρ, can be calculated as the Euclidean norm of its corresponding vector range, $\boldsymbol{\rho}$, which is the subtraction between the satellite position state vector, $\mathbf{r}$, and the site position state vector, $\mathbf{r}_{\text{site}}$.

$$\rho = \|\boldsymbol{\rho}\| = \|\mathbf{r} - \mathbf{r}_{\text{site}}\| = \sqrt{\left(r_x - r_{\text{site}_x}\right)^2 + \left(r_y - r_{\text{site}_y}\right)^2 + \left(r_z - r_{\text{site}_z}\right)^2} \qquad (3.14)$$

Having specified an epoch (e.g., $t_0 = 0$ s), the satellite position state vector can be found following the steps of the previous sub-section whereas the site position state vector can be calculated via Equations (3.9). This latter set of equations need both the Local Sidereal Time, θ_{LST}, which can be obtained by using Equation (3.8), and the Greenwich Mean Sidereal Time at t_0, $\theta_{\mathrm{GMST}}(t_0)$, which is calculated via Equation (3.10). Remember that $\theta_{\mathrm{GMST\,0h}}$ has been defined to be equal to 0.0 rad. In this way, all ideal range observations of different sites needed at t_0 can be obtained. Note that the ECI coordinate system is the coordinate system used to provide both $\mathbf{r}$ and $\mathbf{r_{site}}$ vectors.

On the other hand, in order to calculate the ideal range-rate observations, two definitions must be given. First, the range-rate will be defined as the dot product between the relative velocity of the satellite to the site, $\mathbf{v_{rel}}$, and the unit range vector, $\hat{\boldsymbol{\rho}}$ (see Equation [3.15]).

$$\dot{\rho} = \mathbf{v_{rel}} \cdot \hat{\boldsymbol{\rho}} = \mathbf{v_{rel}} \cdot \frac{\boldsymbol{\rho}}{\rho} \tag{3.15}$$

Second, $\mathbf{v_{rel}}$ will be defined as

$$\mathbf{v_{rel}} = \mathbf{v} - \mathbf{v_{site}} \tag{3.16}$$

where $\mathbf{v}$ is the satellite velocity state vector, and $\mathbf{v_{site}}$ is the site velocity state vector. Both vectors are given in the ECI coordinate system. $\mathbf{v}$ can be calculated following the steps of the previous sub-section whereas $\mathbf{v_{site}}$ can be obtained via Equation (3.17),

$$\mathbf{v_{site}} = \omega_{\oplus} \begin{bmatrix} -r_J \\ r_I \\ 0 \end{bmatrix} \tag{3.17}$$

where $\omega_{\oplus}$ is the Earth's mean angular rotation (see Table 3.1) and the r components are obtained from Equations (3.9). Thus, the relative velocity can be defined as the satellite velocity in an ECEF coordinate system. Figure 3.20 shows all the geometry involved in the range-rate observations computation in order to clarify all equations used.

In addition, Figures 3.21 and 3.22 illustrate the ideal range and range-rate histories respectively that, for example, the Barcelona location will provide from the ideal simulated satellite orbit created. Thus, one may have an overview of the shape and order of magnitude of range and range-rate curves along time. Both figures start at epoch $t_0 = 0$ s and last one satellite orbit.

At this point, all theoretical bases and ways to obtain the ideal parameters have already been explained. This ideal system may now provide valuable information of how Trilateration and Gibbs methods work. The following sections analyse both methods, first from the ideal range and range-rate observations, and, second, adding noise to these ideal observations. This latter step will show a more real case of the precision obtained by using both methods.

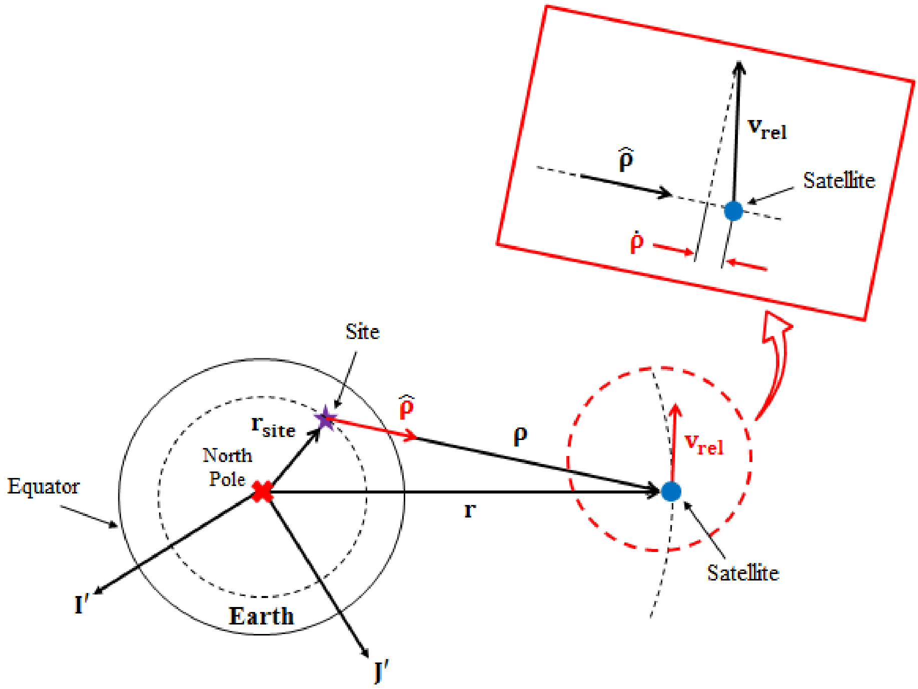

Figure 3.20: *Geometry of range-rate observations computation.*

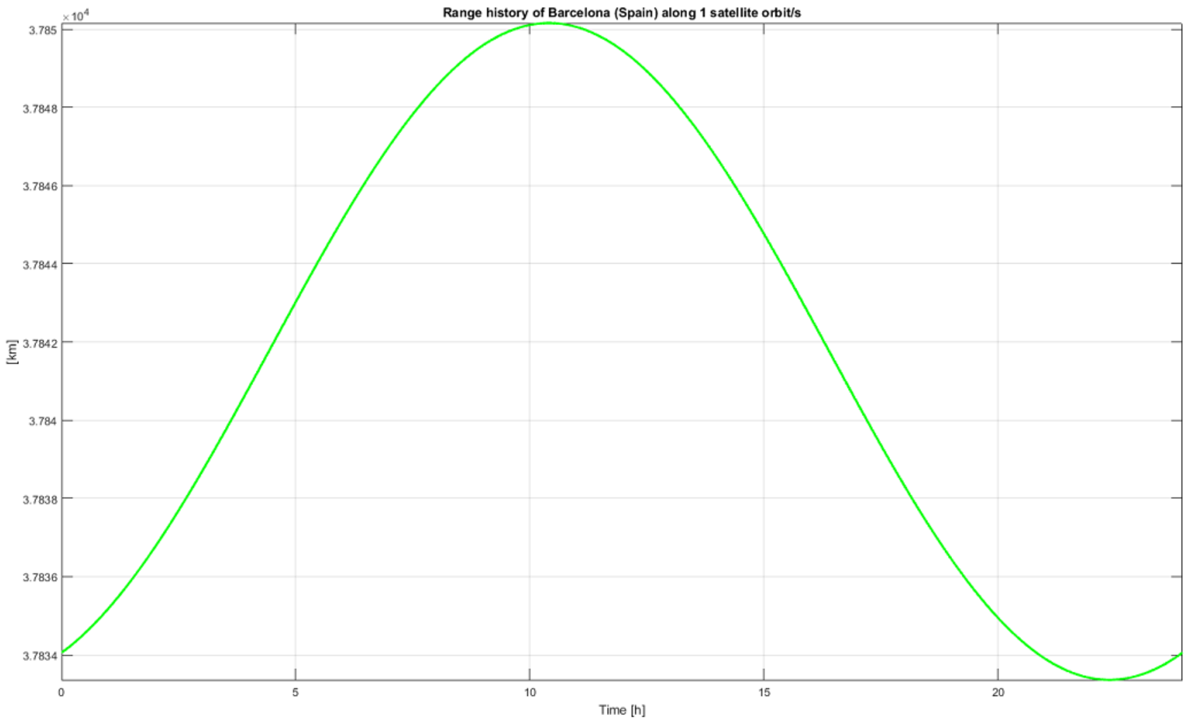

Figure 3.21: *Ideal range history of Barcelona location along one satellite orbit.*

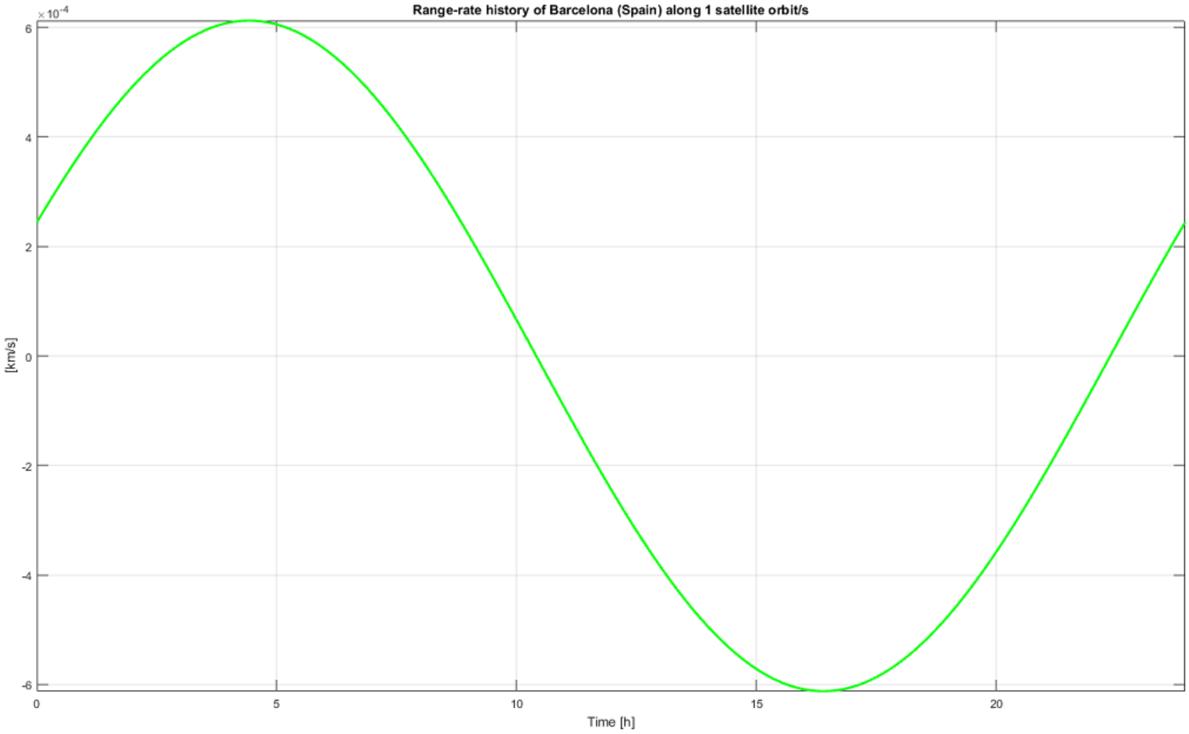

Figure 3.22: *Ideal range-rate history of Barcelona location along one satellite orbit.*

3.5. TRILATERATION AND GIBBS METHODS ANALYSES

As commented in section 3.2, Trilateration method may calculate a satellite state vector, which will be called approximate satellite state vector from now on, from range and range-rate observations of three different sites at the same epoch. It has also been explained that if only range observations were available, the approximate satellite state vector would be provided from range observations of three different sites at three different epochs by using both Trilateration and Gibbs methods.

This section will analyse the results obtained in both cases taking into account that Gibbs method will fail if consecutive range observations are given in two epochs that are very close in time (i.e., a few seconds of difference). Thus, as GEOSAR mission may need long integration times in order to obtain higher resolution images (i.e., $4-6$ h), epochs distanced $9\,000$ s will be used when range observations are only given.

Table 3.5 summarizes all conditions taken into account when the simulation of both cases (settings) has been run. The reader may consult Appendix A for further information about all Matlab functions used to perform such simulations.

The important thing when evaluating all settings is their precision, especially in the range history. Thus, considering the worst case of GEOSAR mission (i.e., the X-band, $\lambda \sim 3$ cm), the error in range history of each location site under the L-band coverage (see Figure 3.14 and Table 3.3) should be maintained over 3 cm during all synthetic aperture. For this reason, the error will be obtained at two different epochs: a) the initial epoch when the approximate satellite state vector is given, and b) an epoch 6 h later from the initial epoch, t_f. In this way, the errors at the beginning and end of the radar synthetic aperture will be shown. Remember that, on the other hand, autofocus synthetic aperture techniques can be used to refine the range history predicted from the orbital model, so that the precision requirement could be relaxed in the order of magnitude of tens of centimetres.

Setting A	Setting B
Location of the three sites: (01) Barcelona (Spain) (02) Betzdorf (Luxemburg) (03) Milan (Italy)	**Location of the three sites:** (01) Barcelona (Spain) (02) Betzdorf (Luxemburg) (03) Milan (Italy)
IDEAL DATA - **Type of observations generated:** RANGE. - **Epoch/s when the observations are generated:** $t_0 = 0$ s, $t_1 = 9\,000$ s, and $t_2 = 18\,000$ s.	**IDEAL DATA** - **Type of observations generated:** RANGE and RANGE-RATE. - **Epoch/s when the observations are generated:** $t_0 = 0$ s.
APPROXIMATE DATA - **Method/s used:** TRILATERATION and GIBBS. - **Epoch when the approximate satellite state vector is given:** $t_1 = 9\,000$ s.	**APPROXIMATE DATA** - **Method/s used:** TRILATERATION. - **Epoch when the approximate satellite state vector is given:** $t_0 = 0$ s.

Table 3.5: *Summary of all conditions considered on settings A and B.*

The error, ξ, will be calculated following Equation 3.18, so that all interesting approximate values obtained from settings of Table 3.5 will be compared to the ideal ones. As said before, the most important parameters to be compared are range observations[1]; however, the satellite state vector values and their errors will also be studied since they directly affect the determination of range observations. In addition, the range-rate observation values and their errors will also be shown when the evaluated setting uses these observations in order to obtain the initial approximate state vector. Finally, the classical orbital elements values and their errors will also be considered as an alternative view of the satellite state vector.

$$\xi = \text{approximate value} - \text{ideal value} \tag{3.18}$$

The results will be organised in tables that the reader may consult in Appendix B. All values shown in these tables will be presented with many decimal figures in order to better quantify the precision of each setting used. In this section, the main results will be depicted by means of different plots, which will show either the comparison between ideal and approximate values of a specific

[1] The approximate range and range-rate observations can be obtained following section 3.4f once the approximate satellite state vector is calculated.

parameter or the evolution of the errors of one particular parameter. In any case, the results will be plotted along one satellite orbit from the initial epoch of each setting.

a) Results Analysis of Setting A

In this case, plots of errors have been selected since there are no visual differences between ideal and approximate parameters. In this way, Figures 3.23 and 3.24 show the errors on each satellite state vector component, and Figure 3.25 illustrates the error in range history of Barcelona location (one of the sites used to calculate the initial approximate satellite state vector).

As seen from the figures below, the errors in the satellite state vector are quite smooth during the first hours, and then they begin to disturb. This fact affects the errors in range history, which its values are less predictable in the last 12 hours. However, one can see from the tables of Appendix A or from the figures shown here that the order of magnitude of all errors is very small. For example, the errors in range observations of each site evaluated are less than nanometres at t_1 (initial epoch), and less than micrometres at t_f (6 hours after the initial epoch). Therefore, one may conclude that the precision of the whole system when using both Trilateration and Gibbs methods is very high. Remember that all system built is an ideal case where perturbations and noise are not taking into account, so that this precision could be expected.

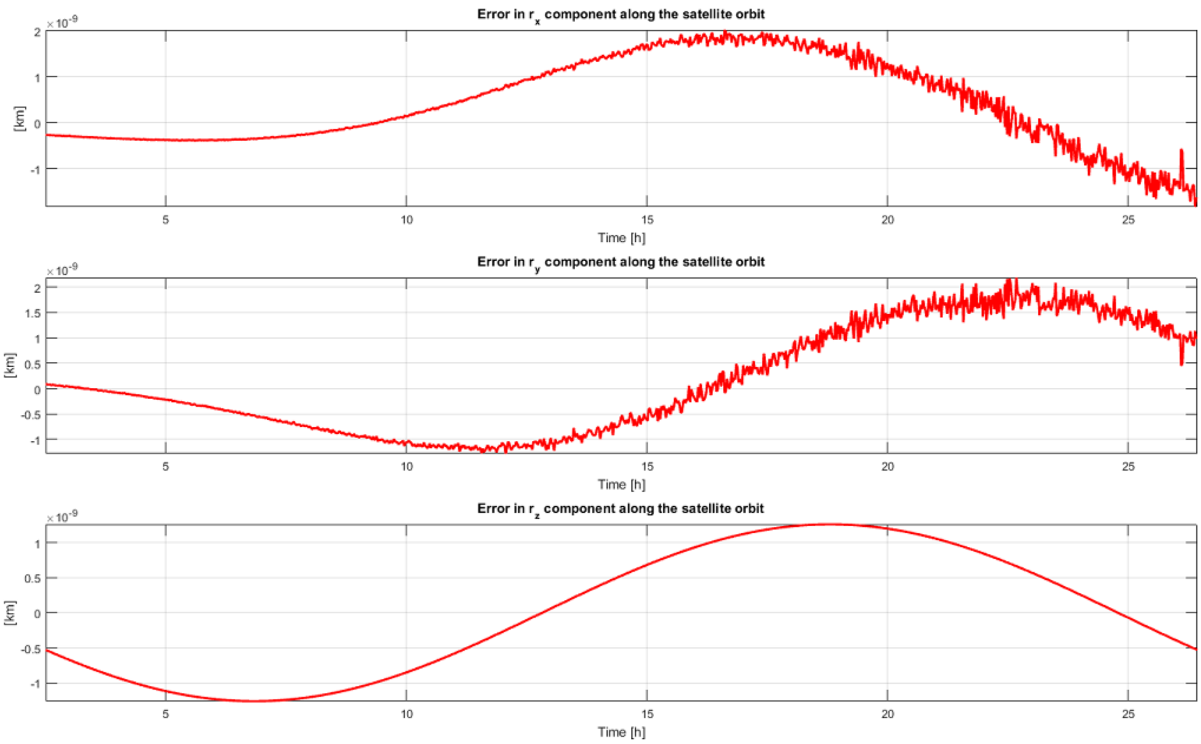

Figure 3.23: *Errors in the satellite position state vector along one satellite orbit (setting A).*

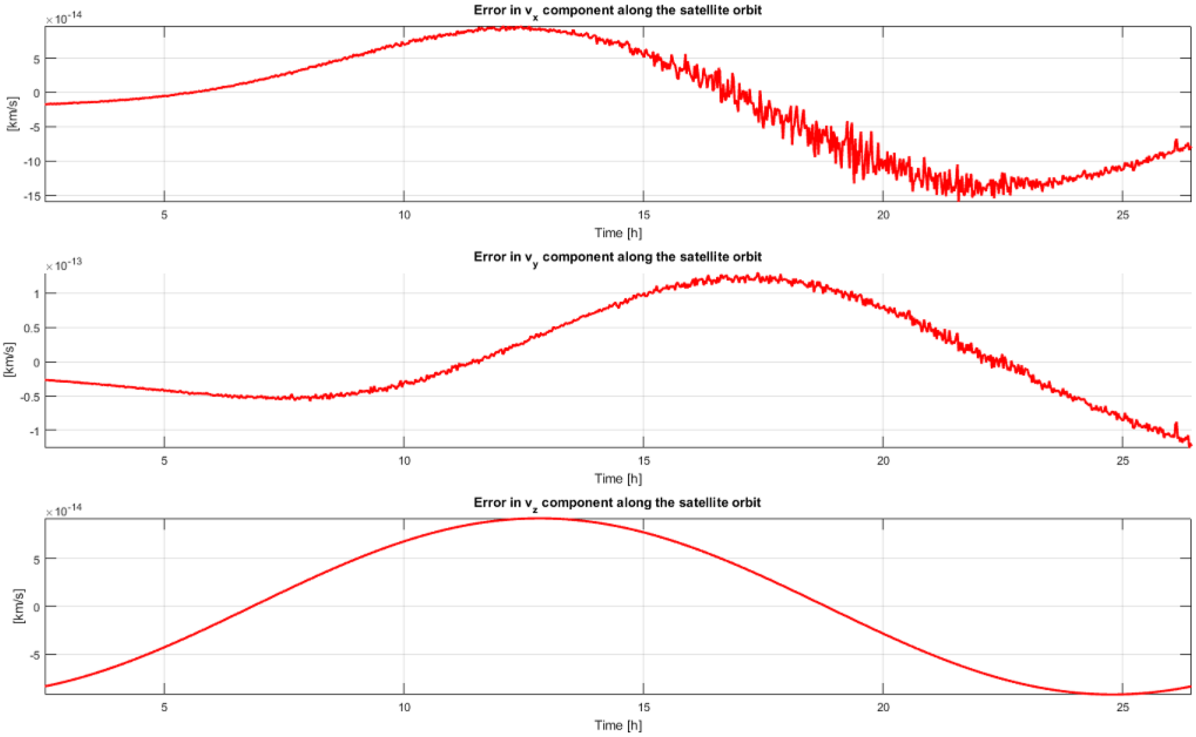

Figure 3.24: *Errors in the satellite velocity state vector along one satellite orbit (setting A).*

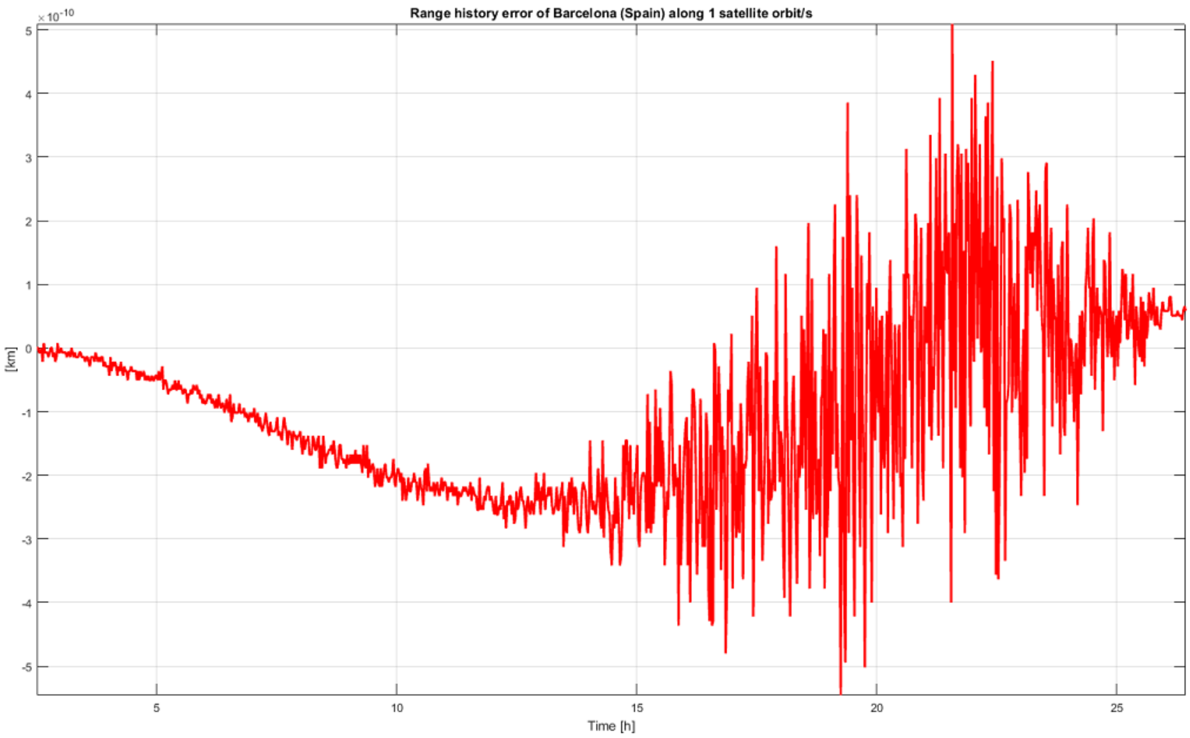

Figure 3.25: *Errors in the range history of Barcelona location along one satellite orbit (setting A).*

b) Results Analysis of Setting B

This setting provides similar order of magnitude errors than setting A, so that the use of ideal range and range-rate observations does not improve the precision of the system obtained in the previous subsection where range observations were only used. In this way, both settings A and B work in a very similar way when perturbations and noise are not considered.

Figure 3.26 illustrates an example of the error in range-rate history of Barcelona location. As seen from the figure, the errors are of the order of magnitude of tens of picometres per second. They are therefore really small.

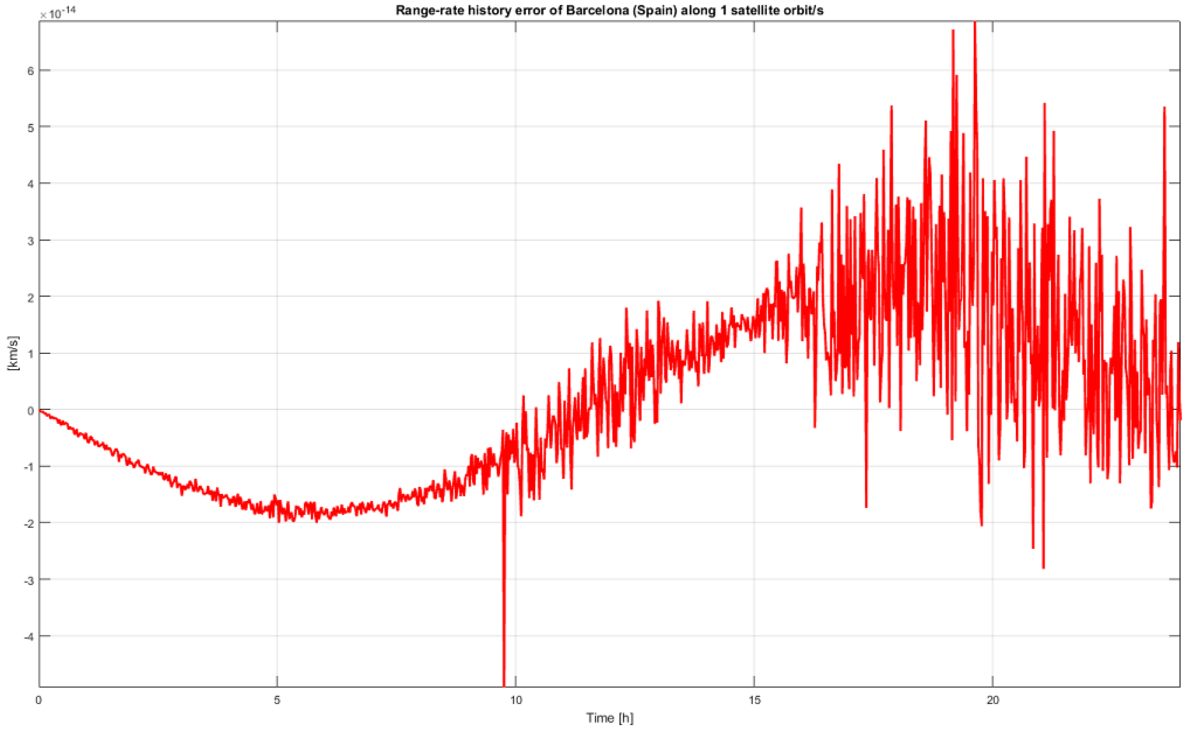

Figure 3.26: *Errors in the range-rate history of Barcelona location along one satellite orbit (setting B).*

Trilateration method alone or combined with Gibbs method almost provides the same and very high precision results when all parameters are considered ideal. As commented before, this is an ideal case that has been useful to evaluate the order of magnitude of errors of all Matlab functions used during both simulations. In order to get closer to reality, let us add noise to the ideal range and range-rate observations and see how the precision of both settings is affected. In this way, the quantity of noise to be added must consequently be calculated. Next section shows how to calculate and what value acquires this noise quantity by using the parameters of GEOSAR mission. After that, section 3.7 will show the new results obtained when adding such noise on ideal range and range-rate observations.

3.6. NOISE OF RANGE AND RANGE-RATE OBSERVATIONS

Levanon (1988) develops the Cramer-Rao lower bounds for both time delay and frequency estimations. From these lower bounds, the standard deviation of range and range-rate observations may be derived. Thus, knowing some specific parameters of GEOSAR mission, one may calculate the quantity of noise to be added to the ideal range and range-rate observations of the previous section. Let us see how these quantities are obtained.

Assuming that the delay measurement is performed after synchronous detection when the signal is at baseband, the Cramer-Rao lower bound for delay estimation can be calculated as

$$\sigma_\tau^2 = \frac{N_0}{2E\beta^2} \tag{3.19}$$

where E/N_0 is the Signal-to-Noise Ratio and β is called the RMS (Root Mean Square) bandwidth, which can be expressed as the Fourier transform of the envelope of the complex signal as

$$\beta^2 = \frac{(2\pi)^2 \int_{-\infty}^{\infty} f^2 |G(f)|^2 df}{\int_{-\infty}^{\infty} |G(f)|^2 df} \tag{3.20}$$

Now, considering a linear FM signal (i.e., the GEOSAR mission case), the Fourier transform of the signal envelope can be approximated by

$$G(f) = \begin{cases} 1, & B/2 \le f \le B/2 \\ 0, & \text{elsewhere} \end{cases}$$

where B is the band-limited width of the signal. Using this $G(f)$ in Equation (3.20), the value of β^2 of a linear FM signal can be obtained as

$$\beta^2 = \frac{(2\pi)^2 \int_{-B/2}^{B/2} f^2 df}{\int_{-B/2}^{B/2} df} = \frac{(2\pi)^2 \left[\frac{f^3}{3}\right]_{-B/2}^{B/2}}{[f]_{-B/2}^{B/2}} = \frac{(2\pi)^2 \left(\frac{B^3}{8} + \frac{B^3}{8}\right)}{3\left(\frac{B}{2} + \frac{B}{2}\right)} = \frac{(2\pi)^2 2B^3}{24B} = \frac{1}{3}\pi^2 B^2$$

which yields the Cramer-Rao lower bound for time delay of a FM signal.

$$\sigma_\tau^2 = \frac{3}{\pi^2 B^2 \left(2\frac{E}{N_0}\right)} \tag{3.21}$$

Knowing that the relation between range resolution, $\Delta\rho$, and time delay, τ, in a radar case can be obtained as

$$\Delta\rho = \frac{c\tau}{2} \tag{3.22}$$

where c is the speed of light, the standard deviation of range measurements, σ_ρ, can consequently be calculated as

$$\sigma_\rho = \sqrt{\sigma_\rho^2} = \sqrt{\frac{c^2}{4}\sigma_\tau^2} = \frac{c}{2}\sqrt{\frac{3}{\pi^2 B^2 \left(2\frac{E}{N_0}\right)}} \tag{3.23}$$

On the other hand, Levanon defines the Cramer-Rao lower bound on frequency estimation as

$$\sigma_{f_D}^2 = \frac{1}{\alpha^2 \left(2\frac{E}{N_0}\right)} \tag{3.24}$$

where E/N_0 is the Signal-to-Noise Ratio and α is called the RMS time duration, which is defined as

$$\alpha^2 = \frac{(2\pi)^2 \int_{-\infty}^{\infty} t^2 |q(t)|^2 dt}{\int_{-\infty}^{\infty} |q(t)|^2 dt} \tag{3.25}$$

where $q(t)$ is the complex representation of the signal. Now, considering the linear FM signal of a single-frequency pulse of duration T and envelope A (i.e., the GEOSAR mission case), the signal envelope $q(t)$ can be approximated by

$$q(t) = \begin{cases} A, & T/2 \leq t \leq T/2 \\ 0, & \text{elsewhere} \end{cases}$$

Substituting this $q(t)$ in Equation (3.25), the value of α^2 of a linear FM signal can be obtained as

$$\alpha^2 = \frac{(2\pi)^2 \int_{-T/2}^{T/2} t^2 A^2 dt}{\int_{-T/2}^{T/2} A^2 dt} = \frac{(2\pi)^2 \left[\frac{t^3}{3}\right]_{-T/2}^{T/2}}{[t]_{-T/2}^{T/2}} = \frac{(2\pi)^2 \left(\frac{T^3}{8} + \frac{T^3}{8}\right)}{3\left(\frac{T}{2} + \frac{T}{2}\right)} = \frac{(2\pi)^2 2T^3}{24T} = \frac{1}{3}\pi^2 T^2$$

which yields the Cramer-Rao lower bound for frequency of a FM signal

$$\sigma_{f_D}^2 = \frac{3}{\pi^2 T^2 \left(2\frac{E}{N_0}\right)} \tag{3.26}$$

As in the previous case, a relation between the frequency Doppler, f_D, and the range-rate, $\dot{\rho}$, must be established. This is done via Equation (3.27),

$$v_\mathrm{r} = -\frac{\lambda}{2} f_D \tag{3.27}$$

where λ is the signal wavelength, and v_r is the radial speed between the radar and the target. Both v_r and $\dot{\rho}$ can be considered the same value. Thus, the standard deviation of range-rate observations, σ_{v_r}, can consequently be calculated as

$$\sigma_{v_\mathrm{r}} = \sqrt{\sigma_{v_\mathrm{r}}^2} = \sqrt{\frac{\lambda^2}{4}\sigma_{f_D}^2} = \frac{\lambda}{2}\sqrt{\frac{3}{\pi^2 T^2 \left(2\frac{E}{N_0}\right)}} \tag{3.28}$$

Once both standard deviations have been defined, let us calculate their value on the particular context of GEOSAR mission. In Casado (2016), all parameters needed to calculate σ_ρ and σ_{v_r} are provided, which are summarized in Table 3.6. It has been considered the worst case, so that all parameters have been selected from the frequency at lower band (i.e., the L-band) and no sub-apertures[1] have been taken into account.

[1] During the processing of the radar signal obtained in all synthetic aperture, it may be considered to process the signal into smaller apertures, called sub-apertures, in order to achieve better performance.

PARAMETERS OF GEOSAR MISSION		
Parameter	**Notation**	**Value**
Frequency (L-band)	f	1.27×10^9 Hz
Signal-to-Noise Ratio	E/N_0	24.8 dB
Bandwidth	B	3.6 MHz
Pulse duration	T	0.763 s

Table 3.6: *Parameters of GEOSAR mission needed to obtain σ_ρ and σ_{v_r}.*

Thus, from parameters of Table 3.6, the standard deviation values of range and range-rate observations yield

$$\sigma_\rho = \frac{c}{2}\sqrt{\frac{3}{\pi^2 B^2 \left(2\frac{E}{N_0}\right)}} = \frac{3 \times 10^8\ \frac{\mathrm{m}}{\mathrm{s}}}{2}\sqrt{\frac{3}{\pi^2 \times (3.6 \times 10^6\ \mathrm{Hz})^2 \times 2 \times 10^{2.48}}} = 0.935\ \mathrm{m}$$

$$\sigma_{v_r} = \frac{\lambda}{2}\sqrt{\frac{3}{\pi^2 T^2 \left(2\frac{E}{N_0}\right)}} = \frac{3 \times 10^8\ \frac{\mathrm{m}}{\mathrm{s}}}{2 \times 1.27 \times 10^9\ \mathrm{Hz}}\sqrt{\frac{3}{\pi^2 \times (0.763\ \mathrm{s})^2 \times 2 \times 10^{2.48}}} = 3.47 \times 10^{-3}\ \frac{\mathrm{m}}{\mathrm{s}}$$

Therefore, the precision of Trilateration and Gibbs methods can now be re-evaluated taking into account both standard deviation values. However, in order to introduce a little margin in the numbers obtained above and work with simpler numbers, let us round σ_ρ and σ_{v_r}, and choose the values of Table 3.7.

STANDARD DEVIATION OF RANGE AND RANGE-RATE OBSERVATIONS		
Parameter	**Notation**	**Value**
Standard deviation of range observations	σ_ρ	1 m
Standard deviation of range-rate observations	σ_{v_r}	$5\ \frac{\mathrm{mm}}{\mathrm{s}}$

Table 3.7: *Standard deviation of range and range-rate observations.*

3.7. TRILATERATION AND GIBBS METHODS ANALYSES ADDING NOISE

This section will analyse how the effect of adding noise to the ideal range and range-rate observations will affect the approximate satellite state vector calculation, and therefore the range values acquisition. This noise will follow a normal distribution with mean equal to 0 for all observations, and standard deviation equal to one of the two values of Table 3.7. In addition, each quantity of noise added to each range and range-rate observation will be different. Thus, for example, the ideal range observation of Barcelona location at epoch t_1 will contain a different quantity of noise that the same observation at epoch t_2 or the range observation of Betzdorf location at epoch t_1. In this way, all samples will be independent of one another. Once the noisy observations have been created, then the approximate satellite state vector will be found and all errors will be computed in the same way as Section 3.5.

Repeating the same simulation different times will provide different results since the noise is randomly added to the observations. For this reason, this section will show the results of only one simulation using the same configuration of setting B (Section 3.5), but with noisy observations. Thus, the reader may have an overview of the effect of adding noise on the initial orbit determination. In order to better quantify the effect of noise, a statistical simulation must be performed. This will be done in the following section.

As in Section 3.5, the reader may consult the numerical results in Appendix B. Here, some plots will be depicted in the following figures showing either the evolution of the errors or the comparison between the ideal and approximate values of one particular parameter along one satellite orbit.

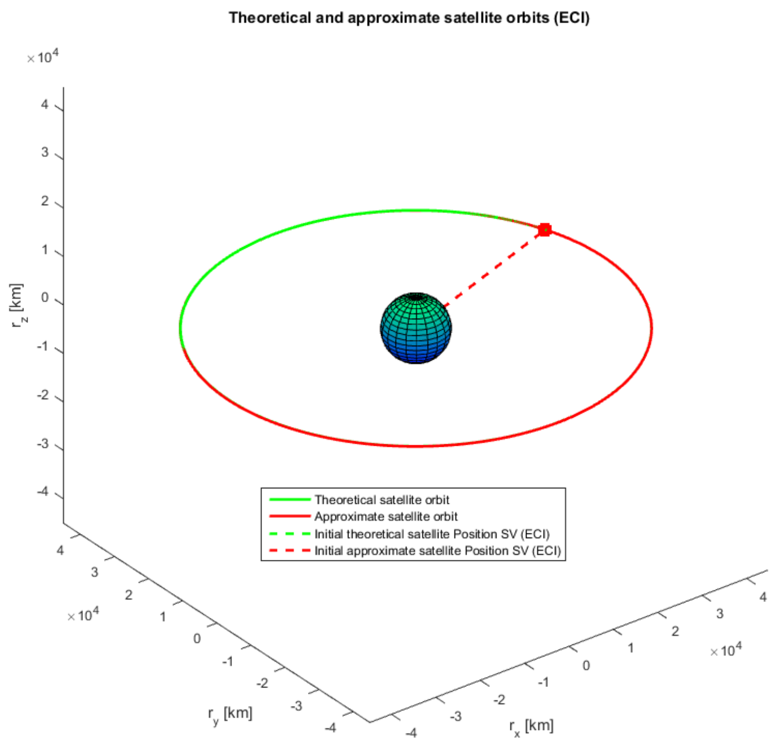

Figure 3.27: *Ideal (in green) and approximate (in red) satellite orbits around the Earth (setting B + noise).*

From Figure 3.27, one can start to differentiate between the ideal (in green) and approximate (in red) satellite orbits. The approximate satellite orbit is no longer strictly equatorial since it has a little inclination (see Table B.12). In addition, the eccentricity value has increased more than four times the ideal value. All of this is due to the fact that the errors in the approximate satellite state vectors are becoming higher. One may also appreciate the magnitude of such errors in Figures 3.28 and 3.29.

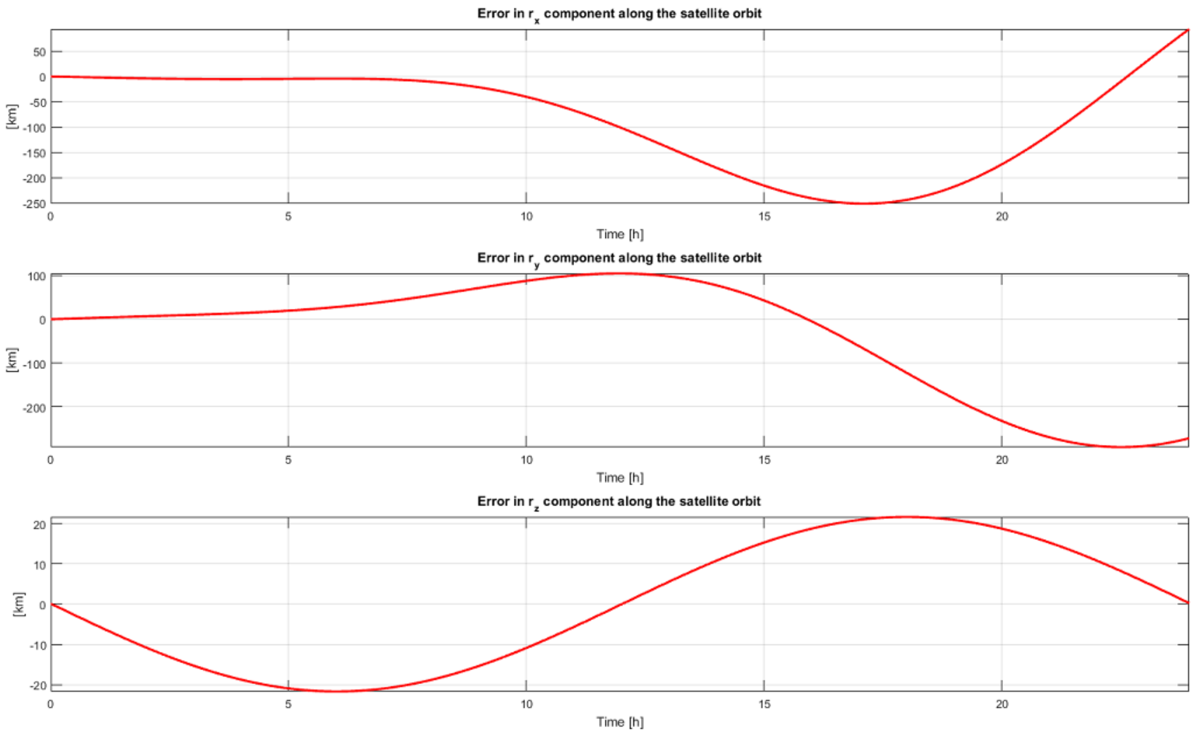

Figure 3.28: *Errors in the satellite position state vector along one satellite orbit (setting B + noise).*

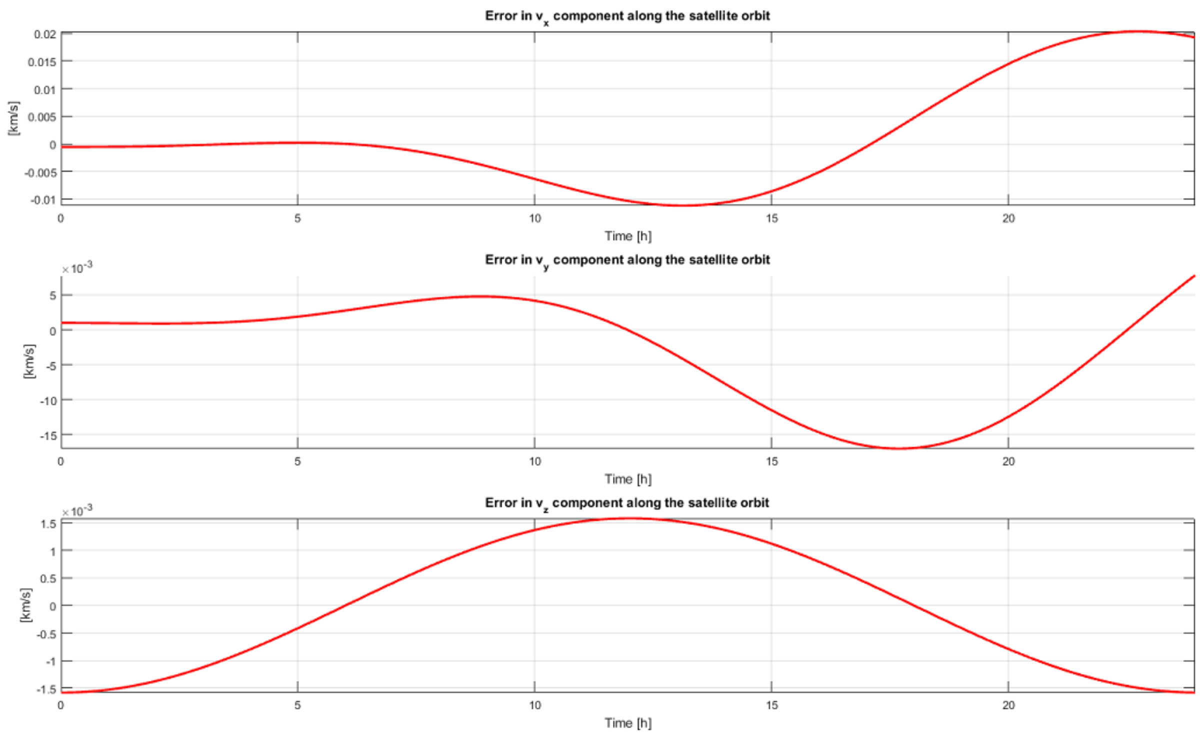

Figure 3.29: *Errors in the satellite velocity state vector along one satellite orbit (setting B + noise).*

At the initial epoch, t_0, the magnitude of the errors between the ideal and approximate satellite position state vectors are of tens and hundreds of metres, whereas, at final epoch, t_f, the magnitude of the errors increases up to tens of kilometres. For the satellite velocity state vector case, the errors are more constant and in the order of magnitude of metres per second. Such errors obviously affect the range history of each site becoming around 1 m at t_0 and reaching the 30 km at t_f (see Appendix B). This fact is illustrated in Figure 3.30, where the ideal and approximate range histories of Barcelona location have been depicted. As seen in this figure, there is a significant difference between both curves mainly due to the difference in the eccentricities of both satellite orbits.

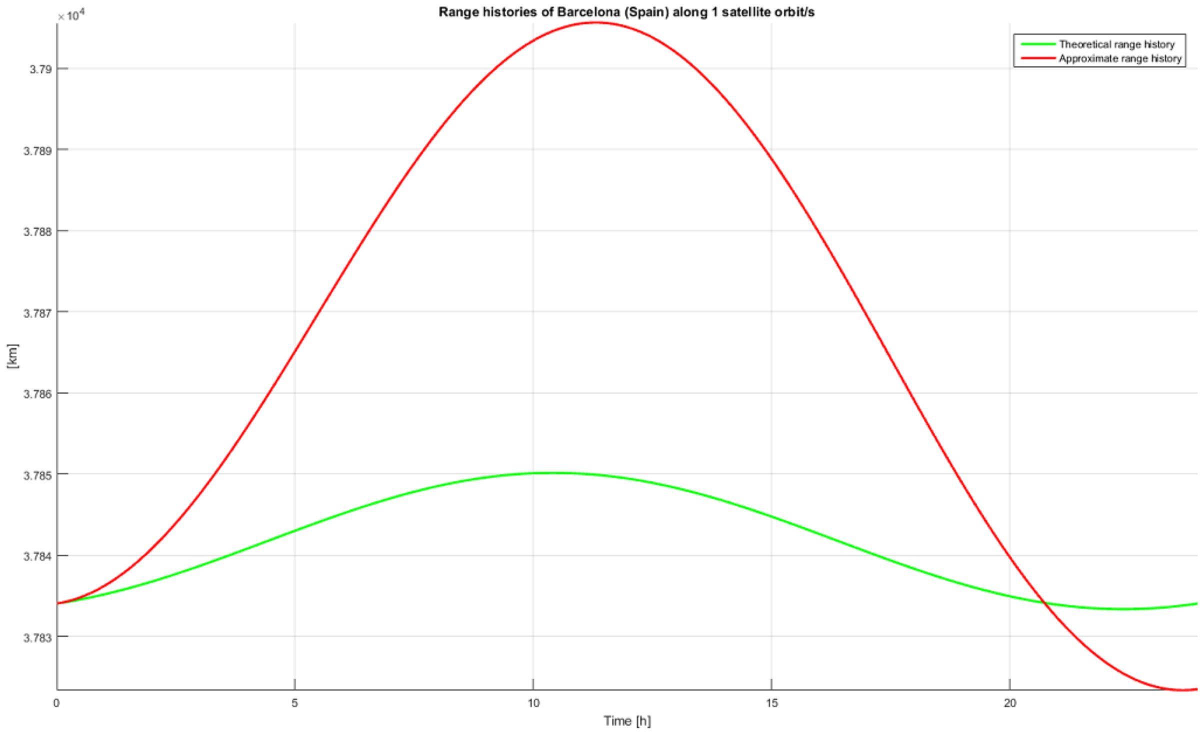

Figure 3.30: *Ideal (in green) and approximate (in red) range histories of Barcelona location along one satellite orbit (setting B + noise).*

One thing to highlight is that the same noise added to the ideal range and range-rate observations is obtained when computing the error in the range and range-rate observations after the approximate satellite state vector is calculated at the initial epoch (see Table 3.8). This fact ensures that the system built works properly since Trilateration and Gibbs methods are geometric methods and provide exact results.

In order to conclude the analysis of adding noise in a single simulation, Figure 3.31 shows the ideal and approximate range-rate histories of Barcelona location along one satellite orbit. From this figure, one may also see the difference between both curves. However, the range-rate history suffers less degradation due to noise compared to the range history. After one satellite orbit, the ideal and approximate range-rate observations are very similar, whereas this fact does not occur between the final values of the ideal and approximate range observations. Therefore, in order not to exceed the amount of figures shown, only those figures that affect the satellite state vector and range history will be depicted in the following sections.

NOISE ADDED AND ERROR OBTAINED IN ρ AND $\dot{\rho}$ OBSERVATIONS AT $t_0 = 0$ s				
Num.	**Site**	**Noise added** (σ_ρ or σ_{v_r})	**Error obtained** (between ideal and approximate observations)	**Error** (between noise added and error obtained)
RANGE OBSERVATIONS [km]				
01	BCN	0.000 537 667 140	0.000 537 667 147	0.000 000 000 007
02	BET	-0.000 433 592 022	-0.000 433 592 017	0.000 000 000 005
03	MIL	0.000 725 404 225	0.000 725 404 243	0.000 000 000 018
RANGE-RATE OBSERVATIONS [km/s]				
01	BCN	0.000 004 310 867	0.000 004 310 867	0.000 000 000 000
02	BET	0.000 013 847 185	0.000 013 847 185	0.000 000 000 000
03	MIL	-0.000 001 024 830	-0.000 001 024 830	0.000 000 000 000

Table 3.8: *Difference between the noises added to the ideal ρ and $\dot{\rho}$ observations and the error obtained between the ideal and approximate ρ and $\dot{\rho}$ observations at epoch t_0.*

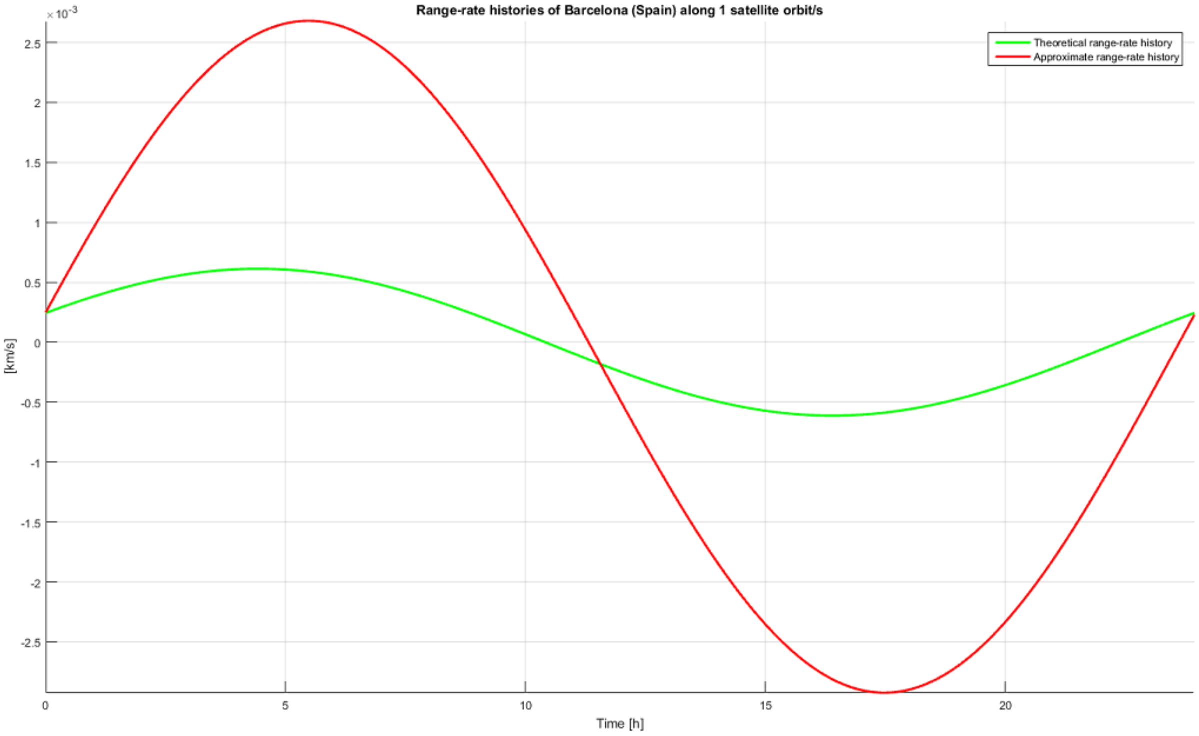

Figure 3.31: *Ideal (in green) and approximate (in red) range-rate histories of Barcelona location along one satellite orbit (setting B + noise).*

3.8. STATISTICAL ANALYSES OF TRILATERATION AND GIBBS METHODS

Since every simulation run when adding noise to the ideal range and range-rate observations gives similar but different results, there is a need to perform a statistical analysis in order to better delimit all results obtained and to better evaluate the precision of the system.

This section will provide these statistics showing the results of the different parameters analysed by means of histograms. The numerical results will also be given in tables as previous sections showing the mean and standard deviation of the errors in each parameter (consult Appendix B). The main parameters to be analysed will be the satellite state vector and range observations of different locations; however, the range-rate observations will also be discussed if needed. Following the same criteria as Section 3.5, the results will be shown at two different epochs simulating the initial and final epochs of the radar synthetic aperture (i.e., t_0 and $t_f = t_0 + 6$ h respectively).

First, the precision of settings A and B plus noise, which will be called setting C and D respectively from now on (see Table 3.9), will be studied. Then, as both settings will not achieve the required precision, other settings will be evaluated. Thus, a complete overview of the Trilateration and Gibbs methods performance will be acquired. Finally, the most important results will be collected all together and shown in a table in Section 3.9. As last remark, it has been considered to repeat the simulation of each setting 1 000 times in order to perform such statistics.

Setting C	Setting D
Location of the three sites: (01) Barcelona (Spain) (02) Betzdorf (Luxemburg) (03) Milan (Italy)	**Location of the three sites:** (01) Barcelona (Spain) (02) Betzdorf (Luxemburg) (03) Milan (Italy)
IDEAL DATA - **Type of observations generated:** RANGE. - **Epoch/s when the observations are generated:** $t_0 = 0$ s, $t_1 = 9\,000$ s, and $t_2 = 18\,000$ s.	**IDEAL DATA** - **Type of observations generated:** RANGE and RANGE-RATE. - **Epoch/s when the observations are generated:** $t_0 = 0$ s.
NOISE ADDED - **Range observations:** MEAN: 0 m / STD.: 1 m.	**NOISE ADDED** - **Range observations:** MEAN: 0 m / STD.: 1 m. - **Range-rate observations:** MEAN: 0 mm/s / STD.: 5 mm/s.
APPROXIMATE DATA - **Method/s used:** TRILATERATION and GIBBS. - **Epoch when the approximate satellite state vector is given:** $t_1 = 9\,000$ s.	**APPROXIMATE DATA** - **Method/s used:** TRILATERATION. - **Epoch when the approximate satellite state vector is given:** $t_0 = 0$ s.

Table 3.9: *Summary of all conditions considered on settings C and D.*

a) Results Analysis of Setting C

Adding noise to the ideal range observations obviously affect the initial satellite state vector determination. In this case, 1 m of standard deviation noise in range observations lead to locate the initial satellite position state vector with errors of 50 to 150 metres on each of its components compared to the initial ideal values. On the other hand, the errors in each component of the initial satellite velocity state vector are around 10 millimetres per second (see Figure 3.32).

Such errors in the satellite state vector will degrade over time. After 6 h, some errors have increased, especially those relating to the satellite position state vector, whereas the other errors have similar values (see Figure 3.33). Although the augmented quantity is not very high, the impact on the final range observations is severe. One may see from tables of Appendix B that the errors on range values of the different locations are of few metres at initial epoch, and become more than 100 m at final epoch. This fact highlights the importance of determining the initial satellite sate vector on a very precise way.

One may have realised that setting C does not fulfil the precision requirements of GEOSAR mission; however, it has been useful to evaluate the performance of Trilateration and Gibbs methods when the initial parameters (range observations) are noisy. Remember that only three observations of Barcelona, three of Betzdorf and three of Milan locations have been used in order to calculate the satellite state vector.

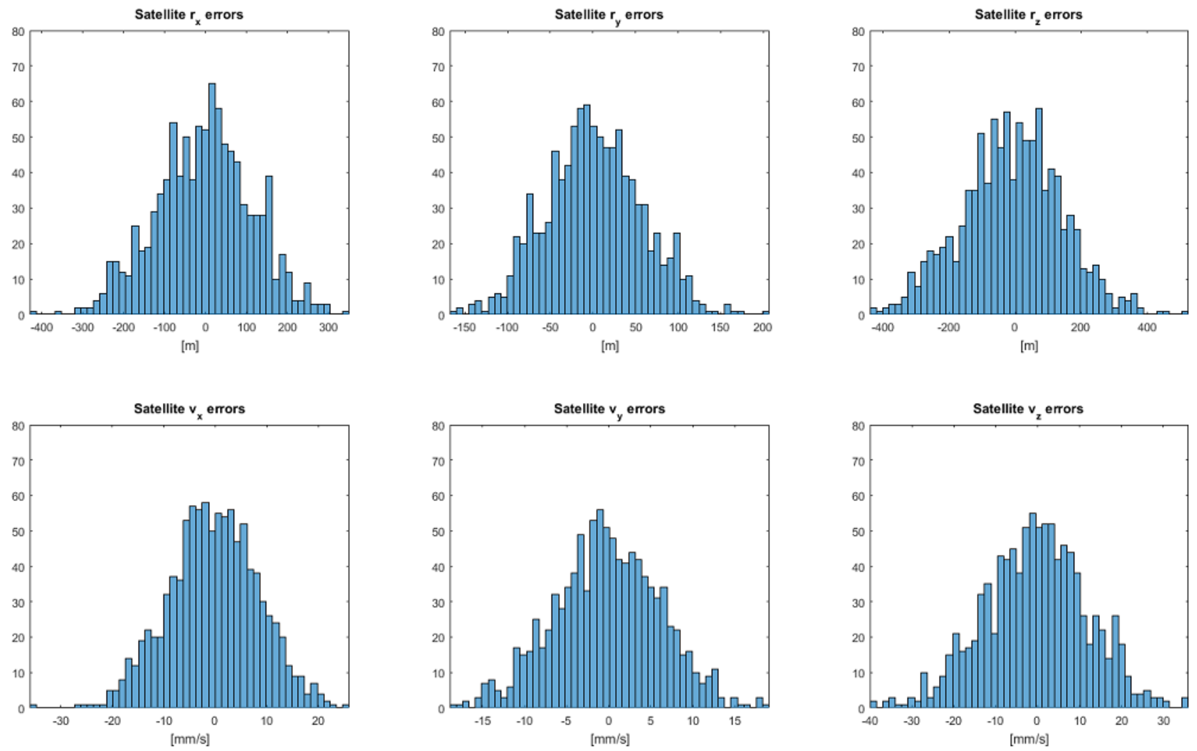

Figure 3.32: *Statistical errors in the satellite state vector at initial epoch,* $t_1 = 9\ 000$ s *(setting C).*

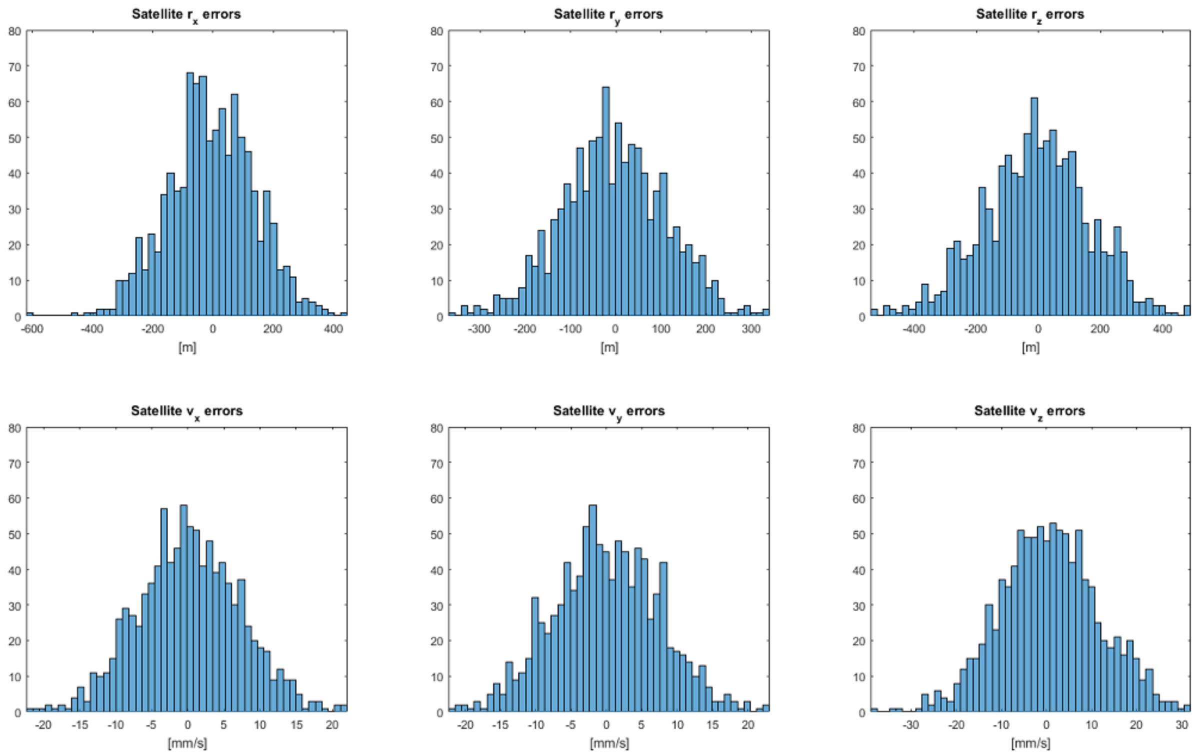

Figure 3.33: *Statistical errors in the satellite state vector at final epoch,* $t_{\mathrm{f}} = 30\ 600$ s *(setting C).*

As commented in the previous section, the same initial noise, added to the ideal range observations of Barcelona, Betzdorf and Milan locations, is obtained after computing the initial range errors (i.e., the difference between the ideal and approximate values) of these three sites. This fact is illustrated in the following figures. In this way, another sign is obtained in order to ensure the proper functionality of whole simulation.

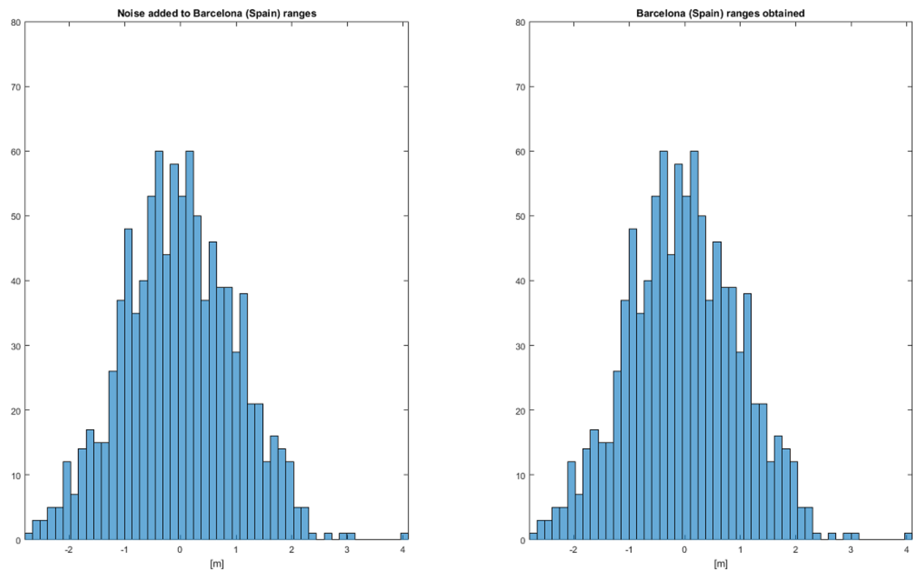

Figure 3.34: *Statistical noise added to the ideal* ρ *observations and errors obtained between the ideal and approximate* ρ *observations of Barcelona location at initial epoch,* $t_1 = 9\ 000$ s *(setting C).*

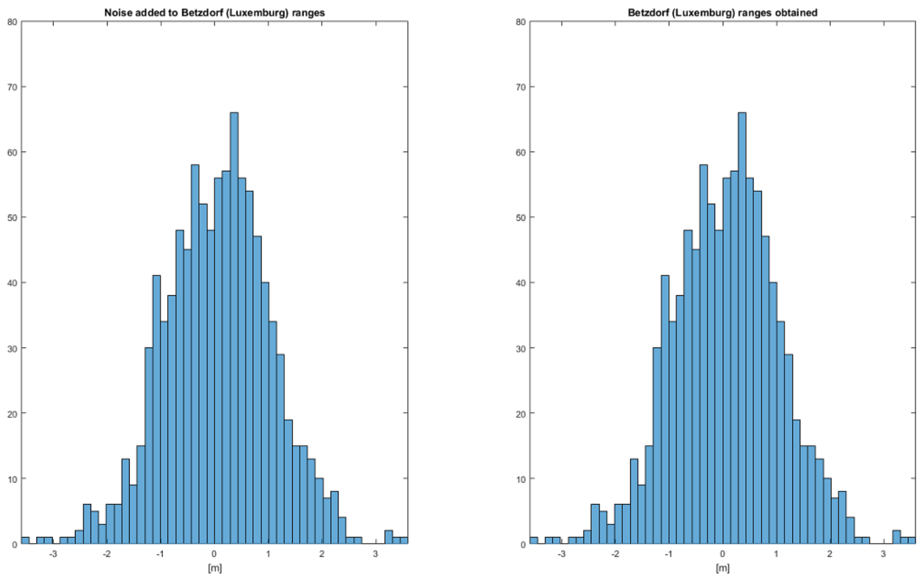

Figure 3.35: *Statistical noise added to the ideal ρ observations and errors obtained between the ideal and approximate ρ observations of Betzdorf location at initial epoch, $t_1 = 9\,000$ s (setting C).*

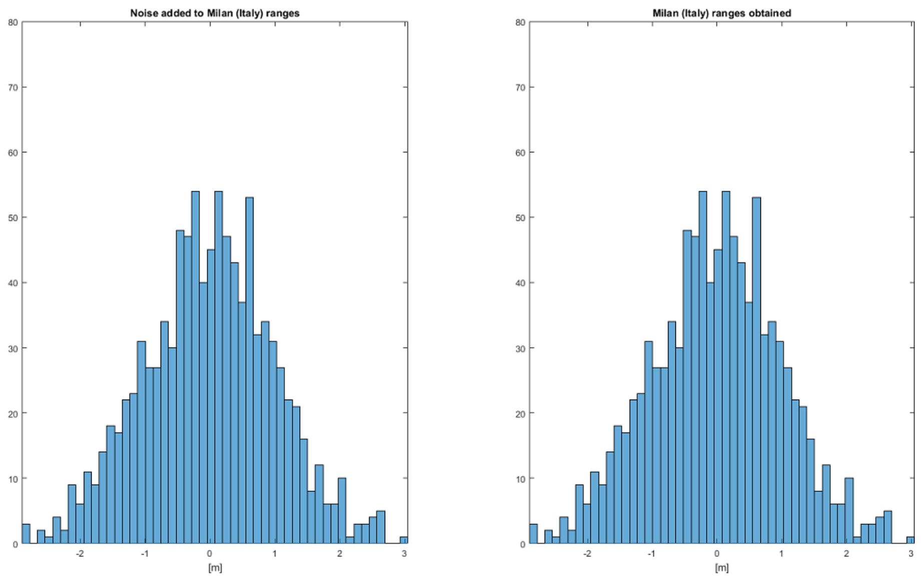

Figure 3.36: *Statistical noise added to the ideal ρ observations and errors obtained between the ideal and approximate ρ observations of Milan location at initial epoch, $t_1 = 9\,000$ s (setting C).*

b) Results Analysis of Setting D

Now, noisy range-rate observations of the three sites are also used. In this case, all observations are provided at same initial epoch, and Trilateration is the only method used in order to calculate the initial satellite state vector.

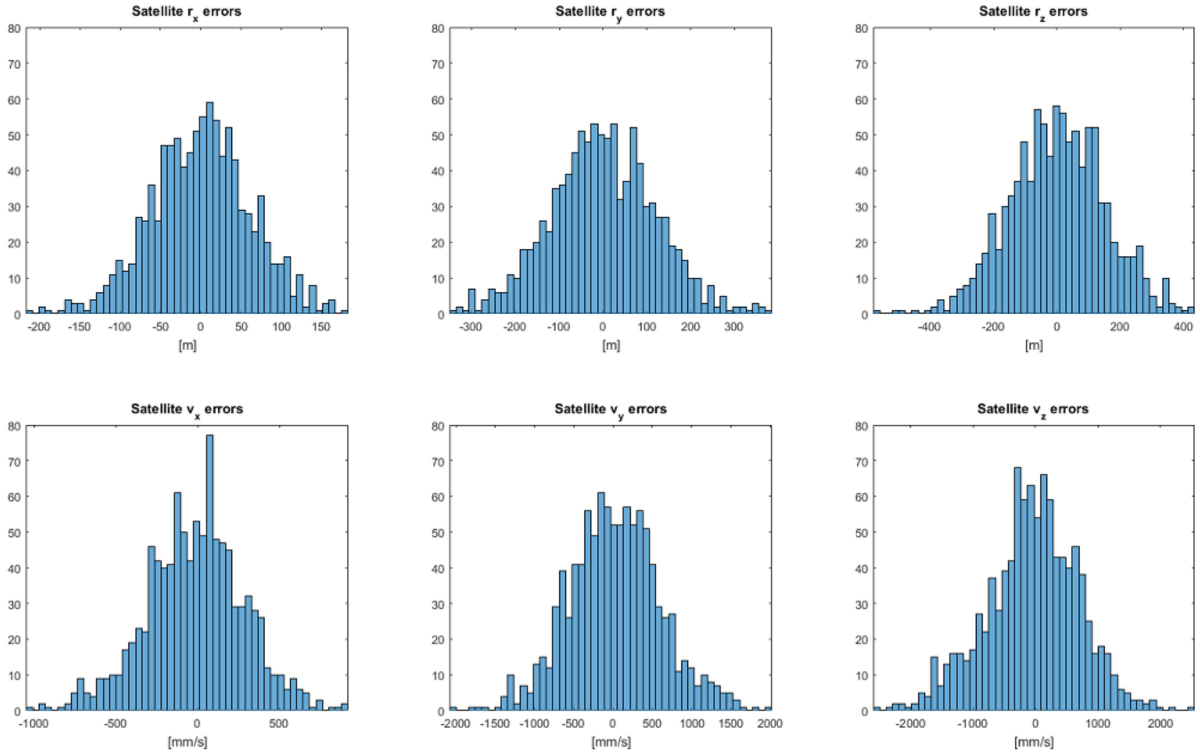

Figure 3.37: *Errors in the satellite state vector at initial epoch,* $t_0 = 0$ s *(setting D).*

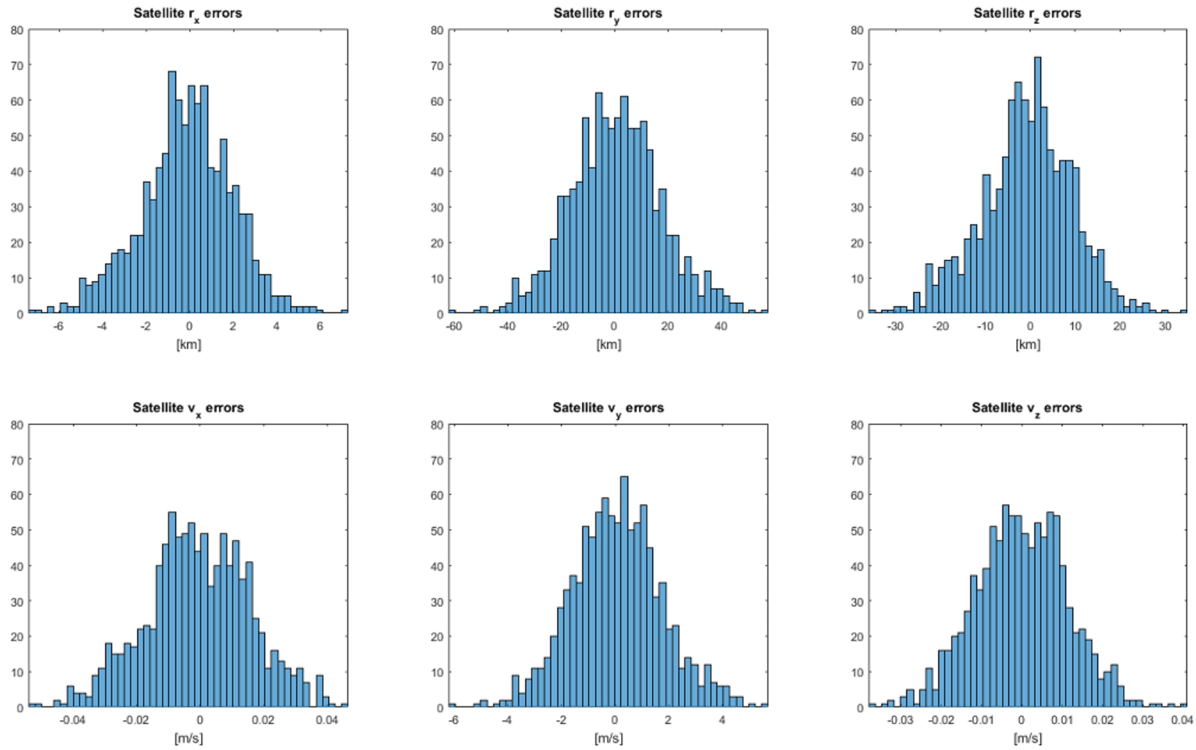

Figure 3.38: *Errors in the satellite state vector at final epoch,* $t_\mathrm{f} = 21\,600$ s *(setting D).*

The results obtained by the simulation show similar order of magnitude errors in the initial satellite position state vector compared to setting C; however, the errors in the initial satellite velocity state vector are two orders of magnitude above (see Figure 3.37). This fact does not degrade the initial range observations obtained by setting C since such values are related to the position of the satellite state vector. But, on the other hand, having a less precise initial state vector, lead to a worse propagation of it over time (see Figure 3.38), and therefore higher errors in the obtained range observations at final epoch. Thus, setting C provided errors of 100 m in range observations at final epoch, and setting D gives now errors of 17 km per each site.

As regards the range-rate observations, they start with errors of a few millimetres per second at initial epoch, and reach around 1.2 metres per second error in each site at final epoch. Again, the errors are too high. If setting C did not fulfil the precision requirements of GEOSAR mission, neither does setting D, which has even greater errors. Both settings, specifically Trilateration and Gibbs methods, are not designed to calculate the satellite orbit with precision in presence of perturbations or noise. They are used as methods to initially determine the satellite orbit. Then, from this initial point and more observations from the satellite orbit, other methods or techniques may improve substantially the initial point precision, and therefore the satellite orbit estimation around the Earth. One of these techniques will be discussed in Chapter 4.

At this point, the correct functionality of the whole system built can finally be proved by showing some statistics related to range-rate observations. Thus, Figures 3.39, 3.40 and 3.41 illustrate the statistics of the noise added to the ideal range-rate observations of Barcelona, Betzdorf and Milan locations at initial epoch compared to the errors obtained (i.e., the difference between the ideal and approximate values) in these observations at these three locations at same initial epoch. As seen in the figures, the statistics are the same so that the system works properly.

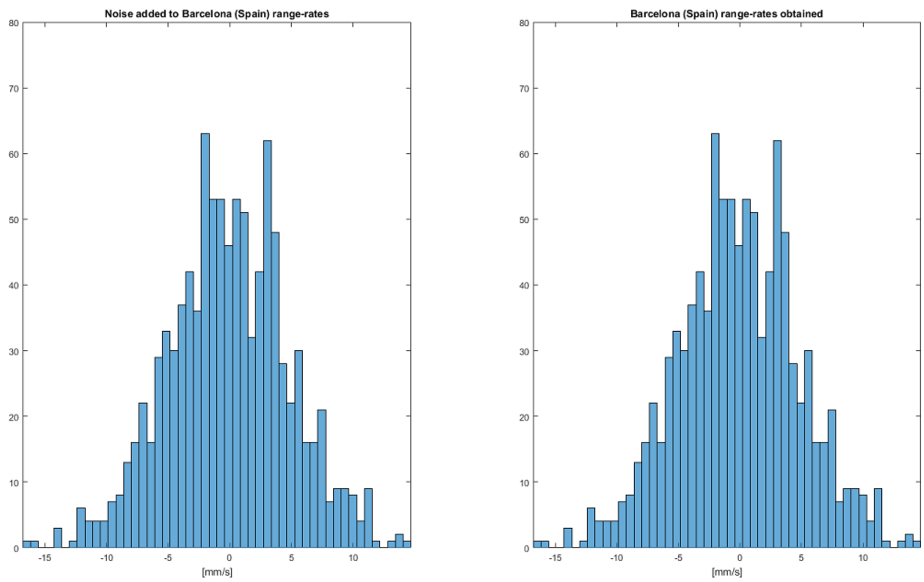

Figure 3.39: *Statistical noise added to the ideal $\dot{\rho}$ observations and errors obtained between the ideal and approximate $\dot{\rho}$ observations of Barcelona location at initial epoch, $t_0 = 0$ s (setting D).*

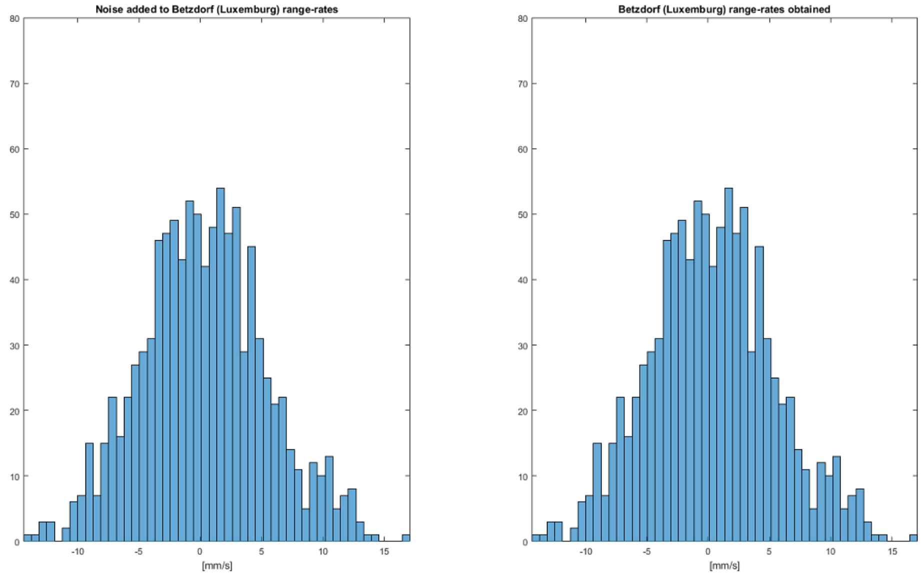

Figure 3.40: *Statistical noise added to the ideal $\dot{\rho}$ observations and errors obtained between the ideal and approximate $\dot{\rho}$ observations of Betzdorf location at initial epoch, $t_0 = 0$ s (setting D).*

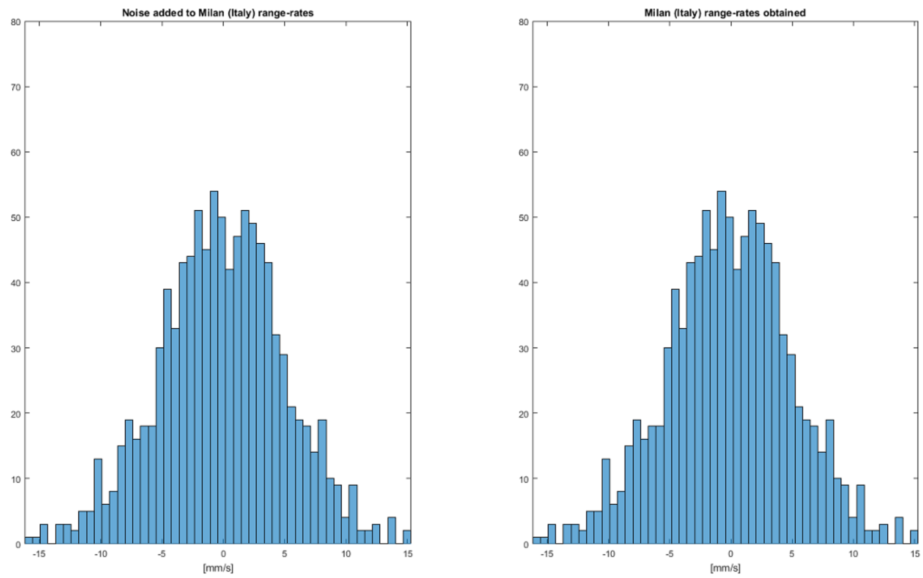

Figure 3.41: *Statistical noise added to the ideal $\dot{\rho}$ observations and errors obtained between the ideal and approximate $\dot{\rho}$ observations of Milan location at initial epoch, $t_0 = 0$ s (setting D).*

Before concluding Trilateration and Gibbs methods analyses, let us evaluate two more situations. First, let us see how the precision of the system is affected when adding a different quantity of noise to the initial observations. In particular, if range observations are degraded with noise of 1 km standard deviation instead of 1 m, how will the errors of the different parameters be? Second, the three sites selected to initially determine the satellite orbit are very close from the satellite point of view. If the triangle forming these three sites is enlarged, how will the initial satellite state vector precision change? Both questions will be discussed in the following sub-sections.

c) Results Analysis of Setting E

This sub-section will analyse how the errors in the satellite state vector and range observations are affected if the initial ideal range observations of the three sites are degraded with 1 km standard deviation Gaussian noise. Table 3.10 summarizes all conditions considered in the simulation.

Setting E

Location of the three sites:
(01) Barcelona (Spain)
(02) Betzdorf (Luxemburg)
(03) Milan (Italy)

IDEAL DATA
- **Type of observations generated:**
  RANGE.
- **Epoch/s when the observations are generated:**
  $t_0 = 0$ s,
  $t_1 = 9\,000$ s, and
  $t_2 = 18\,000$ s.

NOISE ADDED
- **Range observations:**
  MEAN: 0 m / STD.: 1 km.

APPROXIMATE DATA
- **Method/s used:**
  TRILATERATION and GIBBS.
- **Epoch when the approximate satellite state vector is given:**
  $t_1 = 9\,000$ s.

Table 3.10: *Summary of all conditions considered on setting E.*

Figures 3.42 and 3.43 show the statistical results of the errors obtained in the satellite state vector at initial and final epochs respectively. Increasing three orders of magnitude the quantity of noise added to range observations with regard to setting C ($\sigma_\rho = 1$ m) lead to errors three order of magnitude higher in setting E. In setting C, the errors in the initial satellite position state vector were of 50 to 150 metres, whereas, in setting D, these errors become 50 to 150 kilometres. The same rule happens to the other parameters at both initial and final epochs.

As commented in Section 3.3, Trilateration and Gibbs methods are both geometrical methods, so that the order of magnitude of the errors given into the analysis of setting E could be expected. Thus, when determining the initial position of the satellite vector, it will be of the utmost importance the quality of observations (i.e., range and range-rate observations) in order to use them on Trilateration and Gibbs methods.

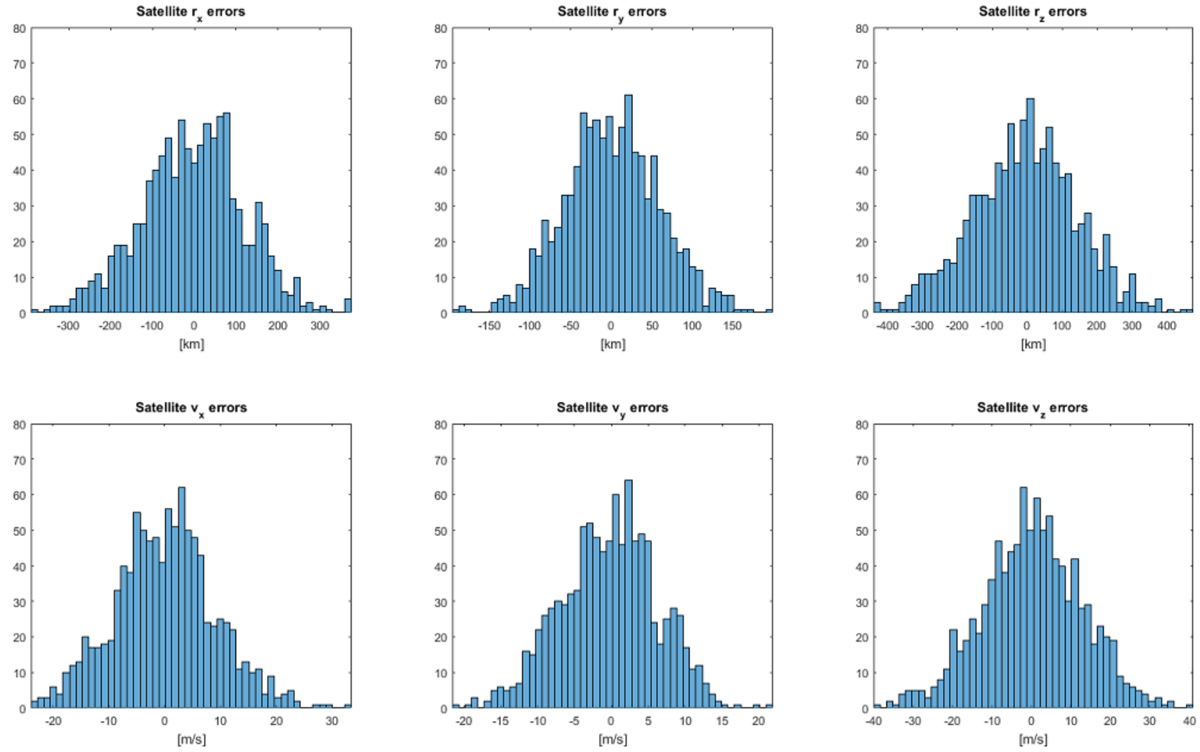

Figure 3.42: *Errors in the satellite state vector at initial epoch, $t_1 = 9\ 000$ s (setting E).*

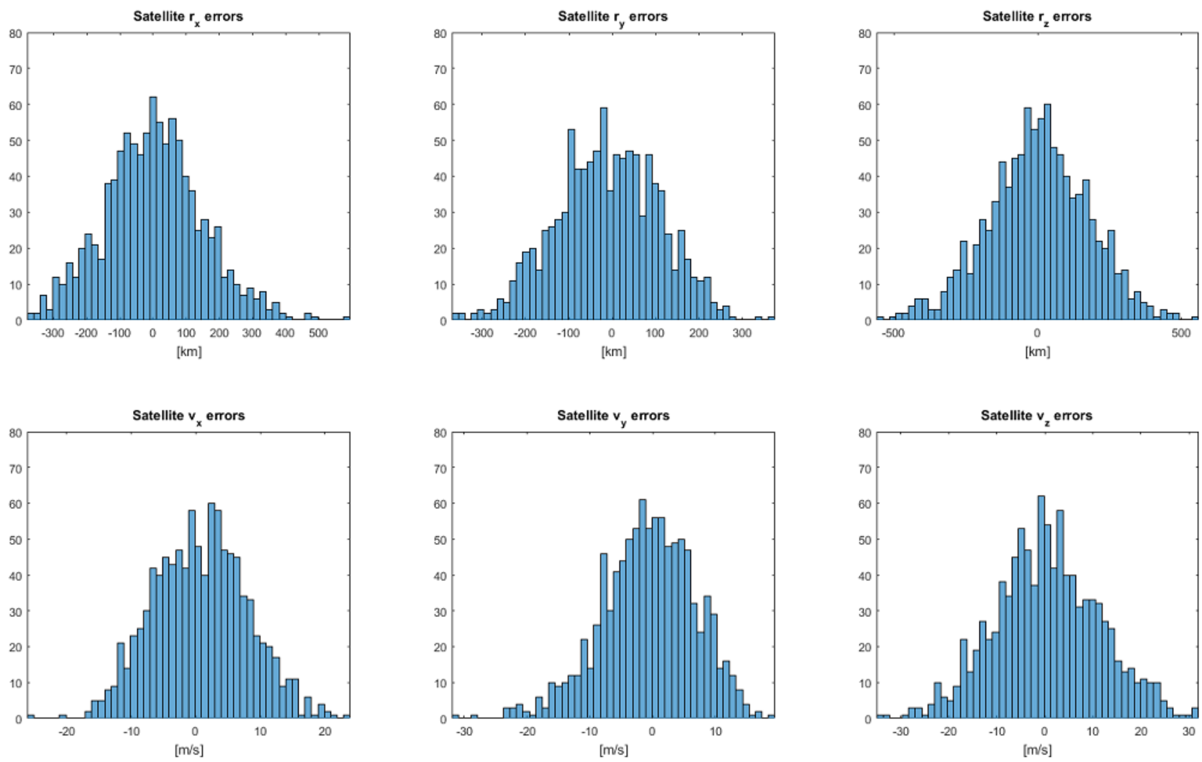

Figure 3.43: *Errors in the satellite state vector at final epoch, $t_f = 30\ 600$ s (setting E).*

d) Results Analysis of Setting F

This sub-section and the following one will show how the enlargement of the triangle forming the three sites affects the errors obtained in the satellite state vector, and range and range-rate observations. The selection of these new three sites has been done considering locations that are on the edges of Europe although they are out of the satellite L-band beam coverage. For this reason, Las Palmas de Gran Canaria (Spain), Reykjavik (Iceland), and Ankara (Turkey) locations have been chosen.

The simulations of setting F (this sub-section) and setting G (next sub-section) will be performed considering noise values of settings C and D respectively (i.e., $\sigma_\rho = 1\ \mathrm{m}$ and $\sigma_{v_r} = 5\ \mathrm{mm/s}$). All conditions taken into account in the simulation of both settings are summarized in Table 3.11.

Setting F	Setting G
Location of the three sites: (04) Las Palmas de Gran Canaria (Spain) (05) Reykjavik (Iceland) (06) Ankara (Turkey)	**Location of the three sites:** (04) Las Palmas de Gran Canaria (Spain) (05) Reykjavik (Iceland) (06) Ankara (Turkey)
IDEAL DATA - **Type of observations generated:** RANGE. - **Epoch/s when the observations are generated:** $t_0 = 0$ s, $t_1 = 9\,000$ s, and $t_2 = 18\,000$ s.	**IDEAL DATA** - **Type of observations generated:** RANGE and RANGE-RATE. - **Epoch/s when the observations are generated:** $t_0 = 0$ s.
NOISE ADDED - **Range observations:** MEAN: 0 m / STD.: 1 m.	**NOISE ADDED** - **Range observations:** MEAN: 0 m / STD.: 1 m. - **Range-rate observations:** MEAN: 0 $\mathrm{mm/s}$ / STD.: 5 $\mathrm{mm/s}$.
APPROXIMATE DATA - **Method/s used:** TRILATERATION and GIBBS. - **Epoch when the approximate satellite state vector is given:** $t_1 = 9\,000$ s.	**APPROXIMATE DATA** - **Method/s used:** TRILATERATION. - **Epoch when the approximate satellite state vector is given:** $t_0 = 0$ s.

Table 3.11: *Summary of all conditions considered on settings F and G.*

Using this new triangle of sites, the errors in the initial satellite state vector have decreased one order of magnitude. The results of setting C showed, for example, satellite position state vector errors between 50 and 150 metres, whereas setting F obtains errors of 5 to 25 metres (see Figure 3.44). This improvement in the satellite state vector initial determination allows that the initial range observation errors of all sites under the satellite L-band beam coverage remain below 1 metre. Such error was only provided in Bern location when analysing setting C. That is to say, the only site evaluated whose location is inside the triangle formed by Barcelona, Betzdorf and Milan sites.

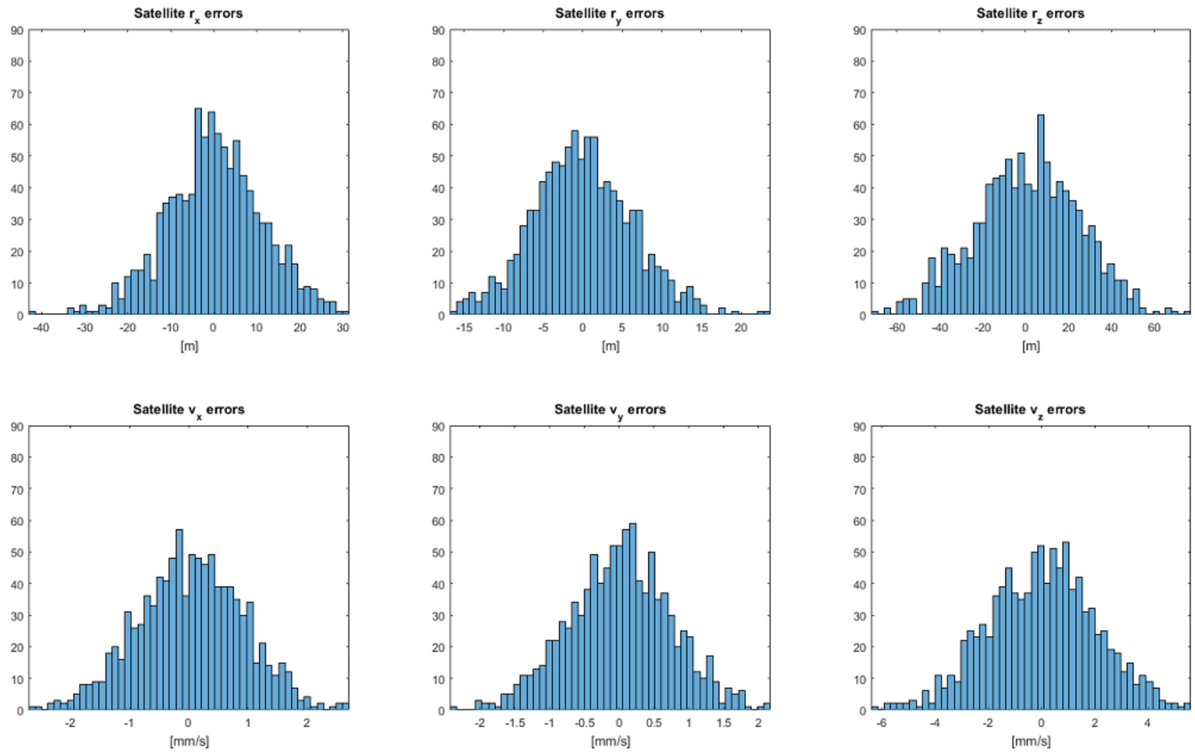

Figure 3.44: *Errors in the satellite state vector at initial epoch,* $t_1 = 9\ 000$ s *(setting F).*

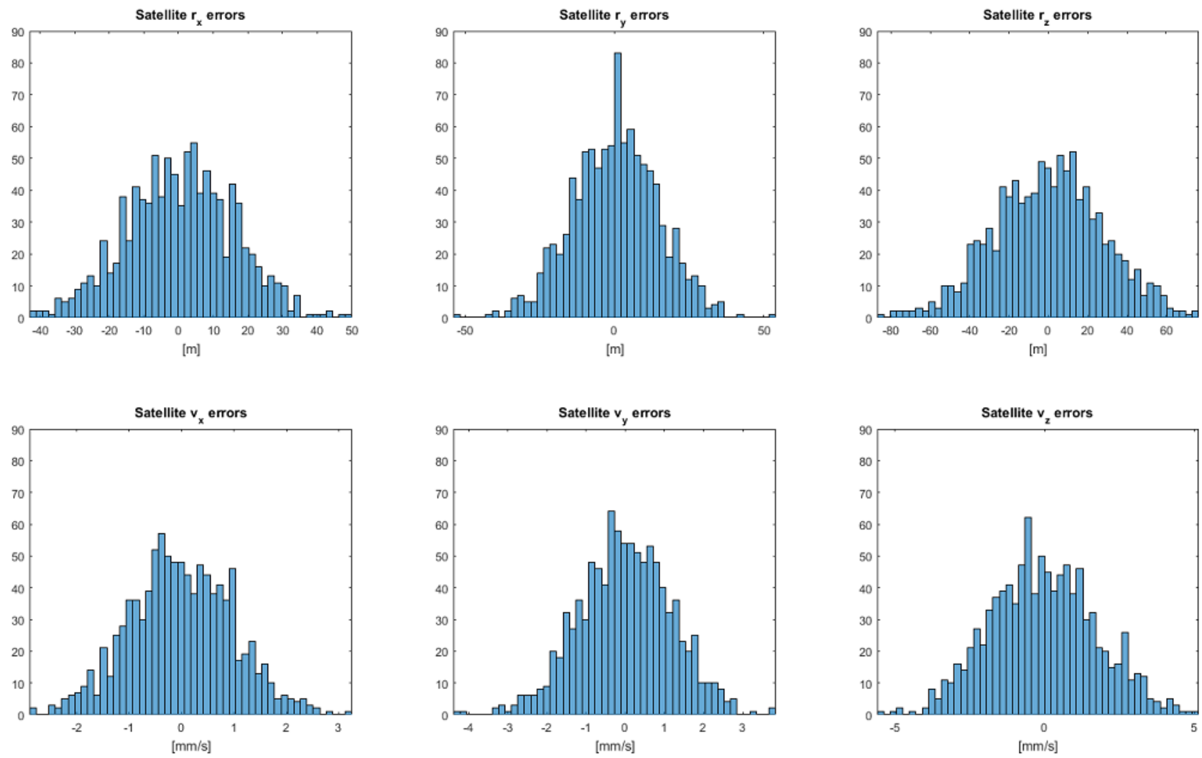

Figure 3.45: *Errors in the satellite state vector at final epoch,* $t_f = 30\ 600$ s *(setting F).*

In addition, this better determination of the initial satellite state vector leads to fewer errors in the satellite propagation (see Figure 3.45), and therefore the final range observations are closer to the ideal values. However, the precision requirements of GEOSAR mission are far to be fulfilled by means of setting F. One may see from tables of Appendix B that the range observation errors at final epoch are around 14 metres, which are a great improvement with regard to those achieved in setting C (~100 metres), but not sufficient.

e) Results Analysis of Setting G

Setting G is the last configuration that is going to be simulated. This setting includes range-rate observation errors as setting D does.

The simulation results can be summarized in two points. On one hand, there is an improvement of one order of magnitude on the errors of all parameters evaluated of setting G with regard to the errors obtained in setting D, which is the same as happened in the previous sub-section. On the other hand, the errors of setting G at final epoch are higher than those obtained in setting F. This fact also happened between settings D and C. Therefore, setting G does not fulfil GEOSAR mission requirements as one could expect from the simulations of previous settings.

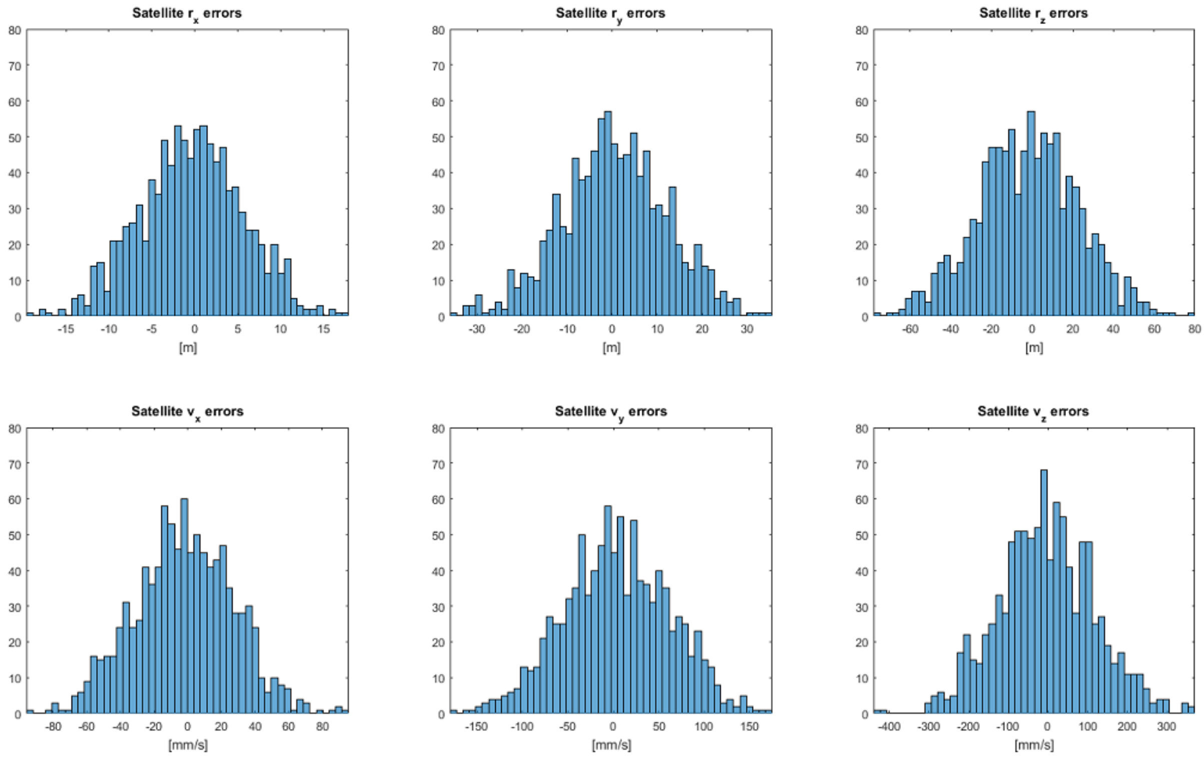

Figure 3.46: *Errors in the satellite state vector at initial epoch,* $t_0 = 0$ s *(setting G).*

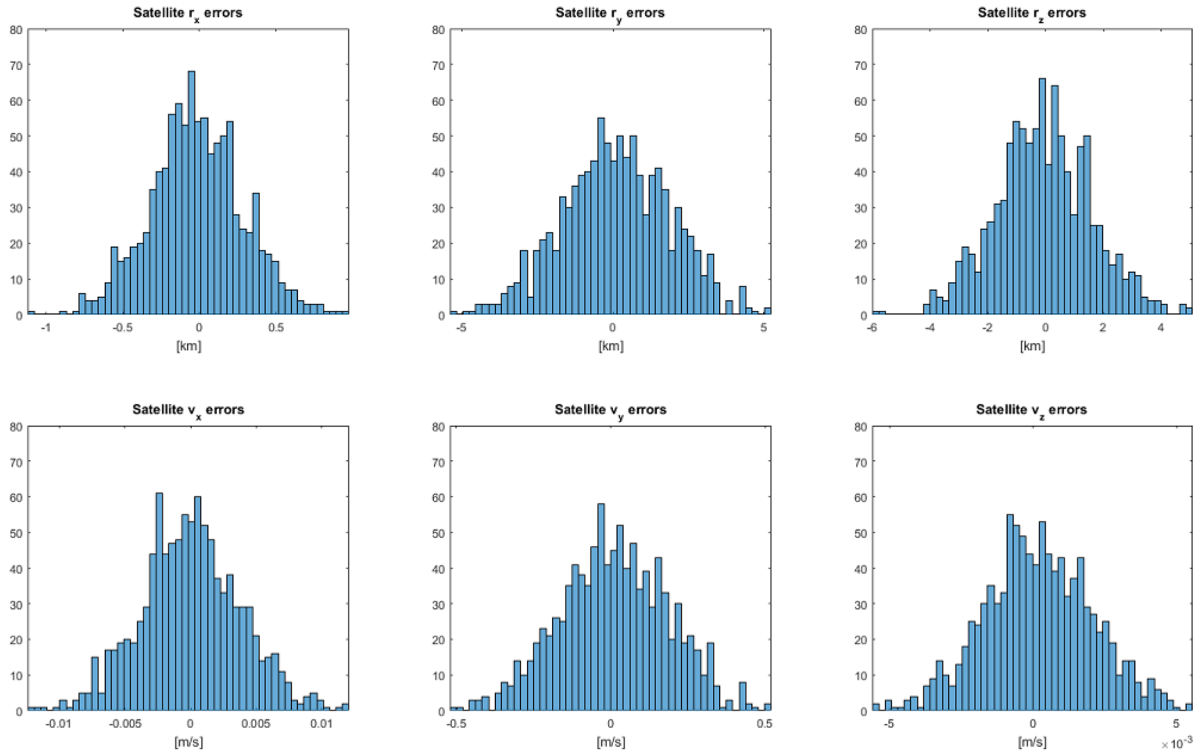

Figure 3.47: *Errors in the satellite state vector at final epoch,* $t_f = 21\,600$ s *(setting G).*

3.9. RESULTS SUMMARY

Table 3.12 summarizes the main results obtained of all settings evaluated along Chapter 3. Thus, the reader can compare the performance of the different settings.

As a conclusion of the chapter, Trilateration and Gibbs methods are required to initially calculate one satellite state vector from observation data. They perform such operation through very few observations of different sites, so that a poor precision on the final result could be expected. On the other hand, GEOSAR mission requirements are very high with respect actual orbit positioning of GEO satellites. Therefore, other techniques must be studied, which use a large amount of observation data, in order to refine the initial orbit determination offered by Trilateration and Gibbs methods. One of these techniques is discussed and evaluated in the following chapter, which is based on differential correction.

RESULTS SUMMARY OF ALL SETTINGS OF CHAPTER 3				
Set.	**Errors in satellite Postion SV (r)**	**Errors in satellite Velocity SV (v)**	**Errors in Range observations (ρ)**	**Errors in Range-rate observations ($\dot{\rho}$)**
INITIAL EPOCH				
A	80 pm – 550 pm	less than $\frac{\text{pm}}{\text{s}}$	less than $\frac{\text{pm}}{\text{s}}$ – 30 pm	–
B	140 pm – 870 pm	less than $\frac{\text{pm}}{\text{s}}$	less than $\frac{\text{pm}}{\text{s}}$ – 10 pm	less than $\frac{\text{pm}}{\text{s}}$
C	50 m – 160 m	$5\ \frac{\text{mm}}{\text{s}} - 15\ \frac{\text{mm}}{\text{s}}$	0.5 m – 7 m	–
D	50 m – 160 m	$0.2\ \frac{\text{m}}{\text{s}} - 0.8\ \frac{\text{m}}{\text{s}}$	0.5 m – 7 m	$3\ \frac{\text{mm}}{\text{s}} - 35\ \frac{\text{mm}}{\text{s}}$
E	50 km – 160 km	$6\ \frac{\text{m}}{\text{s}} - 15\ \frac{\text{m}}{\text{s}}$	0.5 km – 7 km	–
F	5 m – 25 m	$0.7\ \frac{\text{mm}}{\text{s}} - 2.1\ \frac{\text{mm}}{\text{s}}$	0.5 m – 1.1 m	–
G	5 m – 25 m	$25\ \frac{\text{mm}}{\text{s}} - 125\ \frac{\text{mm}}{\text{s}}$	0.5 m – 1.1 m	$2.8\ \frac{\text{mm}}{\text{s}} - 5.1\ \frac{\text{mm}}{\text{s}}$
FINAL EPOCH				
A	140 pm – 870 pm	less than $\frac{\text{pm}}{\text{s}}$	150 pm – 230 pm	–
B	1 pm – 300 pm	less than $\frac{\text{pm}}{\text{s}}$	250 pm – 270 pm	less than $\frac{\text{pm}}{\text{s}}$
C	110 m – 180 m	$5\ \frac{\text{mm}}{\text{s}} - 15\ \frac{\text{mm}}{\text{s}}$	101 m – 110 m	–
D	1 km – 20 km	$10\ \frac{\text{mm}}{\text{s}} - 2\ \frac{\text{m}}{\text{s}}$	17.0 km – 17.5 km	$1.1\ \frac{\text{m}}{\text{s}} - 1.4\ \frac{\text{m}}{\text{s}}$
E	110 km – 180 km	$7\ \frac{\text{m}}{\text{s}} - 12\ \frac{\text{m}}{\text{s}}$	104 km – 110 km	–
F	14 m – 28 m	$0.9\ \frac{\text{mm}}{\text{s}} - 1.8\ \frac{\text{mm}}{\text{s}}$	14.2 m – 14.6 m	–
G	0.3 km – 1.8 km	$1\ \frac{\text{mm}}{\text{s}} - 180\ \frac{\text{mm}}{\text{s}}$	1.65 km – 1.74 km	$110\ \frac{\text{mm}}{\text{s}} - 135\ \frac{\text{mm}}{\text{s}}$

Table 3.12: *Summary of all simulation results performed in Chapter 3. This table shows the value range of the errors between ideal and approximate values of different parameters.*

4

Differential Correction Techniques

Orbit determination requires estimation, which is intimately tied to initial orbit determination (studied in the previous chapter), prediction, and uncertainty estimates. Regardless of the observational data source used for orbit determination, one should make the algorithms general enough to process them. In other words, estimation must be versatile in predicting, filtering, and smoothing data. For estimation, predicting is simply using existing observations to find future states. One must consider that estimation techniques are intimately tied to propagation methods. On the other hand, filtering is determining the current state using current (and past) observations. And, finally, smoothing techniques improve previous state solutions by combining them with future data.

The techniques presented in this chapter are often referred to as differential correction techniques since the methods of solution require iteration or incremental updates to the state. On the one hand, Least Squares techniques use all data available in order to improve the determination of the initial state. On the other, Kalman Filter techniques compute the best estimate of the state of a time-varying process by using a predictor-corrector technique ideally suited for computer applications, given imperfect observations and uncertain dynamics. The selection of using a Least Squares vs. a Kalman Filter evokes tremendous discussion. Ultimately, the requirements are the deciding factor. If the need is for continuous near real-time updates, Kalman Filter approaches are preferred. If the objective is for routine position determination, the Least Squares techniques suffice.

Comparisons of the two techniques are limited, however, Montenbruck et al. (2000) compare Least Squares and Kalman Filter approaches to orbit determination. While they note differences and conclude that the Least Squares approach is better, the positional comparisons are shown to be remarkably close.

This document will only use Least Squares techniques in order to determine the satellite orbit of GEOSAR mission. All data will be available after the radar synthetic aperture and there is no need to continuously monitor the satellite position. In addition, some problems arising from the covariance propagation when using Kalman Filter techniques will be avoided.

Chapter 4 will begin introducing the Least Squares techniques to the reader. Then, these techniques will be particularized to orbit determination and specially to orbit determination for the GEOSAR mission. Remember that GEOSAR mission will provide either range and range-rate measurements or only range measurements, so that both cases will be considered when explaining the final algorithm. Finally, such algorithm will be evaluated performing different statistical simulations and showing their results. As in the previous chapter, the objective is looking for precision. Thus, the results will show how the errors in range history of different sites under the satellite L-band beam coverage evolve along the radar synthetic aperture.

As there is no real data available since the satellite of GEOSAR mission is not in orbit, the simulations performed during this chapter will use the ideal observations built by the same configuration of Chapter 3. Therefore, the Least Squares algorithm developed within this chapter will only consider the interaction between the Earth and the satellite (i.e., no perturbations will be taken into account).

The explanations of this chapter will follow Vallado (2013). The reader is address to it in order to complete all concepts discussed within Chapter 4.

4.1. LEAST SQUARES FUNDAMENTALS

Least Squares techniques are defined as an optimization problem, which fits the measurements to an appropriate mathematical model minimizing the sum of the squares of the residuals. The residuals will be the difference in the actual observations and those obtained using the state vector solution. Thus, defining the residuals as

$$\bar{r} = y_0 - y_c$$

where y_0 are the observed values of the dependent variable, and y_c are the computed values of the dependent variable, the Least Squares criterion (for N observations) satisfies

$$J = \sum_{i=1}^{N} \bar{r}_i^2 = \text{a minimum} \tag{4.1}$$

where J is also known as cost function.

In order to better understand the Least Squares technique, let us first obtain a solution for a linear mathematical model.

a) Linear Least Squares

Linear unweighted Least Squares is the simplest estimation technique. It assumes that all data is given equal weighting or importance and defines the mathematical model in a linear way. Thus, the computed value of the dependent variable per each data point, y_{c_i}, is defined as

$$y_{c_i} = \alpha + \beta x_{0_i}$$

where x_{0_i} are the observed values of the independent variable per each data point, and α and β are the values to be estimated such that the sum of the squares of the residuals, $\bar{r}_i^2$, is a minimum.

$$J = \sum_{i=1}^{N} \bar{r}_i^2 = \sum_{i=1}^{N} \left(y_{0_i} - y_{c_i}\right)^2 = \sum_{i=1}^{N} \left[y_{0_i} - \left(\alpha + \beta x_{0_i}\right)\right]^2 = f(\alpha, \beta) = \text{a minimum}$$

In order to find this minimum, the first derivative with respect to α and β parameters of the cost function to zero must be performed. The function above has two variables whose both partial derivatives are equal to 0 at the minimum, so that the equation can be split in two:

$$\frac{\partial}{\partial \alpha} J = \frac{\partial}{\partial \alpha} \sum_{i=1}^{N} \bar{r}_i^2 = \sum_{i=1}^{N} \frac{\partial \bar{r}_i^2}{\partial \alpha} = \sum_{i=1}^{N} 2\bar{r}_i \frac{\partial \bar{r}_i}{\partial \alpha} = 0 \;\; \Rightarrow \;\; \sum_{i=1}^{N} \bar{r}_i \frac{\partial \bar{r}_i}{\partial \alpha} = 0$$

$$\frac{\partial}{\partial \beta} J = \frac{\partial}{\partial \beta} \sum_{i=1}^{N} \bar{r}_i^2 = \sum_{i=1}^{N} \frac{\partial \bar{r}_i^2}{\partial \beta} = \sum_{i=1}^{N} 2\bar{r}_i \frac{\partial \bar{r}_i}{\partial \beta} = 0 \;\; \Rightarrow \;\; \sum_{i=1}^{N} \bar{r}_i \frac{\partial \bar{r}_i}{\partial \beta} = 0$$

By using the residual definition, the previous equations become

$$\sum_{i=1}^{N} \bar{r}_i \frac{\partial \bar{r}_i}{\partial \alpha} = \sum_{i=1}^{N} \bar{r}_i \frac{\partial\left(y_{0_i} - \alpha - \beta x_{0_i}\right)}{\partial \alpha} = \sum_{i=1}^{N} \bar{r}_i(-1) = -\bar{r}_1 - \bar{r}_2 - \cdots - \bar{r}_N = 0$$

$$\sum_{i=1}^{N} \bar{r}_i \frac{\partial \bar{r}_i}{\partial \beta} = \sum_{i=1}^{N} \bar{r}_i \frac{\partial\left(y_{0_i} - \alpha - \beta x_{0_i}\right)}{\partial \beta} = \sum_{i=1}^{N} \bar{r}_i\left(-x_{0_i}\right) = -\bar{r}_1 x_{0_1} - \bar{r}_2 x_{0_2} - \cdots - \bar{r}_N x_{0_N} = 0$$

which can be expressed in matrix notation as

$$\begin{bmatrix} 1 & 1 & \cdots & 1 \\ x_{0_1} & x_{0_2} & \cdots & x_{0_N} \end{bmatrix} \begin{bmatrix} \bar{r}_1 \\ \bar{r}_2 \\ \vdots \\ \bar{r}_N \end{bmatrix} = \begin{bmatrix} 0 \\ 0 \end{bmatrix}$$

Now, substituting the definition of the residual, $\bar{r}_i$, yield

$$\begin{bmatrix} 1 & 1 & \cdots & 1 \\ x_{0_1} & x_{0_2} & \cdots & x_{0_N} \end{bmatrix} \begin{bmatrix} y_{0_1} - \left(\alpha + \beta x_{0_1}\right) \\ y_{0_2} - \left(\alpha + \beta x_{0_2}\right) \\ \vdots \\ y_{0_N} - \left(\alpha + \beta x_{0_N}\right) \end{bmatrix} = \begin{bmatrix} 0 \\ 0 \end{bmatrix} \qquad (4.2)$$

where α and β parameters have appeared. Applying the distributive law to the second matrix and separating α and β result in

$$\begin{bmatrix} 1 & 1 & \cdots & 1 \\ x_{0_1} & x_{0_2} & \cdots & x_{0_N} \end{bmatrix} \begin{bmatrix} y_{0_1} \\ y_{0_2} \\ \vdots \\ y_{0_N} \end{bmatrix} - \begin{bmatrix} 1 & 1 & \cdots & 1 \\ x_{0_1} & x_{0_2} & \cdots & x_{0_N} \end{bmatrix} \begin{bmatrix} 1 & x_{0_1} \\ 1 & x_{0_2} \\ \vdots & \vdots \\ 1 & x_{0_N} \end{bmatrix} \begin{bmatrix} \alpha \\ \beta \end{bmatrix} = \begin{bmatrix} 0 \\ 0 \end{bmatrix}$$

Notice, in this case, that α and β parameters can be separated because the selected mathematical model is linear.

The next step is to rearrange the matrix addition in order to place the α and β parameters on one side

$$\begin{bmatrix} 1 & 1 & \cdots & 1 \\ x_{0_1} & x_{0_2} & \cdots & x_{0_N} \end{bmatrix} \begin{bmatrix} 1 & x_{0_1} \\ 1 & x_{0_2} \\ \vdots & \vdots \\ 1 & x_{0_N} \end{bmatrix} \begin{bmatrix} \alpha \\ \beta \end{bmatrix} = \begin{bmatrix} 1 & 1 & \cdots & 1 \\ x_{0_1} & x_{0_2} & \cdots & x_{0_N} \end{bmatrix} \begin{bmatrix} y_{0_1} \\ y_{0_2} \\ \vdots \\ y_{0_N} \end{bmatrix}$$

The equation above can be defined in a symbolic form as

$$\mathbf{A}^T \mathbf{A} \hat{\mathbf{X}} = \mathbf{A}^T \mathbf{b}$$

where $\mathbf{A}$ is the partial-derivative matrix ($N \times 2$), $\hat{\mathbf{X}}$ is the solution, state vector or state space (2×1), and $\mathbf{b}$ is the observation matrix ($N \times 1$). These equations are called the normal equations. Although $\mathbf{A}$ and $\mathbf{A}^T$ are not usually square matrices, the matrix product $\mathbf{A}^T\mathbf{A}$ is always square. Thus, the matrix product may be inverted provided it is positive definite (not singular)[1].

[1] A matrix $\mathbf{Y}$ is positive definite when $\mathbf{x}^T\mathbf{Y}\mathbf{x} > 0$ for all $\mathbf{x}$. This is also the observability requirement.

Finally, solving for $\hat{\mathbf{X}}$, the general solution of Least Squares technique for the linear unweighted case is provided.

$$\hat{\mathbf{X}} = (\mathbf{A}^T\mathbf{A})^{-1}\mathbf{A}^T\mathbf{b} \tag{4.3}$$

The overall process is sometimes called parameter estimation because the final objective is to determine the α and β parameters.

In order to account for differences in the accuracy of measurements, weights, w_i, must be introduced. The residuals are weighted using the inverses of the standard deviations of each observation classes, usually by a sensor type or location. Thus, all the observations (of the same type) from a particular sensor are assumed to have similar characteristics. Applying the Least Squares criterion (i.e., Equation [4.1]) to the weighted residuals produces the cost function

$$J = \sum_{i=1}^{N} w_i^2 \bar{r}_i^2 = \bar{\mathbf{r}}^T\mathbf{W}\bar{\mathbf{r}} = (\mathbf{b}-\mathbf{AX})^T\mathbf{W}(\mathbf{b}-\mathbf{AX})$$

where

$$\bar{\mathbf{r}} = \begin{bmatrix} y_{0_1} - y_{c_1} \\ y_{0_2} - y_{c_2} \\ \vdots \\ y_{0_N} - y_{c_N} \end{bmatrix}, \mathbf{A} = \begin{bmatrix} 1 & x_{0_1} \\ 1 & x_{0_2} \\ \vdots & \vdots \\ 1 & x_{0_N} \end{bmatrix}, \mathbf{X} = \begin{bmatrix} \alpha \\ \beta \end{bmatrix}, \text{and } \mathbf{W} = \begin{bmatrix} w_1^2 & 0 & \dots & 0 \\ 0 & w_2^2 & & \vdots \\ \vdots & & \ddots & 0 \\ 0 & \cdots & 0 & w_N^2 \end{bmatrix}$$

The matrix $\mathbf{W}$ is called the weighting matrix whose diagonal elements are defined as

$$w_i = \begin{bmatrix} \frac{1}{\sigma_1} & 0 & \cdots & 0 \\ 0 & \frac{1}{\sigma_2} & \ddots & \vdots \\ \vdots & \ddots & \ddots & 0 \\ 0 & \cdots & 0 & \frac{1}{\sigma_M} \end{bmatrix}$$

where M refers to the total number of observation classes (i.e., range measurements, angular measurements, measurements of different sensors…) related to one observation (time epoch).

Before finding the minimum, let us expand the cost function

$$J = (\mathbf{b}-\mathbf{AX})^T\mathbf{W}(\mathbf{b}-\mathbf{AX}) = \mathbf{b}^T\mathbf{Wb} - 2\mathbf{b}^T\mathbf{WAX} + \mathbf{X}^T\mathbf{A}^T\mathbf{WAX}$$

In this way, setting the derivative with respect to $\mathbf{X}$ of the cost function equal to zero, one can obtain the best estimate of the state.

$$\frac{\partial J}{\partial \mathbf{X}} = -2\mathbf{b}^T\mathbf{WA} + 2\hat{\mathbf{X}}^T\mathbf{A}^T\mathbf{WA} = 0$$

After a few matrix operations, the solution state can be calculated as

$$\hat{\mathbf{X}} = (\mathbf{A}^T\mathbf{WA})^{-1}\mathbf{A}^T\mathbf{Wb} \tag{4.4}$$

where it has been assumed that $\mathbf{A}^T\mathbf{WA}$ is invertible (the observability criteria). Note also that $\mathbf{W}^T = \mathbf{W}$.

Equation (4.4) provides the general solution of linear Least Squares technique. However, orbit determination is not a linear case. Least Squares method can be applied to nonlinear problems by linearizing the problem, obtaining an approximate solution, and iterating in order to refine the answer. Next subsection introduces the nonlinear Least Squares technique.

b) Nonlinear Least Squares

In this case, the measurement-state relationship (i.e., the mathematical model used) is a nonlinear function of the state (e.g., $y = f(x) = \alpha \sin(x + \beta)$ where, in this case, α and β are again the parameters to be estimated). Thus, when applying the derivative to the cost function and rearranging all parameters as the previous subsection (Equation [4.2]), one may realise that α and β, or at least one of them, cannot be separated, so that the solution state, $\widehat{\mathbf{X}}$, cannot be reached.

Fortunately, the nonlinear equations can be approximated to linear equations by means of Taylor series, provided that one can neglect the higher order terms in the Taylor series. In this way, if the measurement-state relationship is calculated as a function $y = f(\alpha, \beta)$ about a nominal α_n and β_n, the computed value of the dependent variable, y_c, can be obtained as

$$y_{\mathrm{c}} = f(\alpha, \beta, x_0) = g(\alpha, \beta) \text{ for any given } x_0$$

whose Taylor series is

$$y_{\mathrm{c}} = y|_{\alpha_n,\beta_n} + (\alpha - \alpha_n)\left.\frac{\partial y}{\partial \alpha}\right|_{\alpha_n,\beta_n} + (\beta - \beta_n)\left.\frac{\partial y}{\partial \beta}\right|_{\alpha_n,\beta_n} + \frac{(\alpha - \alpha_n)^2}{2!}\left.\frac{\partial^2 y}{\partial \alpha^2}\right|_{\alpha_n,\beta_n} + \frac{(\beta - \beta_n)^2}{2!}\left.\frac{\partial^2 y}{\partial \beta^2}\right|_{\alpha_n,\beta_n} + \cdots$$

Because higher power (second order and above) of $(\alpha - \alpha_n)$ and $(\beta - \beta_n)$ are neglected in the linearization, the formulation provides corrections to a known state as $\Delta\alpha = \alpha - \alpha_n$ and $\Delta\beta = \beta - \beta_n$. The nonlinear Least Squares problem consequently requires an a priori estimate of the state for solution, which will be called nominal state vector.

At this point, the computed value of the dependent variable per each data point, y_{c_i}, can be obtained as

$$y_{\mathrm{c}_i} = y_{n_i} + \Delta\alpha \frac{\partial y_{n_i}}{\partial \alpha} + \Delta\beta \frac{\partial y_{n_i}}{\partial \beta}$$

where

$$y_{n_i} = y_i|_{\alpha_n,\beta_n}, \qquad \frac{\partial y_{n_i}}{\partial (a)} = \left.\frac{\partial y_i}{\partial (a)}\right|_{a=\alpha_n,\beta_n}$$

Now, the values of the observations and the partial derivatives can be calculated by using the initial estimates of the state (α_n, β_n) from above. Thus, Equation (4.2) for a nonlinear Least Squares problem, which has been linearized, becomes

$$\mathbf{A}^T \begin{bmatrix} y_{0_1} - \left(y_{n_1} + \Delta\alpha \dfrac{\partial y_{n_1}}{\partial \alpha} + \Delta\beta \dfrac{\partial y_{n_1}}{\partial \beta} \right) \\ y_{0_2} - \left(y_{n_2} + \Delta\alpha \dfrac{\partial y_{n_2}}{\partial \alpha} + \Delta\beta \dfrac{\partial y_{n_2}}{\partial \beta} \right) \\ \vdots \\ y_{0_N} - \left(y_{n_N} + \Delta\alpha \dfrac{\partial y_{n_N}}{\partial \alpha} + \Delta\beta \dfrac{\partial y_{n_N}}{\partial \beta} \right) \end{bmatrix} = \begin{bmatrix} 0 \\ 0 \end{bmatrix}$$

In the linear case, the partial-derivative matrix, **A**, contained partial derivatives of the residuals, $\partial r_i / \partial \alpha$; however, in this case, it contains partials of the measurements, $\partial y_{n_i} / \partial \alpha$.

Applying the distributive law and separating the state parameters $(\Delta\alpha, \Delta\beta)$, the equation above results in

$$\mathbf{A}^T \begin{bmatrix} y_{0_1} - y_{n_1} \\ y_{0_2} - y_{n_2} \\ \vdots \\ y_{0_N} - y_{n_N} \end{bmatrix} - \mathbf{A}^T \begin{bmatrix} \dfrac{\partial y_{n_1}}{\partial \alpha} & \dfrac{\partial y_{n_1}}{\partial \beta} \\ \dfrac{\partial y_{n_2}}{\partial \alpha} & \dfrac{\partial y_{n_2}}{\partial \beta} \\ \vdots & \vdots \\ \dfrac{\partial y_{n_N}}{\partial \alpha} & \dfrac{\partial y_{n_N}}{\partial \beta} \end{bmatrix} \begin{bmatrix} \Delta\alpha \\ \Delta\beta \end{bmatrix} = \begin{bmatrix} 0 \\ 0 \end{bmatrix}$$

Some features of this equation must be considered. First, the matrix containing $y_{0_i} - y_{n_i}$ looks like the **b** matrix, except it contains differences between the measured and nominal y values. It will be called residual matrix and will be noted with symbol $\tilde{\mathbf{b}}$. Second, the matrix containing the observation partials is the transpose of $\mathbf{A}^T$, so that it is the **A** matrix. Finally, the matrix containing $\Delta\alpha$ and $\Delta\beta$ corresponds to the $\hat{\mathbf{X}}$ matrix, except it is now the corrections to α and β. For this reason, it will be called $\delta\tilde{\mathbf{x}}$. Substituting the newly defined matrices, the equation above becomes

$$\mathbf{A}^T \tilde{\mathbf{b}} - \mathbf{A}^T \mathbf{A} \delta\tilde{\mathbf{x}} = 0$$

and assuming observability, the estimated corrections to the state are

$$\delta\hat{\mathbf{x}} = (\mathbf{A}^T \mathbf{A})^{-1} \mathbf{A}^T \tilde{\mathbf{b}} \tag{4.5}$$

Equation (4.5) is identical to the linear Least Squares equation, except that

1) **A**, $\tilde{\mathbf{b}}$, and $\delta\hat{\mathbf{x}}$ are defined in the derivation.

2) **A**, $\mathbf{A}^T$, and $\delta\hat{\mathbf{x}}$ use the previous estimates of α_n and β_n.

3) It is an approximate solution due to the use of a truncated Taylor series.

4) An initial nominal state (α_n and β_n in this case) must be calculated. This is important because the initial nominal value must be near the global minimum value. Otherwise, the iteration may diverge or, in some cases, converge on an incorrect value.

Points (2) and (3) imply the need to iterate in order to improve the estimates whereas, in the linear case, the solutions of α and β were obtained directly.

The steps for the most general form of differential correction using Gaussian Least Squares[1] are:

1) Compute y_{n_i} corresponding to each x_{0_i}.

2) Compute each residual $\bar{r}_i = y_{0_i} - y_{n_i}$.

3) Compute each partial derivative, $\partial y_{n_i}/\partial\alpha$ and $\partial y_{n_i}/\partial\beta$, using α_n, β_n.

4) Form $\mathbf{A}$, $\mathbf{A}^T$, and $\tilde{\mathbf{b}}$.

5) Solve for $\Delta\alpha$ and $\Delta\beta$ using Equation (4.5).

6) Find $\alpha_{n_{\text{new}}} = \alpha_{n_{\text{old}}} + \Delta\alpha$ and $\beta_{n_{\text{new}}} = \beta_{n_{\text{old}}} + \Delta\beta$.

7) If the stopping criterion is reached, quit. Otherwise, return to step (1). A specific criterion for stopping the algorithm will not be used when performing the Least Squares technique in the following simulations. It will be used a certain number of iterations in order to evaluate the algorithm performance. Consult Vallado (2013) for stopping criterions.

All this process is termed differential correction since the state is corrected each iteration.

Weighting the observations may also be addressed. Weighting appears in the solution of the nonlinear problem exactly as it does in the linear case. Thus, the differential-correction equation for nonlinear, weighted Least Squares becomes

$$\delta\hat{\mathbf{x}} = (\mathbf{A}^T\mathbf{W}\mathbf{A})^{-1}\mathbf{A}^T\mathbf{W}\tilde{\mathbf{b}} \tag{4.6}$$

where $\mathbf{W}$ is again the weighting matrix of dimension $N \times N$.

4.2. APPYING LEAST SQUARES TECHNIQUE TO ORBIT DETERMINATION

The differential-correction technique described previously (i.e, the nonlinear Least Squares) is a powerful tool, which can accurately estimate an orbit state from radar, optical, or other measurements of the motion.

When applying differential correction to orbit determination, several situations must be handled:

1) Several element sets may be chosen in order to define the state space, $\hat{\mathbf{X}}$, such as the position and velocity vectors, $\{r_I, r_J, r_K, v_I, v_J, v_K\}$, or an element set composed of Classical Orbital Elements

[1] Gauss has been credited with discovering the Least Squares method with some help from Legendre.

(see Section 3.2). The simulations performed within this document will use the position and velocity vectors since they work well for special orbits such as circular and elliptical equatorial orbits (i.e., GEOSAR mission case).

2) More than one observation is required at each observation time. GEOSAR mission fulfils this requirement since at least three observations (i.e., one range observation for each of the three sites) are provided at each epoch. Remember that the sites may also offer range-rate observations. In this latter case, six observations would be provided at each observation time.

3) The measurements are nonlinear, complex functions of the state.

Considering such requirements, let us formulate the Least Squares technique to the context of GEOSAR mission. It has been said that each site can provide only range measurements or range and range-rate measurements at each time t_i. Thus, the observed values of the dependent variable at time t_i, y_{0_i}, can be expressed as

$$y_{0_i} = \begin{bmatrix} \rho_{1_0} \\ \rho_{2_0} \\ \rho_{3_0} \end{bmatrix} \text{ at } t_i \quad \text{or} \quad y_{0_i} = \begin{bmatrix} \rho_{1_0} \\ \dot{\rho}_{1_0} \\ \rho_{2_0} \\ \dot{\rho}_{2_0} \\ \rho_{3_0} \\ \dot{\rho}_{3_0} \end{bmatrix} \text{ at } t_i$$

In order to calculate the residuals, some predicted measurements from the position and velocity vectors must be obtained:

$$y_{c_i} = \begin{bmatrix} \rho_{1_c} \\ \rho_{2_c} \\ \rho_{3_c} \end{bmatrix} \text{ at } t_i \quad \text{or} \quad y_{c_i} = \begin{bmatrix} \rho_{1_c} \\ \dot{\rho}_{1_c} \\ \rho_{2_c} \\ \dot{\rho}_{2_c} \\ \rho_{3_c} \\ \dot{\rho}_{3_c} \end{bmatrix} \text{ at } t_i$$

Because y_{c_i} is a nonlinear function of the position and velocity vectors, it must be expressed using a first-order Taylor series. In this approach, the computed measurement must be obtained as a Taylor-series expansion about a nominal trajectory. Thus, vector y_{c_i} becomes

$$y_{c_i} = y_{n_i} + \Delta r_I \frac{\partial y_{n_i}}{\partial r_I} + \Delta r_J \frac{\partial y_{n_i}}{\partial r_J} + \Delta r_K \frac{\partial y_{n_i}}{\partial r_K} + \Delta v_I \frac{\partial y_{n_i}}{\partial v_I} + \Delta v_J \frac{\partial y_{n_i}}{\partial v_J} + \Delta v_K \frac{\partial y_{n_i}}{\partial v_K}$$

The nominal trajectory is $y_{n_i} = f(r_I, r_J, r_K, v_I, v_J, v_K, t_i)$, a function of the nominal state vector at each observation time[1].

Once y_{0_i} and y_{c_i} have been defined, the residuals, $\bar{r}_i$, can be calculated as

$$\bar{r}_i = y_{0_i} - y_{c_i} = y_{0_i} - \left(y_{n_i} + \Delta r_I \frac{\partial y_{n_i}}{\partial r_I} + \cdots + \Delta v_K \frac{\partial y_{n_i}}{\partial v_K} \right)$$

[1] The requirement for nominal vectors often means that the initial orbit must be determined (see Chapter 3) in order to form each vector from the observations. The vectors are then propagated to a common epoch, where the nominal vector is formed.

Assuming that each measurement is weighted using its appropriate standard deviation,

$$w_{\rho_j} = \frac{1}{\sigma_{\rho_j}}, w_{\dot{\rho}_j} = \frac{1}{\sigma_{\dot{\rho}_j}} \quad \text{where} \quad j = 1, 2, 3$$

the cost function, J, can be formulated

$$J = \sum_{i=1}^{N} (w_i \bar{r}_i)^T (w_i \bar{r}_i)$$

where

$$w_i = \begin{bmatrix} w_{\rho_1} & 0 & 0 \\ 0 & w_{\rho_2} & 0 \\ 0 & 0 & w_{\rho_3} \end{bmatrix} \quad \text{or} \quad w_i = \begin{bmatrix} w_{\rho_1} & 0 & 0 & 0 & 0 & 0 \\ 0 & w_{\dot{\rho}_1} & 0 & 0 & 0 & 0 \\ 0 & 0 & w_{\rho_2} & 0 & 0 & 0 \\ 0 & 0 & 0 & w_{\dot{\rho}_2} & 0 & 0 \\ 0 & 0 & 0 & 0 & w_{\rho_3} & 0 \\ 0 & 0 & 0 & 0 & 0 & w_{\dot{\rho}_3} \end{bmatrix}$$

At this point, the cost function minimum must be obtained. Therefore, the first derivative with respect to all state parameters (Δr_I, Δr_J, Δr_K, Δv_I, Δv_J, and Δv_K) to zero must be calculated, which produces six scalar equations:

$$\sum_{i=1}^{N} w_i^2 \bar{r}_i \frac{\partial \bar{r}_i}{\partial \Delta r_I} = \sum_{i=1}^{N} w_i^2 \bar{r}_i \frac{\partial}{\partial \Delta r_I}\left(y_{0_i} - y_{n_i} - \Delta r_I \frac{\partial y_{n_i}}{\partial r_I} - \cdots - \Delta v_K \frac{\partial y_{n_i}}{\partial v_K}\right) = \sum_{i=1}^{N} w_i^2 \bar{r}_i \left(-\frac{\partial y_{n_i}}{\partial r_I}\right) = 0$$

$$\vdots$$

$$\sum_{i=1}^{N} w_i^2 \bar{r}_i \frac{\partial \bar{r}_i}{\partial \Delta v_K} = \sum_{i=1}^{N} w_i^2 \bar{r}_i \frac{\partial}{\partial \Delta v_K}\left(y_{0_i} - y_{n_i} - \Delta r_I \frac{\partial y_{n_i}}{\partial r_I} - \cdots - \Delta v_K \frac{\partial y_{n_i}}{\partial v_K}\right) = \sum_{i=1}^{N} w_i^2 \bar{r}_i \left(-\frac{\partial y_{n_i}}{\partial v_K}\right) = 0$$

Setting the equations above in matrix form results in

$$(-1)\begin{bmatrix} \frac{\partial y_{n_1}}{\partial r_I} & \frac{\partial y_{n_2}}{\partial r_I} & \cdots & \frac{\partial y_{n_N}}{\partial r_I} \\ \frac{\partial y_{n_1}}{\partial r_J} & \frac{\partial y_{n_2}}{\partial r_J} & \cdots & \frac{\partial y_{n_N}}{\partial r_J} \\ \vdots & \vdots & & \vdots \\ \frac{\partial y_{n_1}}{\partial v_K} & \frac{\partial y_{n_2}}{\partial v_K} & \cdots & \frac{\partial y_{n_N}}{\partial v_K} \end{bmatrix} \begin{bmatrix} w_1^2 \bar{r}_1 \\ w_2^2 \bar{r}_2 \\ \vdots \\ w_N^2 \bar{r}_N \end{bmatrix} = \begin{bmatrix} 0 \\ \vdots \\ 0 \end{bmatrix}$$

Now, substituting the definition of the residual, $\bar{r}_i$, yield

$$\begin{bmatrix} \frac{\partial y_{n_1}}{\partial r_I} & \frac{\partial y_{n_2}}{\partial r_I} & \cdots & \frac{\partial y_{n_N}}{\partial r_I} \\ \frac{\partial y_{n_1}}{\partial r_J} & \frac{\partial y_{n_2}}{\partial r_J} & \cdots & \frac{\partial y_{n_N}}{\partial r_J} \\ \vdots & \vdots & & \vdots \\ \frac{\partial y_{n_1}}{\partial v_K} & \frac{\partial y_{n_2}}{\partial v_K} & \cdots & \frac{\partial y_{n_N}}{\partial v_K} \end{bmatrix} \begin{bmatrix} w_1^2 \left[y_{0_1} - \left(y_{n_1} + \Delta r_I \frac{\partial y_{n_1}}{\partial r_I} + \cdots + \Delta v_K \frac{\partial y_{n_1}}{\partial v_K}\right)\right] \\ w_2^2 \left[y_{0_2} - \left(y_{n_2} + \Delta r_I \frac{\partial y_{n_2}}{\partial r_I} + \cdots + \Delta v_K \frac{\partial y_{n_2}}{\partial v_K}\right)\right] \\ \vdots \\ w_N^2 \left[y_{0_N} - \left(y_{n_N} + \Delta r_I \frac{\partial y_{n_N}}{\partial r_I} + \cdots + \Delta v_K \frac{\partial y_{n_N}}{\partial v_K}\right)\right] \end{bmatrix} = \begin{bmatrix} 0 \\ \vdots \\ 0 \end{bmatrix}$$

Finally, rearranging the matrices, Equation (4.6) is obtained.

$$\begin{bmatrix} \frac{\partial y_{n_1}}{\partial r_I} & \frac{\partial y_{n_2}}{\partial r_I} & \cdots & \frac{\partial y_{n_N}}{\partial r_I} \\ \frac{\partial y_{n_1}}{\partial r_J} & \frac{\partial y_{n_2}}{\partial r_J} & \cdots & \frac{\partial y_{n_N}}{\partial r_J} \\ \vdots & \vdots & & \vdots \\ \frac{\partial y_{n_1}}{\partial v_K} & \frac{\partial y_{n_2}}{\partial v_K} & \cdots & \frac{\partial y_{n_N}}{\partial v_K} \end{bmatrix} \begin{bmatrix} w_1^2 & 0 & \dots & 0 \\ 0 & w_2^2 & & \vdots \\ \vdots & & \ddots & 0 \\ 0 & \cdots & 0 & w_N^2 \end{bmatrix} \begin{bmatrix} \frac{\partial y_{n_1}}{\partial r_I} & \frac{\partial y_{n_1}}{\partial r_J} & \cdots & \frac{\partial y_{n_1}}{\partial v_K} \\ \frac{\partial y_{n_2}}{\partial r_I} & \frac{\partial y_{n_2}}{\partial r_J} & \cdots & \frac{\partial y_{n_2}}{\partial v_K} \\ \vdots & \vdots & & \vdots \\ \frac{\partial y_{n_N}}{\partial r_I} & \frac{\partial y_{n_N}}{\partial r_J} & \cdots & \frac{\partial y_{n_N}}{\partial v_K} \end{bmatrix} \begin{bmatrix} \Delta r_I \\ \Delta r_J \\ \vdots \\ \Delta v_K \end{bmatrix} =$$

$$= \begin{bmatrix} \frac{\partial y_{n_1}}{\partial r_I} & \frac{\partial y_{n_2}}{\partial r_I} & \cdots & \frac{\partial y_{n_N}}{\partial r_I} \\ \frac{\partial y_{n_1}}{\partial r_J} & \frac{\partial y_{n_2}}{\partial r_J} & \cdots & \frac{\partial y_{n_N}}{\partial r_J} \\ \vdots & \vdots & & \vdots \\ \frac{\partial y_{n_1}}{\partial v_K} & \frac{\partial y_{n_2}}{\partial v_K} & \cdots & \frac{\partial y_{n_N}}{\partial v_K} \end{bmatrix} \begin{bmatrix} w_1^2 & 0 & \dots & 0 \\ 0 & w_2^2 & & \vdots \\ \vdots & & \ddots & 0 \\ 0 & \cdots & 0 & w_N^2 \end{bmatrix} \begin{bmatrix} y_{0_1} - y_{n_1} \\ y_{0_2} - y_{n_2} \\ \vdots \\ y_{0_N} - y_{n_N} \end{bmatrix}$$

where

$$\delta\hat{\mathbf{x}} = \begin{bmatrix} \Delta r_I \\ \Delta r_J \\ \Delta r_K \\ \Delta v_I \\ \Delta v_J \\ \Delta v_K \end{bmatrix}, \mathbf{A} = \begin{bmatrix} \frac{\partial y_{n_1}}{\partial r_I} & \frac{\partial y_{n_1}}{\partial r_J} & \cdots & \frac{\partial y_{n_1}}{\partial v_K} \\ \frac{\partial y_{n_2}}{\partial r_I} & \frac{\partial y_{n_2}}{\partial r_J} & \cdots & \frac{\partial y_{n_2}}{\partial v_K} \\ \vdots & \vdots & & \vdots \\ \frac{\partial y_{n_N}}{\partial r_I} & \frac{\partial y_{n_N}}{\partial r_J} & \cdots & \frac{\partial y_{n_N}}{\partial v_K} \end{bmatrix}, \mathbf{W} = \begin{bmatrix} w_1^2 & 0 & \dots & 0 \\ 0 & w_2^2 & & \vdots \\ \vdots & & \ddots & 0 \\ 0 & \cdots & 0 & w_N^2 \end{bmatrix}, \text{and } \tilde{\mathbf{b}} = \begin{bmatrix} y_{0_1} - y_{n_1} \\ y_{0_2} - y_{n_2} \\ \vdots \\ y_{0_N} - y_{n_N} \end{bmatrix}$$

In order to clarify the dimension of each vector and matrix above and its elements, Figures 4.1, 4.2 and 4.3 illustrates the structure of all of them, except for vector $\delta\hat{\mathbf{x}}$ whose dimensions are 6×1. The vectors and matrices structure takes into account the two possible cases of GEOSAR mission: a) only range measurements, and b) range and range-rate measurements. Thus, one may see an overview of how each observation is split in M measurements (observed values).

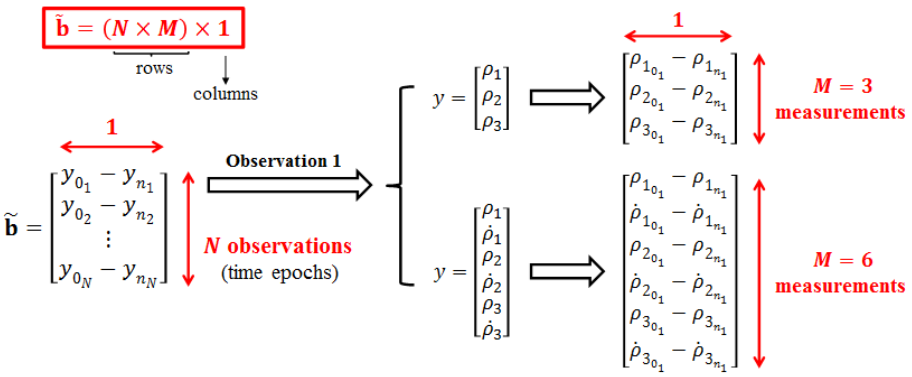

Figure 4.1: *Dimensions and structure of vector* $\tilde{\mathbf{b}}$.

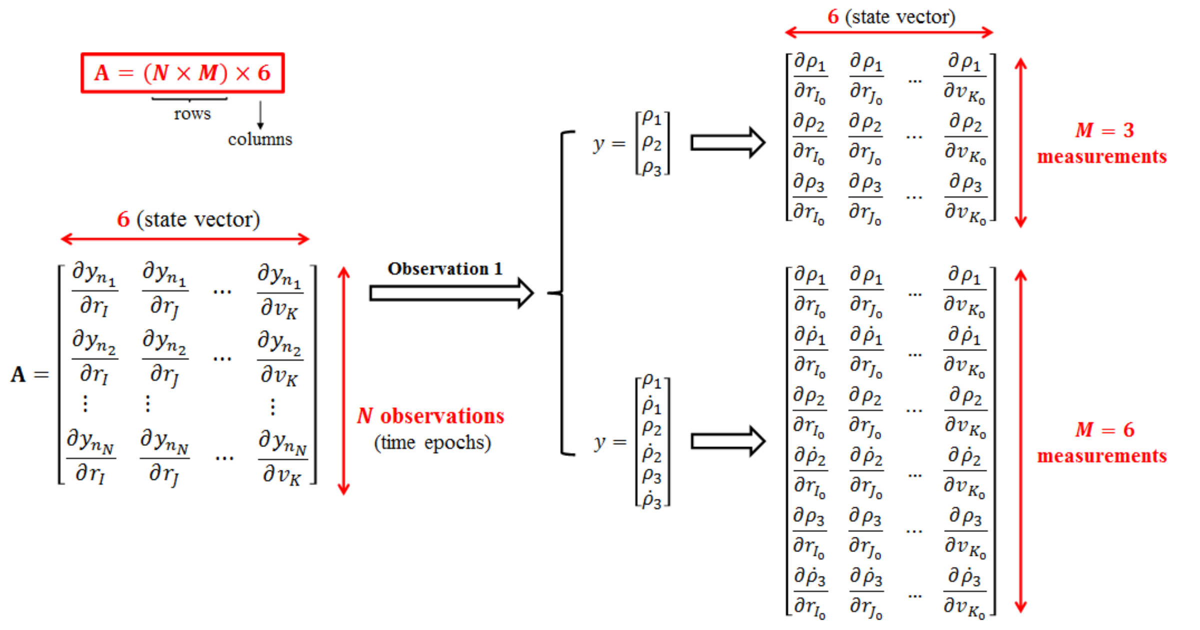

Figure 4.2: *Dimensions and structure of matrix* **A**.

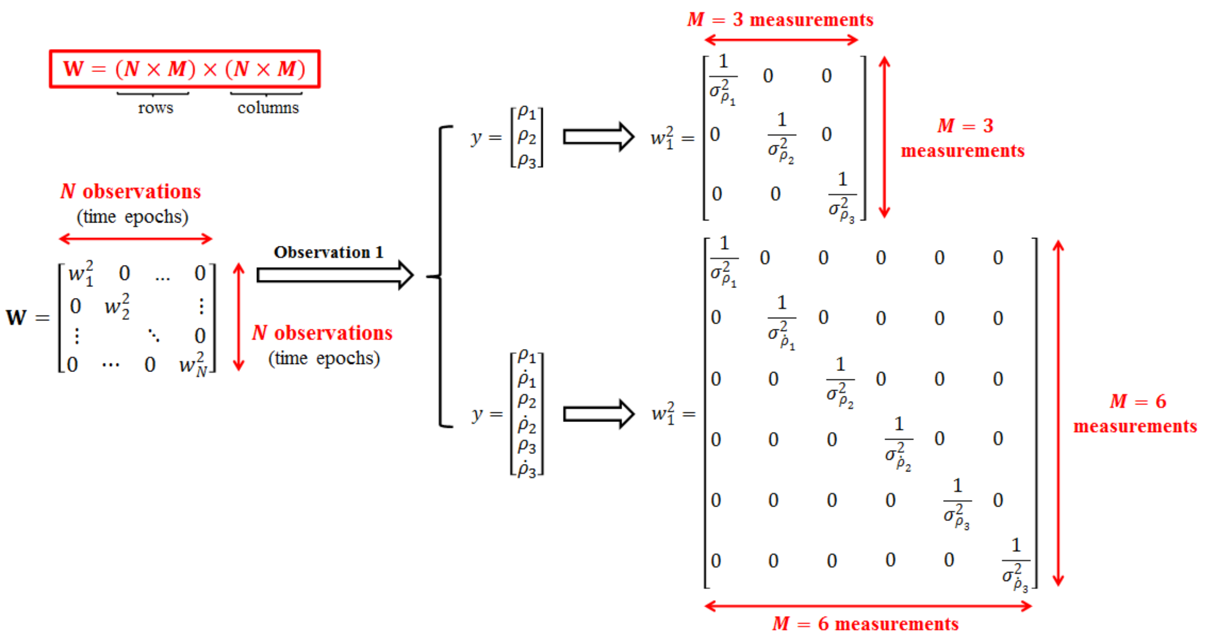

Figure 4.3: *Dimensions and structure of matrix* **W**.

Now, it must be explained how to calculate matrix **A**. The **A** matrix describes how changes in the initial state (position and velocity vectors) affect the computed observations (measurements). These are sometimes called sensitivity partial derivatives. In order to find these nonlinear, time-dependent derivatives, the first step is to break up the partial derivative using the chain rule:

$$\mathbf{A} = \frac{\partial \text{observations}}{\partial \hat{\mathbf{X}}_0} = \frac{\partial \text{observations}}{\partial \hat{\mathbf{X}}} \frac{\partial \hat{\mathbf{X}}}{\partial \hat{\mathbf{X}}_0} = \mathbf{H\Phi} \tag{4.7}$$

Equation (4.7) distinguishes the observation partial derivatives, **H**, from the partial derivative of the state over time. This latter matrix, **Φ**, is called the matrix of variational equations, or the error state transition matrix, and it relates the state errors at time t ($\boldsymbol{\delta}\hat{\mathbf{x}}$), to the state errors at time t_0 ($\boldsymbol{\delta}\hat{\mathbf{x}}_0$). Both matrices, **H** and **Φ**, can be calculated using analytical or numerical integration techniques, or by finite differencing. This document will use finite differencing, so that the reader may consult Vallado (2013) or Montenbruck et al. (2000) for further information about analytical or numerical integration techniques, which consider perturbations.

It is fairly simple to approximate the complete matrix **A** using finite differencing. This technique takes small differences of the state in order to determine their effect on the system. In addition, the technique is independent of any particular propagation method.

$$\frac{\partial \text{observations}}{\partial \hat{\mathbf{X}}_0} \cong \frac{f\left(\hat{\mathbf{X}} + \delta_i\right) - f\left(\hat{\mathbf{X}}\right)}{\delta_i} \tag{4.8}$$

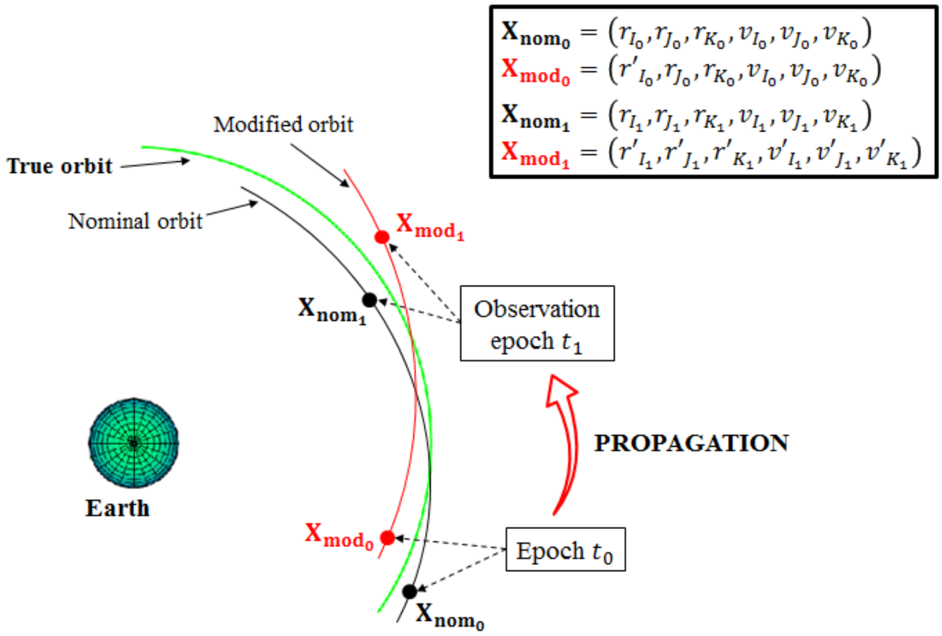

Figure 4.4: *Determination of the first modified orbit when using finite differencing.*

The main idea is to take the partial derivative of the observations (at the observation times) with respect to the state at the epoch time. In order to do this, one must proceed as follows:

1) Generate position and velocity vectors at the times of the observations from the nominal state at epoch t_0. Although one can choose any epoch time, the beginning or the end of the data are most common.

2) Determine six additional trajectories varying each component of the position and velocity vectors. Figure 4.4 illustrates the first modified trajectory when the first component of the nominal state vector, r_{I_0}, is perturbed.

3) Compute each partial derivative from the observations and each varied trajectories. Thus, an approximation to the partial derivative is achieved.

Step (2) must be performed modifying each state element with a percentage of the vector magnitude rather than a fixed delta. Thus, the value of δ_i of Equation (4.8) can be determined as the modified state minus the nominal state,

$$\delta_i = \widehat{\mathbf{X}}_{\mathrm{mod}_i} - \widehat{\mathbf{X}}_{\mathrm{nom}_i}$$

and each observation can be calculated as the modified observation minus the nominal observation. As a result, the approximation of the derivative of each observation with respect to an element of the state becomes

$$\frac{\partial \mathrm{observations}}{\partial \widehat{\mathbf{X}}_0} \cong \frac{\mathrm{obs}_{\mathrm{mod}} - \mathrm{obs}_{\mathrm{nom}}}{\delta_i}$$

Figure 4.5 shows how the partial derivatives are calculated when using finite differencing in the first possible case of GEOSAR mission (i.e., when only range measurements are provided).

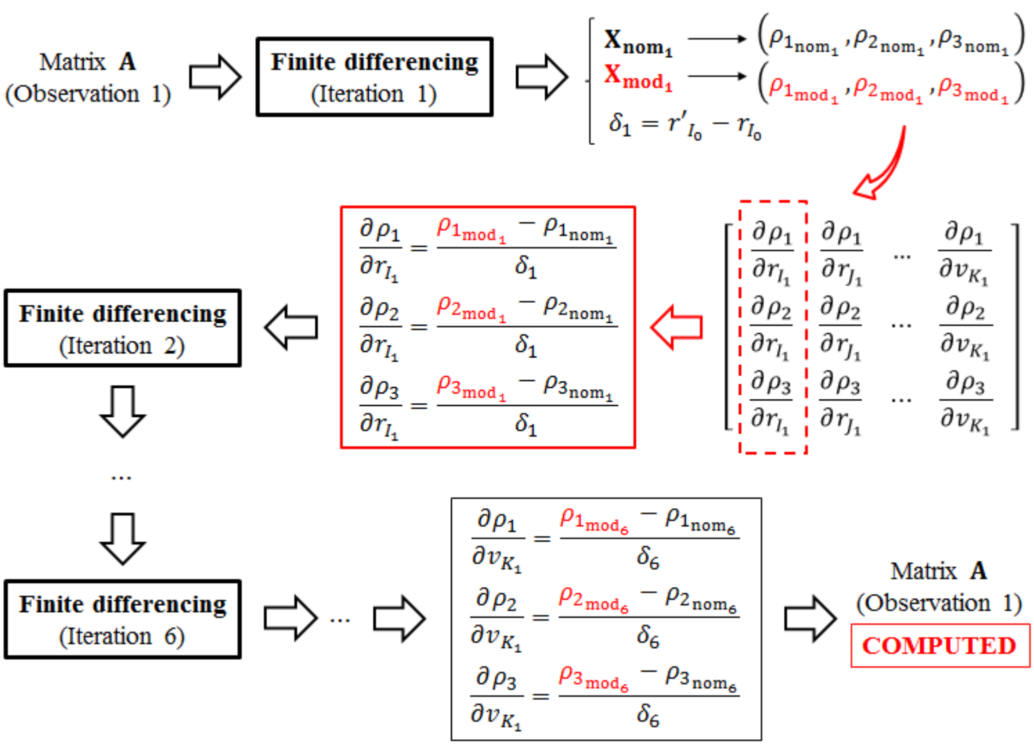

Figure 4.5: *Partial derivatives calculation when using finite differencing.*

In order to conclude the explanation of finite differencing technique, Table 4.1 summarizes all steps performed by this technique in algorithm form.

FINITE DIFFERENCING ALGORITHM
FOR $j = 1$ to 6 (i.e., number of state vector components) 1) Propagate the nominal state vector from t_0 (i.e., the epoch where the nominal state vector is given) to the observation time t_i. 2) Compute all observed values from the nominal state vector at t_i (i.e., $\rho_{1_{\text{nom}_i}}$, $\dot{\rho}_{1_{\text{nom}_i}}$, …). 3) Calculate the modified state vector at t_0. • $\delta_j = \widehat{\mathbf{X}}_{\text{nom}_j} \times 0.01$ (i.e., modify by 1 % the original component value). • $\widehat{\mathbf{X}}_{\text{mod}_j} = \widehat{\mathbf{X}}_{\text{nom}_j} + \delta_j$. 4) Propagate the modified state vector from t_0 to t_i. 5) Compute all observed values from the modified state vector at t_i (i.e., $\rho_{1_{\text{mod}_j}}$, $\dot{\rho}_{1_{\text{mod}_j}}$, …). 6) Compute the **A** matrix elements for each observed value. • $\frac{\partial \text{obs}}{\partial \text{component}} \approx \frac{\delta \text{obs}_j}{\delta_j} = \frac{\text{obs}_{\text{mod}} - \text{obs}_{\text{nom}}}{\delta_j}$. 7) Reset the modified component $\widehat{\mathbf{X}}_{\text{mod}_j}$ to its original value $\widehat{\mathbf{X}}_{\text{nom}_j}$. END LOOP

Table 4.1: *Finite differencing algorithm.*

Once the calculation of **A** matrix has been explained, Equation (4.6) can be performed. The resulting $\delta\hat{\mathbf{x}}$ value must be added to the nominal state vector. At this point, the convergence must be checked. The simulations performed into this document will not follow any convergence criteria, so that the final algorithm will iterate a fixed number of iterations in order to evaluate its performance.

Table 4.2 shows the complete Least Squares algorithm related to orbit determination in the GEOSAR mission context, which will be used in the simulations of the following section.

In order to conclude this section, it must be said that Least Squares may process successive batches of data in order not to redo all calculations performed when new data is provided. Such technique is called sequential batch Least Squares and uses Bayes estimation. The reader may consult Vallado (2013) for further information about this technique since it will not be used within the simulations of this document.

LEAST SQUARES ALGORITHM
Compute the nominal state vector at time t_0, $\hat{\mathbf{X}}_{\text{nom}_0}$ by using one of the methods of Chapter 3. FOR $i = 1$ to 100 (i.e., total number of Least Squares iterations) FOR $j = 1$ to N (i.e., total number of observations) 1) Propagate the nominal state vector from t_0 to the observation time t_j. 2) Compute all observed values from the nominal state vector at t_j (i.e., $\rho_{1_{\text{nom}_j}}$, $\dot{\rho}_{1_{\text{nom}_j}}$, …). 3) Find vector $\tilde{\mathbf{b}}$ corresponding to observation j, $\tilde{\mathbf{b}}_j$. • $\tilde{\mathbf{b}}_j = \left[y_{\text{obs}_j} - y_{\text{nom}_j}\right] = \begin{bmatrix} \rho_{1_{\text{obs}_j}} - \rho_{1_{\text{nom}_j}} \\ \rho_{2_{\text{obs}_j}} - \rho_{2_{\text{nom}_j}} \\ \rho_{3_{\text{obs}_j}} - \rho_{3_{\text{nom}_j}} \end{bmatrix}$, or • $\tilde{\mathbf{b}}_j = \left[y_{\text{obs}_j} - y_{\text{nom}_j}\right] = \begin{bmatrix} \rho_{1_{\text{obs}_j}} - \rho_{1_{\text{nom}_j}} \\ \dot{\rho}_{1_{\text{obs}_j}} - \dot{\rho}_{1_{\text{nom}_j}} \\ \rho_{2_{\text{obs}_j}} - \rho_{2_{\text{nom}_j}} \\ \dot{\rho}_{2_{\text{obs}_j}} - \dot{\rho}_{2_{\text{nom}_j}} \\ \rho_{3_{\text{obs}_j}} - \rho_{3_{\text{nom}_j}} \\ \dot{\rho}_{3_{\text{obs}_j}} - \dot{\rho}_{3_{\text{nom}_j}} \end{bmatrix}$ 4) Perform Finite Differencing for the $\mathbf{A}$ matrix corresponding to observation j, $\mathbf{A}_j$. END FOR 5) Concatenate all vectors $\tilde{\mathbf{b}}_j$ and matrices $\mathbf{A}_j$ in order to build vector $\tilde{\mathbf{b}}$ and matrix $\mathbf{A}$. 6) Compute the transpose of matrix $\mathbf{A}$, $\mathbf{A}^T$. 7) Compute the weighting matrix, $\mathbf{W}$. 8) Compute $(\mathbf{A}^T\mathbf{W}\mathbf{A})^{-1}$. 9) Find $\delta\hat{\mathbf{x}}$ from Equation (4.6). 10) Update the nominal state vector. • $\hat{\mathbf{X}}_{\text{nom}_0} = \hat{\mathbf{X}}_{\text{nom}_0} + \delta\hat{\mathbf{x}}$ END LOOP

Table 4.2: *Least Squares algorithm.*

4.3. RESULTS ANALYSES OF LEAST SQUARES TECHNIQUE

This section will analyse the precision of Least Squares technique when different simulations of the Least Squares algorithm of the previous section are performed. Each simulation will be independent of the other since the quantity of noise added to the ideal range and range-rate observations will be random and delimited by the same standard deviation calculated in Section 3.6. Thus, the results obtained in each simulation will be different, and therefore there is a need to perform statistical simulations. All Matlab functions and scripts used in such simulations are listed and briefly explained in Appendix A.

The simulations proceeding will be similar to those performed in Chapter 3. First, different settings will be analysed considering either range and range-rate observations or only range observations. Second, each statistical simulation will use 1 000 samples (i.e., the complete Least Squares algorithm will be repeated 1 000 times on each statistical simulation). Third, the noisy observations will be provided equally spaced in a time span of 6 h, which will simulate the radar synthetic aperture duration. Forth, the amount of observations given will be 1 000 in all simulations, so that the interval of time between observations will be of 20 seconds approximately. During the simulation of the first setting, 10 and 100 observations will also be used. In this way, the reader will see how the available number of observations affects the final precision of Least Squares technique. Finally, the initial state vector will be given at $t_0 = 0$ s for all settings used. Thus, in this section, there will not be distinction in the initial epoch selected depending on the initial observations provided. Remember that Least Squares technique uses all available data in order to improve the initial state.

In Chapter 3, it has been explained the methods used in order to obtain the initial nominal state vector when range and range-rate observations are given. Now, in Chapter 4, more than 3 observations are available[1], so that the determination of the initial state may be improved by means of averaging the initial state vectors calculated when using different observations of different epochs. Imagine that range and range-rate observations are available. One state vector can be calculated at each observation epoch by means of Trilateration method. Propagating all of them to the same epoch, let us say the initial epoch t_0, and performing an average of all of these vectors, the initial state vector estimate is improved. Thus, Least Squares technique needs less iterations in order to converge. However, it may happen that the initial estimate is too close to the real one (e.g., a few metres of difference in the satellite position state vector), and this fact entails problems when the partial-derivative matrix, $\mathbf{A}$, is calculated (i.e., matrix $\mathbf{A}$ is not full rank, so that $(\mathbf{A}^T\mathbf{W}\mathbf{A})^{-1}$ cannot be calculated). Therefore, there is no need to obtain a very precise initial nominal state vector when using Least Squares technique.

In order to see better how Least Squares technique works, the initial nominal state vector has been chosen manually. That is to say, as the ideal satellite state vector value at epoch t_0 is known, one may vary its values in an appropriate way in order to obtain the initial nominal state vector. Table 4.3 shows the initial nominal state vector used as a starting point for all settings that are going to be simulated.

Previous to show the results, it must be said that the Least Squares algorithm has been set to iterate 100 times per each sample of the statistical simulation. Thus, some intermediate results will also be collected in order to evaluate the Least Squares performance. The results will show the errors in the approximate satellite state vector (i.e., how the initial nominal state vector errors vary along the Least Squares iterations), and the errors in the range and range-rate observations of the same locations evaluated in the simulations of the previous chapter.

[1] Remember that, when only range observations are given, the range observations must be provided at three different epochs in order to calculate the initial state vector.

	SATELLITE STATE VECTOR AT $t_0 = 0$ s		Initial error
	Ideal value	Initial nominal value	
r_x [km]	39 811.324 342 080 086	39 861.324 342 080 086	50.000 000 000 000
r_y [km]	13 863.769 945 143 404	13 813.769 945 143 402	-50.000 000 000 002
r_z [km]	0.000 000 000 000	50.000 000 000 000	50.000 000 000 000
v_x [km/s]	-1.011 153 178 968	-1.611 153 178 968	-0.600 000 000 000
v_y [km/s]	2.904 251 340 218	3.304 251 340 218	0.400 000 000 000
v_z [km/s]	0.000 000 000 000	-0.500 000 000 000	-0.500 000 000 000

Table 4.3: *Initial nominal state vector at* $t_0 = 0$ s.

a) Results Analysis of Setting H

Table 4.4 summarizes all conditions taken into account when performing the statistical simulation of setting H.

Setting H

Location of the three sites in order to obtain the initial nominal state vector:
(01) Barcelona (Spain) / (02) Betzdorf (Luxemburg) / (03) Milan (Italy).

IDEAL DATA
- **Type of observations generated:** RANGE.
- **Number of observations generated per type and site:** 1 000.
- **Time span:** 6 h.

NOISE ADDED
- **Range observations:** MEAN: 0 m / STD.: 1 m.

APPROXIMATE DATA
- **Technique used:** LEAST SQUARES.
- **Epoch when the approximate satellite state vector is given:** $t_0 = 0$ s.

Table 4.4: *Summary of all conditions considered on setting H.*

As setting H is the first simulation to be analysed, some issues of the Least Squares algorithm will be evaluated in order to achieve a better understanding of how it works. In this way, first, it will be studied the algorithm convergence considering the use of 10, 100, and 1 000 range observations per site. Then, it will be shown the statistical simulations of these three cases in order to evaluate the Least Squares performance depending on the number of observations used. Finally, it will be discussed the need of using the matrix weighting, **W**.

Least Squares Algorithm Convergence

The convergence of Least Squares algorithm will be first evaluated by means of the values that the vector corrections to the state vector, $\delta\hat{\mathbf{x}}$, will take along the 100 iterations of the algorithm. Remember that vector $\delta\hat{\mathbf{x}}$ stands for the quantities to add or subtract to the initial nominal state vector in order to meet the ideal (or real) state vector value. Therefore, the algorithm convergence will be achieved when all components of $\delta\hat{\mathbf{x}}$ tend to zero. Table 4.5 shows these values related to the first, last, and two intermediate algorithm iterations when 10, 100, and 1 000 observations are available.

VECTOR CORRECTIONS TO THE STATE VECTOR ($\delta\hat{\mathbf{x}}$)				
	1 iteration	**5 iterations**	**10 iterations**	**100 iterations**
10 observations				
Δr_I [km]	-3 398.688 743 392 164	7.551 466 757 265	-0.000 000 005 521	0.000 000 014 671
Δr_J [km]	7 404.570 041 511 945	-22.351 284 190 081	0.000 000 047 278	-0.000 000 004 605
Δr_K [km]	-3 763.973 795 325 485	48.420 613 556 557	0.000 000 102 210	0.000 000 100 552
Δv_I [km/s]	-0.137 931 905 765	0.000 952 662 549	-0.000 000 000 004	0.000 000 000 001
Δv_J [km/s]	-0.897 575 778 875	0.000 431 719 380	-0.000 000 000 003	-0.000 000 000 001
Δv_k [km/s]	-0.847 552 955 657	-0.003 174 745 293	-0.000 000 000 015	-0.000 000 000 004
100 observations				
Δr_I [km]	-2 797.376 035 418 503	-0.724 838 847 395	-0.000 000 023 078	0.000 000 027 056
Δr_J [km]	6 083.544 042 823 009	-1.014 973 379 256	0.000 000 127 740	-0.000 000 078 793
Δr_K [km]	-2 528.329 262 221 871	2.425 283 473 699	0.000 000 202 795	-0.000 000 021 910
Δv_I [km/s]	0.021 368 880 662	0.000 280 478 520	-0.000 000 000 012	0.000 000 000 008
Δv_J [km/s]	-0.785 378 631 189	-0.000 026 171 636	-0.000 000 000 006	0.000 000 000 003
Δv_k [km/s]	-0.571 238 823 219	0.000 022 713 295	-0.000 000 000 039	0.000 000 000 019
1000 observations				
Δr_I [km]	-2 727.787 691 748 790	-1.331 548 925 731	-0.000 000 072 754	-0.000 000 024 384
Δr_J [km]	5 921.967 312 268 461	0.011 342 024 704	0.000 000 058 583	0.000 000 021 923
Δr_K [km]	-2 412.261 924 791 630	-0.031 730 686 798	-0.000 000 396 257	-0.000 000 126 927
Δv_I [km/s]	0.040 031 559 759	0.000 182 871 545	-0.000 000 000 006	-0.000 000 000 002
Δv_J [km/s]	-0.771 984 625 893	-0.000 031 330 161	0.000 000 000 002	0.000 000 000 000
Δv_k [km/s]	-0.538 811 531 308	0.000 125 882 791	0.000 000 000 005	0.000 000 000 001

Table 4.5: *Initial, final, and two intermediate values of vector $\delta\hat{\mathbf{x}}$ considering 10, 100, and 1 000 observations.*

From the table above, one may say that the algorithm converges to one point in all three cases provided that all components of $\delta\hat{\mathbf{x}}$ tend to zero. In addition, one may conclude that the more observations are available, the more rapidly the algorithm will converge. This fact can also be seen in Figure 4.6 where the evolution of all $\delta\hat{\mathbf{x}}$ components has been depicted. This figure only shows the first 10 iterations since the evolution of $\delta\hat{\mathbf{x}}$ components is very little from iteration 10 and cannot be observable in all plots.

Up to now, it has been proved that all $\delta\hat{\mathbf{x}}$ components tend to zero; however, nothing has been said about the point where the algorithm has converged. This fact is illustrated in Figures 4.7 and 4.8 where the evolution of the initial nominal position and velocity vectors along the Least Squares algorithm iterations have been depicted respectively. As in Figure 4.6, only the first 10 iterations have been plotted.

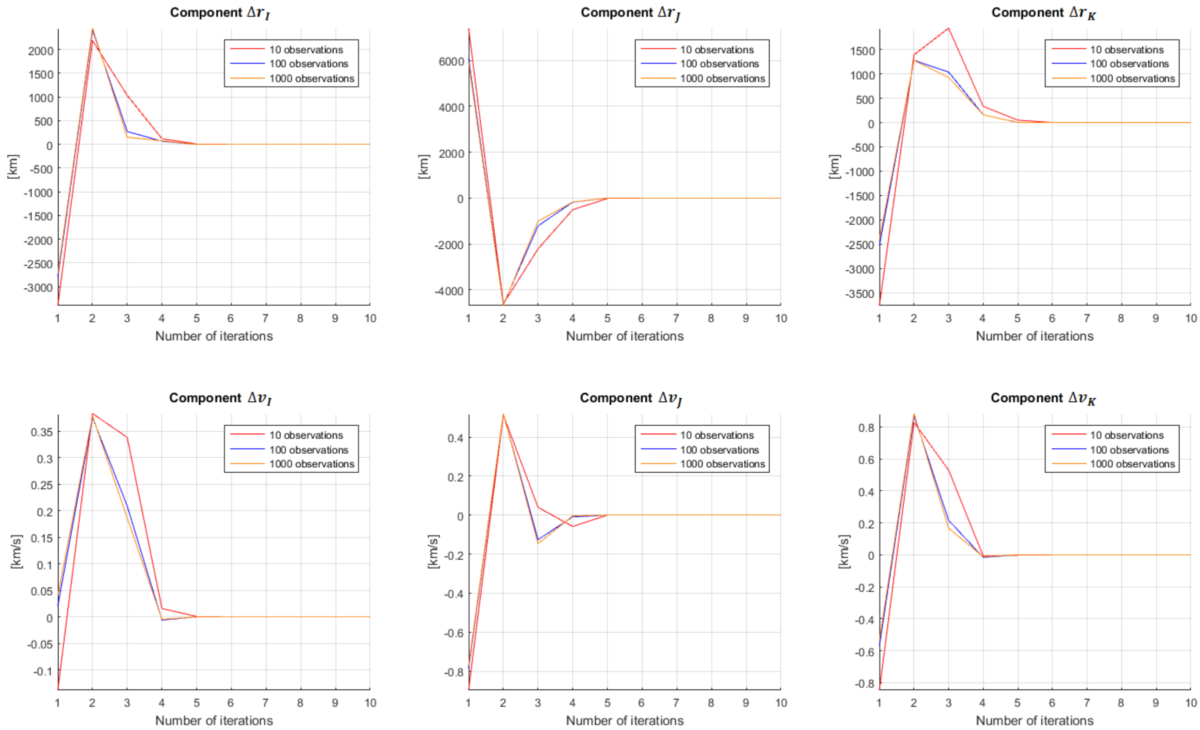

Figure 4.6: *Evolution of $\delta\hat{\mathbf{x}}$ components along the first 10 iterations of Least Squares algorithm considering 10 (in red), 100 (in blue), and 1 000 (in orange) observations.*

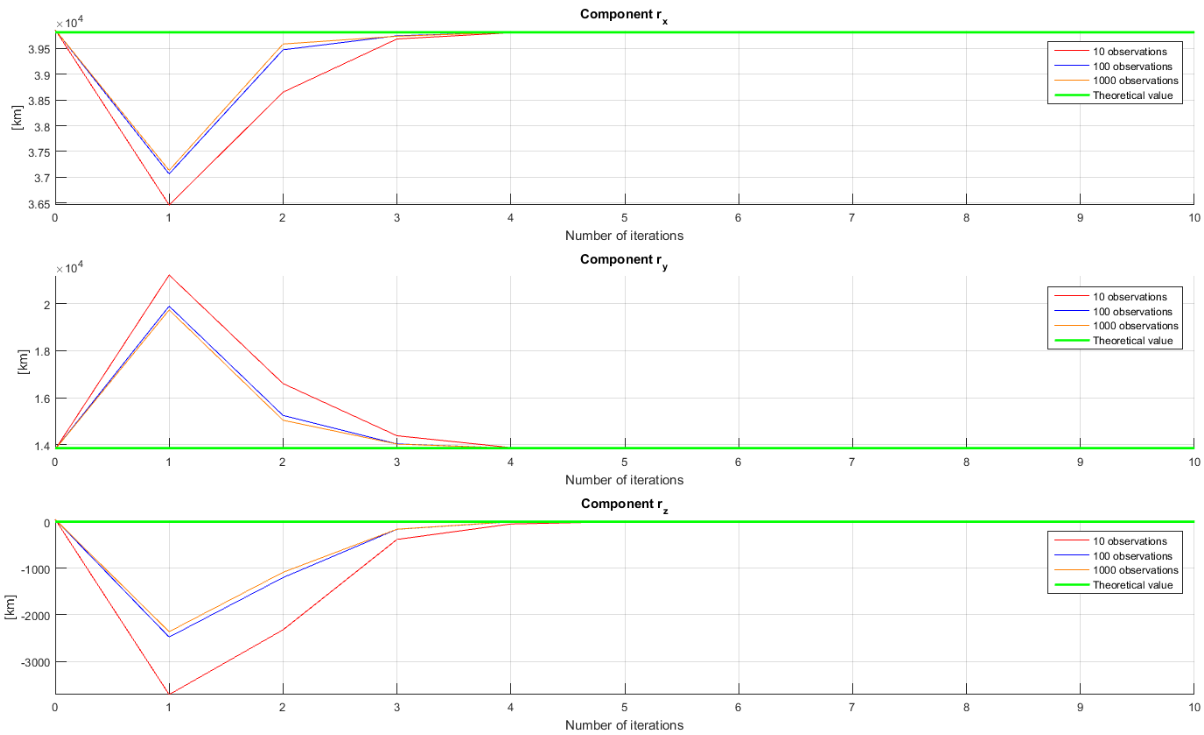

Figure 4.7: *Evolution of the initial nominal position state vector along the first 10 iterations of Least Squares algorithm considering 10 (in red), 100 (in blue), and 1 000 (in orange) observations.*

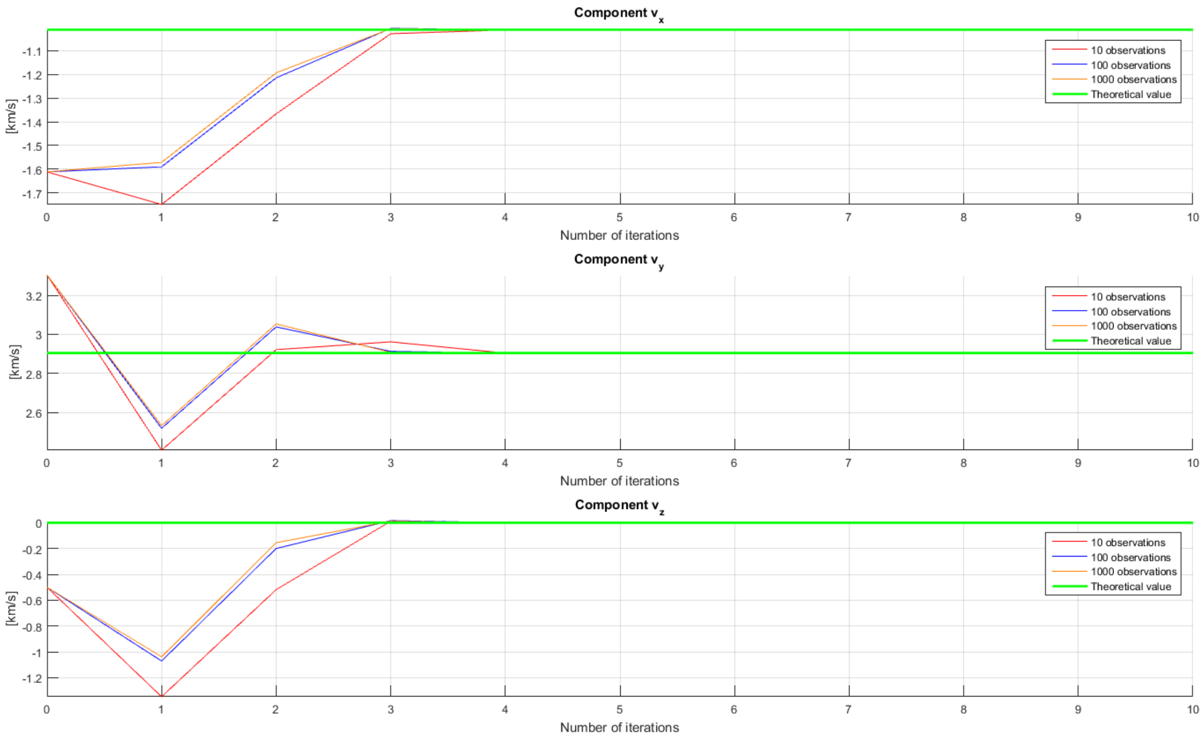

Figure 4.8: *Evolution of the initial nominal velocity state vector along the first 10 iterations of Least Squares algorithm considering 10 (in red), 100 (in blue), and 1 000 (in orange) observations.*

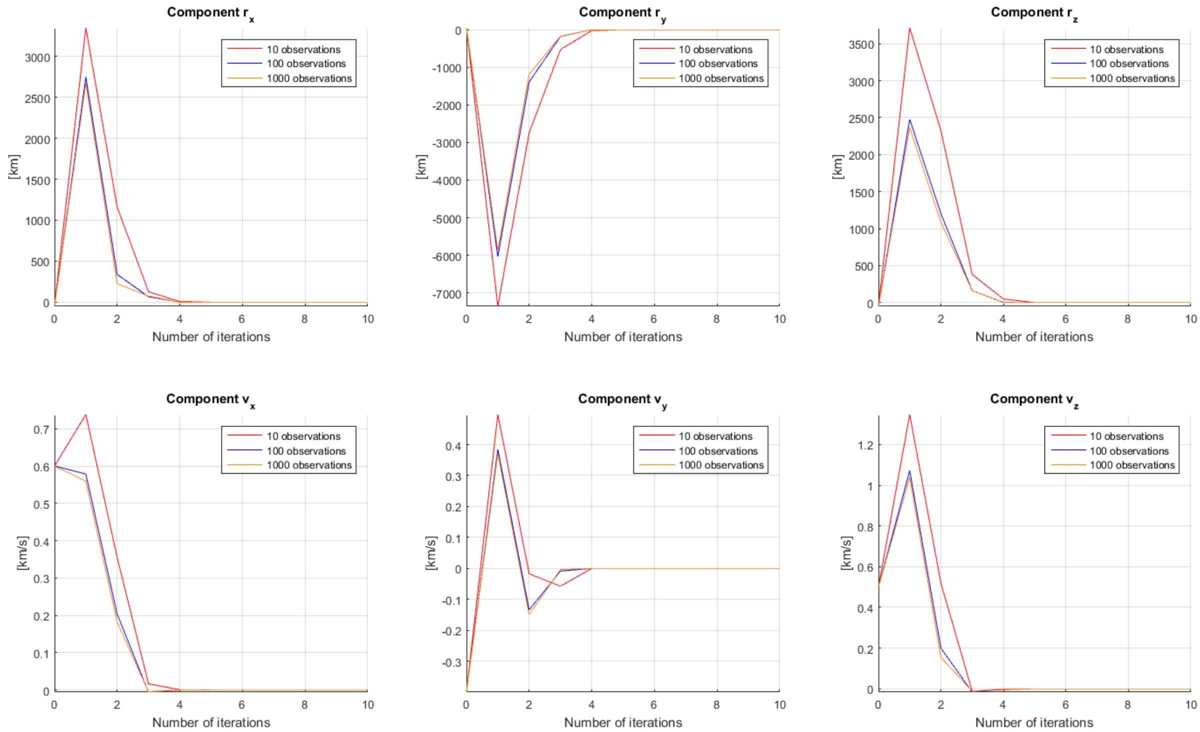

Figure 4.9: *Evolution of the errors between the ideal and nominal state vectors along the first 10 iterations of Least Squares algorithm and considering 10 (in red), 100 (in blue), and 1 000 (in orange) observations.*

From Figures 4.7 and 4.8, one may see that all components converge to the ideal value, and therefore the algorithm convergence has been totally proved.

Finally, Figure 4.9 shows the evolution of the errors obtained between the ideal and nominal state vector values. From this figure, one may see the magnitude of the errors. However, in order to better analyse such errors, a statistical simulation must be performed since each Least Squares algorithm simulation provides different results.

Statistical Simulation of Setting H (10, 100, and 1 000 Observations)
Appendix C shows the main results obtained during each statistical simulation of setting H. First, the evolution of the errors in the nominal state vector is listed, and then, the final errors in the range observations are provided. Both set of errors are calculated at two different epochs simulating the initial and final epochs of the radar synthetic aperture.

Least Squares algorithm needs a few iterations in order to converge to the final state vector. During the first iteration, the nominal state vector is moved far away from its ideal position; however, from this distant point, the algorithm is able to meet the ideal position more precisely than the methods used in Chapter 3. It must also be said that, from iteration 10, the Least Squares algorithm achieve very little or no gain with respect to the precision obtained. Thus, the tolerance of iteration 10 would be used as an escape criterion when performing Least Squares technique in a more real case.

		ORDER OF MAGNITUDE OF THE ERRORS OF SETTING H AT t_0 AND t_f			
		3 observations (setting C)	**10 observations**	**100 observations**	**1 000 observations**
r	t_0	117 / 56 / 151 m	15 / 30 / 52 m	4 / 9 / 17 m	1 / 3 / 5 m
	t_f	143 / 114 / 169 m	44 / 22 / 63 m	14 / 7 / 21 m	4 / 2 / 7 m
v	t_0	9 / 6 / 12 $\frac{\mathrm{mm}}{\mathrm{s}}$	1 / 2 / 5 $\frac{\mathrm{mm}}{\mathrm{s}}$	0.8 / 0.3 / 1.5 $\frac{\mathrm{mm}}{\mathrm{s}}$	0.2 / 0.1 / 0.5 $\frac{\mathrm{mm}}{\mathrm{s}}$
	t_f	7 / 8 / 11 $\frac{\mathrm{mm}}{\mathrm{s}}$	1 / 3 / 4 $\frac{\mathrm{mm}}{\mathrm{s}}$	0.2 / 1 / 1.2 $\frac{\mathrm{mm}}{\mathrm{s}}$	0.08 / 0.3 / 0.4 $\frac{\mathrm{mm}}{\mathrm{s}}$
ρ	t_0	0.6 to 6.7 m	0.4 to 1.7 m	0.2 to 0.5 m	5.6 to 17 cm
	t_f	102 to 108 m	0.4 to 2.5 m	0.2 to 0.8 m	5.4 to 26 cm

Table 4.6: *Summary of the order of magnitude errors of setting H. This table shows the error obtained on each* **r** *and* **v** *components as well as the range values of the error in ρ observations of all sites evaluated.*

Table 4.6 summarizes the errors obtained (i.e., their standard deviations) when using 10, 100, and 1 000 observations. The errors calculated when setting C was simulated have also been added. In this way, one may compare the precision of all same configurations. As seen from the table, the errors in the satellite state vector decrease one order of magnitude when using 1 000 observations instead of 10, and are two orders of magnitude below of those errors obtained when simulating setting C. This fact clearly affect the precision of range observations, which goes from a few metres on setting C to a few centimetres on setting H when using 1 000 observations.

In order to better see how the final range observation errors are distributed among all locations studied, it has been considered adding Figures 4.10, 4.11, and 4.12.

By using Least Squares technique, the precision requirement of GEOSAR mission may be fulfilled. All locations under the satellite L-band beam coverage, except those at the edges, have a range observation precision of the same order of magnitude of the radar X-band wavelength. In addition, such requirement is achieved at both initial and final epochs. However, one must consider that the simulation has been performed without taking into account any kind of perturbations, so that some precision deterioration could be expected when adding third body effects, solar radiation pressure, etc. But, on the other hand, more observations might be used in order to increase the precision obtained. For instance, one could use 10 000 observations (time epochs) instead of 1 000. This fact has not been proved within this document since the statistical simulation was computationally expensive.

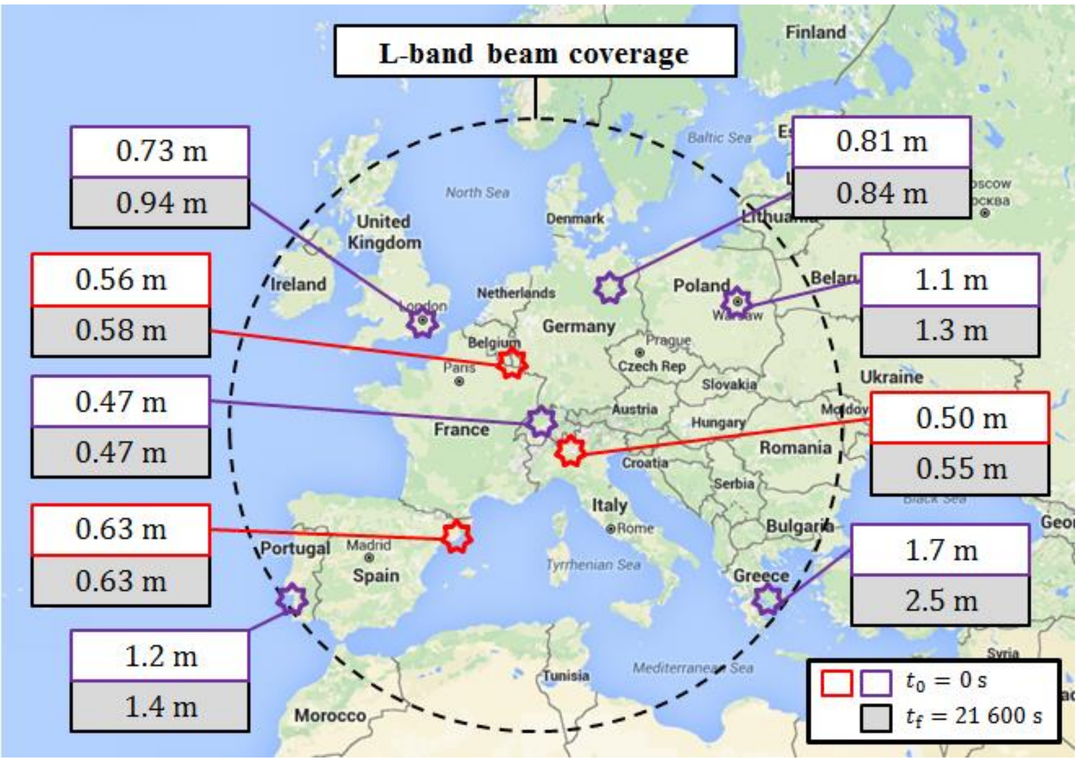

Figure 4.10: *Precision of setting H when using 10 observations. Red and purple squares illustrate ρ errors at initial epoch, t_0, whereas black squares show ρ errors at final epoch, t_f.*

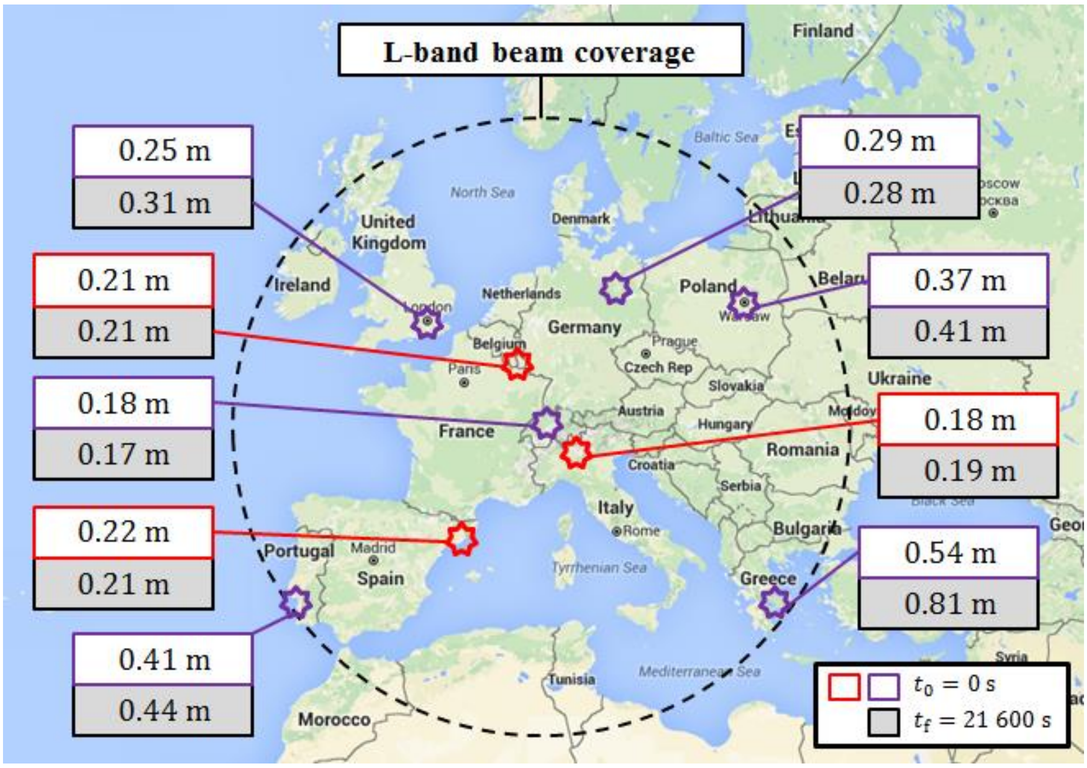

Figure 4.11: *Precision of setting H when using 100 observations. Red and purple squares illustrate ρ errors at initial epoch, t_0, whereas black squares show ρ errors at final epoch, t_f.*

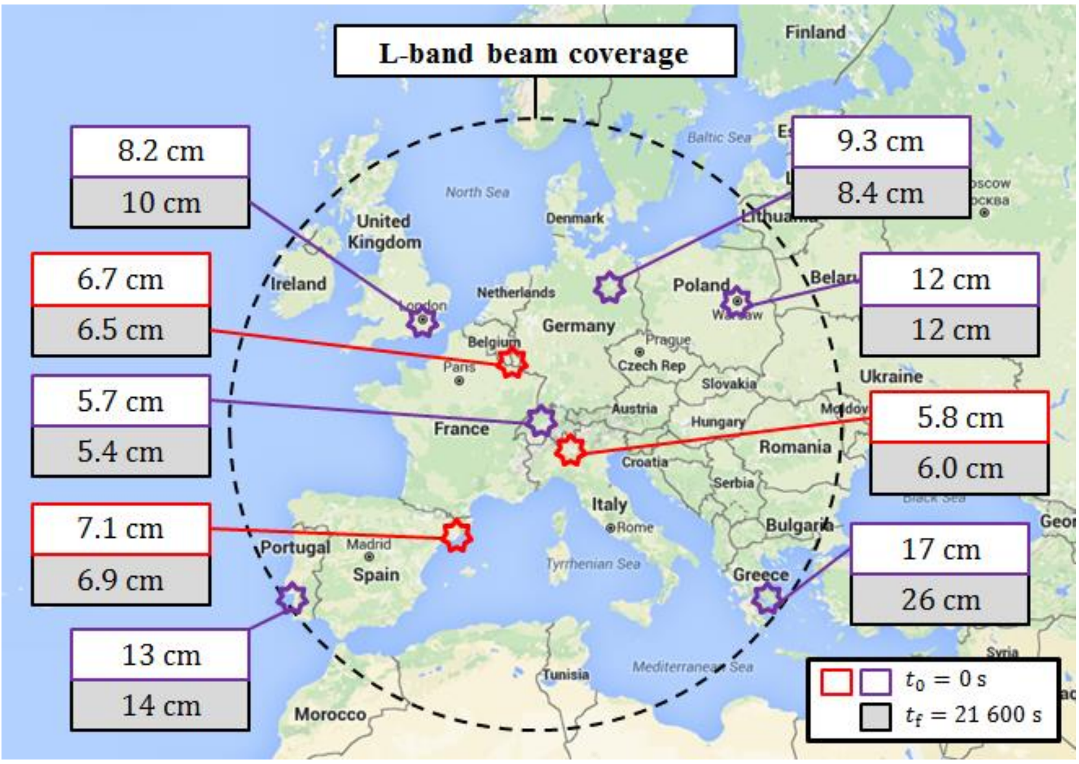

Figure 4.12: *Precision of setting H when using 1 000 observations. Red and purple squares illustrate ρ errors at initial epoch, t_0, whereas black squares show ρ errors at final epoch, t_f.*

<u>Matrix Weighting, **W**</u>

In order to conclude the analysis of setting H, it has been tested without setting the matrix **W**. The reason to do this is that all ideal range observations coming from different sites have been perturbed considering the same level of noise (i.e., $\sigma_{\rho_i} = 1$ m where $i = 1, 2, 3$). Thus, the use or not of matrix **W** for improving the precision of the Least Squares algorithm will be evaluated in this case of study. Table 4.7 shows a comparison of the errors found in setting H.

		ERRORS OF SETTING H AT t_0 AND t_f	
		1 000 observations (using **W**)	**1 000 observations** (without using **W**)
r	t_0	1 / 3 / 5 m	1 / 3 / 5 m
	t_f	4 / 2 / 7 m	4 / 2 / 7 m
v	t_0	0.2 / 0.1 / 0.5 $\frac{\text{mm}}{\text{s}}$	0.3 / 0.09 / 0.5 $\frac{\text{mm}}{\text{s}}$
	t_f	0.08 / 0.3 / 0.4 $\frac{\text{mm}}{\text{s}}$	0.08 / 0.3 / 0.4 $\frac{\text{mm}}{\text{s}}$
ρ	t_0	5.6 to 17 cm	5.6 to 17 cm
	t_f	5.4 to 26 cm	5.3 to 26 cm

Table 4.7: *Summary of the errors of setting H (matrix* **W** *use). This table shows the error obtained on each* **r** *and* **v** *components as well as the range values of the error in ρ observations of all sites evaluated.*

As seen from the table above, the use of matrix **W** does not improve the precision of Least Squares algorithm. Although matrix **W** is not useful in this case, it must be taken into account when performing the algorithm in a real case.

b) Results Analysis of Setting I

The next setting to be analysed considers range and range-rate observations. Let us see whether the use of range-rate observations improve the precision acquired in the previous sub-section. All conditions taken into account within the simulation are summarized in Table 4.8.

The simulation of Least Squares algorithm adding range-rate observations is run similarly than the one only using range observations. That is to say, after the first iteration, the initial nominal state vector is moved far away. Then, from this distant point, the algorithm converges a few iterations later. One can see this fact from the tables of Appendix C.

Table 4.9 compares the results between settings D and I, which have similar configurations. It has also been added setting H in order to compare its precision to the one obtained through setting I. As seen from the table, setting I improves the precision of setting D in two, three or even in four order of magnitudes. However, it does not improve the precision of setting H since similar or almost identical results are obtained.

Setting I
Location of the three sites in order to obtain the initial nominal state vector: (01) Barcelona (Spain) / (02) Betzdorf (Luxemburg) / (03) Milan (Italy). IDEAL DATA - **Type of observations generated:** RANGE and RANGE-RATE. - **Number of observations generated per type and site:** 1 000. - **Time span:** 6 h. NOISE ADDED - **Range observations:** MEAN: 0 m / STD.: 1 m. - **Range-rate observations:** MEAN: 0 mm/s / STD.: 5 mm/s. APPROXIMATE DATA - **Technique used:** LEAST SQUARES. - **Epoch when the approximate satellite state vector is given:** $t_0 = 0$ s.

Table 4.8: *Summary of all conditions considered on setting I.*

		COMPARISON BETWEEN ERRORS OF SETTINGS D, H, I		
		Setting D (3 observations)	**Setting H** (1 000 observations)	**Setting I** (1 000 observations)
r	t_0	62 / 120 / 150 m	1 / 3 / 5 m	2 / 3 / 6 m
	t_f	2 / 17 / 10 km	4 / 2 / 7 m	4 / 2 / 6 m
v	t_0	0.3 / 0.6 / 0.7 $\frac{m}{s}$	0.2 / 0.1 / 0.5 $\frac{mm}{s}$	0.3 / 0.09 / 0.5 $\frac{mm}{s}$
	t_f	0.02 / 1.7 / 0.01 $\frac{m}{s}$	0.08 / 0.3 / 0.4 $\frac{mm}{s}$	0.08 / 0.3 / 0.4 $\frac{mm}{s}$
ρ	t_0	0.6 to 6.9 m	5.6 to 17 cm	5.6 to 17 cm
	t_f	17.0 to 17.5 km	5.4 to 26 cm	5.4 to 25 cm

Table 4.9: *Comparison between the errors of settings D, H, and I. This table shows the error obtained on each* **r** *and* **v** *components as well as the range values of the error in ρ observations of all sites evaluated.*

Therefore, the precision requirement of GEOSAR mission is also fulfilled by means of setting I, especially for those locations in the centre of the satellite L-band beam coverage. Figure 4.13 shows how the errors in range observations are distributed among all sites evaluated.

Before concluding Chapter 4, it has been considered to add the analysis of two more settings. Setting J will reduce the error added in the ideal range observations one order of magnitude. On the other hand, setting K will do the same but in the range-rate observations. In this way, it will be shown which case offers better capabilities for improving the precision required on GEOSAR mission.

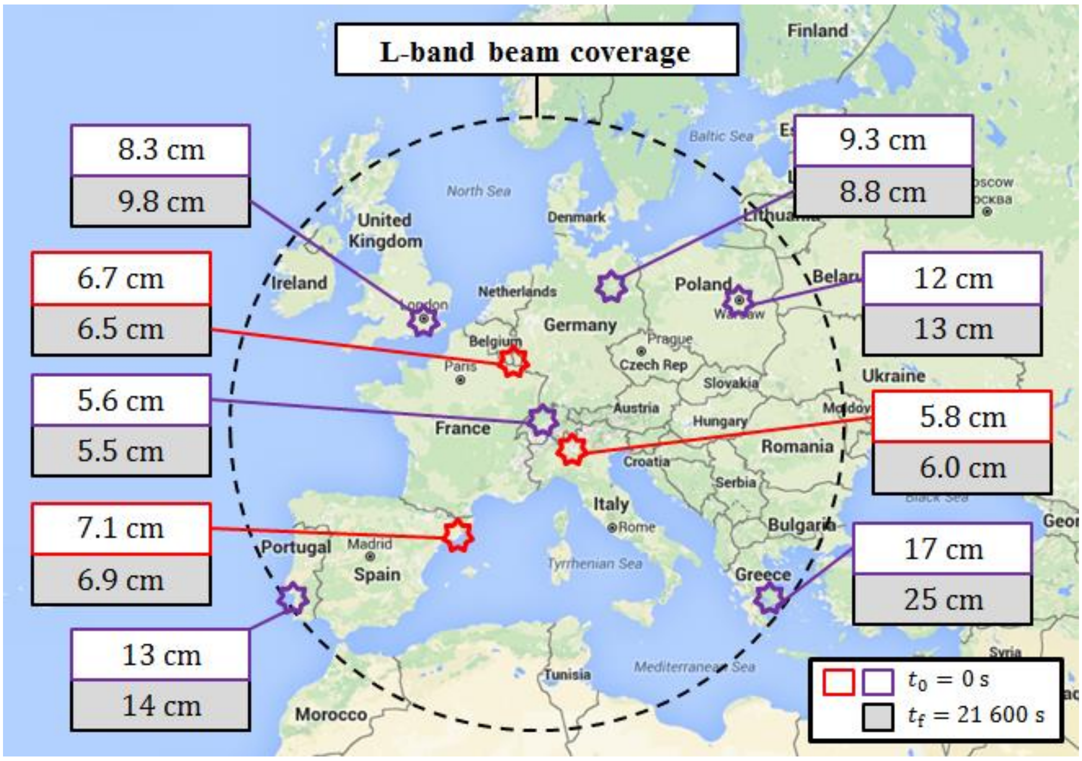

Figure 4.13: *Precision of setting I. Red and purple squares illustrate ρ errors at initial epoch, t_0, whereas black squares show ρ errors at final epoch, t_f.*

c) Results Analysis of Setting J

Table 4.10 summarizes all conditions taken into account in the simulation of setting J, which they are the same of those used for setting H, but the standard deviation noise to the range observations has reduced one order of magnitude.

Setting J

Location of the three sites in order to obtain the initial nominal state vector:
(01) Barcelona (Spain) / (02) Betzdorf (Luxemburg) / (03) Milan (Italy).

IDEAL DATA
- **Type of observations generated:** RANGE.
- **Number of observations generated per type and site:** 1 000.
- **Time span:** 6 h.

NOISE ADDED
- **Range observations:** MEAN: 0 m / STD.: 0.1 m.

APPROXIMATE DATA
- **Technique used:** LEAST SQUARES.
- **Epoch when the approximate satellite state vector is given:** $t_0 = 0$ s.

Table 4.10: *Summary of all conditions considered on setting J.*

		ERRORS OF SETTINGS H AND J	
		Setting H (1 000 observations)	**Setting J** (1 000 observations)
r	t_0	1 / 3 / 5 m	0.1 / 0.3 / 0.5 m
	t_f	4 / 2 / 7 m	0.4 / 0.2 / 0.7 m
v	t_0	0.2 / 0.1 / 0.5 $\frac{\text{mm}}{\text{s}}$	27 / 10 / 49 $\frac{\mu\text{m}}{\text{s}}$
	t_f	0.08 / 0.3 / 0.4 $\frac{\text{mm}}{\text{s}}$	8 / 35 / 39 $\frac{\mu\text{m}}{\text{s}}$
ρ	t_0	5.6 to 17 cm	5.7 to 17 mm
	t_f	5.4 to 26 cm	5.5 to 27 mm

Table 4.11: *Comparison between settings H and J. This table shows the error obtained on each* **r** *and* **v** *components as well as the range values of the error in* ρ *observations of all sites evaluated.*

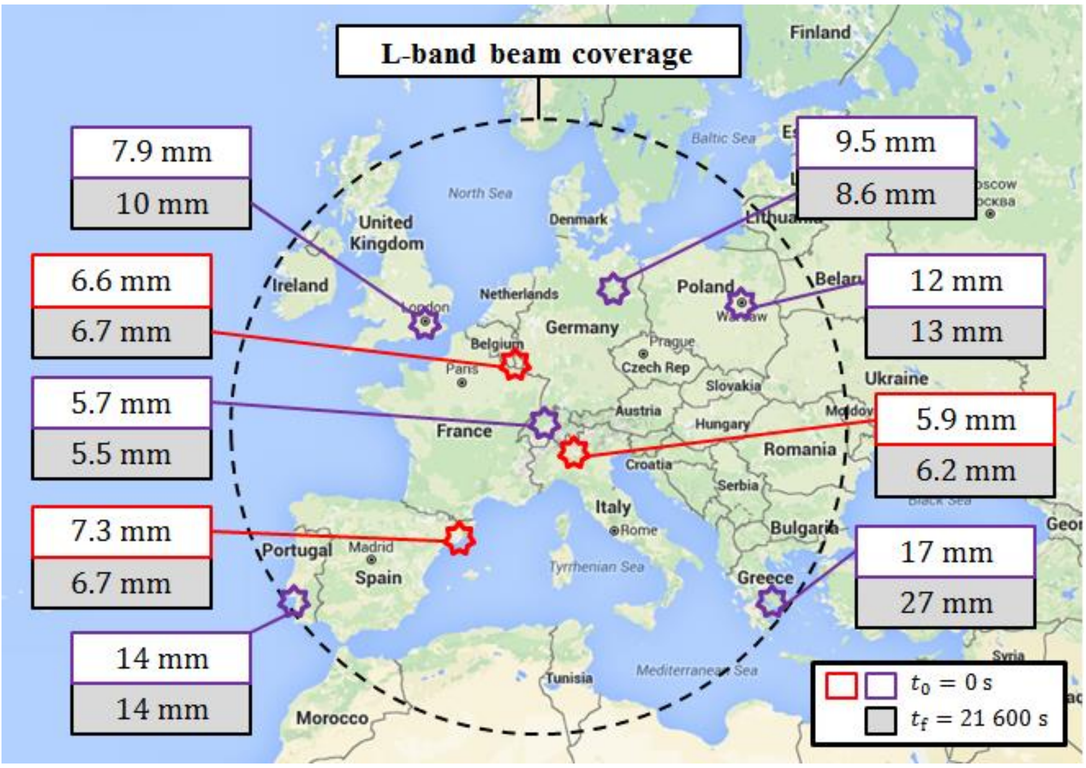

Figure 4.14: *Precision of setting J. Red and purple squares illustrate* ρ *errors at initial epoch,* t_0*, whereas black squares show* ρ *errors at final epoch,* t_f.

The simulation results show a reduction of one order of magnitude of the errors obtained in the satellite state vector as well as in the range observations with respect to setting H (see Table 4.11). Thus, the precision requirement of GEOSAR mission is completely fulfilled in all locations under the satellite L-band beam coverage. Therefore, it is highlighted the need of being provided of very precise range observations.

Following the same format of previous sub-sections, Figure 4.14 illustrates how the range observation errors are distributed along all sites evaluated.

d) Results Analysis of Setting K

The analyses of different settings will conclude studying setting K. One may find the information of all conditions considered in the simulation of setting K in Table 4.12.

Setting K

Location of the three sites in order to obtain the initial nominal state vector:
(01) Barcelona (Spain) / (02) Betzdorf (Luxemburg) / (03) Milan (Italy).

IDEAL DATA
- **Type of observations generated:** RANGE and RANGE-RATE.
- **Number of observations generated per type and site:** 1 000.
- **Time span:** 6 h.

NOISE ADDED
- **Range observations:** MEAN: 0 m / STD.: 1 m.
- **Range-rate observations:** MEAN: 0 $\mathrm{mm/s}$ / STD.: 0.5 $\mathrm{mm/s}$.

APPROXIMATE DATA
- **Technique used:** LEAST SQUARES.
- **Epoch when the approximate satellite state vector is given:** $t_0 = 0$ s.

Table 4.12: *Summary of all conditions considered on setting K.*

The simulation results (see Table 4.13) show a very little error decrease in the satellite state vector with respect to setting I. This fact implies a small improvement in the precision of setting K; however, it does not achieve the precision obtained by using setting J, which is one order of magnitude below. Therefore, it has been shown that decreasing the errors of the range observations provides better precision results than only decreasing the errors of the range-rate observations.

Finally, the range observation errors are shown in Figure 4.15.

		COMPARISON BETWEEN ERRORS OF SETTINGS I, J, K		
		Setting I (1 000 observations)	**Setting J** (1 000 observations)	**Setting K** (1 000 observations)
r	t_0	2 / 3 / 6 m	0.1 / 0.3 / 0.5 m	1 / 3 / 5 m
	t_f	4 / 2 / 6 m	0.4 / 0.2 / 0.7 m	4 / 2 / 6 m
v	t_0	0.3 / 0.09 / 0.5 $\frac{\text{mm}}{\text{s}}$	27 / 10 / 49 $\frac{\mu\text{m}}{\text{s}}$	0.3 / 0.09 / 0.4 $\frac{\text{mm}}{\text{s}}$
	t_f	0.08 / 0.3 / 0.4 $\frac{\text{mm}}{\text{s}}$	8 / 35 / 39 $\frac{\mu\text{m}}{\text{s}}$	0.08 / 0.3 / 0.4 $\frac{\text{mm}}{\text{s}}$
ρ	t_0	5.6 to 17 cm	5.7 to 17 mm	4.9 to 17 cm
	t_f	5.4 to 25 cm	5.5 to 27 mm	4.7 to 25 cm

Table 4.13: *Comparison between the errors of settings I, J, and K. This table shows the error obtained on each* **r** *and* **v** *components as well as the range values of the error in ρ observations of all sites evaluated.*

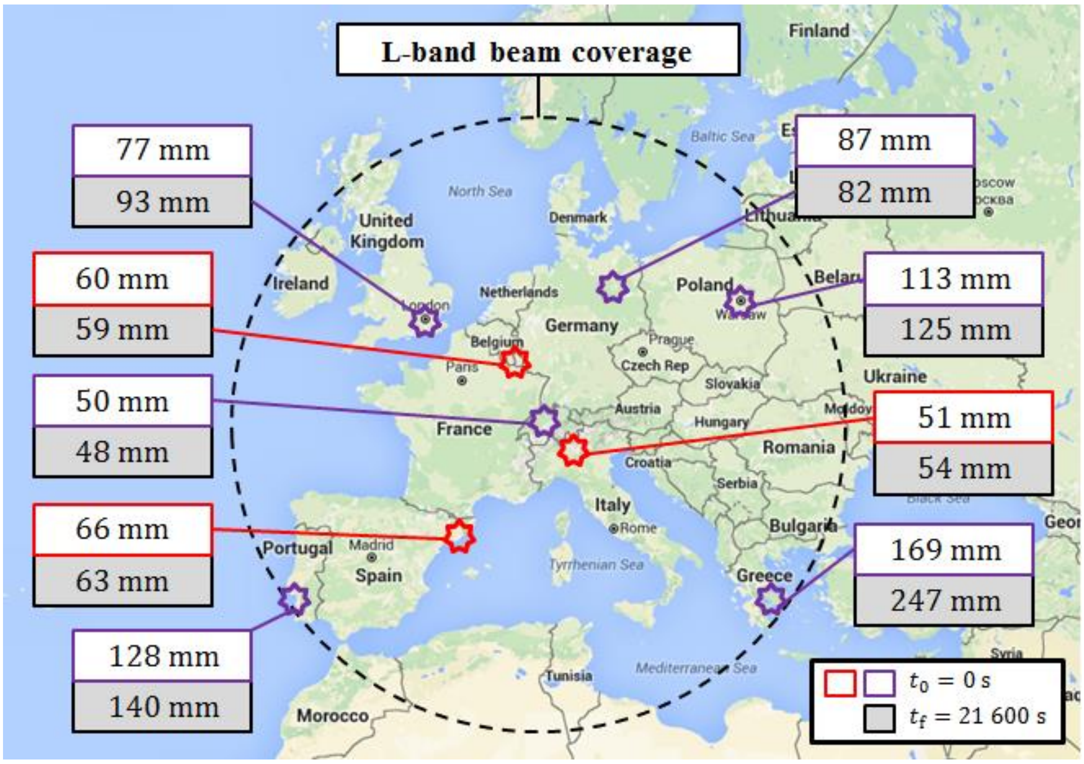

Figure 4.15: *Precision of setting K. Red and purple squares illustrate ρ errors at initial epoch, t_0, whereas black squares show ρ errors at final epoch, t_f.*

4.4. RESULTS SUMMARY

The following table summarizes the main results obtained of all simulated settings along Chapter 4.

RESULTS SUMMARY OF ALL CHAPTER 4 SETTINGS				
Set.	**Errors in satellite Postion SV (r)**	**Errors in satellite Velocity SV (v)**	**Errors in Range observations (ρ)**	**Errors in Range-rate observations ($\dot{\rho}$)**
INITIAL EPOCH ($t_0 = 0$ s)				
H (10)	15 / 30 / 52 m	1 / 2 / 5 $\frac{\text{mm}}{\text{s}}$	0.4 to 1.7 m	–
H (100)	4 / 9 / 17 m	0.8 / 0.3 / 1.5 $\frac{\text{mm}}{\text{s}}$	0.2 to 0.5 m	–
H (1 000)	1 / 3 / 5 m	0.2 / 0.1 / 0.5 $\frac{\text{mm}}{\text{s}}$	5.6 to 17 cm	–
I (1 000)	2 / 3 / 6 m	0.3 / 0.09 / 0.5 $\frac{\text{mm}}{\text{s}}$	5.6 to 17 cm	11 to 14 $\frac{\mu\text{m}}{\text{s}}$
J (1 000)	0.1 / 0.3 / 0.5 m	27 / 10 / 49 $\frac{\mu\text{m}}{\text{s}}$	5.7 to 17 mm	–
K (1 000)	1 / 3 / 5 m	0.3 / 0.09 / 0.4 $\frac{\text{mm}}{\text{s}}$	4.9 to 17 cm	8.7 to 12 $\frac{\mu\text{m}}{\text{s}}$
FINAL EPOCH ($t_f = 21\,600$ s)				
H (10)	44 / 22 / 63 m	1 / 3 / 4 $\frac{\text{mm}}{\text{s}}$	0.4 to 2.5 m	–
H (100)	14 / 7 / 21 m	0.2 / 1 / 1.2 $\frac{\text{mm}}{\text{s}}$	0.2 to 0.8 m	–
H (1 000)	4 / 2 / 7 m	0.08 / 0.3 / 0.4 $\frac{\text{mm}}{\text{s}}$	5.4 to 26 cm	–
I (1 000)	4 / 2 / 6 m	0.08 / 0.3 / 0.4 $\frac{\text{mm}}{\text{s}}$	5.4 to 25 cm	11 to 14 $\frac{\mu\text{m}}{\text{s}}$
J (1 000)	0.4 / 0.2 / 0.7 m	8 / 35 / 39 $\frac{\mu\text{m}}{\text{s}}$	5.5 to 27 mm	–
K (1 000)	4 / 2 / 6 m	0.08 / 0.3 / 0.4 $\frac{\text{mm}}{\text{s}}$	4.7 to 25 cm	8.5 to 12 $\frac{\mu\text{m}}{\text{s}}$

Table 4.14: *Summary of all simulation results performed in Chapter 4. This table shows the error obtained on each* **r** *and* **v** *components as well as the range values of the error in ρ and $\dot{\rho}$ observations of all sites evaluated.*

CONCLUSIONS

This document has introduced the topic of orbit determination methods and techniques to the reader in the context of GEOSAR mission.

First, Chapter 1 has explained the GEOSAR mission main features. In this way, the advantages of the mission versus LEOSAR missions, and the new set of application that this fact involves have been listed. However, GEOSAR mission introduces some constraints. One of these limitations lies on the lack of knowledge with precision about the orbit that the satellite describes around the Earth. Such precision is related to the range history between the radar antenna and each scene point under the satellite L-band beam coverage. Therefore, in order to obtain well-focused images, the range history of every site must remain in the order of magnitude of the radar X-band wavelength (i.e., $\lambda \sim 3$ cm). Thus, this document has introduced different methods and techniques in order to determine the satellite orbit with such precision.

After Chapter 2 has shown how a SAR radar works with some examples, Chapter 3 has started to present methods for orbit determination from range and range-rate measurements. In this way, Trilateration and Gibbs methods have been discussed. On the one hand, Trilateration method alone may calculate an initial satellite state vector if both types of measurements are available. On the other hand, Gibbs method may help Trilateration method in order to find the initial state vector if only range measurements are given. Many simulations have been performed in order to evaluate the precision of both methods. Such simulations have shown that the combination of both methods results to be the best approach to initially determine the satellite orbit. However, the required precision is far to be accomplished, so that other techniques had to be studied.

Finally, Chapter 4 has introduced Least Squares and Kalman filter techniques, which are called differential correction techniques. At the beginning of the chapter, it has been discussed the pros and cons of both techniques resulting Least Squares the technique to be used in order to determine the satellite orbit. In this way, the complete formulation of Least Squares technique has been explained, and then, it has been adapted to the orbit determination problem. At this point, some simulations have been performed in order to evaluate the precision of Least Squares technique. Such simulations have resulted in range observation errors of the same order of magnitude than the required precision of GEOSAR mission. However, all errors found are above the 3 centimetres of the radar X-band wavelength. This fact implies that the Least Squares technique must be used in collaboration to other techniques, for instance, autofocusing techniques. In this way, the mission precision for the satellite orbit determination may be completely ensured.

As a final remark, it had been shown that decreasing the errors in the range observations used in Least Squares technique provide better precision results than reducing the errors in the range-rate observations.

Future work

This document may be used as a first overview of satellite orbit determination in GEOSAR mission. All methods and techniques explained within the document are clearly useful for orbit determination. However, some modifications in the algorithms must be performed in order to take into account perturbations. Since there were no real data available, the precision of all methods has been evaluated from an ideal simulated orbit, which presented similar issues of a real GEO orbit but did not consider perturbations. One must know that perturbations affect the satellite movement along its orbit, and does the estimation of its orbit more difficult to calculate in a precise way.

On the other hand, care must be taken when defining time. Since there were no specific dates of real observables, time has treated in a more easy way. But, the appearance of real data will imply to define time by using time references described briefly in Section 2.4. Knowing the time, one may locate one site over the Earth's surface more precisely, and therefore the range measurement between the satellite and site will be calculated with less error.

Since GEOSAR mission has no launching date yet, it will be difficult to achieve real data soon in order to prove the methods and techniques discussed within this document. However, this real data may be obtained from the alternative system based on a ground-based interferometer, which has been presented in Chapter 1. An interferometer will provide different measurements, so that all methods and techniques explained along this document must be adapted to such system.

Finally, the feasibility of Kalman filter techniques in the context of GEOSAR mission may also be proved instead of using Least Squares techniques. And, in case that the precision requirements are not obtained, autofocusing techniques may also be studied.

APPENDIX A

Appendix A illustrates the block diagram of all Matlab scripts and functions involved on each group of simulations performed along this document. At the end of this Appendix, a brief explanation of every script or function used into the simulations is provided.

A.1. MATLAB SCRIPTS AND FUNCTIONS OF SECTIONS 3.5 AND 3.7

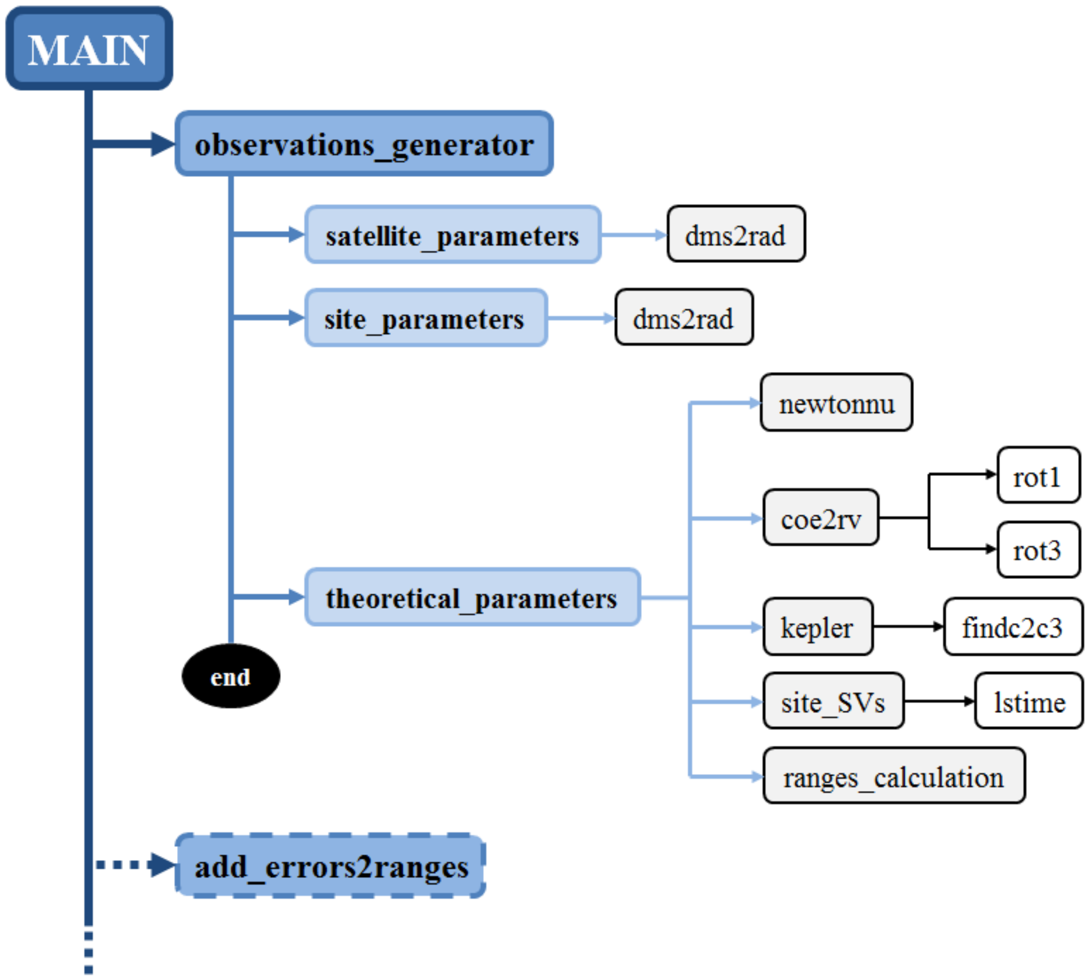

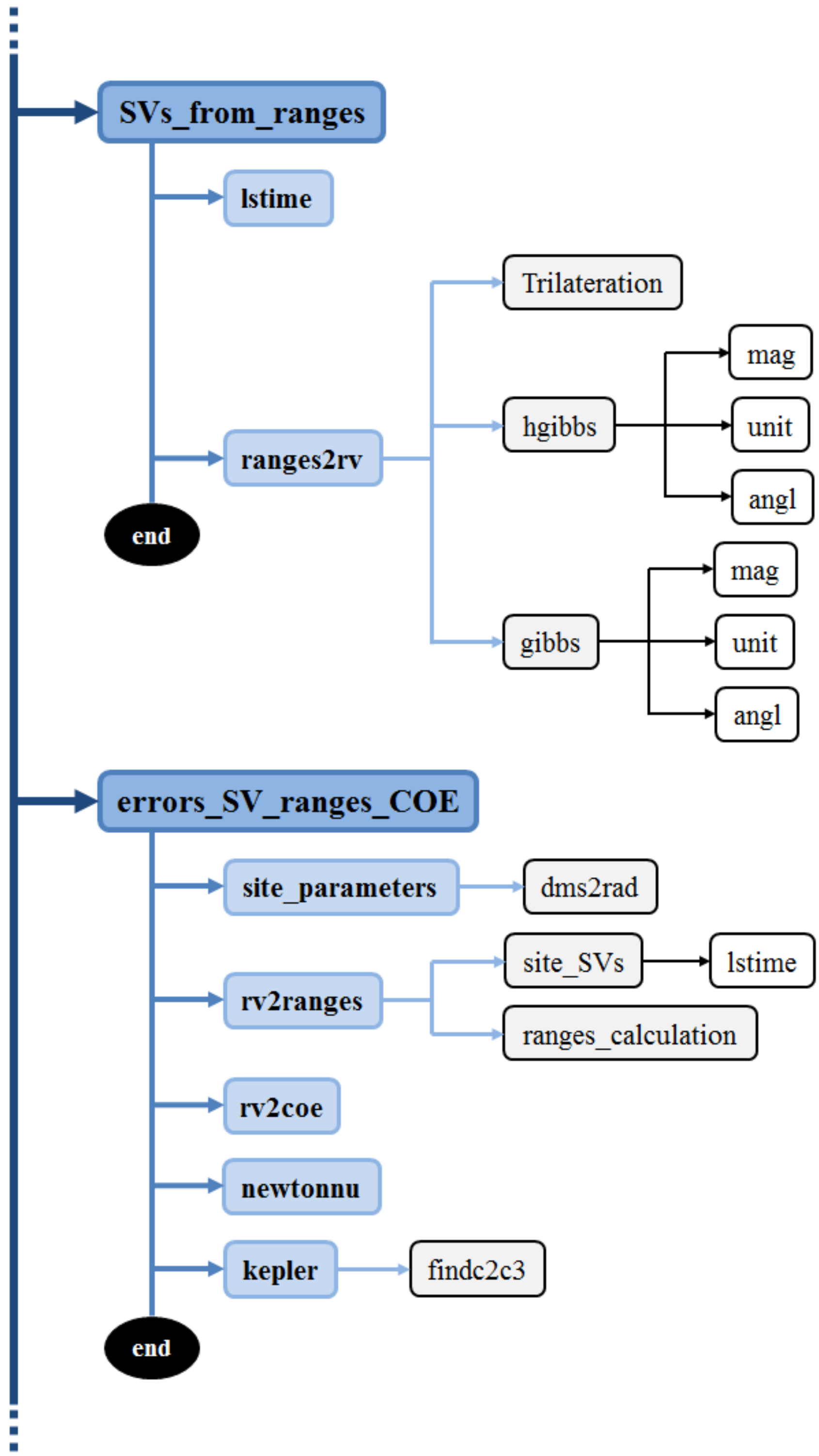
SVs_from_ranges
lstime
Trilateration
mag
hgibbs
unit
ranges2rv
angl
end
mag
unit
gibbs
angl
errors_SV_ranges_COE
site_parameters
dms2rad
site_SVs
lstime
rv2ranges
ranges_calculation
rv2coe
newtonnu
kepler
findc2c3
end

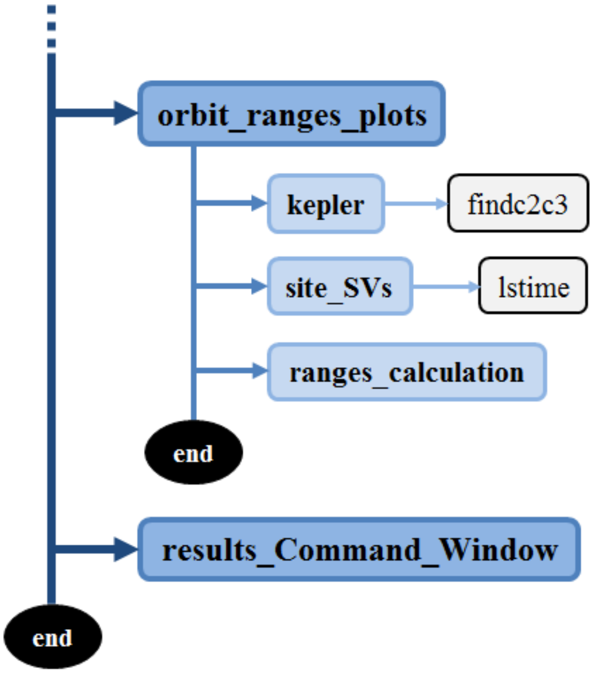

Figure A.1: *Block diagram of Matlab scripts and functions used in Sections 3.5 and 3.7.*

A.2. MATLAB SCRIPTS AND FUNCTIONS OF SECTION 3.8

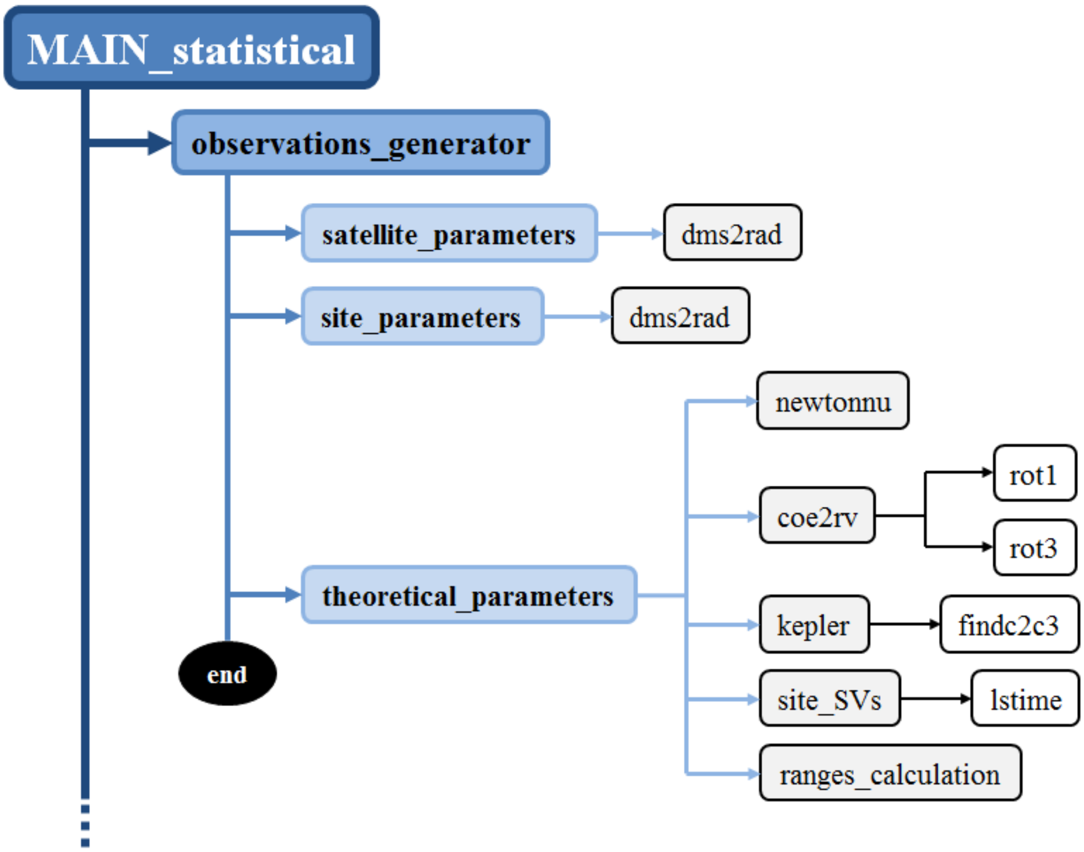

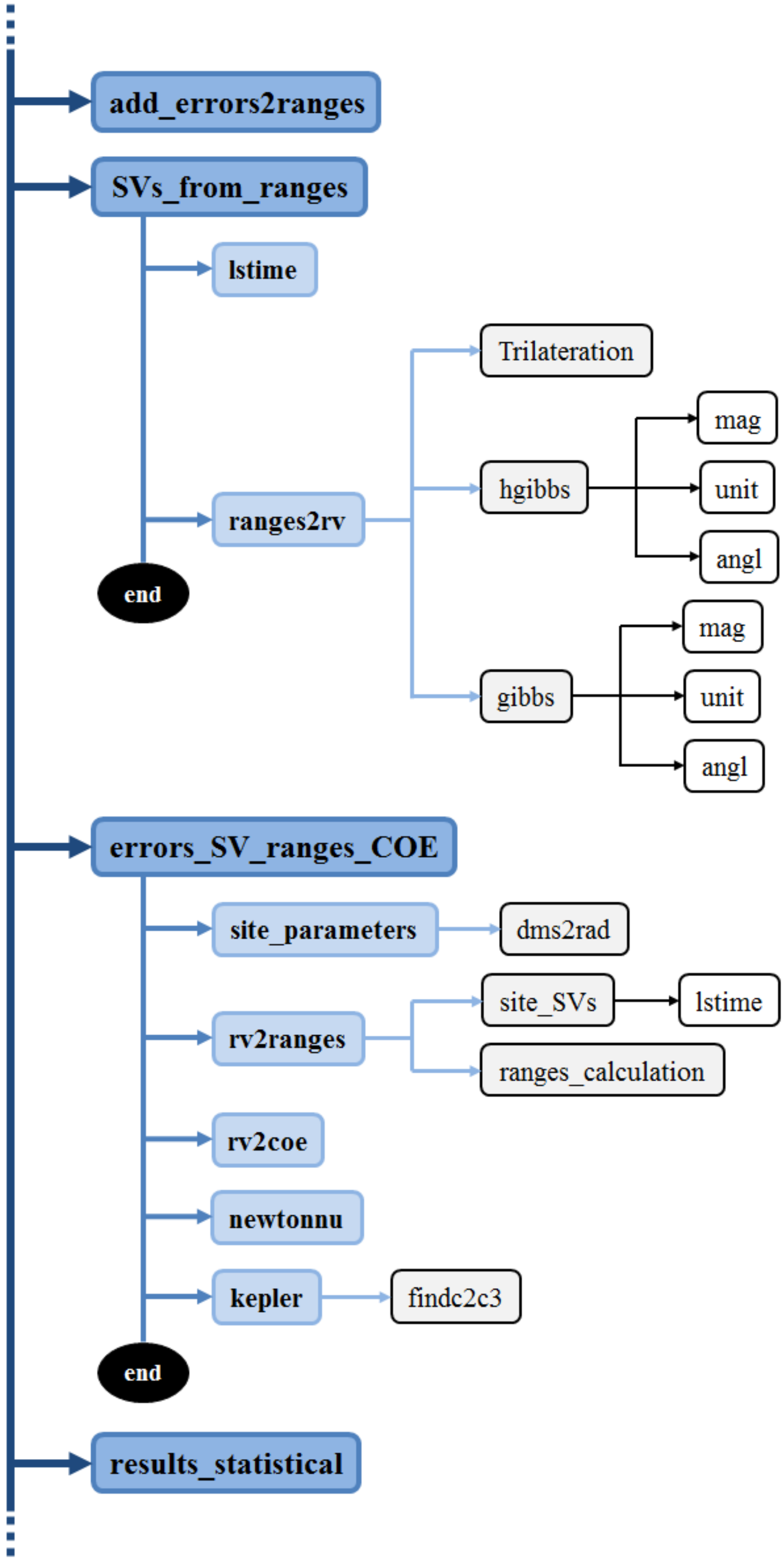
add_errors2ranges
SVs_from_ranges
lstime
Trilateration
mag
hgibbs
unit
ranges2rv
angl
end
mag
gibbs
unit
angl
errors_SV_ranges_COE
site_parameters
dms2rad
site_SVs
lstime
rv2ranges
ranges_calculation
rv2coe
newtonnu
kepler
findc2c3
end
results_statistical

Figure A.2: *Block diagram of Matlab scripts and functions used in Section 3.8.*

A.3. MATLAB SCRIPTS AND FUNCTIONS OF SECTION 4.3

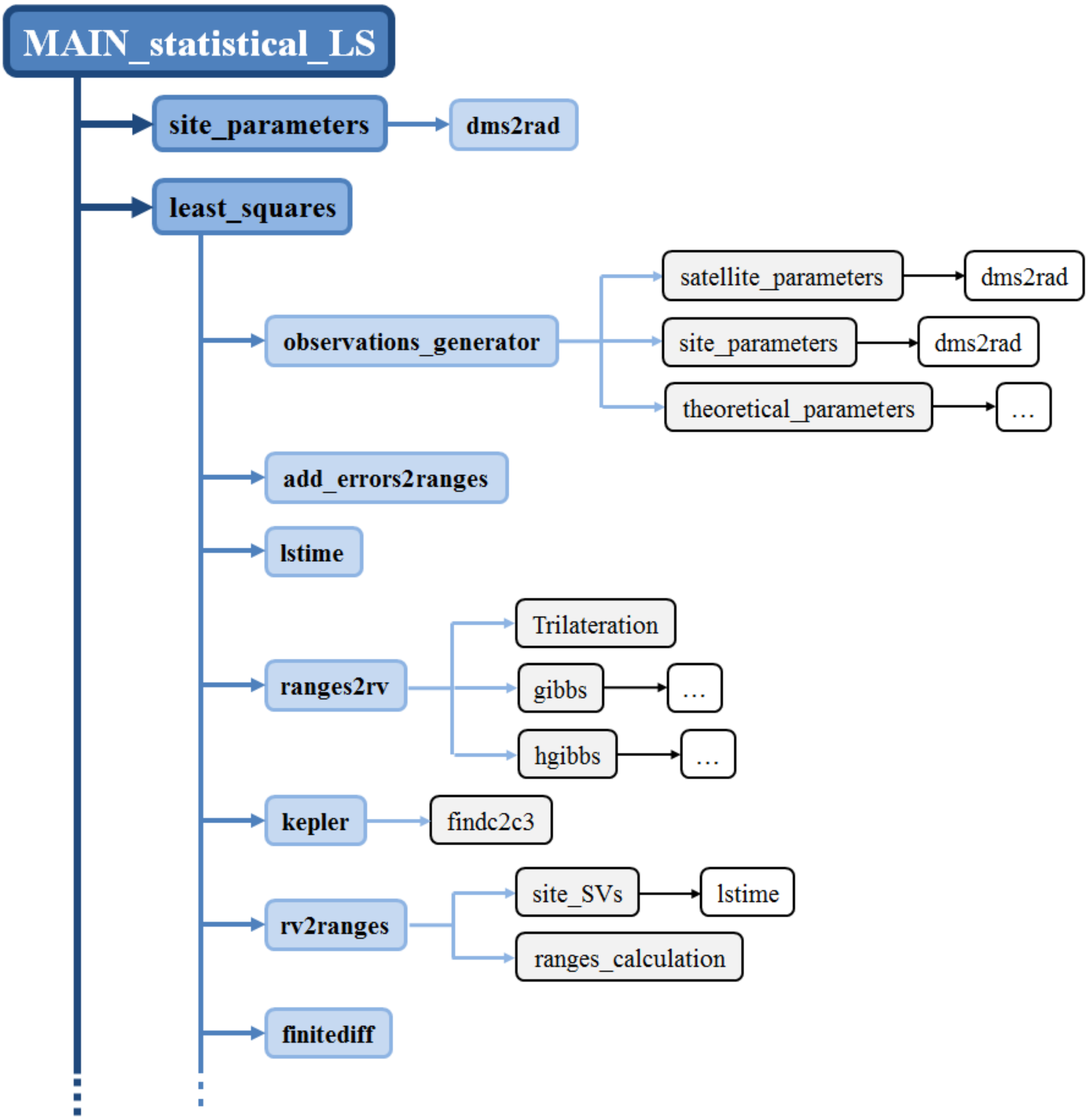

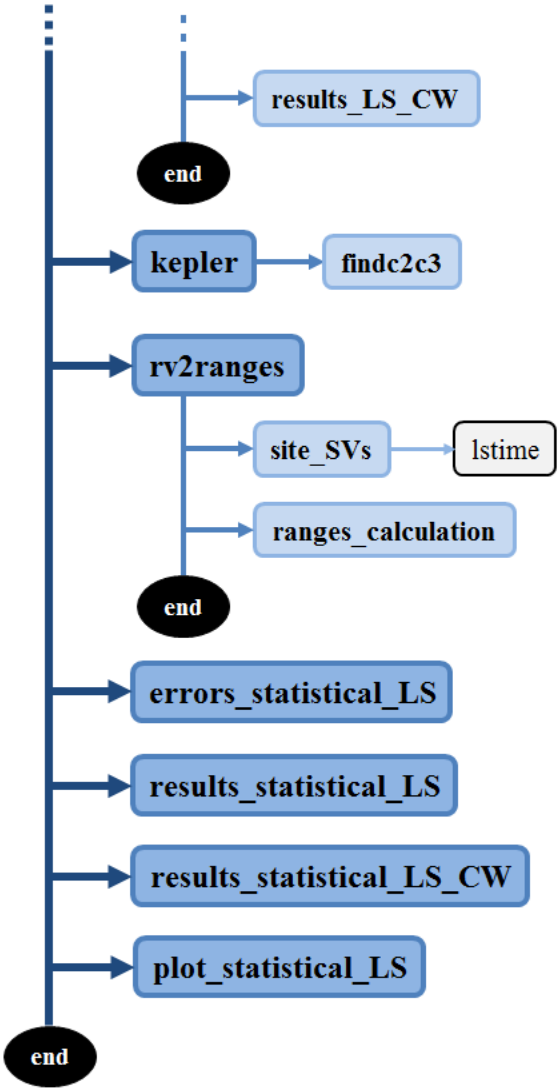

Figure A.3: *Block diagram of Matlab scripts and functions used in Section 4.3.*

A.4. SUMMARY OF ALL MATLAB FUNCTIONS AND SCRIPTS USED

Script/Function name	Summary
add_errors2ranges (script)	It adds uniform or Gaussian noise to the range and range-rate observations generated by script observations_generator.
angl (function)	It calculates the angle between two vectors.
coe2rv (function)	It finds the position and velocity vectors in a geocentric equatorial system, IJK, given the Classical Orbital Elements.
dms2rad (function)	It converts degrees, minutes and seconds into radians.
errors_statistical_LS (script)	It computes the statistical errors obtained in the satellite state vector, and in range and range-rate observations when the Least Squares technique is performed.

errors_SV_ranges_COE (script)	It computes the errors between ideal and approximate values of the satellite state vector, range and range-rate observations, and Classical Orbital Elements.
findc2c3 (function)	It calculates the c2 and c3 functions in order for using them in the universal variable calculation of z.
finitediff (function)	It perturbs the components of the state vector in order to obtain matrix **A** when performing Least Squares technique.
gibbs (function)	It performs the Gibbs' method of orbit determination, i.e. it determines the velocity at the middle epoch of the 3 given position vectors.
hgibbs (function)	It implements the Herrick-Gibbs approximation for orbit determination, and finds the middle velocity vector for the 3 given position vectors.
kepler (function)	It solves Kepler's problem for orbit determination and returns a future geocentric equatorial, IJK, position and velocity vector. The solution uses universal variables.
least_squares (script)	It performs the complete Least Squares algorithm by using finite differencing.
lstime (function)	It finds the Local Sidereal Time, θ_{LST}, at a given location.
mag (function)	It finds the magnitude of a vector.
MAIN (script)	It performs the complete simulation of the initial orbit determination of Chapter 3.
MAIN_statistical (script)	It performs the complete statistical simulation of the initial orbit determination of Chapter 3.
MAIN_statistical_LS (script)	It performs the complete statistical simulation of Least Squares algorithm of Chapter 4.
newtonnu (function)	It solves Kepler's equation when the true anomaly is known. The mean and eccentric, parabolic, or hyperbolic anomaly are also found.
observations_generator (script)	It generates N range and range-rate (if chosen) observations of three different sites selected by the user from an ideal simulated geostationary satellite orbit. It also provides the ideal parameters generated of this satellite orbit.
orbit_ranges_plots (script)	It calculates the evolution of the ideal and approximate satellite orbits, and range and range-rate histories. Then it plots the results.
plot_statistical (script)	It plots the statistical results performed within the script results_statistical.
plot_statistical_LS (script)	It plots the statistical results calculated within the script results_statitical_LS.
ranges2rv (function)	It computes the satellite state vector from a set of range and range-rate observations of three different sites by using Trilateration, Gibbs or Herrick-Gibbs methods.
ranges_calculation (function)	It computes the range and range-rate observations given the satellite and site state vectors.
results_Command_Window (script)	It shows, by Command Window, some results obtained in scripts: observations_generator, add_errors2ranges, SVs_from_ranges, errors_SV_ranges_COE, and orbit_ranges_plot.

results_LS_CW (script)	It shows, by Command Window, some results related to script least_squares.
results_statistical (script)	It shows, by Command Window, the results obtained within the script MAIN_statistical.
results_statistical_LS (script)	It computes the statistical results of Least Squares algorithm when performing the statistical simulation of it.
results_statistical_LS_CW (script)	It shows, by Command Window, the statistical results obtained within the script results_statistical_LS.
rot1 (function)	It performs a rotation about the first axis.
rot3 (function)	It performs a rotation about the third axis.
rv2coe (function)	It finds the Classical Orbital Elements given the geocentric equatorial, IJK, position and velocity vectors.
rv2ranges (function)	It computes the range and range-rate observations of different sites given the satellite state vector at epoch t.
satellite_parameters (function)	It returns the location parameters that define the initial satellite position with respect to the initial Greenwich Mean Sidereal Time (GMST) at epoch $t_0 = 00:00:00$.
site_parameters (function)	It returns the location parameters of one of the sites defined within the function.
site_SVs (function)	It computes the site state vectors given the location parameters of each site and the epochs when these state vectors must be calculated.
SVs_from_ranges (script)	It computes the approximate satellite state vector from a set of observations containing range and range-rate observations of three different sites.
theoretical_parameters (function)	It computes the ideal range and range-rate observations at each epoch of variable t between one site located over the Earth's surface and a satellite located in a near-circular geostationary orbit.
Trilateration (function)	It calculates the satellite state vector at the epoch when the range and range-rate observations of three different sites are provided.
unit (function)	It calculates a unit vector given the original vector.

Table A.1: *Summary of all Matlab functions and scripts used along the PFC.*

APPENDIX B

Appendix B shows the numerical results obtained in all Matlab simulations performed in Chapter 3. These results are related to ideal and approximate values and errors of: the satellite state vector, the Classical Orbital Elements, and the range and range-rate observations. In case of statistical simulations, the results show the ideal value, and the mean and standard deviation of the errors obtained in the satellite state vector, and the range and range-rate observations.

B.1. RESULTS OF SECTION 3.5: SETTING A

	SATELLITE STATE VECTOR		
	Ideal value	**Approximate value**	**Error**
EPOCH $t_1 = 9\,000$ s			
r_x [km]	23 076.206 106 788 981	23 076.206 106 788 715	-0.000 000 000 266
r_y [km]	35 283.375 426 893 952	35 283.375 426 894 039	0.000 000 000 087
r_z [km]	0.000 000 000 000	-0.000 000 000 531	-0.000 000 000 531
v_x [km/s]	-2.573 186 442 040	-2.573 186 442 040	-0.000 000 000 000
v_y [km/s]	1.683 542 939 042	1.683 542 939 042	-0.000 000 000 000
v_z [km/s]	0.000 000 000 000	0.000 000 000 000	-0.000 000 000 000
EPOCH $t_f = 30\,600$ s			
r_x [km]	-35 389.419 322 388 858	-35 389.419 322 389 018	-0.000 000 000 160
r_y [km]	22 934.754 421 927 479	22 934.754 421 926 620	-0.000 000 000 859
r_z [km]	0.000 000 000 000	-0.000 000 001 146	-0.000 000 001 146
v_x [km/s]	-1.672 148 279 220	-1.672 148 279 220	0.000 000 000 000
v_y [km/s]	-2.579 589 570 438	-2.579 589 570 438	-0.000 000 000 000
v_z [km/s]	-0.000 000 000 000	0.000 000 000 000	0.000 000 000 000

Table B.1: *Numerical results of satellite state vector (setting A).*

RANGE OBSERVATIONS (ρ)				
Num.	**Site**	**Ideal value** [km]	**Approximate value** [km]	**Error** [km]
EPOCH t_1 = 9 000 s				
01	BCN	37 837.696 026 402 111	37 837.696 026 402 111	0.000 000 000 000
02	BET	38 446.575 954 225 314	38 446.575 954 225 314	0.000 000 000 000
03	MIL	38 028.921 622 176 684	38 028.921 622 176 684	0.000 000 000 000
07	BRN	38 182.029 368 749 914	38 182.029 368 749 914	0.000 000 000 000
08	LIS	38 042.328 754 617 185	38 042.328 754 617 192	0.000 000 000 007
09	LON	38 742.205 915 905 528	38 742.205 915 905 528	0.000 000 000 000
10	BRL	38 622.189 255 594 414	38 622.189 255 594 414	0.000 000 000 000
11	WAR	38 576.603 473 887 648	38 576.603 473 887 641	-0.000 000 000 007
12	ATH	37 347.330 742 545 055	37 347.330 742 545 033	-0.000 000 000 022
EPOCH t_f = 30 600 s				
01	BCN	37 849.125 818 200 402	37 849.125 818 200 220	-0.000 000 000 182
02	BET	38 458.054 469 152 936	38 458.054 469 152 768	-0.000 000 000 167
03	MIL	38 040.427 889 373 103	38 040.427 889 372 928	-0.000 000 000 175
07	BRN	38 193.517 922 760 664	38 193.517 922 760 497	-0.000 000 000 167
08	LIS	38 053.631 863 541 596	38 053.631 863 541 428	-0.000 000 000 167
09	LON	38 753.630 333 962 217	38 753.630 333 962 057	-0.000 000 000 160
10	BRL	38 633.731 442 392 957	38 633.731 442 392 789	-0.000 000 000 167
11	WAR	38 588.212 889 795 912	38 588.212 889 795 737	-0.000 000 000 175
12	ATH	37 359.011 566 637 222	37 359.011 566 637 004	-0.000 000 000 218

Table B.2: *Numerical results of range observations (setting A).*

CLASSICAL ORBITAL ELEMENTS (COE)				
COE	**Unit**	**Ideal value**	**Approximate value**	**Error**
EPOCH t_1 = 9 000 s				
$\boldsymbol{a}$	[km]	42 164.169 460 970 334	42 164.169 460 970 174	-0.000 000 000 160
$\boldsymbol{e}$	–	0.000 200 000 000	0.000 200 000 000	-0.000 000 000 000
$\boldsymbol{p}$	[km]	42 164.167 774 403 555	42 164.167 774 403 410	-0.000 000 000 145
$\boldsymbol{i}$	[°]	0.000 000 000 000	0.000 000 000 000	0.000 000 000 000
$\boldsymbol{\Omega}$	[°]	undefined	undefined	-
$\boldsymbol{\omega}$	[°]	undefined	undefined	-
$\boldsymbol{\nu_0}$	[°]	56.814 314 616 910	56.814 314 616 744	-0.000 000 000 166
$\boldsymbol{\tilde{\omega}_{\mathrm{true}}}$	[°]	0.000 000 000 000	0.000 000 000 000	0.000 000 000 000
$\boldsymbol{u_0}$	[°]	undefined	undefined	-
$\boldsymbol{\lambda_{\mathrm{true}_0}}$	[°]	56.814 314 616 910	56.814 314 616 744	-0.000 000 000 166

EPOCH $t_f = 30\,600$ s

				Error
a	[km]	42 164.169 460 970 334	42 164.169 460 970 166	-0.000 000 000 167
e	–	0.000 200 000 000	0.000 200 000 000	-0.000 000 000 000
p	[km]	42 164.167 774 403 555	42 164.167 774 403 395	-0.000 000 000 160
i	[°]	0.000 000 000 000	0.000 000 000 000	0.000 000 000 000
Ω	[°]	undefined	undefined	-
ω	[°]	undefined	undefined	-
ν_0	[°]	147.054 013 879 961	147.054 013 879 872	-0.000 000 000 089
$\tilde{\omega}_{\text{true}}$	[°]	0.000 000 000 000	0.000 000 000 000	0.000 000 000 000
u_0	[°]	undefined	undefined	-
λ_{true_0}	[°]	147.054 013 879 961	147.054 013 879 872	-0.000 000 000 089

__Table B.3:__ Numerical results of Classical Orbital Elements (setting A).

B.2. RESULTS OF SECTION 3.5: SETTING B

SATELLITE STATE VECTOR	Ideal value	Approximate value	Error
EPOCH $t_0 = 0$ s			
r_x [km]	39 811.324 342 080 086	39 811.324 342 080 072	-0.000 000 000 015
r_y [km]	13 863.769 945 143 404	13 863.769 945 143 476	0.000 000 000 036
r_z [km]	-0.000 000 000 015	0.000 000 000 073	0.000 000 000 036
v_x [km/s]	-1.011 153 178 968	-1.011 153 178 968	0.000 000 000 000
v_y [km/s]	2.904 251 340 218	2.904 251 340 218	-0.000 000 000 000
v_z [km/s]	0.000 000 000 000	0.000 000 000 000	0.000 000 000 000
EPOCH $t_f = 21\,600$ s			
r_x [km]	-14 048.210 875 367 075	-14 048.210 875 367 071	0.000 000 000 004
r_y [km]	39 758.040 138 460 929	39 758.040 138 460 681	0.000 000 000 281
r_z [km]	0.000 000 000 004	-0.000 000 000 247	0.000 000 000 281
v_x [km/s]	-2.899 009 362 761	-2.899 009 362 761	0.000 000 000 000
v_y [km/s]	-1.023 728 690 437	-1.023 728 690 437	-0.000 000 000 000
v_z [km/s]	-0.000 000 000 000	-0.000 000 000 000	-0.000 000 000 000

__Table B.4:__ Numerical results of satellite state vector (setting B).

RANGE OBSERVATIONS (ρ)				
Num.	**Site**	**Ideal value** [km]	**Approximate value** [km]	**Error** [km]
EPOCH $t_0 = 0$ s				
01	BCN	37 834.053 693 001 108	37 834.053 693 001 115	0.000 000 000 007
02	BET	38 443.051 174 980 268	38 443.051 174 980 275	0.000 000 000 007
03	MIL	38 025.423 177 105 964	38 025.423 177 105 971	0.000 000 000 007
07	BRN	38 178.508 556 331 370	38 178.508 556 331 377	0.000 000 000 007
08	LIS	38 038.478 209 228 619	38 038.478 209 228 626	0.000 000 000 007
09	LON	38 738.600 812 036 675	38 738.600 812 036 675	0.000 000 000 000
10	BRL	38 618.783 379 768 545	38 618.783 379 768 553	0.000 000 000 007
11	WAR	38 573.312 333 845 846	38 573.312 333 845 854	0.000 000 000 007
12	ATH	37 344.093 302 991 045	37 344.093 302 991 045	0.000 000 000 000
EPOCH $t_f = 21\,600$ s				
01	BCN	37 845.136 629 696 470	37 845.136 629 696 208	-0.000 000 000 262
02	BET	38 453.982 609 793 478	38 453.982 609 793 216	-0.000 000 000 262
03	MIL	38 036.328 990 781 658	38 036.328 990 781 396	-0.000 000 000 262
07	BRN	38 189.439 026 046 719	38 189.439 026 046 457	-0.000 000 000 262
08	LIS	38 049.809 535 903 398	38 049.809 535 903 143	-0.000 000 000 255
09	LON	38 749.625 490 385 479	38 749.625 490 385 210	-0.000 000 000 269
10	BRL	38 629.568 681 622 295	38 629.568 681 622 033	-0.000 000 000 262
11	WAR	38 583.959 484 721 621	38 583.959 484 721 352	-0.000 000 000 269
12	ATH	37 354.695 527 400 443	37 354.695 527 400 181	-0.000 000 000 262

Table B.5: *Numerical results of range observations (setting B).*

CLASSICAL ORBITAL ELEMENTS (COE)				
COE	**Unit**	**Ideal value**	**Approximate value**	**Error**
EPOCH $t_0 = 0$ s				
a	[km]	42 164.169 460 970 312	42 164.169 460 970 064	-0.000 000 000 247
e	–	0.000 200 000 000	0.000 200 000 000	-0.000 000 000 000
p	[km]	42 164.167 774 403 555	42 164.167 774 403 279	-0.000 000 000 276
i	[°]	0.000 000 000 000	0.000 000 000 000	0.000 000 000 000
Ω	[°]	undefined	undefined	-
ω	[°]	undefined	undefined	-
ν_0	[°]	19.200 000 000 009	19.200 000 000 836	0.000 000 000 827
$\tilde{\omega}_{\text{true}}$	[°]	0.000 000 000 000	0.000 000 000 000	0.000 000 000 000
u_0	[°]	undefined	undefined	-
λ_{true_0}	[°]	19.200 000 000 009	19.200 000 000 836	0.000 000 000 827

EPOCH $t_f = 21\ 600$ s

$\boldsymbol{a}$	[km]	42 164.169 460 970 304	42 164.169 460 970 086	-0.000 000 000 218
$\boldsymbol{e}$	–	0.000 200 000 000	0.000 200 000 000	-0.000 000 000 000
$\boldsymbol{p}$	[km]	42 164.167 774 403 526	42 164.167 774 403 300	-0.000 000 000 226
$\boldsymbol{i}$	[°]	0.000 000 000 000	0.000 000 000 000	0.000 000 000 000
$\boldsymbol{\Omega}$	[°]	undefined	undefined	-
$\boldsymbol{\omega}$	[°]	undefined	undefined	-
$\boldsymbol{\nu_0}$	[°]	109.460 486 499 160	109.460 486 499 685	0.000 000 000 524
$\tilde{\boldsymbol{\omega}}_{\mathbf{true}}$	[°]	0.000 000 000 000	0.000 000 000 000	0.000 000 000 000
$\boldsymbol{u_0}$	[°]	undefined	undefined	-
$\boldsymbol{\lambda}_{\mathbf{true}_0}$	[°]	109.460 486 499 160	109.460 486 499 685	0.000 000 000 524

Table B.6: *Numerical results of Classical Orbital Elements (setting B).*

RANGE-RATE OBSERVATIONS ($\dot{\rho}$)

Num.	**Site**	**Ideal value** [km/s]	**Approximate value** [km/s]	**Error** [km/s]
EPOCH $t_0 = 0$ s				
01	BCN	0.000 243 981 046	0.000 243 981 046	-0.000 000 000 000
02	BET	0.000 228 394 049	0.000 228 394 049	-0.000 000 000 000
03	MIL	0.000 224 589 431	0.000 224 589 431	-0.000 000 000 000
07	BRN	0.000 227 712 055	0.000 227 712 055	-0.000 000 000 000
08	LIS	0.000 272 339 131	0.000 272 339 131	-0.000 000 000 000
09	LON	0.000 239 431 262	0.000 239 431 262	-0.000 000 000 000
10	BRL	0.000 212 360 938	0.000 212 360 938	-0.000 000 000 000
11	WAR	0.000 196 782 202	0.000 196 782 202	-0.000 000 000 000
12	ATH	0.000 188 748 825	0.000 188 748 825	0.000 000 000 000
EPOCH $t_f = 21\ 600$ s				
01	BCN	0.000 560 626 939	0.000 560 626 939	-0.000 000 000 000
02	BET	0.000 565 211 901	0.000 565 211 901	-0.000 000 000 000
03	MIL	0.000 567 152 627	0.000 567 152 627	-0.000 000 000 000
07	BRN	0.000 565 822 125	0.000 565 822 125	-0.000 000 000 000
08	LIS	0.000 550 314 761	0.000 550 314 761	-0.000 000 000 000
09	LON	0.000 560 950 171	0.000 560 950 171	-0.000 000 000 000
10	BRL	0.000 570 630 327	0.000 570 630 327	-0.000 000 000 000
11	WAR	0.000 576 172 939	0.000 576 172 939	-0.000 000 000 000
12	ATH	0.000 580 934 546	0.000 580 934 546	-0.000 000 000 000

Table B.7: *Numerical results of range-rate observations (setting B).*

B.3. RESULTS OF SECTION 3.7: SETTING B + NOISE

NOISE ADDED TO RANGE OBSERVATIONS AT $t_0 = 0$ s			
Num.	**Site**	**Mean** [km]	**Standard deviation** [km]
01	BCN	0.000 000 000 000	0.000 537 667 140
02	BET	0.000 000 000 000	-0.000 433 592 022
03	MIL	0.000 000 000 000	0.000 725 404 225

Table B.8: *Numerical results of the noise added to range observations at initial epoch (setting B + noise).*

NOISE ADDED TO RANGE-RATE OBSERVATIONS AT $t_0 = 0$ s			
Num.	**Site**	**Mean** [km/s]	**Standard deviation** [km/s]
01	BCN	0.000 000 000 000	0.000 004 310 867
02	BET	0.000 000 000 000	0.000 013 847 185
03	MIL	0.000 000 000 000	-0.000 001 024 830

Table B.9: *Numerical results of the noise added to range-rate observations at initial epoch (setting B + noise).*

	SATELLITE STATE VECTOR		
	Ideal value	**Approximate value**	**Error**
EPOCH $t_0 = 0$ s			
r_x [km]	39 811.324 342 080 086	39 811.365 775 960 876	0.041 433 880 790
r_y [km]	13 863.769 945 143 404	13 863.704 826 079 083	-0.065 119 064 320
r_z [km]	0.000 000 000 000	0.128 662 579 438	0.128 662 579 438
v_x [km/s]	-1.011 153 178 968	-1.011 713 812 592	-0.000 560 633 624
v_y [km/s]	2.904 251 340 218	2.905 228 419 887	0.000 977 079 669
v_z [km/s]	0.000 000 000 000	-0.001 581 919 610	-0.001 581 919 610
EPOCH $t_f = 21\,600$ s			
r_x [km]	-14 048.210 875 367 075	-14 052.447 524 146 140	-4.236 648 779 066
r_y [km]	39 758.040 138 460 929	39 785.824 830 923 550	27.784 692 462 621
r_z [km]	0.000 000 000 000	-21.697 656 431 888	-21.697 656 431 888
v_x [km/s]	-2.899 009 362 761	-2.899 022 545 707	-0.000 013 182 946
v_y [km/s]	-1.023 728 690 437	-1.020 975 865 168	0.002 752 825 269
v_z [km/s]	-0.000 000 000 000	-0.000 003 827 423	-0.000 003 827 423

Table B.10: *Numerical results of satellite state vector (setting B + noise).*

RANGE OBSERVATIONS (ρ)				
Num.	**Site**	**Ideal value** [km]	**Approximate value** [km]	**Error** [km]
EPOCH $t_0 = 0$ s				
01	BCN	37 834.053 693 001 108	37 834.054 230 668 255	0.000 537 667 147
02	BET	38 443.051 174 980 268	38 443.050 741 388 251	-0.000 433 592 017
03	MIL	38 025.423 177 105 964	38 025.423 902 510 207	0.000 725 404 243
07	BRN	38 178.508 556 331 370	38 178.508 755 516 385	0.000 199 185 015
08	LIS	38 038.478 209 228 619	38 038.477 744 405 391	-0.000 464 823 228
09	LON	38 738.600 812 036 675	38 738.599 345 585 506	-0.001 466 451 169
10	BRL	38 618.783 379 768 545	38 618.783 389 391 559	0.000 009 623 014
11	WAR	38 573.312 333 845 846	38 573.313 393 922 865	0.001 060 077 018
12	ATH	37 344.093 302 991 045	37 344.098 271 158 415	0.004 968 167 370
EPOCH $t_f = 21\,600$ s				
01	BCN	37 845.136 629 696 470	37 874.770 851 403 351	29.634 221 706 881
02	BET	38 453.982 609 793 478	38 483.973 901 242 141	29.991 291 448 663
03	MIL	38 036.328 990 781 658	38 066.214 892 452 292	29.885 901 670 634
07	BRN	38 189.439 026 046 719	38 219.353 441 842 606	29.914 415 795 887
08	LIS	38 049.809 535 903 398	38 079.158 423 171 444	29.348 887 268 046
09	LON	38 749.625 490 385 479	38 779.601 111 043 070	29.975 620 657 591
10	BRL	38 629.568 681 622 295	38 659.720 734 556 664	30.152 052 934 369
11	WAR	38 583.959 484 721 621	38 614.177 746 458 212	30.218 261 736 591
12	ATH	37 354.695 527 400 443	37 384.479 588 293 689	29.784 060 893 246

Table B.11: *Numerical results of range observations (setting B + noise).*

CLASSICAL ORBITAL ELEMENTS (COE)				
COE	**Unit**	**Ideal value**	**Approximate value**	**Error**
EPOCH $t_0 = 0$ s				
a	[km]	42 164.169 460 970 312	42 194.613 477 875 355	30.444 016 905 043
e	–	0.000 200 000 000	0.000 909 845 318	0.000 709 845 318
p	[km]	42 164.167 774 403 555	42 194.578 548 393 642	30.410 773 990 086
i	[°]	0.000 000 000 000	0.029 463 150 371	0.029 463 150 371
Ω	[°]	undefined	199.539 960 718 384	199.539 960 718 384
ω	[°]	undefined	179.893 028 161 531	179.893 028 161 531
ν_0	[°]	19.200 000 000 009	359.766 908 973 045	340.566 908 973 035
$\tilde{\omega}_{\text{true}}$	[°]	0.000 000 000 000	undefined	-
u_0	[°]	undefined	undefined	-
λ_{true_0}	[°]	19.200 000 000 009	undefined	-

EPOCH $t_f = 21\ 600$ s

				Error
a	[km]	42 164.169 460 970 304	42 194.613 477 875 333	30.444 016 905 029
e	–	0.000 200 000 000	0.000 909 845 318	0.000 709 845 318
p	[km]	42 164.167 774 403 526	42 194.578 548 393 612	30.410 773 990 086
i	[°]	0.000 000 000 000	0.029 463 150 371	0.029 463 150 371
Ω	[°]	undefined	199.539 960 718 384	199.539 960 718 384
ω	[°]	undefined	179.893 028 161 473	179.893 028 161 473
ν_0	[°]	109.460 486 499 160	90.020 352 336 123	-19.440 134 163 037
$\tilde{\omega}_{true}$	[°]	0.000 000 000 000	undefined	-
u_0	[°]	undefined	undefined	-
λ_{true_0}	[°]	109.460 486 499 160	undefined	-

Table B.12: *Numerical results of Classical Orbital Elements (setting B + noise).*

RANGE-RATE OBSERVATIONS ($\dot{\rho}$)				
Num.	**Site**	**Ideal value** [km/s]	**Approximate value** [km/s]	**Error** [km/s]
EPOCH $t_0 = 0$ s				
01	BCN	0.000 243 981 046	0.000 248 291 913	0.000 004 310 867
02	BET	0.000 228 394 049	0.000 242 241 234	0.000 013 847 185
03	MIL	0.000 224 589 431	0.000 223 564 601	-0.000 001 024 830
07	BRN	0.000 227 712 055	0.000 233 656 531	0.000 005 944 476
08	LIS	0.000 272 339 131	0.000 293 435 693	0.000 021 096 562
09	LON	0.000 239 431 262	0.000 267 723 969	0.000 028 292 707
10	BRL	0.000 212 360 938	0.000 218 254 665	0.000 005 893 727
11	WAR	0.000 196 782 202	0.000 187 315 570	-0.000 009 466 632
12	ATH	0.000 188 748 825	0.000 129 890 237	-0.000 058 858 588
EPOCH $t_f = 21\ 600$ s				
01	BCN	0.000 560 626 939	0.002 654 130 867	0.002 093 503 928
02	BET	0.000 565 211 901	0.002 694 071 148	0.002 128 859 247
03	MIL	0.000 567 152 627	0.002 708 050 691	0.002 140 898 064
07	BRN	0.000 565 822 125	0.002 697 928 254	0.002 132 106 129
08	LIS	0.000 550 314 761	0.002 571 307 098	0.002 020 992 337
09	LON	0.000 560 950 171	0.002 660 561 661	0.002 099 611 490
10	BRL	0.000 570 630 327	0.002 738 766 736	0.002 168 136 409
11	WAR	0.000 576 172 939	0.002 783 622 972	0.002 207 450 033
12	ATH	0.000 580 934 546	0.002 816 550 615	0.002 235 616 069

Table B.13: *Numerical results of range-rate observations (setting B + noise).*

B.4. RESULTS OF SECTION 3.8: SETTING C

NOISE ADDED TO RANGE OBSERVATIONS AT $t_1 = 9\,000$ s			
Num.	**Site**	**Mean** [km]	**Standard deviation** [km]
01	BCN	-0.000 020 794 635	0.001 001 491 045
02	BET	0.000 065 381 263	0.000 990 369 202
03	MIL	-0.000 010 505 824	0.000 999 585 034

Table B.14: *Statistical results of the noise added to range observations at initial epoch (setting C).*

RANGE OBSERVATIONS (ρ)				
Num.	**Site**	**Ideal value** [km]	**Error** [km]	
			Mean	**Standard deviation**
EPOCH $t_1 = 9\,000$ s				
01	BCN	37 837.696 026 402 111	-0.000 020 794 636	0.001 001 491 045
02	BET	38 446.575 954 225 314	0.000 065 381 261	0.000 990 369 203
03	MIL	38 028.921 622 176 684	-0.000 010 505 826	0.000 999 585 034
07	BRN	38 182.029 368 749 914	0.000 022 277 605	0.000 647 420 212
08	LIS	38 042.328 754 617 185	0.000 014 524 901	0.003 088 182 987
09	LON	38 742.205 915 905 528	0.000 123 810 304	0.002 220 811 393
10	BRL	38 622.189 255 594 414	0.000 053 819 387	0.001 487 446 178
11	WAR	38 576.603 473 887 648	-0.000 000 487 978	0.002 826 341 719
12	ATH	37 347.330 742 545 055	-0.000 262 248 383	0.006 701 227 195
EPOCH $t_f = 30\,600$ s				
01	BCN	37 849.125 818 200 402	0.003 229 178 696	0.106 116 551 598
02	BET	38 458.054 469 152 936	0.003 236 956 763	0.104 823 979 930
03	MIL	38 040.427 889 373 103	0.003 168 286 400	0.104 747 398 201
07	BRN	38 193.517 922 760 664	0.003 203 213 421	0.104 880 971 769
08	LIS	38 053.631 863 541 596	0.003 353 629 527	0.108 007 819 194
09	LON	38 753.630 333 962 217	0.003 318 412 393	0.105 453 419 099
10	BRL	38 633.731 442 392 957	0.003 171 451 640	0.103 747 735 929
11	WAR	38 588.212 889 795 912	0.003 076 117 304	0.102 815 631 311
12	ATH	37 359.011 566 637 222	0.002 856 473 494	0.103 004 113 990

Table B.15: *Statistical results of range observations (setting C).*

SATELLITE STATE VECTOR			
	Ideal value	**Error**	
		Mean	**Standard deviation**
EPOCH $t_1 = 9\,000$ s			
r_x [km]	23 076.206 106 788 981	-0.003 842 348 683	0.116 666 925 830
r_y [km]	35 283.375 426 893 952	0.001 119 548 941	0.056 142 626 758
r_z [km]	0.000 000 000 000	-0.008 971 507 131	0.150 660 482 757
v_x [km/s]	-2.573 186 442 040	-0.000 000 360 000	0.000 008 633 632
v_y [km/s]	1.683 542 939 042	-0.000 000 182 964	0.000 006 246 387
v_z [km/s]	0.000 000 000 000	-0.000 000 499 875	0.000 012 300 785
EPOCH $t_f = 30\,600$ s			
r_x [km]	-35 389.419 322 388 858	-0.005 656 660 153	0.142 900 699 936
r_y [km]	22 934.754 421 927 479	-0.004 628 160 410	0.114 204 786 750
r_z [km]	0.000 000 000 000	-0.006 816 147 554	0.168 727 153 936
v_x [km/s]	-1.672 148 279 220	0.000 000 184 632	0.000 007 073 899
v_y [km/s]	-2.579 589 570 438	-0.000 000 064 263	0.000 007 518 829
v_z [km/s]	-0.000 000 000 000	0.000 000 656 216	0.000 010 983 308

Table B.16: *Statistical results of satellite state vector (setting C).*

B.5. RESULTS OF SECTION 3.8: SETTING D

NOISE ADDED TO RANGE OBSERVATIONS AT $t_0 = 0$ s			
Num.	**Site**	**Mean** [km]	**Standard deviation** [km]
01	BCN	0.000 007 075 273	0.000 954 952 523
02	BET	-0.000 016 803 836	0.000 999 457 606
03	MIL	-0.000 003 828 291	0.001 013 639 293

Table B.17: *Statistical results of the noise added to range observations at initial epoch (setting D).*

NOISE ADDED TO RANGE-RATE OBSERVATIONS AT $t_0 = 0$ s			
Num.	**Site**	**Mean** [km/s]	**Standard deviation** [km/s]
01	BCN	-0.000 000 124 367	0.000 004 894 309
02	BET	0.000 000 294 824	0.000 005 057 132
03	MIL	-0.000 000 149 263	0.000 005 094 707

Table B.18: *Statistical results of the noise added to range-rate observations at initial epoch (setting D).*

RANGE OBSERVATIONS (ρ)

Num.	Site	Ideal value [km]	Error [km] Mean	Error [km] Standard deviation
EPOCH $t_0 = 0$ s				
01	BCN	37 834.053 693 001 108	0.000 007 075 277	0.000 954 952 523
02	BET	38 443.051 174 980 268	-0.000 016 803 831	0.000 999 457 606
03	MIL	38 025.423 177 105 964	-0.000 003 828 284	0.001 013 639 293
07	BRN	38 178.508 556 331 370	-0.000 008 756 149	0.000 648 793 275
08	LIS	38 038.478 209 228 619	0.000 013 303 092	0.003 172 591 514
09	LON	38 738.600 812 036 675	-0.000 023 070 197	0.002 300 991 661
10	BRL	38 618.783 379 768 545	-0.000 021 902 804	0.001 476 513 832
11	WAR	38 573.312 333 845 846	-0.000 018 486 489	0.002 908 291 393
12	ATH	37 344.093 302 991 045	0.000 028 636 768	0.006 940 341 927
EPOCH $t_f = 21\,600$ s				
01	BCN	37 845.136 629 696 470	0.710 064 597 740	17.194 602 433 949
02	BET	38 453.982 609 793 478	0.720 554 883 344	17.343 079 403 691
03	MIL	38 036.328 990 781 658	0.716 680 203 892	17.318 322 025 947
07	BRN	38 189.439 026 046 719	0.717 916 902 765	17.320 408 916 631
08	LIS	38 049.809 535 903 398	0.703 313 125 439	17.035 369 200 413
09	LON	38 749.625 490 385 479	0.721 053 566 825	17.313 093 709 566
10	BRL	38 629.568 681 622 295	0.724 510 770 026	17.428 527 444 918
11	WAR	38 583.959 484 721 621	0.725 387 526 973	17.481 859 284 098
12	ATH	37 354.695 527 400 443	0.710 219 078 426	17.360 789 159 842

Table B.19: *Statistical results of range observations (setting D).*

RANGE-RATE OBSERVATIONS ($\dot{\rho}$)

Num.	Site	Ideal value [km/s]	Error [km/s] Mean	Error [km/s] Standard deviation
EPOCH $t_0 = 0$ s				
01	BCN	0.000 243 981 046	-0.000 000 124 367	0.000 004 894 309
02	BET	0.000 228 394 049	0.000 000 294 824	0.000 005 057 132
03	MIL	0.000 224 589 431	-0.000 000 149 263	0.000 005 094 707
07	BRN	0.000 227 712 055	0.000 000 048 884	0.000 003 383 013
08	LIS	0.000 272 339 131	0.000 000 196 579	0.000 015 646 600
09	LON	0.000 239 431 262	0.000 000 671 420	0.000 011 101 081
10	BRL	0.000 212 360 938	0.000 000 161 363	0.000 007 752 932
11	WAR	0.000 196 782 202	-0.000 000 210 994	0.000 014 541 946
12	ATH	0.000 188 748 825	-0.000 001 720 667	0.000 033 562 133

EPOCH $t_f = 21\ 600$ s

01	BCN	0.000 560 626 939	0.000 050 351 944	0.001 215 446 991
02	BET	0.000 565 211 901	0.000 051 140 778	0.001 236 985 820
03	MIL	0.000 567 152 627	0.000 051 416 697	0.001 244 283 557
07	BRN	0.000 565 822 125	0.000 051 216 883	0.001 238 944 948
08	LIS	0.000 550 314 761	0.000 048 716 844	0.001 171 383 486
09	LON	0.000 560 950 171	0.000 050 478 906	0.001 219 213 403
10	BRL	0.000 570 630 327	0.000 052 023 622	0.001 260 891 744
11	WAR	0.000 576 172 939	0.000 052 909 712	0.001 284 814 369
12	ATH	0.000 580 934 546	0.000 053 558 613	0.001 301 879 697

Table B.20: *Statistical results of range-rate observations (setting D).*

SATELLITE STATE VECTOR			
	Ideal value	Error	
		Mean	Standard deviation
EPOCH $t_0 = 0$ s			
r_x [km]	39 811.324 342 080 086	0.000 268 174 643	0.061 898 243 421
r_y [km]	13 863.769 945 143 404	-0.000 131 102 625	0.120 189 082 665
r_z [km]	0.000 000 000 000	0.001 752 361 514	0.150 967 284 766
v_x [km/s]	-1.011 153 178 968	-0.000 015 081 728	0.000 298 147 864
v_y [km/s]	2.904 251 340 218	0.000 022 838 521	0.000 581 275 665
v_z [km/s]	0.000 000 000 000	-0.000 050 439 729	0.000 743 176 478
EPOCH $t_f = 21\ 600$ s			
r_x [km]	-14 048.210 875 367 075	-0.138 466 305 982	2.098 900 569 503
r_y [km]	39 758.040 138 460 929	0.629 012 483 030	17.040 050 731 314
r_z [km]	0.000 000 000 000	-0.692 942 617 556	10.190 570 394 388
v_x [km/s]	-2.899 009 362 761	-0.000 000 702 934	0.000 016 477 585
v_y [km/s]	-1.023 728 690 437	0.000 062 031 977	0.001 688 435 116
v_z [km/s]	-0.000 000 000 000	-0.000 000 186 739	0.000 011 417 112

Table B.21: *Statistical results of satellite state vector (setting D).*

B.6. RESULTS OF SECTION 3.8: SETTING E

NOISE ADDED TO RANGE OBSERVATIONS AT $t_1 = 9\ 000$ s			
Num.	**Site**	**Mean** [km]	**Standard deviation** [km]
01	BCN	-0.032 512 355 075	0.990 224 081 084
02	BET	0.000 624 884 542	1.009 062 541 120
03	MIL	-0.050 884 426 181	0.985 956 913 669

Table B.22: *Statistical results of the noise added to range observations at initial epoch (setting E).*

RANGE OBSERVATIONS (ρ)

Num.	Site	Ideal value [km]	Error [km] Mean	Error [km] Standard deviation
EPOCH $t_1 = 9\,000$ s				
01	BCN	37 837.696 026 402 111	-0.032 512 355 076	0.990 224 081 084
02	BET	38 446.575 954 225 314	0.000 624 884 540	1.009 062 541 120
03	MIL	38 028.921 622 176 684	-0.050 884 426 182	0.985 956 913 668
07	BRN	38 182.029 368 749 914	-0.026 534 838 313	0.646 554 965 419
08	LIS	38 042.328 754 617 185	0.022 914 666 003	3.221 222 236 165
09	LON	38 742.205 915 905 528	0.050 216 339 532	2.324 621 277 815
10	BRL	38 622.189 255 594 414	-0.028 523 882 592	1.433 944 953 140
11	WAR	38 576.603 473 887 648	-0.083 828 924 968	2.862 158 601 816
12	ATH	37 347.330 742 545 055	-0.258 454 672 248	6.878 881 439 188
EPOCH $t_f = 30\,600$ s				
01	BCN	37 849.125 818 200 402	-6.288 550 770 242	107.882 405 765 730
02	BET	38 458.054 469 152 936	-6.428 043 535 146	106.688 345 838 139
03	MIL	38 040.427 889 373 103	-6.435 099 219 613	106.495 591 077 952
07	BRN	38 193.517 922 760 664	-6.420 953 108 421	106.681 669 485 819
08	LIS	38 053.631 863 541 596	-6.087 339 942 798	109.875 074 665 772
09	LON	38 753.630 333 962 217	-6.362 939 492 749	107.420 794 498 492
10	BRL	38 633.731 442 392 957	-6.544 132 085 281	105.570 111 606 237
11	WAR	38 588.212 889 795 912	-6.644 503 999 983	104.535 524 397 077
12	ATH	37 359.011 566 637 222	-6.632 765 425 843	104.335 352 709 917

Table B.23: *Statistical results of range observations (setting E).*

SATELLITE STATE VECTOR

	Ideal value	Error Mean	Error Standard deviation
EPOCH $t_1 = 9\,000$ s			
r_x [km]	23 076.206 106 788 981	-4.124 581 228 867	121.720 532 918 644
r_y [km]	35 283.375 426 893 952	1.015 302 556 406	58.588 548 994 502
r_z [km]	0.000 000 000 000	-6.144 603 168 485	149.234 382 398 849
v_x [km/s]	-2.573 186 442 040	0.000 034 960 719	0.008 978 175 308
v_y [km/s]	1.683 542 939 042	-0.000 353 135 071	0.006 529 509 732
v_z [km/s]	0.000 000 000 000	0.000 176 505 538	0.012 673 089 619

EPOCH $t_f = 30\ 600$ s

	Ideal value	Error Mean	Error Standard deviation
r_x [km]	-35 389.419 322 388 858	1.697 418 123 979	147.521 768 475 264
r_y [km]	22 934.754 421 927 479	-10.353 228 819 781	118.069 957 282 002
r_z [km]	0.000 000 000 000	2.591 282 794 655	173.760 712 319 894
v_x [km/s]	-1.672 148 279 220	0.000 714 119 301	0.007 264 669 915
v_y [km/s]	-2.579 589 570 438	-0.000 707 565 863	0.007 445 796 793
v_z [km/s]	-0.000 000 000 000	0.000 456 036 687	0.010 884 328 392

Table B.24: *Statistical results of satellite state vector (setting E).*

B.7. RESULTS OF SECTION 3.8: SETTING F

NOISE ADDED TO RANGE OBSERVATIONS AT $t_1 = 9\ 000$ s			
Num.	**Site**	**Mean** [km]	**Standard deviation** [km]
04	LPG	0.000 030 256 899	0.001 002 632 811
05	REY	-0.000 007 978 140	0.001 022 218 217
06	ANK	0.000 046 053 714	0.000 993 014 698

Table B.25: *Statistical results of the noise added to range observations at initial epoch (setting F).*

SATELLITE STATE VECTOR

	Ideal value	Error	
		Mean	Standard deviation
EPOCH $t_1 = 9\ 000$ s			
r_x [km]	23 076.206 106 788 981	0.000 359 133 482	0.010 999 995 561
r_y [km]	35 283.375 426 893 952	-0.000 085 138 000	0.006 209 583 964
r_z [km]	0.000 000 000 000	0.000 826 007 842	0.024 072 703 630
v_x [km/s]	-2.573 186 442 040	0.000 000 029 162	0.000 000 882 855
v_y [km/s]	1.683 542 939 042	0.000 000 011 014	0.000 000 732 739
v_z [km/s]	0.000 000 000 000	0.000 000 001 979	0.000 002 008 423
EPOCH $t_f = 30\ 600$ s			
r_x [km]	-35 389.419 322 388 858	0.000 488 610 291	0.015 299 427 680
r_y [km]	22 934.754 421 927 479	0.000 281 858 699	0.014 176 421 690
r_z [km]	0.000 000 000 000	0.000 023 545 211	0.027 540 061 269
v_x [km/s]	-1.672 148 279 220	-0.000 000 012 722	0.000 000 970 585
v_y [km/s]	-2.579 589 570 438	-0.000 000 003 055	0.000 001 175 189
v_z [km/s]	-0.000 000 000 000	-0.000 000 060 237	0.000 001 755 614

Table B.26: *Statistical results of satellite state vector (setting F).*

RANGE OBSERVATIONS (ρ)				
Num.	**Site**	**Ideal value** [km]	**Error** [km]	
			Mean	**Standard deviation**
EPOCH t_1 = 9 000 s				
01	BCN	37 837.696 026 402 111	0.000 019 998 491	0.000 598 104 638
02	BET	38 446.575 954 225 314	0.000 011 968 222	0.000 714 705 975
03	MIL	38 028.921 622 176 684	0.000 018 954 116	0.000 646 144 337
04	LPG	37 730.308 575 272 822	0.000 030 256 903	0.001 002 632 811
05	REY	40 447.716 714 274 029	-0.000 007 978 142	0.001 022 218 218
06	ANK	37 620.731 260 024 579	0.000 046 053 716	0.000 993 014 698
07	BRN	38 182.029 368 749 914	0.000 015 943 760	0.000 663 886 005
08	LIS	38 042.328 754 617 185	0.000 016 867 671	0.000 680 957 206
09	LON	38 742.205 915 905 528	0.000 006 628 946	0.000 757 257 889
10	BRL	38 622.189 255 594 414	0.000 012 953 037	0.000 792 970 410
11	WAR	38 576.603 473 887 648	0.000 017 883 284	0.000 836 272 936
12	ATH	37 347.330 742 545 055	0.000 041 999 290	0.000 832 316 292
EPOCH t_f = 30 600 s				
01	BCN	37 849.125 818 200 402	-0.000 276 227 181	0.014 439 621 250
02	BET	38 458.054 469 152 936	-0.000 269 610 712	0.014 408 347 978
03	MIL	38 040.427 889 373 103	-0.000 267 961 806	0.014 396 681 592
04	LPG	37 741.515 485 508 971	-0.000 298 549 309	0.014 561 379 407
05	REY	40 459.065 252 813 991	-0.000 279 222 399	0.014 478 627 518
06	ANK	37 632.500 945 118 300	-0.000 242 363 041	0.014 267 309 424
07	BRN	38 193.517 922 760 664	-0.000 269 308 119	0.014 404 692 650
08	LIS	38 053.631 863 541 596	-0.000 288 240 213	0.014 502 245 076
09	LON	38 753.630 333 962 217	-0.000 274 336 964	0.014 436 335 634
10	BRL	38 633.731 442 392 957	-0.000 262 730 222	0.014 372 494 319
11	WAR	38 588.212 889 795 912	-0.000 256 006 235	0.014 334 869 038
12	ATH	37 359.011 566 637 222	-0.000 252 436 373	0.014 319 784 911

Table B.27: *Statistical results of range observations (setting F).*

B.8. RESULTS OF SECTION 3.8: SETTING G

NOISE ADDED TO RANGE OBSERVATIONS AT t_0 = 0 s			
Num.	**Site**	**Mean** [km]	**Standard deviation** [km]
04	LPG	-0.000 011 590 789	0.001 018 744 790
05	REY	0.000 090 799 603	0.001 049 616 126
06	ANK	-0.000 018 023 079	0.001 003 659 869

Table B.28: *Statistical results of the noise added to range observations at initial epoch (setting G).*

NOISE ADDED TO RANGE-RATE OBSERVATIONS AT $t_0 = 0$ s			
Num.	**Site**	**Mean** [km/s]	**Standard deviation** [km/s]
04	LPG	-0.000 000 031 771	0.000 004 990 862
05	REY	0.000 000 098 369	0.000 004 970 079
06	ANK	-0.000 000 385 005	0.000 005 014 528

Table B.29: *Statistical results of the noise added to range-rate observations at initial epoch (setting G).*

RANGE OBSERVATIONS (ρ)				
Num.	**Site**	**Ideal value** [km]	**Error** [km]	
			Mean	**Standard deviation**
EPOCH $t_0 = 0$ s				
01	BCN	37 834.053 693 001 108	0.000 025 764 508	0.000 598 561 248
02	BET	38 443.051 174 980 268	0.000 048 604 630	0.000 712 547 116
03	MIL	38 025.423 177 105 964	0.000 032 848 830	0.000 639 097 012
04	LPG	37 726.272 782 221 386	-0.000 011 590 789	0.001 018 744 789
05	REY	40 444.031 239 730 401	0.000 090 799 606	0.001 049 616 126
06	ANK	37 617.666 306 731 175	-0.000 018 023 079	0.001 003 659 869
07	BRN	38 178.508 556 331 370	0.000 039 289 394	0.000 659 000 053
08	LIS	38 038.478 209 228 619	0.000 026 442 025	0.000 694 987 184
09	LON	38 738.600 812 036 675	0.000 058 720 357	0.000 764 302 752
10	BRL	38 618.783 379 768 545	0.000 050 025 138	0.000 785 163 598
11	WAR	38 573.312 333 845 846	0.000 041 913 691	0.000 823 628 922
12	ATH	37 344.093 302 991 045	-0.000 013 724 601	0.000 838 438 661
EPOCH $t_f = 21\,600$ s				
01	BCN	37 845.136 629 696 470	0.113 154 989 828	1.701 901 589 788
02	BET	38 453.982 609 793 478	0.114 255 313 435	1.713 109 098 993
03	MIL	38 036.328 990 781 658	0.113 976 397 583	1.712 893 791 970
04	LPG	37 737.833 258 773 469	0.110 186 517 018	1.665 902 722 591
05	REY	40 455.138 465 738 593	0.114 559 076 988	1.707 171 595 565
06	ANK	37 628.054 814 066 825	0.114 392 373 306	1.733 537 119 433
07	BRN	38 189.439 026 046 719	0.114 041 031 403	1.712 193 853 289
08	LIS	38 049.809 535 903 398	0.112 172 788 264	1.686 343 783 715
09	LON	38 749.625 490 385 479	0.114 150 409 778	1.708 828 059 552
10	BRL	38 629.568 681 622 295	0.114 792 879 207	1.721 206 807 406
11	WAR	38 583.959 484 721 621	0.115 055 184 762	1.727 483 140 005
12	ATH	37 354.695 527 400 443	0.113 854 944 790	1.723 842 226 669

Table B.30: *Statistical results of range observations (setting G).*

RANGE-RATE OBSERVATIONS ($\dot{\rho}$)

Num.	**Site**	**Ideal value** [km/s]	**Error** [km/s] **Mean**	**Error** [km/s] **Standard deviation**
EPOCH $t_0 = 0$ s				
01	BCN	0.000 243 981 046	-0.000 000 078 524	0.000 002 829 472
02	BET	0.000 228 394 049	-0.000 000 062 611	0.000 003 386 262
03	MIL	0.000 224 589 431	-0.000 000 110 872	0.000 003 054 289
04	LPG	0.000 297 263 023	-0.000 000 031 771	0.000 004 990 862
05	REY	0.000 250 880 941	0.000 000 098 369	0.000 004 970 079
06	ANK	0.000 165 555 535	-0.000 000 385 005	0.000 005 014 528
07	BRN	0.000 227 712 055	-0.000 000 087 145	0.000 003 135 776
08	LIS	0.000 272 339 131	-0.000 000 003 826	0.000 003 305 663
09	LON	0.000 239 431 262	-0.000 000 009 610	0.000 003 607 503
10	BRL	0.000 212 360 938	-0.000 000 100 028	0.000 003 784 186
11	WAR	0.000 196 782 202	-0.000 000 159 483	0.000 004 027 778
12	ATH	0.000 188 748 825	-0.000 000 315 837	0.000 004 157 103
EPOCH $t_f = 21\,600$ s				
01	BCN	0.000 560 626 939	0.000 008 084 726	0.000 120 170 862
02	BET	0.000 565 211 901	0.000 008 220 009	0.000 122 372 946
03	MIL	0.000 567 152 627	0.000 008 268 125	0.000 123 112 684
04	LPG	0.000 542 035 994	0.000 007 571 614	0.000 111 937 348
05	REY	0.000 555 506 558	0.000 007 968 441	0.000 118 436 842
06	ANK	0.000 588 604 579	0.000 008 858 204	0.000 132 470 260
07	BRN	0.000 565 822 125	0.000 008 233 427	0.000 122 570 039
08	LIS	0.000 550 314 761	0.000 007 803 142	0.000 115 683 478
09	LON	0.000 560 950 171	0.000 008 105 566	0.000 120 563 874
10	BRL	0.000 570 630 327	0.000 008 372 392	0.000 124 812 180
11	WAR	0.000 576 172 939	0.000 008 525 751	0.000 127 251 771
12	ATH	0.000 580 934 546	0.000 008 639 959	0.000 128 978 427

Table B.31: *Statistical results of range-rate observations (setting G).*

SATELLITE STATE VECTOR			
	Ideal value	Error: Mean	Error: Standard deviation
EPOCH $t_0 = 0$ s			
r_x [km]	39 811.324 342 080 086	-0.000 387 366 344	0.005 959 348 757
r_y [km]	13 863.769 945 143 404	0.000 454 205 423	0.011 730 818 246
r_z [km]	0.000 000 000 000	-0.001 984 728 364	0.024 854 585 822
v_x [km/s]	-1.011 153 178 968	-0.000 002 180 298	0.000 029 332 037
v_y [km/s]	2.904 251 340 218	0.000 003 790 617	0.000 058 548 037
v_z [km/s]	0.000 000 000 000	-0.000 004 761 136	0.000 120 527 136
EPOCH $t_f = 21\,600$ s			
r_x [km]	-14 048.210 875 367 075	-0.016 556 064 088	0.302 695 363 054
r_y [km]	39 758.040 138 460 929	0.108 028 284 059	1.764 757 959 772
r_z [km]	0.000 000 000 000	-0.065 276 042 319	1.652 626 790 413
v_x [km/s]	-2.899 009 362 761	-0.000 000 008 128	0.000 003 784 674
v_y [km/s]	-1.023 728 690 437	0.000 010 674 790	0.000 174 989 687
v_z [km/s]	-0.000 000 000 000	0.000 000 164 641	0.000 001 882 529

Table B.32: *Statistical results of satellite state vector (setting G).*

APPENDIX C

Appendix C shows the numerical results obtained in all Matlab statistical simulations performed in Chapter 4. These results are related to the mean and standard deviation of the errors in the satellite state vector, and the range and range-rate observations.

C.1. RESULTS OF SECTION 4.3: SETTING H

a) 10 observations

RANGE OBSERVATIONS (ρ) AFTER 100 LS ITERATIONS

Num.	Site	Ideal value [km]	Error [km] Mean	Error [km] Standard deviation
EPOCH $t_0 = 0$ s				
01	BCN	37 834.053 693 001 108	-0.000 021 985 243	0.000 630 787 855
02	BET	38 443.051 174 980 268	-0.000 024 767 247	0.000 560 073 395
03	MIL	38 025.423 177 105 964	-0.000 012 878 201	0.000 503 176 644
07	BRN	38 178.508 556 331 370	-0.000 018 808 537	0.000 471 408 115
08	LIS	38 038.478 209 228 619	-0.000 041 892 249	0.001 214 243 512
09	LON	38 738.600 812 036 675	-0.000 038 287 380	0.000 734 115 508
10	BRL	38 618.783 379 768 545	-0.000 014 660 243	0.000 807 455 746
11	WAR	38 573.312 333 845 846	0.000 000 730 986	0.001 077 123 467
12	ATH	37 344.093 302 991 045	0.000 038 965 419	0.001 741 682 544

EPOCH $t_f = 21\,600$ s

01	BCN	37 845.136 629 696 470	-0.000 019 379 361	0.000 625 846 249
02	BET	38 453.982 609 793 478	-0.000 029 474 680	0.000 584 067 512
03	MIL	38 036.328 990 781 658	-0.000 004 589 864	0.000 548 007 265
07	BRN	38 189.439 026 046 719	-0.000 016 685 846	0.000 472 987 357
08	LIS	38 049.809 535 903 398	-0.000 055 324 092	0.001 410 584 120
09	LON	38 749.625 490 385 479	-0.000 056 033 121	0.000 938 104 981
10	BRL	38 629.568 681 622 295	-0.000 011 628 733	0.000 836 314 796
11	WAR	38 583.959 484 721 621	0.000 017 838 984	0.001 278 244 541
12	ATH	37 354.695 527 400 443	0.000 098 969 964	0.002 546 747 265

Table C.1: *Statistical results of range observations (setting H with 10 observations).*

SATELLITE STATE VECTOR

EPOCH $t_0 = 0$ s

	Ideal value	LS (Iter.)	Error: Mean	Error: Standard deviation
r_x [km]	39 811.324 342 080 086	001	-3 348.715 059 713 256	0.012 768 375 080
		005	0.140 738 014 856	0.014 747 394 503
		010	0.000 507 727 770	0.014 744 377 508
		100	0.000 507 712 444	0.014 744 379 387
r_y [km]	13 863.769 945 143 404	001	7 354.628 326 153 779	0.028 858 004 929
		005	-0.106 686 695 679	0.030 052 160 175
		010	-0.001 007 805 667	0.030 048 544 293
		100	-0.001 007 742 257	0.030 048 544 756
r_z [km]	0.000 000 000 000	001	-3 714.001 680 310 728	0.049 972 809 200
		005	0.149 007 136 586	0.052 422 816 149
		010	0.001 150 281 391	0.052 416 480 446
		100	0.001 150 350 317	0.052 416 446 636
v_x [km/s]	-1.011 153 178 968	001	-0.737 937 815 336	0.000 002 921 888
		005	-0.000 008 601 758	0.000 002 603 013
		010	0.000 000 105 815	0.000 002 602 921
		100	0.000 000 105 809	0.000 002 602 922
v_y [km/s]	2.904 251 340 218	001	-0.497 579 433 802	0.000 002 040 366
		005	0.000 008 463 373	0.000 000 868 280
		010	0.000 000 024 593	0.000 000 868 037
		100	0.000 000 024 590	0.000 000 868 037
v_z [km/s]	0.000 000 000 000	001	-1.347 559 455 396	0.000 005 596 347
		005	-0.000 011 666 079	0.000 004 608 225
		010	0.000 000 183 366	0.000 004 608 880
		100	0.000 000 183 347	0.000 004 608 881

EPOCH $t_f = 21\ 600$ s

r_x [km]	-14 048.210 875 367 075	001	-10 476.498 484 164 631	0.035 221 350 209
		005	-0.016 855 803 350	0.043 952 521 368
		010	0.001 899 711 124	0.043 947 076 870
		100	0.001 899 615 283	0.043 947 091 942
r_y [km]	39 758.040 138 460 929	001	-6 486.796 924 776 097	0.019 610 172 239
		005	0.284 597 148 697	0.022 489 936 721
		010	0.001 032 148 676	0.022 477 374 572
		100	0.001 032 078 890	0.022 477 385 589
r_z [km]	0.000 000 000 000	001	-18 683.638 722 227 672	0.087 948 132 827
		005	-0.160 648 193 583	0.063 235 958 483
		010	0.002 508 958 347	0.063 244 843 499
		100	0.002 508 702 773	0.063 244 862 618
v_x [km/s]	-2.899 009 362 761	001	0.166 336 443 981	0.000 000 708 473
		005	-0.000 009 622 119	0.000 000 829 369
		010	-0.000 000 023 571	0.000 000 829 261
		100	-0.000 000 023 570	0.000 000 829 261
v_y [km/s]	-1.023 728 690 437	001	-0.360 467 995 554	0.000 003 402 911
		005	0.000 033 300 418	0.000 003 341 045
		010	0.000 000 143 578	0.000 003 339 718
		100	0.000 000 143 568	0.000 003 339 719
v_z [km/s]	-0.000 000 000 000	001	0.186 562 342 948	0.000 003 592 318
		005	-0.000 010 816 228	0.000 003 819 130
		010	-0.000 000 084 686	0.000 003 818 667
		100	-0.000 000 084 691	0.000 003 818 665

Table C.2: *Statistical results of satellite state vector (setting H with 10 observations).*

b) 100 observations

RANGE OBSERVATIONS (ρ) AFTER 100 LS ITERATIONS

Num.	**Site**	**Ideal value** [km]	**Error** [km] **Mean**	**Error** [km] **Standard deviation**
EPOCH $t_0 = 0$ s				
01	BCN	37 834.053 693 001 108	0.000 011 553 484	0.000 222 999 071
02	BET	38 443.051 174 980 268	-0.000 001 990 323	0.000 206 172 160
03	MIL	38 025.423 177 105 964	0.000 000 018 007	0.000 183 104 085
07	BRN	38 178.508 556 331 370	-0.000 000 015 215	0.000 177 337 188
08	LIS	38 038.478 209 228 619	0.000 025 728 903	0.000 408 104 335
09	LON	38 738.600 812 036 675	0.000 001 051 072	0.000 253 155 197
10	BRL	38 618.783 379 768 545	-0.000 010 398 525	0.000 286 000 491
11	WAR	38 573.312 333 845 846	-0.000 016 189 459	0.000 365 824 870
12	ATH	37 344.093 302 991 045	-0.000 006 343 591	0.000 540 105 173

EPOCH $t_f = 21\ 600$ s

01	BCN	37 845.136 629 696 470	0.000 002 817 166	0.000 213 144 866
02	BET	38 453.982 609 793 478	0.000 005 804 237	0.000 206 021 686
03	MIL	38 036.328 990 781 658	-0.000 000 409 032	0.000 193 601 359
07	BRN	38 189.439 026 046 719	0.000 002 576 529	0.000 172 910 702
08	LIS	38 049.809 535 903 398	0.000 011 166 829	0.000 439 132 920
09	LON	38 749.625 490 385 479	0.000 012 245 353	0.000 311 714 674
10	BRL	38 629.568 681 622 295	0.000 001 709 606	0.000 277 384 814
11	WAR	38 583.959 484 721 621	-0.000 005 348 105	0.000 405 393 755
12	ATH	37 354.695 527 400 443	-0.000 025 725 529	0.000 811 046 538

Table C.3: *Statistical results of range observations (setting H with 100 observations).*

SATELLITE STATE VECTOR

EPOCH $t_0 = 0$ s

	Ideal value	LS (Iter.)	Error: Mean	Error: Standard deviation
r_x [km]	39 811.324 342 080 086	001	-2 747.374 325 585 931	0.004 146 849 876
		005	-0.005 299 178 589	0.004 521 005 301
		010	-0.000 097 115 434	0.004 521 148 648
		100	-0.000 097 133 988	0.004 521 136 296
r_y [km]	13 863.769 945 143 404	001	6 033.535 176 245 816	0.009 704 448 769
		005	0.013 809 326 909	0.009 404 098 553
		010	0.000 435 919 487	0.009 404 391 635
		100	0.000 435 934 555	0.009 404 359 237
r_z [km]	0.000 000 000 000	001	-2 478.342 498 907 589	0.016 397 486 902
		005	-0.029 047 632 121	0.017 013 920 467
		010	0.000 506 979 619	0.017 013 913 856
		100	0.000 506 878 979	0.017 013 953 208
v_x [km/s]	-1.011 153 178 968	001	-0.578 630 555 378	0.000 000 974 684
		005	-0.000 001 445 831	0.000 000 815 724
		010	-0.000 000 035 074	0.000 000 815 733
		100	-0.000 000 035 075	0.000 000 815 729
v_y [km/s]	2.904 251 340 218	001	-0.385 378 072 371	0.000 000 714 399
		005	0.000 000 249 565	0.000 000 287 048
		010	-0.000 000 016 321	0.000 000 287 060
		100	-0.000 000 016 321	0.000 000 287 060
v_z [km/s]	0.000 000 000 000	001	-1.071 237 749 339	0.000 001 932 899
		005	0.000 003 021 132	0.000 001 496 201
		010	-0.000 000 046 316	0.000 001 496 178
		100	-0.000 000 046 315	0.000 001 496 180

EPOCH $t_f = 21\ 600$ s

r_x [km]	-14 048.210 875 367 075	001	-8 548.390 778 414 758	0.012 133 914 830
		005	-0.019 060 666 552	0.013 620 143 714
		010	-0.000 452 119 889	0.013 620 356 490
		100	-0.000 452 160 534	0.013 620 291 342
r_y [km]	39 758.040 138 460 929	001	-6 532.343 853 471 367	0.005 753 698 587
		005	0.010 077 547 226	0.007 086 387 543
		010	-0.000 252 452 032	0.007 086 806 648
		100	-0.000 252 465 348	0.007 086 774 143
r_z [km]	0.000 000 000 000	001	-14 326.473 931 763 925	0.027 692 388 556
		005	0.041 558 633 499	0.020 538 101 548
		010	-0.000 637 403 147	0.020 537 780 090
		100	-0.000 637 384 745	0.020 537 806 848
v_x [km/s]	-2.899 009 362 761	001	0.177 185 347 266	0.000 000 201 065
		005	0.000 000 343 279	0.000 000 254 009
		010	0.000 000 007 811	0.000 000 254 019
		100	0.000 000 007 812	0.000 000 254 019
v_y [km/s]	-1.023 728 690 437	001	-0.505 585 645 680	0.000 000 697 863
		005	0.000 000 464 568	0.000 001 049 856
		010	-0.000 000 040 915	0.000 001 049 909
		100	-0.000 000 040 917	0.000 001 049 905
v_z [km/s]	-0.000 000 000 000	001	0.205 791 572 405	0.000 001 108 719
		005	0.000 002 105 265	0.000 001 238 952
		010	-0.000 000 036 772	0.000 001 238 951
		100	-0.000 000 036 764	0.000 001 238 954

Table C.4: *Statistical results of satellite state vector (setting H with 100 observations).*

c) 1 000 observations

RANGE OBSERVATIONS (ρ) AFTER 100 LS ITERATIONS

Num.	**Site**	**Ideal value** [km]	**Error** [km]	
			Mean	**Standard deviation**
EPOCH $t_0 = 0$ s				
01	BCN	37 834.053 693 001 108	-0.000 001 777 038	0.000 071 012 805
02	BET	38 443.051 174 980 268	-0.000 001 860 663	0.000 067 246 589
03	MIL	38 025.423 177 105 964	-0.000 001 913 580	0.000 058 008 732
07	BRN	38 178.508 556 331 370	-0.000 001 880 110	0.000 056 978 953
08	LIS	38 038.478 209 228 619	-0.000 001 558 577	0.000 131 749 702
09	LON	38 738.600 812 036 675	-0.000 001 761 370	0.000 082 746 150
10	BRL	38 618.783 379 768 545	-0.000 001 979 483	0.000 093 098 695
11	WAR	38 573.312 333 845 846	-0.000 002 108 893	0.000 118 072 018
12	ATH	37 344.093 302 991 045	-0.000 002 253 608	0.000 170 057 396

EPOCH t_f = 21 600 s

01	BCN	37 845.136 629 696 470	0.000 000 557 739	0.000 069 278 537
02	BET	38 453.982 609 793 478	0.000 000 557 934	0.000 064 956 620
03	MIL	38 036.328 990 781 658	0.000 000 460 472	0.000 059 577 369
07	BRN	38 189.439 026 046 719	0.000 000 510 769	0.000 053 827 942
08	LIS	38 049.809 535 903 398	0.000 000 751 058	0.000 142 939 197
09	LON	38 749.625 490 385 479	0.000 000 677 961	0.000 101 756 609
10	BRL	38 629.568 681 622 295	0.000 000 457 484	0.000 083 655 145
11	WAR	38 583.959 484 721 621	0.000 000 316 663	0.000 123 922 691
12	ATH	37 354.695 527 400 443	0.000 000 008 972	0.000 257 925 962

Table C.5: *Statistical results of range observations (setting H).*

SATELLITE STATE VECTOR

EPOCH t_0 = 0 s

	Ideal value	LS (Iter.)	Error: Mean	Error: Standard deviation
r_x [km]	39 811.324 342 080 086	001	-2 677.786 964 536 734	0.001 318 997 334
		005	-0.010 626 476 347	0.001 438 366 518
		010	-0.000 005 365 480	0.001 438 359 759
		100	-0.000 005 446 527	0.001 438 368 282
r_y [km]	13 863.769 945 143 404	001	5 871.966 257 355 713	0.003 163 605 546
		005	0.020 768 959 952	0.003 012 023 221
		010	0.000 008 172 583	0.003 012 052 792
		100	0.000 008 231 089	0.003 012 070 365
r_z [km]	0.000 000 000 000	001	-2 362.258 797 119 339	0.005 289 591 483
		005	-0.035 126 056 733	0.005 483 035 341
		010	-0.000 002 130 912	0.005 483 072 193
		100	-0.000 002 590 748	0.005 483 043 009
v_x [km/s]	-1.011 153 178 968	001	-0.559 968 250 472	0.000 000 313 683
		005	-0.000 001 200 920	0.000 000 262 389
		010	-0.000 000 000 482	0.000 000 262 386
		100	-0.000 000 000 489	0.000 000 262 388
v_y [km/s]	2.904 251 340 218	001	-0.371 984 502 881	0.000 000 232 936
		005	-0.000 000 344 739	0.000 000 092 659
		010	-0.000 000 000 120	0.000 000 092 664
		100	-0.000 000 000 118	0.000 000 092 664
v_z [km/s]	0.000 000 000 000	001	-1.038 811 150 367	0.000 000 622 655
		005	0.000 003 708 427	0.000 000 474 169
		010	-0.000 000 000 661	0.000 000 474 165
		100	-0.000 000 000 653	0.000 000 474 159

EPOCH $t_f = 21\ 600$ s

r_x [km]	-14 048.210 875 367 075	001	-8 315.714 256 233 945	0.003 929 811 676
		005	-0.018 496 798 384	0.004 382 018 752
		010	-0.000 009 250 633	0.004 381 969 183
		100	-0.000 009 418 790	0.004 382 008 881
r_y [km]	39 758.040 138 460 929	001	-6 468.689 501 788 756	0.001 981 644 527
		005	-0.004 954 134 618	0.002 282 212 241
		010	-0.000 004 148 325	0.002 282 312 448
		100	-0.000 004 199 171	0.002 282 323 456
r_z [km]	0.000 000 000 000	001	-13 854.833 771 147 956	0.008 839 328 329
		005	0.051 010 595 018	0.006 508 273 915
		010	-0.000 009 053 048	0.006 508 216 793
		100	-0.000 008 937 975	0.006 508 137 137
v_x [km/s]	-2.899 009 362 761	001	0.176 220 721 205	0.000 000 064 635
		005	0.000 000 753 490	0.000 000 080 385
		010	0.000 000 000 337	0.000 000 080 385
		100	0.000 000 000 341	0.000 000 080 385
v_y [km/s]	-1.023 728 690 437	001	-0.514 435 890 555	0.000 000 208 955
		005	-0.000 001 313 125	0.000 000 337 747
		010	-0.000 000 000 751	0.000 000 337 757
		100	-0.000 000 000 759	0.000 000 337 759
v_z [km/s]	-0.000 000 000 000	001	0.204 004 621 229	0.000 000 359 307
		005	0.000 002 545 565	0.000 000 399 340
		010	0.000 000 000 158	0.000 000 399 343
		100	0.000 000 000 192	0.000 000 399 341

Table C.6: *Statistical results of satellite state vector (setting H).*

d) 1 000 observations (without weighting matrix)

RANGE OBSERVATIONS (ρ) AFTER 100 LS ITERATIONS

Num.	**Site**	**Ideal value** [km]	**Error** [km]	
			Mean	**Standard deviation**
EPOCH $t_0 = 0$ s				
01	BCN	37 834.053 693 001 108	-0.000 001 628 950	0.000 071 177 743
02	BET	38 443.051 174 980 268	-0.000 000 165 003	0.000 066 023 878
03	MIL	38 025.423 177 105 964	-0.000 000 567 517	0.000 057 450 768
07	BRN	38 178.508 556 331 370	-0.000 000 468 230	0.000 056 227 648
08	LIS	38 038.478 209 228 619	-0.000 002 792 055	0.000 132 087 723
09	LON	38 738.600 812 036 675	-0.000 000 265 194	0.000 080 803 802
10	BRL	38 618.783 379 768 545	0.000 000 552 792	0.000 092 101 806
11	WAR	38 573.312 333 845 846	0.000 000 911 101	0.000 117 310 536
12	ATH	37 344.093 302 991 045	-0.000 000 738 031	0.000 167 360 833

EPOCH $t_f = 21\ 600$ s

01	BCN	37 845.136 629 696 470	0.000 001 397 873	0.000 069 634 476
02	BET	38 453.982 609 793 478	-0.000 000 320 364	0.000 065 575 654
03	MIL	38 036.328 990 781 658	0.000 000 970 807	0.000 059 048 938
07	BRN	38 189.439 026 046 719	0.000 000 431 707	0.000 053 855 658
08	LIS	38 049.809 535 903 398	0.000 001 134 534	0.000 141 822 478
09	LON	38 749.625 490 385 479	-0.000 001 211 874	0.000 102 556 738
10	BRL	38 629.568 681 622 295	-0.000 000 318 861	0.000 083 227 715
11	WAR	38 583.959 484 721 621	0.000 000 443 080	0.000 121 552 935
12	ATH	37 354.695 527 400 443	0.000 004 961 733	0.000 255 372 313

Table C.7: *Statistical results of range observations (setting H without weighting matrix).*

SATELLITE STATE VECTOR

EPOCH $t_0 = 0$ s

	Ideal value	LS (Iter.)	Error: Mean	Error: Standard deviation
r_x [km]	39 811.324 342 080 086	001	-2 677.786 949 746 548	0.001 297 433 765
		005	-0.010 619 491 499	0.001 411 273 828
		010	0.000 001 516 604	0.001 411 289 148
		100	0.000 001 253 456	0.001 411 285 953
r_y [km]	13 863.769 945 143 404	001	5 871.966 200 124 976	0.003 147 108 709
		005	0.020 730 906 342	0.002 982 883 974
		010	-0.000 029 803 123	0.002 982 953 845
		100	-0.000 029 665 123	0.002 982 931 529
r_z [km]	0.000 000 000 000	001	-2 362.258 856 687 308	0.005 260 674 370
		005	-0.035 193 300 474	0.005 402 048 546
		010	-0.000 069 955 764	0.005 402 075 357
		100	-0.000 071 604 097	0.005 402 168 986
v_x [km/s]	-1.011 153 178 968	001	-0.559 968 245 768	0.000 000 309 463
		005	-0.000 001 197 243	0.000 000 259 710
		010	0.000 000 003 186	0.000 000 259 711
		100	0.000 000 003 171	0.000 000 259 711
v_y [km/s]	2.904 251 340 218	001	-0.371 984 497 543	0.000 000 232 779
		005	-0.000 000 342 851	0.000 000 092 867
		010	0.000 000 001 771	0.000 000 092 872
		100	0.000 000 001 781	0.000 000 092 871
v_z [km/s]	0.000 000 000 000	001	-1.038 811 134 506	0.000 000 626 093
		005	0.000 003 720 572	0.000 000 478 738
		010	0.000 000 011 494	0.000 000 478 732
		100	0.000 000 011 542	0.000 000 478 715

EPOCH $t_f = 21\ 600$ s

r_x [km]	-14 048.210 875 367 075	001	-8 315.714 196 681 018	0.003 874 792 808
		005	-0.018 443 966 932	0.004 315 008 723
		010	0.000 043 356 914	0.004 315 027 184
		100	0.000 042 878 132	0.004 315 081 414
r_y [km]	39 758.040 138 460 929	001	-6 468.689 456 032 478	0.001 999 247 430
		005	-0.004 912 305 802	0.002 262 239 465
		010	0.000 037 615 802	0.002 262 354 655
		100	0.000 037 515 266	0.002 262 380 757
r_z [km]	0.000 000 000 000	001	-13 854.833 547 229 373	0.008 880 598 667
		005	0.051 177 442 015	0.006 571 597 525
		010	0.000 157 919 908	0.006 571 514 620
		100	0.000 158 594 463	0.006 571 289 358
v_x [km/s]	-2.899 009 362 761	001	0.176 220 721 428	0.000 000 064 383
		005	0.000 000 753 072	0.000 000 079 181
		010	-0.000 000 000 076	0.000 000 079 182
		100	-0.000 000 000 064	0.000 000 079 181
v_y [km/s]	-1.023 728 690 437	001	-0.514 435 891 777	0.000 000 203 702
		005	-0.000 001 307 588	0.000 000 334 341
		010	0.000 000 004 775	0.000 000 334 355
		100	0.000 000 004 756	0.000 000 334 357
v_z [km/s]	-0.000 000 000 000	001	0.204 004 627 210	0.000 000 360 957
		005	0.000 002 550 416	0.000 000 393 363
		010	0.000 000 005 052	0.000 000 393 365
		100	0.000 000 005 172	0.000 000 393 372

***Table C.8:** Statistical results of satellite state vector (setting H without weighting matrix).*

C.2. RESULTS OF SECTION 4.3: SETTING I

RANGE OBSERVATIONS (ρ) AFTER 100 LS ITERATIONS

Num.	**Site**	**Ideal value** [km]	**Error** [km]	
			Mean	**Standard deviation**
EPOCH $t_0 = 0$ s				
01	BCN	37 834.053 693 001 108	0.000 000 770 829	0.000 071 608 511
02	BET	38 443.051 174 980 268	-0.000 000 827 931	0.000 066 955 836
03	MIL	38 025.423 177 105 964	-0.000 000 870 510	0.000 057 835 021
07	BRN	38 178.508 556 331 370	-0.000 000 730 115	0.000 056 476 678
08	LIS	38 038.478 209 228 619	0.000 003 000 810	0.000 132 173 830
09	LON	38 738.600 812 036 675	-0.000 000 124 237	0.000 082 788 634
10	BRL	38 618.783 379 768 545	-0.000 002 108 565	0.000 093 339 633
11	WAR	38 573.312 333 845 846	-0.000 003 195 748	0.000 118 185 093
12	ATH	37 344.093 302 991 045	-0.000 002 915 545	0.000 173 109 336

EPOCH $t_f = 21\ 600$ s

01	BCN	37 845.136 629 696 470	0.000 001 027 371	0.000 069 052 109
02	BET	38 453.982 609 793 478	0.000 000 945 505	0.000 065 130 765
03	MIL	38 036.328 990 781 658	0.000 000 056 827	0.000 060 386 400
07	BRN	38 189.439 026 046 719	0.000 000 521 567	0.000 054 692 344
08	LIS	38 049.809 535 903 398	0.000 002 904 514	0.000 144 387 518
09	LON	38 749.625 490 385 479	0.000 002 074 127	0.000 098 357 362
10	BRL	38 629.568 681 622 295	-0.000 000 034 092	0.000 087 592 215
11	WAR	38 583.959 484 721 621	-0.000 001 370 335	0.000 128 689 257
12	ATH	37 354.695 527 400 443	-0.000 004 153 027	0.000 250 961 703

Table C.9: *Statistical results of range observations (setting I).*

RANGE-RATE OBSERVATIONS ($\dot{\rho}$) AFTER 100 LS ITERATIONS

Num.	Site	Ideal value [km]	Error [km]	
			Mean	Standard deviation
EPOCH $t_0 = 0$ s				
01	BCN	0.000 243 981 046	-0.000 000 000 026	0.000 000 011 575
02	BET	0.000 228 394 049	0.000 000 000 066	0.000 000 011 395
03	MIL	0.000 224 589 431	0.000 000 000 027	0.000 000 010 889
07	BRN	0.000 227 712 055	0.000 000 000 040	0.000 000 010 957
08	LIS	0.000 272 339 131	-0.000 000 000 071	0.000 000 013 647
09	LON	0.000 239 431 262	0.000 000 000 077	0.000 000 011 678
10	BRL	0.000 212 360 938	0.000 000 000 097	0.000 000 012 488
11	WAR	0.000 196 782 202	0.000 000 000 099	0.000 000 012 846
12	ATH	0.000 188 748 825	-0.000 000 000 048	0.000 000 012 758
EPOCH $t_f = 21\ 600$ s				
01	BCN	0.000 560 626 939	0.000 000 000 048	0.000 000 011 126
02	BET	0.000 565 211 901	0.000 000 000 065	0.000 000 010 996
03	MIL	0.000 567 152 627	0.000 000 000 043	0.000 000 010 647
07	BRN	0.000 565 822 125	0.000 000 000 053	0.000 000 010 672
08	LIS	0.000 550 314 761	0.000 000 000 071	0.000 000 012 439
09	LON	0.000 560 950 171	0.000 000 000 087	0.000 000 011 413
10	BRL	0.000 570 630 327	0.000 000 000 055	0.000 000 011 614
11	WAR	0.000 576 172 939	0.000 000 000 033	0.000 000 011 780
12	ATH	0.000 580 934 546	-0.000 000 000 043	0.000 000 013 471

Table C.10: *Statistical results of range-rate observations (setting I).*

SATELLITE STATE VECTOR

EPOCH $t_0 = 0$ s

	Ideal value	LS (Iter.)	Error: Mean	Error: Standard deviation
r_x [km]	39 811.324 342 080 086	001	-2 697.830 916 001 658	0.001 327 320 153
		005	-0.009 379 023 830	0.001 455 867 350
		010	-0.000 025 446 978	0.001 455 896 352
		100	-0.000 025 425 499	0.001 455 899 083
r_y [km]	13 863.769 945 143 404	001	5 919.982 215 824 241	0.003 088 347 545
		005	0.019 068 736 037	0.003 010 298 329
		010	0.000 077 815 866	0.003 010 389 998
		100	0.000 077 775 678	0.003 010 392 880
r_z [km]	0.000 000 000 000	001	-2 382.515 465 341 180	0.005 426 048 743
		005	-0.033 719 771 772	0.005 656 490 556
		010	0.000 034 430 493	0.005 656 476 292
		100	0.000 034 479 023	0.005 656 492 066
v_x [km/s]	-1.011 153 178 968	001	-0.565 160 766 587	0.000 000 309 688
		005	-0.000 001 249 854	0.000 000 259 910
		010	-0.000 000 006 193	0.000 000 259 914
		100	-0.000 000 006 189	0.000 000 259 914
v_y [km/s]	2.904 251 340 218	001	-0.375 793 434 857	0.000 000 222 982
		005	-0.000 000 206 094	0.000 000 092 389
		010	-0.000 000 002 370	0.000 000 092 393
		100	-0.000 000 002 369	0.000 000 092 393
v_z [km/s]	0.000 000 000 000	001	-1.047 995 976 807	0.000 000 588 884
		005	0.000 003 549 556	0.000 000 458 154
		010	-0.000 000 005 757	0.000 000 458 153
		100	-0.000 000 005 750	0.000 000 458 151

EPOCH $t_f = 21\ 600$ s

r_x [km]	-14 048.210 875 367 075	001	-8 381.040 088 224 710	0.003 874 163 861
		005	-0.018 548 395 607	0.004 333 462 606
		010	-0.000 088 336 892	0.004 333 527 986
		100	-0.000 088 262 954	0.004 333 534 321
r_y [km]	39 758.040 138 460 929	001	-6 490.884 587 991 865	0.001 901 177 357
		005	-0.001 507 908 604	0.002 213 002 323
		010	-0.000 043 356 962	0.002 213 123 877
		100	-0.000 043 316 048	0.002 213 122 347
r_z [km]	0.000 000 000 000	001	-13 987.354 693 985 875	0.008 379 130 683
		005	0.048 825 735 702	0.006 290 482 196
		010	-0.000 079 096 664	0.006 290 478 631
		100	-0.000 079 001 334	0.006 290 446 975
v_x [km/s]	-2.899 009 362 761	001	0.176 608 909 943	0.000 000 065 102
		005	0.000 000 656 975	0.000 000 081 636
		010	0.000 000 001 765	0.000 000 081 638
		100	0.000 000 001 764	0.000 000 081 638
v_y [km/s]	-1.023 728 690 437	001	-0.512 603 976 081	0.000 000 208 491
		005	-0.000 000 901 765	0.000 000 331 146
		010	-0.000 000 007 239	0.000 000 331 162
		100	-0.000 000 007 233	0.000 000 331 162
v_z [km/s]	-0.000 000 000 000	001	0.203 805 441 568	0.000 000 364 693
		005	0.000 002 443 698	0.000 000 411 886
		010	-0.000 000 002 486	0.000 000 411 885
		100	-0.000 000 002 489	0.000 000 411 886

Table C.11: *Statistical results of satellite state vector (setting I).*

C.3. RESULTS OF SECTION 4.3: SETTING J

RANGE OBSERVATIONS (ρ) AFTER 100 LS ITERATIONS

Num.	**Site**	**Ideal value** [km]	**Error** [km]	
			Mean	**Standard deviation**
EPOCH $t_0 = 0$ s				
01	BCN	37 834.053 693 001 108	-0.000 000 070 051	0.000 007 281 977
02	BET	38 443.051 174 980 268	0.000 000 118 833	0.000 006 576 705
03	MIL	38 025.423 177 105 964	-0.000 000 023 310	0.000 005 898 642
07	BRN	38 178.508 556 331 370	0.000 000 036 060	0.000 005 682 753
08	LIS	38 038.478 209 228 619	-0.000 000 040 721	0.000 013 668 476
09	LON	38 738.600 812 036 675	0.000 000 217 092	0.000 007 896 027
10	BRL	38 618.783 379 768 545	0.000 000 118 432	0.000 009 454 451
11	WAR	38 573.312 333 845 846	0.000 000 034 352	0.000 012 264 174
12	ATH	37 344.093 302 991 045	-0.000 000 463 065	0.000 017 173 610

EPOCH $t_f = 21\ 600$ s

01	BCN	37 845.136 629 696 470	0.000 000 378 377	0.000 006 741 494
02	BET	38 453.982 609 793 478	0.000 000 311 810	0.000 006 675 618
03	MIL	38 036.328 990 781 658	0.000 000 223 765	0.000 006 238 949
07	BRN	38 189.439 026 046 719	0.000 000 274 143	0.000 005 564 134
08	LIS	38 049.809 535 903 398	0.000 000 642 659	0.000 013 737 852
09	LON	38 749.625 490 385 479	0.000 000 447 426	0.000 010 380 647
10	BRL	38 629.568 681 622 295	0.000 000 169 470	0.000 008 603 031
11	WAR	38 583.959 484 721 621	-0.000 000 000 508	0.000 012 659 498
12	ATH	37 354.695 527 400 443	-0.000 000 261 115	0.000 026 855 049

Table C.12: *Statistical results of range observations (setting J).*

SATELLITE STATE VECTOR

EPOCH $t_0 = 0$ s

	Ideal value	LS (Iter.)	Error: Mean	Error: Standard deviation
r_x [km]	39 811.324 342 080 086	001	-2 677.786 975 906 893	0.000 133 956 213
		005	-0.010 624 924 629	0.000 143 275 899
		010	-0.000 003 969 278	0.000 143 278 347
		100	-0.000 004 034 020	0.000 143 268 900
r_y [km]	13 863.769 945 143 404	001	5 871.966 278 781 252	0.000 326 164 517
		005	0.020 765 466 505	0.000 309 343 581
		010	0.000 004 770 594	0.000 309 337 189
		100	0.000 004 779 533	0.000 309 340 067
r_z [km]	0.000 000 000 000	001	-2 362.258 840 895 556	0.000 524 489 887
		005	-0.035 139 969 631	0.000 540 902 839
		010	-0.000 016 976 777	0.000 540 920 141
		100	-0.000 017 456 877	0.000 541 020 771
v_x [km/s]	-1.011 153 178 968	001	-0.559 968 253 697	0.000 000 031 988
		005	-0.000 001 200 966	0.000 000 026 899
		010	-0.000 000 000 538	0.000 000 026 898
		100	-0.000 000 000 539	0.000 000 026 897
v_y [km/s]	2.904 251 340 218	001	-0.371 984 504 797	0.000 000 023 883
		005	-0.000 000 344 630	0.000 000 009 735
		010	-0.000 000 000 006	0.000 000 009 735
		100	-0.000 000 000 002	0.000 000 009 737
v_z [km/s]	0.000 000 000 000	001	-1.038 811 154 877	0.000 000 062 718
		005	0.000 003 708 568	0.000 000 049 199
		010	-0.000 000 000 497	0.000 000 049 198
		100	-0.000 000 000 477	0.000 000 049 209

EPOCH $t_f = 21\ 600$ s

r_x [km]	-14 048.210 875 367 075	001	-8 315.714 296 721 295	0.000 400 394 995
		005	-0.018 498 693 109	0.000 443 803 587
		010	-0.000 011 437 950	0.000 443 796 239
		100	-0.000 011 526 996	0.000 443 756 910
r_y [km]	39 758.040 138 460 929	001	-6 468.689 506 980 571	0.000 203 388 262
		005	-0.004 954 835 409	0.000 235 259 872
		010	-0.000 004 930 950	0.000 235 264 923
		100	-0.000 004 929 211	0.000 235 256 287
r_z [km]	0.000 000 000 000	001	-13 854.833 837 052 151	0.000 890 850 710
		005	0.051 012 592 437	0.000 675 327 306
		010	-0.000 006 742 239	0.000 675 306 439
		100	-0.000 006 454 379	0.000 675 467 888
v_x [km/s]	-2.899 009 362 761	001	0.176 220 721 353	0.000 000 006 421
		005	0.000 000 753 317	0.000 000 008 068
		010	0.000 000 000 171	0.000 000 008 068
		100	0.000 000 000 174	0.000 000 008 068
v_y [km/s]	-1.023 728 690 437	001	-0.514 435 888 504	0.000 000 020 534
		005	-0.000 001 313 066	0.000 000 034 776
		010	-0.000 000 000 706	0.000 000 034 776
		100	-0.000 000 000 707	0.000 000 034 775
v_z [km/s]	-0.000 000 000 000	001	0.204 004 623 304	0.000 000 035 826
		005	0.000 002 546 579	0.000 000 039 386
		010	0.000 000 001 240	0.000 000 039 387
		100	0.000 000 001 275	0.000 000 039 394

Table C.13: *Statistical results of satellite state vector (setting J).*

C.4. RESULTS OF SECTION 4.3: SETTING K

RANGE OBSERVATIONS (ρ) AFTER 100 LS ITERATIONS

Num.	**Site**	**Ideal value** [km]	**Error** [km]	
			Mean	**Standard deviation**
EPOCH $t_0 = 0$ s				
01	BCN	37 834.053 693 001 108	-0.000 000 250 183	0.000 065 877 713
02	BET	38 443.051 174 980 268	-0.000 000 862 137	0.000 060 406 739
03	MIL	38 025.423 177 105 964	-0.000 001 237 938	0.000 051 330 092
07	BRN	38 178.508 556 331 370	-0.000 000 998 669	0.000 049 660 534
08	LIS	38 038.478 209 228 619	0.000 001 318 878	0.000 127 815 401
09	LON	38 738.600 812 036 675	-0.000 000 149 690	0.000 076 999 027
10	BRL	38 618.783 379 768 545	-0.000 001 722 737	0.000 087 315 656
11	WAR	38 573.312 333 845 846	-0.000 002 657 805	0.000 113 149 212
12	ATH	37 344.093 302 991 045	-0.000 003 684 519	0.000 168 884 460

EPOCH $t_f = 21\ 600$ s

01	BCN	37 845.136 629 696 470	0.000 001 304 685	0.000 062 961 619
02	BET	38 453.982 609 793 478	0.000 000 262 023	0.000 058 656 129
03	MIL	38 036.328 990 781 658	0.000 000 010 009	0.000 054 287 302
07	BRN	38 189.439 026 046 719	0.000 000 217 327	0.000 047 806 034
08	LIS	38 049.809 535 903 398	0.000 003 204 583	0.000 140 075 764
09	LON	38 749.625 490 385 479	0.000 000 997 310	0.000 093 213 854
10	BRL	38 629.568 681 622 295	-0.000 000 804 564	0.000 082 000 817
11	WAR	38 583.959 484 721 621	-0.000 001 837 791	0.000 124 592 351
12	ATH	37 354.695 527 400 443	-0.000 002 362 806	0.000 246 859 596

Table C.14: *Statistical results of range observations (setting K).*

RANGE-RATE OBSERVATIONS ($\dot{\rho}$) AFTER 100 LS ITERATIONS

Num.	**Site**	**Ideal value** [km]	**Error** [km]	
			Mean	**Standard deviation**
EPOCH $t_0 = 0$ s				
01	BCN	0.000 243 981 046	0.000 000 000 125	0.000 000 009 562
02	BET	0.000 228 394 049	0.000 000 000 115	0.000 000 009 388
03	MIL	0.000 224 589 431	0.000 000 000 114	0.000 000 008 792
07	BRN	0.000 227 712 055	0.000 000 000 115	0.000 000 008 875
08	LIS	0.000 272 339 131	0.000 000 000 141	0.000 000 011 807
09	LON	0.000 239 431 262	0.000 000 000 120	0.000 000 009 729
10	BRL	0.000 212 360 938	0.000 000 000 105	0.000 000 010 599
11	WAR	0.000 196 782 202	0.000 000 000 097	0.000 000 010 971
12	ATH	0.000 188 748 825	0.000 000 000 096	0.000 000 010 956
EPOCH $t_f = 21\ 600$ s				
01	BCN	0.000 560 626 939	-0.000 000 000 007	0.000 000 009 147
02	BET	0.000 565 211 901	-0.000 000 000 030	0.000 000 008 966
03	MIL	0.000 567 152 627	-0.000 000 000 020	0.000 000 008 578
07	BRN	0.000 565 822 125	-0.000 000 000 023	0.000 000 008 602
08	LIS	0.000 550 314 761	0.000 000 000 004	0.000 000 010 672
09	LON	0.000 560 950 171	-0.000 000 000 032	0.000 000 009 419
10	BRL	0.000 570 630 327	-0.000 000 000 037	0.000 000 009 691
11	WAR	0.000 576 172 939	-0.000 000 000 038	0.000 000 009 911
12	ATH	0.000 580 934 546	-0.000 000 000 002	0.000 000 011 692

Table C.15: *Statistical results of range-rate observations (setting K).*

SATELLITE STATE VECTOR

EPOCH $t_0 = 0$ s

	Ideal value	LS (Iter.)	Error: Mean	Error: Standard deviation
r_x [km]	39 811.324 342 080 086	001	-4 145.255 430 893 705	0.001 177 041 479
		005	-2.234 567 985 750	0.001 442 236 533
		010	-0.000 027 469 233	0.001 438 465 081
		100	-0.000 027 476 738	0.001 438 458 445
r_y [km]	13 863.769 945 143 404	001	9 296.634 210 249 404	0.002 728 209 600
		005	3.145 995 000 364	0.002 990 885 288
		010	0.000 063 591 839	0.002 991 743 233
		100	0.000 063 678 013	0.002 991 666 588
r_z [km]	0.000 000 000 000	001	-4 092.703 963 651 105	0.005 190 187 331
		005	-9.691 657 036 666	0.005 468 711 676
		010	-0.000 019 622 573	0.005 455 665 516
		100	-0.000 019 423 490	0.005 455 600 798
v_x [km/s]	-1.011 153 178 968	001	-0.934 667 828 621	0.000 000 269 359
		005	-0.000 297 554 852	0.000 000 257 813
		010	-0.000 000 004 730	0.000 000 257 908
		100	-0.000 000 004 738	0.000 000 257 902
v_y [km/s]	2.904 251 340 218	001	-0.640 724 003 951	0.000 000 190 848
		005	0.000 146 974 540	0.000 000 090 214
		010	-0.000 000 001 373	0.000 000 090 538
		100	-0.000 000 001 378	0.000 000 090 534
v_z [km/s]	0.000 000 000 000	001	-1.677 325 002 805	0.000 000 514 321
		005	0.000 585 291 930	0.000 000 443 992
		010	0.000 000 000 167	0.000 000 445 421
		100	0.000 000 000 138	0.000 000 445 424

EPOCH $t_f = 21\ 600$ s

r_x [km]	-14 048.210 875 367 075	001	-12 925.334 680 520 786	0.003 326 379 109
		005	-4.684 198 415 642	0.004 298 025 187
		010	-0.000 072 073 819	0.004 298 208 091
		100	-0.000 072 183 711	0.004 298 150 078
r_y [km]	39 758.040 138 460 929	001	-6 084.549 398 217 307	0.002 616 983 431
		005	3.521 434 554 237	0.002 184 304 485
		010	-0.000 026 839 579	0.002 188 589 888
		100	-0.000 026 934 738	0.002 188 561 168
r_z [km]	0.000 000 000 000	001	-24 488.696 796 761 662	0.008 841 851 651
		005	8.070 342 332 343	0.006 095 477 377
		010	0.000 002 378 047	0.006 114 824 736
		100	0.000 001 978 307	0.006 114 868 560
v_x [km/s]	-2.899 009 362 761	001	0.126 651 563 028	0.000 000 089 156
		005	0.000 133 636 167	0.000 000 081 072
		010	0.000 000 001 830	0.000 000 080 906
		100	0.000 000 001 831	0.000 000 080 906
v_y [km/s]	-1.023 728 690 437	001	-0.179 011 162 294	0.000 000 372 814
		005	0.000 215 045 428	0.000 000 327 648
		010	-0.000 000 005 141	0.000 000 328 081
		100	-0.000 000 005 153	0.000 000 328 075
v_z [km/s]	-0.000 000 000 000	001	-0.003 861 972 197	0.000 000 432 004
		005	0.000 704 311 394	0.000 000 398 278
		010	0.000 000 001 430	0.000 000 397 317
		100	0.000 000 001 416	0.000 000 397 312

Table C.16: *Statistical results of satellite state vector (setting K).*

REFERENCES

[01] Bate, Roger R., Mueller, Donald D., and White, Jerry E., *Fundamentals of Astrodynamics*, Dover Publications, Inc., New York, 1971.

[02] Casado, D., *Design of an Active Radar Calibrator for Geostationary SAR Missions*, Projecte Final de Carrera (PFC), Universitat Politècnica de Catalunya (UPC), Barcelona, 2016.

[03] Cumming, Ian G., and Wong, Frank H., *Digital Processing of Synthetic Aperture Radar Data: Algorithms and Implementation*, Artech House Publishers, New York, 2005.

[04] Curtis, Howard D., *Orbital Mechanics for Engineering Students*, Elsevier, UK, 2010.

[05] Escobal, Pedro R., *Methods of Orbit Determination*, John Wiley & Sons, New York, 1965.

[06] Fortescue, P., Stark, J., and Swinerd, G., *Spacecraft Systems Engineering*, John Wiley & Sons, Chichester (England), 2003.

[07] International Earth Rotation and Reference Systems Service. 2013. *Announcement of DUT1*. [ONLINE] Available at: http://datacenter.iers.org/eop/-/somos/5Rgv/getTX/17/bulletind-109.txt. [Accessed 15 February 2016]

[08] Levanon, N., *Radar Principles*, John Wiley & Sons, New York, 1988.

[09] Martín, R., *Analysis, Design and Implementation of a Compact Interferometer for Geostationary Orbital Tracking*, Projecte Final de Carrera (PFC), Universitat Politècnica de Catalunya (UPC), Barcelona, 2016.

[10] Montenbruck, O., and Gill, E., *Satellite Orbits: Models, Methods, and Applications*, Springer, New York, 2000.

[11] Monti Guarnieri, A., Perletta, L., Rocca, F., Scapin, D., Tebaldini, S., Broquetas, A., and Ruiz, J., *Design of a Geosynchronous SAR System for Water-Vapour Maps and Deformation Estimation*, ESA Fringe 2011, Frascati, Italy, 19-23 September 2011.

[12] National Aeronautics and Space Administration. *Definition of Two-Line Element Set Coordinate System*. [ONLINE] Available at: http://spaceflight.nasa.gov/realdata/sightings/SSapplications/Post/JavaSSOP/SSOP_Help/tle_def.html. [Accessed 15 February 2016]

[13] National Geospatial-Intelligence Agency. *Office of Geomatics: World Geodetic System 1984 (WGS 84)*. [ONLINE] Available at: http://earth-info.nga.mil/GandG/wgs84/. [Accessed 21 March 2016]

[14] Ruiz Rodon, J., Broquetas, A., Makhoul, E., Monti Guarnieri, A., and Rocca, F., *Nearly Zero Inclination Geosynchronous SAR Mission Analysis With Long Integration Time for Earth Observation*, in Geoscience and Remote Sensing, IEEE Transactions on, vol. 52, no. 10, pp. 6379-6391, October 2014.

[15] Ruiz Rodon, J., Broquetas, A., Makhoul, E., Monti Guarnieri, A., and Rocca, F., *Results on Spatial-Temporal Atmospheric Phase Screen Retrieval from Long-Term GEOSAR Acquisition*, in Geoscience and Remote Sensing Symposium (IGARSS), 2012 IEEE International, vol., no., pp. 3289-3292, 22-27 July 2012.

[16] Ruiz Rodon, J., Broquetas, A., Monti Guarnieri, A., and Rocca, F., *Geosyncrhonous SAR Focusing With Atmospheric Phase Screen Retrieval and Compensation*, in Geoscience and Remote Sensing, IEEE Transactions on, vol. 51, no. 8, pp. 4397-4404, August 2013.

[17] Soumekh, M., *Synthetic Aperture Radar Signal Processing with MATLAB Algorithms*, John Wiley & Sons, New York, 1999.

[18] Tomiyasu, K., and Pacelli, J. L., *Synthetic Aperture Radar Imaging from an Inclined Geosynchronous Orbit*, in IEEE Transactions on Geoscience and Remote Sensing, vol. GE-21, no. 3, pp. 324-329, July 1983.

[19] U.S.S. Command. *Space-Track*. [ONLINE] Available at: https://www.space-track.org. [Accessed 15 February 2016]

[20] Vallado, David A., *Fundamentals of Astrodynamics and Applications*, Microcosm Press, Hawthorne, CA (USA), 2013.

[21] Wadge, G., Monti Guarnieri, A., Hobbs, S. E., and Schulz, D., *Potential atmospheric and terrestrial applications of a geosynchronous radar*, 2014 IEEE Geoscience and Remote Sensing Symposium, pp. 946-949, Quebec City, QC, 2014.